



HAL
open science

Coordination compounds based on 3d-metals with multidentate N- or N₂ donor ligands: Synthesis, structure and properties

Nataliya Plyuta

► **To cite this version:**

Nataliya Plyuta. Coordination compounds based on 3d-metals with multidentate N- or N₂ donor ligands: Synthesis, structure and properties. Inorganic chemistry. Université d'Angers; Kiïvs kij nacionalnij unïversitet imeni Tarasa Ševčenko (Kiïv), 2020. English. NNT : 2020ANGE0020 . tel-04891338

HAL Id: tel-04891338

<https://theses.hal.science/tel-04891338v1>

Submitted on 16 Jan 2025

HAL is a multi-disciplinary open access archive for the deposit and dissemination of scientific research documents, whether they are published or not. The documents may come from teaching and research institutions in France or abroad, or from public or private research centers.

L'archive ouverte pluridisciplinaire **HAL**, est destinée au dépôt et à la diffusion de documents scientifiques de niveau recherche, publiés ou non, émanant des établissements d'enseignement et de recherche français ou étrangers, des laboratoires publics ou privés.

THESE DE DOCTORAT

DE L'UNIVERSITE D'ANGERS
COMUE UNIVERSITE BRETAGNE LOIRE

ECOLE DOCTORALE N° 596
Matière, Molécules, Matériaux
Spécialité : *Chimie inorganique*

Nataliya PLYUTA

Coordination Compounds Based on 3d-Metals with Multidentate N- or N,O-donor Ligands: Synthesis, Structure and Properties

Thèse en cotutelle «université d'Angers et université de Kiev»

Thèse présentée et soutenue à Kiev, le 21/12/2020

Unité de recherche : *Laboratoire MOLTECH-Anjou (UMR 6200), Angers, France;
Faculté de Chimie, Université de Kiev, Ukraine.*

Thèse N° :

Composition du Jury

Rapporteurs :

Pr. Marius Andruh	Professeur	<i>Université de Bucarest</i>	(Romania)
Dr. Sergey Kolotilov	Leading researcher	<i>Institut de chimie physique de NAS</i>	(Ukraine)

Examineurs :

Pr. Nicolas Mercier	Professeur	<i>Université d'Angers</i>	(France)
Dr. Svitlana Petrusenko	Senior researcher	<i>Université de Kiev</i>	(Ukraine)

Directeurs de Thèse :

Dr. Narcis Avarvari	Directeur de Recherches	<i>Université d'Angers</i>	(France)
Pr. Vladimir Kokozay	Professeur	<i>Université de Kiev</i>	(Ukraine)

Co-encadrant de Thèse :

Dr. Thomas Cauchy	Maître de Conférences	<i>Université d'Angers</i>	(France)
--------------------------	-----------------------	----------------------------	----------

Acknowledgment

This work has been done in the MOLTECH-Anjou laboratory (University of Angers, France) and in the Faculty of Chemistry (Taras Shevchenko National University of Kyiv, Ukraine) under the double supervision of Dr. **Narcis Avarvari** (Angers) and Prof. **Vladimir Kokozay** (Kyiv) according to the agreement of the joined thesis.

First and foremost, I would like to thank my supervisors **Narcis Avarvari** and **Vladimir Kokozay** for their time, ideas and knowledge, valuable advices, patience that cannot be underestimated. I would like to extend my sincere thanks to **Svitlana Petrusenko** for invaluable knowledge, insightful suggestions and constructive discussions. I cannot begin to express my thanks to **Thomas Cauchy** who profoundly believed in my abilities and helped me to learn theoretical calculations. They have walked me through all the stages of the writing of this thesis.

I would also like to extend my deepest gratitude to the members of the jury who did me the honor of evaluate this work. The reviewers, Prof. **Marius Andruh** (University of Bucharest) and Dr. **Sergey Kolotilov** (Institut of physical chemistry NAS of Ukraine). The examiners, Prof. **Nicolas Mercier** (University of Angers) and Dr. **Svitlana Petrusenko** (University of Kyiv).

I extend my sincere thanks to all members of MOLTECH-Anjou laboratory, and all those who contributed directly or indirectly to the dissertation. All the people in this department are very kind and warm to me. In particular, I wish to thank **Cecile Meziere** for her help in the laboratory; **Sonia Ouledkram** and **Ingrid Freuze** for mass spectrometry measurements; **Magali Allain** for her help with X-ray analyses; **Valérie Bonnin** for the elemental analyses; **Benjamin Siegler** for NMR spectroscopy measurements.

Special thanks to the Ukrainians in Angers: **Oleh Stetsiuk**, **Serhii Krykun**, **Maxim Dekhtiarenko**, **Alla Skorokhod** and all the master students for helpful advices in work, help, a lot of jokes and spending time together. Many thanks to **Nabil Mroweh** for conversations and reminding me about my English, to **Yohan Chéret** for his kindness, help and support in any moment. Big thanks to **Cristina Oliveras**, **Maurizio Mastropasqua Talamo**, **Kévin Martin** for having a good time in Anger and in Kyiv. I also wish to thank **Marwa Bel Haj Salah** and **Suchithra Ashoka Sahadevan** for unwavering support, **Pablo Simon Marques** and **Jose Maria Andres Castan** for their humor and part of Spanish culture, **Youseef Aidibi** for “hard working” atmosphere in our office.

I am very grateful to all our collaborators Dr. **Evgeny Goreshnik** (Jožef Stefan Institute, Slovenia) and Dr. **Irina Omelchenko** (Institute for Single Crystals, Ukraine) for the X-ray analyses; Prof. **Miguel Julve** and Prof. **Francisco Lloret** (University of Valencia, Spain) for the magnetic measurements; Prof. **Andrew Ozarowski** (National High Magnetic Field Laboratory, USA) for HREPR studies, Prof. **Andreas Hauser** (University of Geneva, Switzerland) for the luminescent investigation; Prof. **N. A. Davidenko** (University of Kyiv, Ukraine) for studying photovoltaic properties of polymer composite films and Dr. **O.V. Pocas** (Institute of Epidemiology and Infectious Diseases, Ukraine) for antimicrobial activity studies.

I would like to thank Prof. **Zoia Voitenko**, who helped me to apply for the scholarship, and to the French Embassy in Ukraine for the financial support of my work.

Finally, I want to thank my family for their love, encouraging and supporting me. Thanks to all my friends for their company, no matter how physically far away we are.

Thank you all!

Content

Acronyms	3
Liste of compounds obtained.	4
General introduction	6
CHAPTER 1. Introduction	7
1.1. Multidentate <i>N</i> - and <i>N, O</i> -donor ligands.	7
1.2. Coordination compounds with Schiff bases derived from <i>o</i> -vanillin	8
1.3. Heterometallic <i>d-s</i> coordination compounds	17
1.4. Coordination compounds with ligands based on 2,1,3-benzothiadiazole.	20
References.	29
CHAPTER 2. Coordination compounds with hydroxylated Schiff bases.	36
2.1. Introduction.	36
2.2. Heterometallic <i>d-s</i> complexes	37
2.3. Tetranuclear Cu(II) complexes.	46
2.4. Mn(II) and Mn(III) complexes.	49
2.4.1. $[\text{Mn}^{\text{II}}_2(\text{HL}^2)_2(\text{NCS})_2] \cdot 2\text{C}_2\text{H}_5\text{OH}$	49
2.4.2. Manganese (III) coordination polymers	51
2.4.3. EPR spectral studies	54
2.5. Tautomerism in H_2L^2	56
2.6. Conclusion.	62
References.	64
CHAPTER 3. Coordination compounds with Schiff base ligands bases on 2,1,3-benzothiadiazole.	67
3.1. Introduction.	67
3.2. Synthesis and crystal structure of Schiff base ligands.	67
3.3. Synthesis and crystal structures of coordination compounds with HL^5 and HL^6	73
3.4. Magnetic properties.	80
3.5. Conclusion	84
References.	85
CHAPTER 4. Coordination compounds with 2,1,3-benzothiadiazole based pyridine and 2,2'-bipyridine ligands.	88
4.1. Introduction.	88

4.2. Synthesis, DFT calculations and crystal structure of ligands L ⁷ - L ¹⁰	88
4.3. Coordination compounds with ligands based on 2,1,3-benzothiadiazole.	93
4.3.1. Crystal structures of coordination compounds with L ⁷	94
4.3.2. Crystal structures of coordination compounds with L ⁸	102
4.3.3. Crystal structures of coordination compounds with L ⁹	103
4.4. Photophysical properties..	110
4.5. Conclusion..	114
References.	115
General conclusions.	117
Appendixes.	120
Appendix 1. Experimental section	120
Appendix 2. Crystallographic data and selected geometrical parameters	140
Appendix 3. Computational details	209

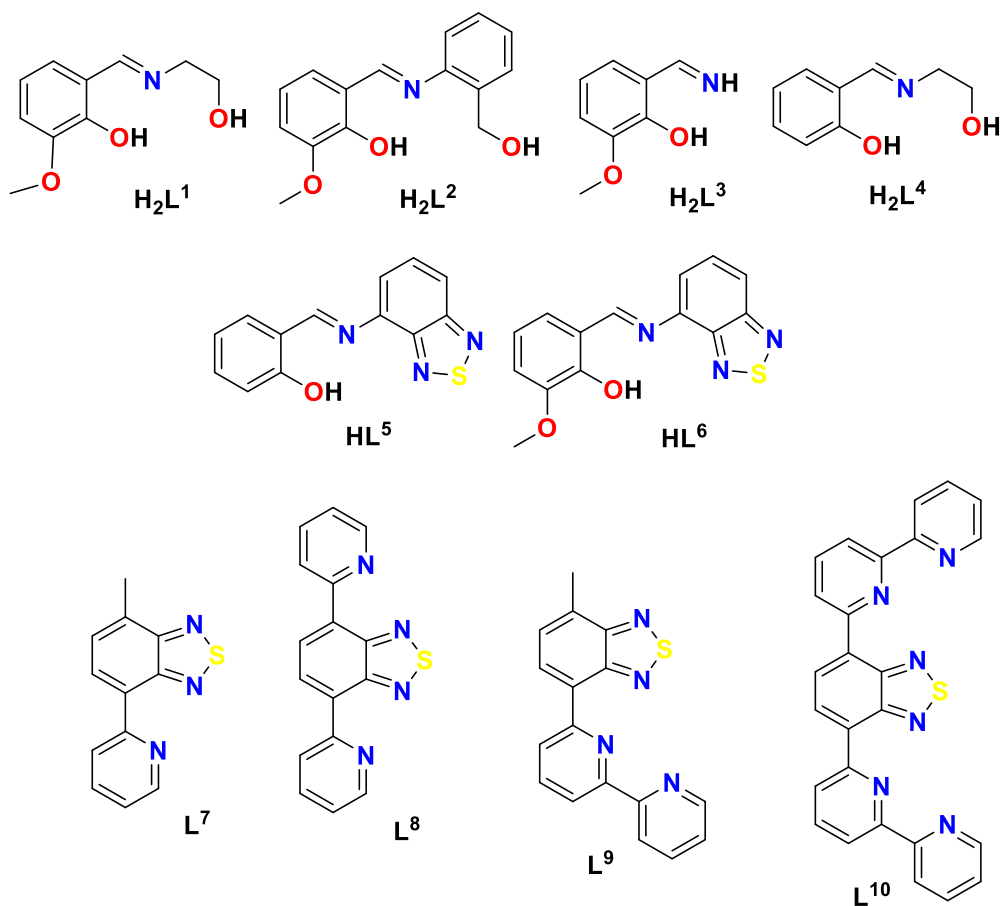
Acronyms

SB	– Schiff base
<i>o</i> -van	– <i>o</i> -vanillin; 2-hydroxy-3-methoxybenzaldehyde
Sal	– salicylaldehyde, 2-hydroxybenzaldehyde
BTD	– 2,1,3-benzothiadiazole
H ₂ L ¹	– 2-[(2-hydroxyethyl)imino]methyl-6-methoxy-phenol
H ₂ L ²	– 3-2-[(2-hydroxymethylbenzyl)imino]methyl-6-methoxy-phenol
HL ³	– 2-iminomethyl-6-methoxy-phenol
H ₂ L ⁴	– 2-[(2-hydroxyethyl)imino]methylphenol
HL ⁵	– 2-[4-(2,1,3-benzothiadiazole)imino]methyl-phenol
HL ⁶	– 2-[4-(2,1,3-benzothiadiazole)imino]methyl-6-methoxy-phenol
L ⁷	– 4-(2-pyridine)-7-methyl-2,1,3-benzothiadiazole
L ⁸	– 4,7-bis(2-pyridine)-2,1,3-benzothiadiazole
L ⁹	– 4-(2,2'-bipyridine)-7-methyl-2,1,3-benzothiadiazole
L ¹⁰	– 4,7-bis(2,2'-bipyridine)-2,1,3-benzothiadiazole
Hea	– monoethanolamine
aba	– 2-aminobenzyl alcohol
DMF	– dimethylformamide
DMSO	– dimethylsulfoxide
Et ₃ N	– triethylamine
OAc ⁻	– acetate anion
Hfac ⁻	– hexafluoroacetylacetonate anion
SMM	– single molecule magnet
LUMO	– lowest unoccupied molecular orbital
HOMO	– highest occupied molecular orbital
py	– pyridine
bipy	– 2,2'-bipyridine
DCM	– dichloromethane
SCE	– saturated calomel electrode
DFT	– density functional theory
TD-DFT	– time-dependent density functional theory
EDD	– electron density difference
THF	– tetrahydrofuran
BVS	– bond valence sum

List of compounds obtained

- 1 $[\text{Cu}_4(\text{L}^1)_4(\text{CH}_3\text{OH})_4] \cdot 2,2\text{CH}_3\text{OH}$
- 2 $[\text{Ca}\{\text{Cu}(\text{HL}^1)_2\}_2]\text{Br}_2$
- 3 $[\text{Ca}\{\text{Cu}(\text{HL}^1)_2\}_2]\text{I}_2 \cdot 0,4\text{H}_2\text{O}$
- 3a $[\text{Ca}\{\text{Cu}(\text{HL}^1)_2\}_2(\text{CH}_3\text{OH})]\text{I}_2$
- 4 $[\text{Ca}\{\text{Cu}(\text{HL}^1)_2\}_2](\text{SCN})_2$
- 5 $[\text{Sr}\{\text{Cu}(\text{HL}^1)_2\}_2(\text{CH}_3\text{OH})]\text{I}_2$
- 6 $[\text{Sr}\{\text{Cu}(\text{HL}^1)_2\}_2(\text{H}_2\text{O})_2](\text{SCN})_2 \cdot 0,65\text{CH}_3\text{OH}$
- 7 $[\text{Sr}\{\text{Cu}(\text{HL}^1)_2\}_2\text{NO}_3]\text{NO}_3 \cdot \text{CH}_3\text{OH}$
- 8 $[\text{Ba}\{\text{Cu}(\text{HL}^1)_2\}_2(\text{CH}_3\text{OH})_2]\text{I}_2$
- 9 $[\text{Ba}\{\text{Cu}(\text{HL}^1)_2\}_2(\text{CH}_3\text{OH})_2](\text{SCN})_2$
- 10 $[\text{Cu}_4(\text{HL}^1)_2(\text{L}^1)_2(\text{NCS})_2(\text{CH}_3\text{OH})_2] \cdot 2\text{CH}_3\text{OH}$
- 11 $[\text{Ca}\{\text{Cu}(\text{HL}^2)_2\}_2]\text{I}_2$
- 12 $[\text{Cu}(\text{L}^3)_2\text{Ca}(\text{NCS})_2(\text{H}_2\text{O})]$
- 13 $\{\text{[Mn}(\text{HL}^1)_2]\text{Cl}\}_n$
- 14 $\{\text{[Mn}(\text{HL}^1)_2]\text{Br}\}_n$
- 15 $[\text{Mn}(\text{HL}^1)_2(\text{NCS})]$
- 16 $\{\text{[Mn}(\text{HL}^4)_2]\text{Br}\}_n$
- 17 $\{\text{[Mn}(\text{HL}^4)_2]\text{I}\}_n$
- 18 $\{\text{[Mn}(\text{HL}^4)_2]\text{NCS}\}_n$
- 19 $[\text{Mn}_2(\text{HL}^2)_2(\text{NCS})_2] \cdot 2\text{C}_2\text{H}_5\text{OH}$
- 20 H_2L^2
- 20a $\text{H}_2\text{L}^2 \cdot \text{CH}_3\text{OH}$
- 20b $\text{H}_2\text{L}^2 \cdot \text{H}_2\text{O}$
- 21 $\text{Cu}(\text{L}^5)_2$
- 22 $\text{Co}(\text{L}^5)_2$
- 23 $\text{Ni}(\text{L}^5)_2$
- 24 $\text{Zn}(\text{L}^5)_2$
- 25 $[\text{Cu}(\text{L}^5)(\text{Hfac})]$
- 26 $\text{Cu}(\text{L}^6)_2$
- 27 $\text{Zn}(\text{L}^6)_2$
- 28 $[\text{Co}(\text{L}^6)_2] \cdot \text{CH}_2\text{Cl}_2$
- 29a $[\text{Co}_2(\text{L}^7)_2\text{Cl}_4(\text{CH}_3\text{OH})_2]$
- 29b $[\text{Co}_2(\text{L}^7)_2\text{Cl}_4]$
- 30 $[\text{CuL}^7\text{Cl}_2]$
- 31 $[\text{ZnL}^7\text{Cl}_2]$
- 32 $[\text{PtL}^7\text{Cl}_2]$
- 33 $[\text{MnL}^7(\text{Hfac})_2]$
- 34 $[\text{CoL}^7(\text{Hfac})_2]$
- 35 $[\text{NiL}^7(\text{Hfac})_2]$
- 36 $[\text{CuL}^7(\text{Hfac})_2]$
- 37 $[\text{ZnL}^7(\text{Hfac})_2]$
- 38 $[\text{CuL}^8(\text{Hfac})_2]$
- 39 $[\text{Cu}_2\text{L}^8(\text{Hfac})_4]$
- 40 $[\text{MnL}^9\text{Cl}_2] \cdot 0,5\text{CH}_2\text{Cl}_2$
- 41 $[\text{CoL}^9(\text{H}_2\text{O})_2\text{Cl}]\text{Cl} \cdot 3\text{H}_2\text{O}$
- 42 $[\text{CoL}^9\text{Cl}_2] \cdot 0,25\text{CH}_2\text{Cl}_2$

- 43 $[\text{NiL}^9(\text{H}_2\text{O})_3]\text{Cl}_2 \cdot 2\text{H}_2\text{O}$
 44 $[\text{Ni}_2(\text{L}^9)_2\text{Cl}_4] \cdot 2\text{H}_2\text{O}$
 45 $[\text{CuL}^9\text{Cl}_2] \cdot \text{H}_2\text{O}$
 46 $[\text{ZnL}^9\text{Cl}_2]$
 47 $[\text{NiL}^9(\text{Hfac})(\text{H}_2\text{O})](\text{Hfac}) \cdot \text{H}_2\text{O}$
 48 $[\text{CuL}^9(\text{Hfac})(\text{H}_2\text{O})](\text{Hfac}) \cdot \text{H}_2\text{O}$
 49 $[\text{CuL}^9(\text{Hfac})(\text{C}_2\text{H}_5\text{OH})](\text{Hfac})$



General Introduction

This thesis is devoted to the synthesis of the new coordination compounds with multidentate *N*- and *N,O*-donor ligands, investigation of their structures and properties.

Chapter one is dedicated to an overview of the reported multidentate ligands for the synthesis of polynuclear complexes based on *3d*-metals. Coordination properties of Schiff base ligands and compounds derived from 2,1,3-benzotriazole were considered in detail. A special focus is made on coordination chemistry of *s*-metals.

Chapter two explores the classical Schiff base ligands in the synthesis of polynuclear complexes by the “direct synthesis” approach. Crystal structures of polynuclear Cu, Mn, Cu/Ca, Cu/Sr, Cu/Ba complexes were discussed. High-field EPR investigation of polymeric manganese (III) complexes combined with DFT calculations were described. The chapter ends with the study of three crystalline pseudo-polymorphs of Schiff base ligand which paves the way to the choice of the experimental conditions for further coordination chemistry studies.

Chapter three reports on the syntheses and coordination chemistry studies of novel Schiff base ligands based on 2,1,3-benzotriazole. A combined experimental and theoretical study is proposed to characterize the coordination possibilities and photophysical properties of these ligands. Crystal structures and magnetic properties for complexes complete this chapter.

Chapter four describes the synthesis of new chelate ligands based on 2,1,3-benzotriazole. The syntheses of series of mono- and binuclear complexes were discussed. The crystallographic results, electrochemical and photophysical properties were supported by DFT and TD-DFT studies.

General conclusions and perspectives summarize the work described in this manuscript and propose an overlook on future directions.

The manuscript includes three appendixes. Appendix 1 describes general information of methods and all synthetic procedures for new ligands and complexes. Appendix 2 contains the main crystallographic parameters and selected bond lengths and angles of the compounds obtained. Appendix 3 includes DFT calculation details.

Chapter 1

INTRODUCTION

1.1. Multidentate *N*- and *N, O*-donor ligands

Synthesis and study of biological and physicochemical properties of metal complexes with multidentate ligands is an actual trend of modern coordination chemistry. The polydentate ligands allow to obtain both stable chelate complexes of molecular type and polynuclear mono- and heterometallic compounds, up to coordination polymers with different degrees of dimensionality. The chelate complexes have a wide practical application (e.g. in medicine, agriculture, chemical industry) and are also used in theoretical research (e.g. modeling active centers of enzymes and other natural compounds, establishing mechanisms of important natural processes). Polymer and polynuclear complexes are interesting mainly for their physical and chemical properties, such as magnetic, electro- and photoconductive, catalytic, sorption, optical properties allowing to consider them as promising objects for the creation of a new variety of functional materials.

Among the great variety of multidentate ligands, which are now actively explored in coordination chemistry, one of the most promising classes is the one of the Schiff bases¹. Schiff bases (SBs) are organic compounds with imine (>C=N-) or azomethine (-CH=N-) groups. Most SBs are oily or crystalline compounds that are insoluble in water but well soluble in organic solvents. The simplest SBs are colourless, more complex SBs have a characteristic intensive colouring and belong to the class of azomethine dyes. Generally, SBs are obtained by condensation of primary amines with aldehydes or ketones:



SBs have an important biological significance because they are intermediate in many enzymatic processes (for example, the biosynthesis of α -amino acids in the body) and are used as strong bactericides (including furacilin and furazolidone). Also SBs are widely studied as effective ligands¹⁻³ for the synthesis of coordination compounds promising for making pharmaceutical preparations with antitumor, antibacterial, antifungal and other biological properties⁴⁻⁶, catalysts⁷, analytical reagents⁸, energy storage⁹ and models of important biochemical processes¹⁰.

In a separate group it can be distinguished salicylidene type of SBs, obtained by condensation with salicylic aldehyde or its derivatives. Such ligands have significant advantages - they have quite simple structures, are commercially available, easily synthesized and modified with high yields. In addition, complexes with this kind of ligands often form crystalline

precipitates, which is important to determine the crystal structure by X-ray analysis. Salen type ligands are the most studied in this group¹¹.

The coordination properties of *o*-vanillin based SB have been less studied, despite the fact that they potentially have an additional donor atom. Today such ligands are attracting significant attention of researchers¹². These ligands can be divided into two main groups: symmetrical and asymmetrical (Fig. 1.1).

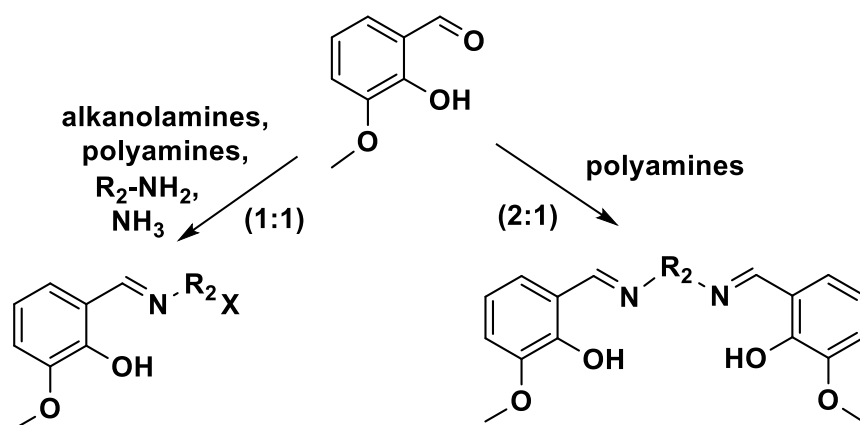


Figure 1.1. Symmetrical and asymmetrical Schiff base ligands.

Symmetrical SBs more often show chelating functions and are used as "blocking ligands" to create building blocks for crystal engineering. At the same time the use of asymmetrical SBs allows to investigate more various coordination compounds, as ligands they are more flexible, showing both chelate and bridge-chelate functions.

In addition, SBs are easily modifiable, which allows to obtain new polydentate ligands with different sets and combinations of donor centers and substitutes.

1.2. Coordination compounds with Schiff bases derived from *o*-vanillin

The ligand H_2L^1 results from the condensation of *o*-vanillin with monoethanolamine (Fig. 1.2). Analysis of CSD data of the complexes with H_2L^1 allowed us to establish the characteristic coordination modes (Table 1.1).

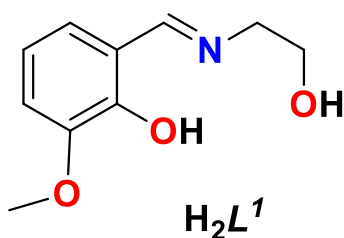


Figure 1.2. Structure of the ligand H_2L^1 .

As shown in Table 1.1 the ligand H_2L^1 realizes mainly chelate-bridging modes due to the four donor atoms (O_{meth} , OH_{ph} , N , OH_{alk}) and the high lability of the alcohol arms (Fig. 1.2). The majority of known complexes shows a polynuclear structure (up to 75%).

Table 1.1. Coordination modes of H_2L^1 .*

Coordination mode (donor sites: OH_{alk} , N , OH_{ph} , O_{meth})	Harris notation ¹³	Compounds
$(HL^1)^-$		
O, N – bidentate chelating	[1.0101]	$M(HL^1)_2$ $M = Cu, Zn$ ^{14,15}
O, N, O' – tridentate chelating	[1.0111]	$[Co(HL^1)_2]X \cdot H_2O$ $X = OAc, NO_3$ ^{16,17} ; $[Ni_2(HL^1)_3(NCO)] \cdot 2H_2O$ ¹⁸ ; $Zn_2(HL^1)_2(OAc)_2$ ¹⁹ ; $[Dy_3(\mu_3-OH)L^1(HL^1)_4](ClO_4)_2 \cdot 1.5C_2H_5OH \cdot 3.5H_2O$ ²⁰
O, O', N, O'' – tetradentate chelating	[1.1111]	$Zn_2(HL^1)_2(OAc)_2$ ¹⁹
O, N, O' – tridentate bridging	[2.01 ₁ 2 ₁ 1 ₁]	$\{[Mn(HL^1)_2]I\}^{21}$; $[Cu(HL^1)(NCS)]_n$ ²² ; $[Ni_2(HL^1)_3(N_3)] \cdot 3H_2O$ ²³
O, O', O', N – tetradentate bridging	[2.1 ₁ 2 ₁ 2 ₁ 0 ₁ 2]	$[Ni_2(HL^1)_3X] \cdot nH_2O$, $X = NCO, N_3$ ^{18,23} ; $\{[Cu_4(L^1)_2(HL^1)_2(H_2O)_2(ppda)]5H_2O\}_n$ ²⁴
O, O, N, O' – tetradentate bridging	[2.02 ₁ 2 ₁ 2 ₁ 2 ₁]	$[Dy_3(\mu_3-OH)L^1(HL^1)_4](ClO_4)_2 \cdot 1.5C_2H_5OH \cdot 3.5H_2O$ ²⁰
O, O', O', O', N – pentadentate bridging	[3.1 ₁ 3 ₁ 2 ₃ 0 ₁ 3]	$[Ni_4(L^1)_2(HL^1)_2(X)_2(solv)_2] \cdot nsolv$, $X = SeCN, NCS$, $solv = C_3H_7NO, H_2O, EtOH$ ^{18,25} ;
O, O', O', N, O'' – pentadentate bridging	[2.1 ₁ 2 ₁ 2 ₁ 2 ₁ 2 ₁]	$[Dy_3(OH)L^1(HL^1)_4](ClO_4)_2 \cdot 1.5C_2H_5OH \cdot 3.5H_2O$ ²⁰ ; $[Dy_4(OH)_2(HL^1)_2(L^1)_2(X)_4] \cdot 4solv$, $X = Cl, N_3$; $solv = MeCN$ $MeOH$ ²⁶ ; $[Cu_4(L^1)_2(HL^1)_2(H_2O)_2](NO_3)_2(pydc)_2 \cdot 9H_2O$ ²⁴ ; $[Cu_4(L^1)_2(HL^1)_2(H_2O)](ClO_4)_2 \cdot 2H_2O$ ²⁷
$O, O', O', N, O'', O'', O''$ – heptadentate bridging	[4.1 ₁ 2 ₁ 2 ₃ 2 ₃ 4 ₁ 2]	$[Dy_6Na_2(L^1)_4(O_2)(PhCOO)_{10}(H_2O)_2]$ ²⁸
$(L^1)^{2-}$		
O, N, O' – tridentate chelating	[1.0111]	$[MoO_2L^1(CH_3OH)]$ ²⁹
O, O', N, O'' – tetradentate chelating	[1.1111]	$[(VO_2)(HL^1)(H_2O)]Na\}_n$ ³⁰
O, O', O', N – tetradentate bridging	[2.1 ₁ 2 ₁ 2 ₁ 0 ₁ 2]	$[Fe_4(L^1)_4(MeOH)_4]$ ³¹
O, N, O', O' – tetradentate bridging	[2.01 ₁ 2 ₁ 2 ₁ 2 ₁]	$[(UO_2)_2(L^1)_2(dmf)_2]$ ³² ; $[Cu_4(L^1)_2(HL^1)_2(H_2O)](ClO_4)_2 \cdot 2H_2O$ ²⁷ ; $[Na_2\{Mn_3(O)\}_2Ln(L^1)_6(O_2CPh)_4(N_3)_2]OH \cdot nsolv$, $Ln = Eu, Gd, Tb, Dy$, $solv = CH_3CN, H_2O$ ³³
O, N, O', O', O' – pentadentate bridging	[3.01 ₁ 3 ₁ 2 ₃ 1 ₁]	$\{[(H_2O)MnL^1]\{MnL^1\}\}_2 \cdot 2(MeOH)_2(EtOH) \cdot 2Cl$ ³⁴ ; $[Dy_3(OH)L^1(HL^1)_4](ClO_4)_2 \cdot 1.5C_2H_5OH \cdot 3.5H_2O$ ²⁰ ; $\{[Cu_4(L^1)_2(HL^1)_2(H_2O)_2(ppda)]5H_2O\}_n$ ²⁴ ; $[Cu_4(L^1)_2(HL^1)_2(H_2O)_2](NO_3)_2(pydc)_2 \cdot 9H_2O$ ²⁴ ; $[Cu_6Dy_3(L^1)_6(OH)_6(H_2O)_5(MeOH)]NO_3 \cdot 2Br \cdot 4H_2O \cdot MeOH$ ³⁵ ; $[Cu_4L^1_4]_nCH_3CN$, $n = 0, 1$ ^{36,37} ; $Ni_4L^1_4(CH_3OH)_4 \cdot 4H_2O$ ³⁷ ; $[Ni_4(L^1)_2(HL^1)_2(X)_2(solv)_2] \cdot nsolv$, $X = SeCN, NCS$, $solv = C_3H_7NO, H_2O, EtOH$ ^{18,25} ;
O, O', O', N, O'', O'' – hexadentate bridging	[3.1 ₁ 2 ₁ 2 ₂ 2 ₃ 1 ₂]	$[Ln_{12}Na_3(OH)_2(L^1)_6(piv)_{12}(CO_3)_6(MeOH)_6]OH \cdot 5MeOH$, $Ln = Gd, Dy$ ³⁸ ;
$O, O', O', N, O'', O'', O''$ – heptadentate bridging	[4.1 ₁ 2 ₁ 2 ₂ 2 ₃ 4 ₁ 2]	$[Co_2Ln_4(OH)_2(piv)_4(L^1)_4(ae)_2](NO_3)_2 \cdot 2H_2O$, $Ln = Eu, Gd, Tb, Dy$ ³⁹

* according to Cambridge Structural Database (CSD)

Thus, five tetranuclear complexes with copper, of cubane type, were obtained and studied. E. Gungor *et al.* have obtained the tetranuclear complex $[\text{Cu}_4\text{L}^1_4]$ by reacting $\text{Cu}(\text{OAc})_2\cdot\text{H}_2\text{O}$, H_2L^1 and Et_3N in ethanol/methanol mixture³⁶. The obtained complex contains the fragment $\{\text{Cu}_4\text{O}_4\}$ and belongs to the class of cubane structures (4+2)⁴⁰, *i.e.* it has four short and two long $\text{Cu}\cdots\text{Cu}$ distances. In the crystal lattice there are three independent fragments of the open cubane type, which differ significantly in their linear and angular parameters. An antiferromagnetic interaction was found ($J = -108.46 \text{ cm}^{-1}$) between the Cu^{II} centers (Fig. 1.3).

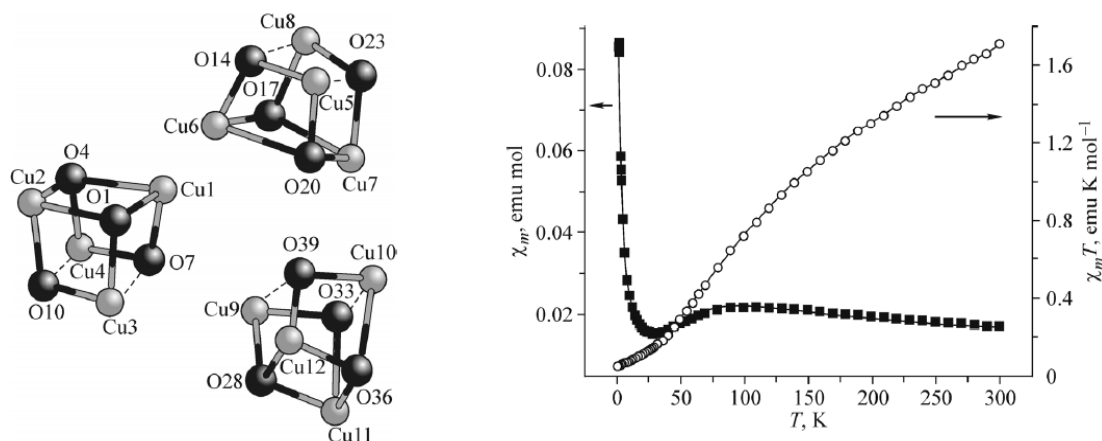


Figure 1.3. Crystal structure of the Cu_4O_4 fragments and temperature dependence of the magnetic susceptibility of the complex $[\text{Cu}_4\text{L}^1_4]$ ³⁶.

The complex $[\text{Cu}_4\text{L}^1_4]\cdot\text{CH}_3\text{CN}$ is representative of the (4+2) class $\{\text{Cu}_4\text{O}_4\}$ of cubane compounds and was obtained by reaction of the ligands with $\text{Cu}(\text{NO}_3)_2\cdot 3\text{H}_2\text{O}$ in acetonitrile (Fig. 1.4). Studies of magnetic properties have shown mainly ferromagnetic interactions between copper atoms³⁷.

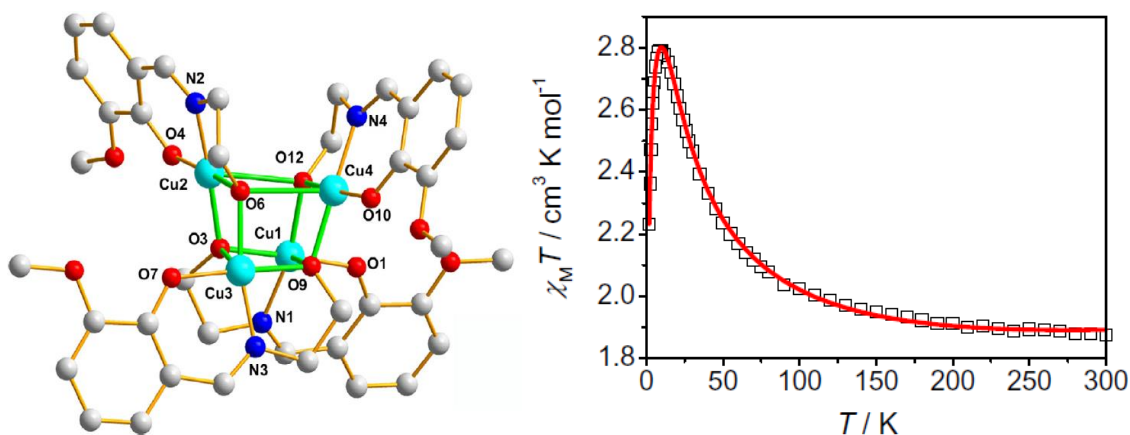


Figure 1.4. Crystal structure and temperature dependence of the magnetic susceptibility of the complex $[\text{Cu}_4\text{L}^1_4]\cdot\text{CH}_3\text{CN}$ ³⁷.

In the complexes $[\text{Cu}_4(L^I)_2(\text{HL}^I)_2(\text{H}_2\text{O})_2](\text{NO}_3)_2(\text{pydc})_2 \cdot 9\text{H}_2\text{O}$ (pydc – pyridine-3,5-dicarboxylate), $\{[\text{Cu}_4(L^I)_2(\text{HL}^I)_2(\text{H}_2\text{O})_2(\text{ppda})] \cdot 5\text{H}_2\text{O}\}_n$ (ppda – 1,4-diacrylate)²⁴ and $[\text{Cu}_4(L^I)_2(\text{HL}^I)_2(\text{H}_2\text{O})](\text{ClO}_4)_2 \cdot 2\text{H}_2\text{O}$ ²⁷ two coordination modes of the ligand are combined (Table 1.1). All complexes consist of a tetranuclear open cubane $\{\text{Cu}_4\text{O}_4\}$ core. In all cases, antiferromagnetic interactions have been observed.

Polynuclear heterometallic *s-f* complexes proved to be promising objects of research. Complexes $[\text{Ln}_{12}\text{Na}_3(\mu_3\text{-OH})_2(L^I)_6(\text{piv})_{12}(\text{CO}_3)_6(\text{MeOH})_6]\text{OH} \cdot 5\text{MeOH}$ (Ln = Gd, Dy, piv – 2,2-dimethylpropanoic acid residue) were synthesized by using lanthanide chlorides and the sodium salt of the 2,2-dimethylpropanoic acid. The obtained compounds are isomorphous and consist of a dodecahedral cluster $\{\text{Dy}_{12}\}$ or $\{\text{Gd}_{12}\}$, inside which there are three sodium ions (Fig. 1.5). Studies of magnetic properties have shown that the compound with the $\{\text{Gd}_{12}\}$ fragment is a good candidate for magnetic refrigeration with a significant change in entropy ($-\Delta S_m$) of $30.99 \text{ J} \cdot \text{kg}^{-1} \text{K}^{-1}$ for $H = 7 \text{ T}$ at 4 K . The compound with the fragment $\{\text{Dy}_{12}\}$ demonstrates the behavior of single molecule magnet (SMM)³⁸.

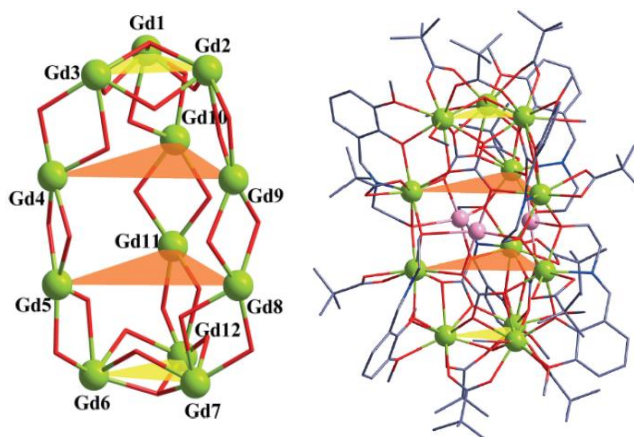


Figure 1.5. Crystal structure of the $\{\text{Gd}_{12}\}$ core in the complex $[\text{Gd}_{12}\text{Na}_3(\mu_3\text{-OH})_2(L^I)_6(\text{piv})_{12}(\text{CO}_3)_6(\text{MeOH})_6]\text{OH} \cdot 5\text{MeOH}$ ³⁸.

The effect of changing the length of the "alcohol arm" of the ligand on the composition and structure of the complexes was studied by Modak³⁵. Thus, when using H_2L^I the nine-core complex $[\text{Cu}_6\text{Dy}_3(L^I)_6(\text{OH})_6(\text{H}_2\text{O})_5(\text{MeOH})]\text{NO}_3 \cdot \text{Br}_2 \cdot 4\text{H}_2\text{O} \cdot \text{MeOH}$ was obtained, while when using a ligand resulting from the condensation of *o*-vanillin with 3-amino-1-propanol, only a five-core complex was obtained. The complex with the $\{\text{Cu}_6\text{Dy}_3\}$ fragment shows antiferromagnetic interactions with slow magnetic relaxation below 2 K (Fig. 1.6).

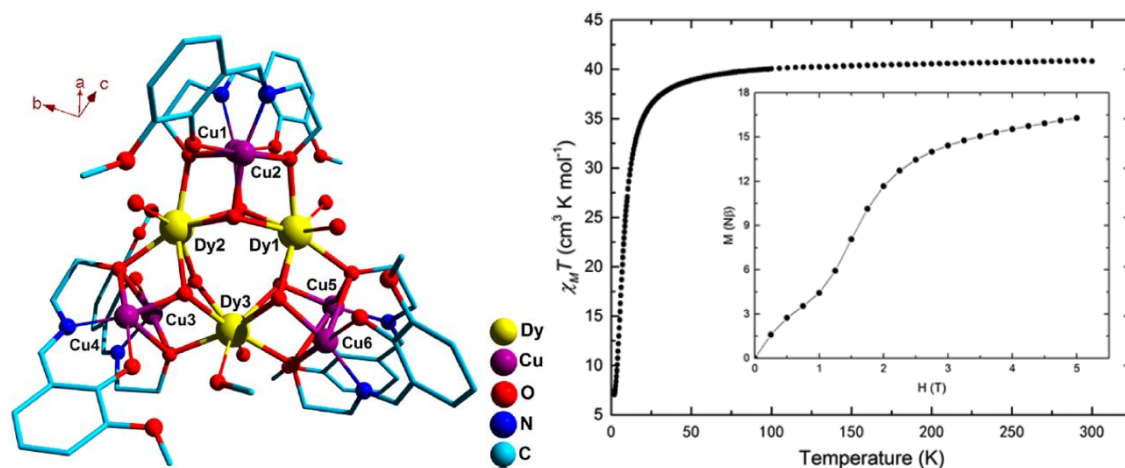


Figure 1.6. Crystal structure and dependence $\chi_m T$ vs T (magnetization at 1.82 K) of the complex $[\text{Cu}_6\text{Dy}_3(\text{L}^1)_6(\text{OH})_6(\text{H}_2\text{O})_5(\text{MeOH})]\text{NO}_3 \cdot \text{Br}_2 \cdot 4\text{H}_2\text{O} \cdot \text{MeOH}$ ³⁵.

Ligand H_2L^2 is the product of condensation of *o*-vanillin with 2-aminobenzyl alcohol and contains four donor sites (O_{meth} , OH_{ph} , N, OH_{alk}). H_2L^2 differs from H_2L^1 by the presence of a benzene ring between the N atom and the OH group (Fig. 1.7). This reduces the flexibility of the alcohol chain but allows additional π - π stacking interactions in the crystal packing of the complexes.

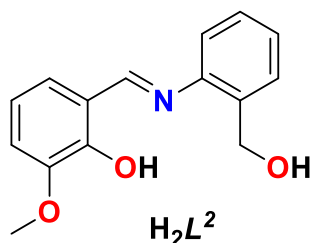


Figure 1.7. Structure of the ligand H_2L^2 .

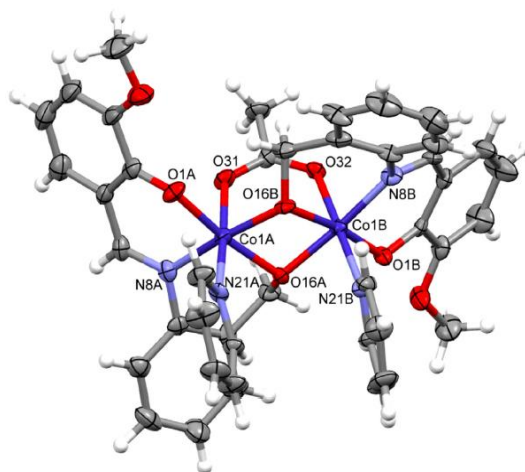
This ligand has been studied quite actively only over the past six years. The currently established coordination properties of H_2L^2 are presented in Table 1.2. Among the 30 known crystal structures, only one complex has a mononuclear structure $[\text{MoO}_2(\text{L}^2)(\text{dmsO})]$, in this compound the ligand displaying a chelating function²⁹. All other coordination compounds have a polynuclear crystal structure due to chelate-bridging properties of the ligand. The complexes show magnetic^{41–47}, biological⁴⁸ and luminescent⁴⁷ properties.

Table 1.2. Coordination modes of H_2L^2 .*

Coordination mode (donor sites: OH_{alk} , N , OH_{ph} , O_{meth})	Harris notation ¹³	Compounds
		$(HL^2)^-$
O, O', O', N, O'' – pentadentate bridging	[3.1 ₁ 2 ₁₂ 1 ₂ 1 ₂]	[Ni₂Ln₂(Ac)₃(HL²)₄(H₂O)₂](NO₃)₃, Ln=Dy, Tb, Ho, Lu ⁴¹; [NiLn(HL²)₂(NO₃)₃], Ln=Gd, Pr ^{41,42}; [M₂Ln(HL²)₄(NO₃)](NO₃)₂, M=Ni, Zn; Ln=La, Gd, Pr ⁴²
		$(L^2)^{2-}$
O, N, O' – tridentate chelating	[1.01111]	[MoO₂(L²)(dmsO)] ²⁹
O, N, O', O' – tetradentate bridging	[2.01 ₁ 2 ₁₂ 1 ₁]	[Co₂(L²)₂(py)₂(OAc)]PF ₆ , [Co₂(L²)₂(4-Mepy)₂(OAc)]PF ₆ ⁴⁸ ; [Co₂Ln (HL ²) ₄ (NO ₃)](NO ₃) ₂ ·CH ₃ OH·H ₂ O, Ln= Nd, Sm, Gd, Tb, Dy ⁴³ ; [Fe₈(μ-O)₄(L²)₈] ⁴⁴
O, N, O', O', O' – pentadentate bridging	[3.01 ₁ 3 ₁₂₃ 1 ₁]	[Ni₄L²₄(H₂O)₄]·4ACN ⁴⁵ ; [Cu₄(L²)₄]·4H ₂ O ⁴⁶ ; [Co₄L²₄(H₂O)₄]·4THF·4H ₂ O ⁴³
$O, O', O', N, O'', O'', O''$ – heptadentate bridging	[4.1 ₁ 2 ₁₂ 3 ₂₃₄ 1 ₂]	[M₇L²₆](NO ₃) ₂ ·nCH ₃ OH, M= Mn, Fe, Co, Cu, Zn ⁴⁷ ; [Cu₆Na₂L²₆](NO ₃) ₂ ·4CH ₃ OH ⁴⁷ ; [Co₇L²₆](NO ₃) ₂ ·2H ₂ O ⁴³ ;

* according to Cambridge Structural Database (CSD)

Binuclear complexes [**Co₂(L²)₂(py)₂(OAc)**]PF₆ and [**Co₂(L²)₂(4-Mepy)₂(OAc)**]PF₆ were prepared by the salt method using Co(OAc)₂·4H₂O ⁴⁸. Each Co(III) ion has distorted octahedral geometry within N₂O₄ coordination environment (Fig. 1.8). Electrochemical and antibacterial properties were investigated for these compounds.

**Figure 1.8.** Crystal structure of the complex [**Co₂(L²)₂(py)₂(OAc)**]PF₆ ⁴⁸.

Heterometallic complexes [**NiLn**(HL²)₂(NO₃)₃] and [**M₂Ln**(HL²)₄(NO₃)](NO₃)₂ (M = Ni, Zn; Ln = La, Gd, Pr) were obtained by the traditional salt method ⁴². The complexes have binuclear neutral and linear trinuclear cationic structures (Fig. 1.9). Magnetic measurements revealed that Ni(II) and Gd(III) ions are coupled ferromagnetically, while Ni(II) and Pr(III) ions are coupled

antiferromagnetically in the binuclear complexes. In order to confirm the nature of the interaction, these results were compared with the data for the trinuclear complexes.

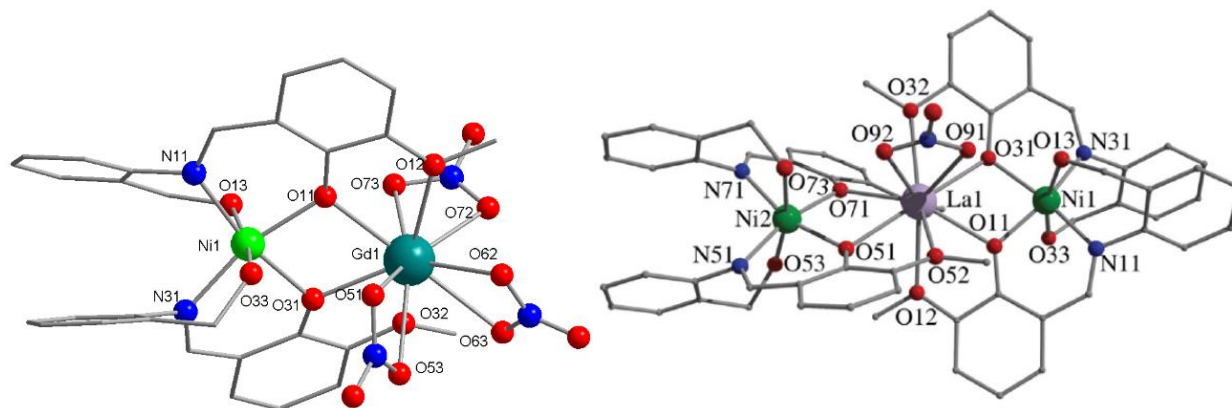


Figure 1.9. Crystal structures of $[\text{NiGd}(\text{HL}^2)_2(\text{NO}_3)_3]$ and $[\text{Ni}_2\text{La}(\text{HL}^2)_4(\text{NO}_3)]^{2+}$.⁴²

For the purpose of creating new magnetic materials⁴³, conditions for the synthesis of tri-, tetra- and heptanuclear complexes ($[\text{Co}_2\text{Ln}(\text{HL}^2)_4(\text{NO}_3)](\text{NO}_3)_2 \cdot \text{CH}_3\text{OH} \cdot \text{H}_2\text{O}$ ($\text{Ln} = \text{Nd}, \text{Sm}, \text{Gd}, \text{Tb}, \text{Dy}$), $[\text{Co}_4\text{L}^2_4(\text{H}_2\text{O})_4] \cdot 4\text{THF} \cdot 4\text{H}_2\text{O}$, $[\text{Co}_7\text{L}^2_6](\text{NO}_3)_2 \cdot 2\text{H}_2\text{O}$) were investigated (Fig. 1.10). Six of the obtained complexes show SMM behavior. The contribution of the Ln^{III} ions to the magnetic behavior in the series of heterometallic $\text{Co}^{\text{II}}-\text{Ln}^{\text{III}}$ complexes has been illustrated.

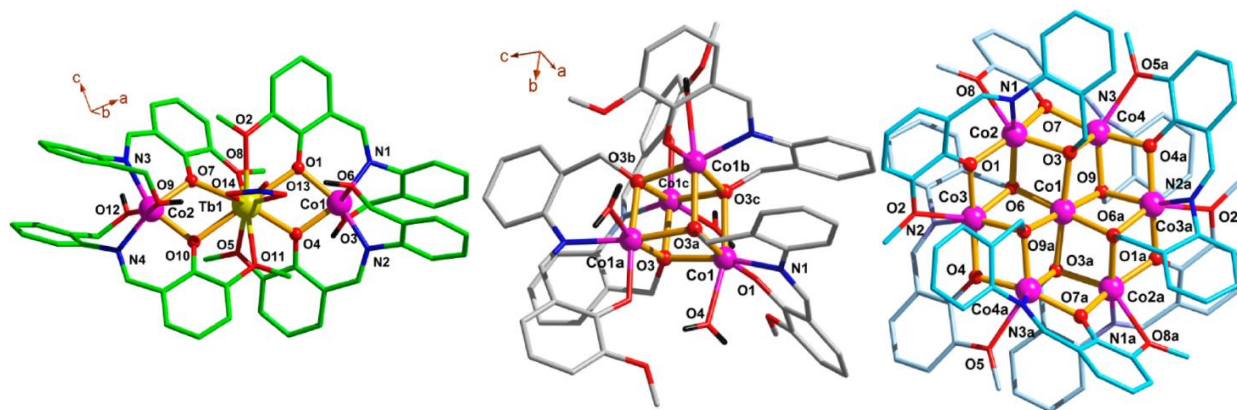


Figure 1.10. Crystal structures of $[\text{Co}_2\text{Tb}(\text{HL}^2)_4(\text{NO}_3)]^{2+}$ (left), $[\text{Co}_4\text{L}^2_4(\text{H}_2\text{O})_4]$ (in the middle) and $[\text{Co}_7\text{L}^2_6]^{2+}$ (right).⁴³

The polynuclear complexes $[\text{M}_7\text{L}^2_6](\text{NO}_3)_2 \cdot 2\text{CH}_3\text{OH}$ ($\text{M} = \text{Mn}, \text{Fe}, \text{Co}, \text{Cu}, \text{Zn}$) were synthesized by the solvothermal method⁴⁷. All complexes are isomorphous and consist of disk-shaped $\{\text{M}^{\text{II}}_7\}$ cores (Fig. 1.11). This is the first time that five isostructural complexes consisting of a heptanuclear fragment have been obtained with the same SB. The crystal structure of $[\text{Fe}_7\text{L}^2_6](\text{NO}_3)_2 \cdot 2\text{CH}_3\text{OH}$ is an extremely rare sample in coordination chemistry of iron (II) of disk-shaped heptanuclear cluster. Magnetic studies have established ferromagnetic interactions in the

Mn^{II}, Fe^{II}, Co^{II} complexes and antiferromagnetic interactions in the Cu^{II} complex. The complex [Co₇L²₆](NO₃)₂·2CH₃OH exhibits SMM behavior. In the solid state the compound [Zn₇L²₆](NO₃)₂·2CH₃OH has luminescent properties with emission maximum at 497 nm when excited at 430 nm.

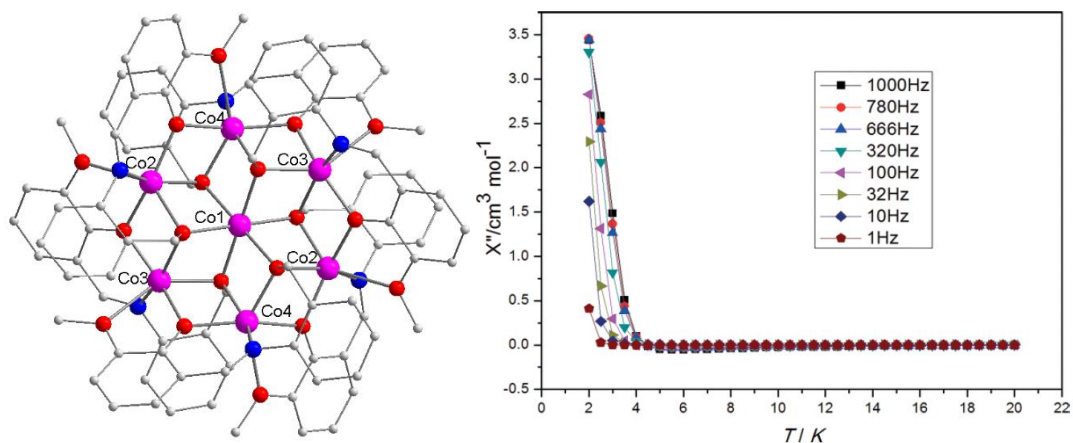


Figure 1.11. Crystal structure of [Co₇L²₆]²⁺ and frequency dependence of the out-of-phase (χ'') ac susceptibility under an applied zero Oe field for [Co₇L²₆](NO₃)₂·2CH₃OH⁴⁷.

The ligand HL³, which is a condensation product of *o*-vanillin and ammonia, contains only three donor centers (O_{met}, OH_{ph}, N), but their specific location around metal ions makes possible to use as both asymmetrical and pseudo-symmetrical ligand. The coordination of two HL³ molecules simulates the structure of a symmetrical Salen-type ligand with the advantage that the connecting element (carbon chain) between the benzene rings is absent. This significantly weakens the steric obstacles for the coordination of metal ions with different radii (Fig. 1.12).

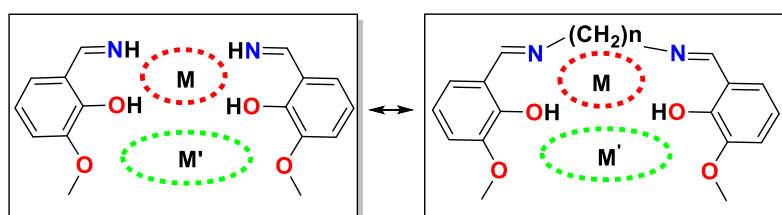


Figure 1.12. Schiff base coordination scheme: asymmetrical HL³ (left) and Salen-type (right).

The ligand HL³ is coordinated only in its deprotonated form and exhibits two coordination modes (bidentate-chelating and tetradentate-bridging) (Table 1.3). Only seven crystal structures of complexes with this ligand are known. Complexes with HL³ reveal magnetic properties^{49–53}, antibacterial and antifungal activity⁵⁴.

Table 1.3. Coordination modes of HL^3 .*

Coordination mode (donor sites: $OH_{alk}, N, OH_{ph}, O_{meth}$)	Harris notation ¹³	Compounds
	$(L^3)^-$	
O, N – bidentate chelating	[1.011]	$[Ni(L^3)_2] \cdot 2H_2O$ ⁴⁹ ; $[Cu(L^3)_2] \cdot H_2O$ ⁵⁴ ; $[Ni_4(L^3)_4(OMe)_4(MeOH)_4] \cdot 2H_2O$ ⁵⁰
O, O', O', N – tetradentate bridging	[2.112 ₁₂ 1 ₂]	$[Ni(L^3)_2Na(ClO_4)(H_2O)]$ ⁴⁹ ; $[Cu(CH_3OH)(L^3)_2Gd(NO_3)_3]$ ⁵¹ ; $[Ni_7(L^3)_6(OMe)_6](ClO_4)_2$ ⁵² ; $[Co_7(L^3)_6(OMe)_6](ClO_4)_2$ ⁵³

* according to Cambridge Structural Database (CSD)

In the study of antibacterial and antifungal activity it was found that the *o*-vanillin based SB complexes are more active than their salicylic analogs⁵⁴.

The tetranuclear complex $[Ni_4(L^3)_4(OMe)_4(MeOH)_4] \cdot 2H_2O$ was synthesized by S. T. Meally and coworkers⁵⁰. The influence of the reaction conditions on the structure and magnetic properties was investigated.

Heptanuclear complexes $[Ni_7(L^3)_6(OMe)_6](ClO_4)_2$ ⁵² and $[Co_7(L^3)_6(OMe)_6](ClO_4)_2$ ⁵³ were obtained by the solvothermal method. The $\{Ni_7\}$ and $\{Co_7\}$ clusters have similar structures to the complexes with the ligand H_2L^2 described above (Fig. 1.11). Magnetic studies indicate the existence of ferromagnetic interaction between divalent metal ions.

The synthesis of complexes $[Ni(L^3)_2Na(ClO_4)(H_2O)]$ ⁴⁹ and $[Cu(CH_3OH)(L^3)_2Ln(NO_3)_3]$ ($Ln = Gd, Yb, Eu, Pr$)⁵¹ was reported by J.-P. Costes. Heterometallic complexes were obtained by reaction of mononuclear copper or nickel complexes with the corresponding metal salts. The complexes have binuclear structures (Fig. 1.13) showing diamagnetic (Ni/Na) and ferromagnetic (Cu/Gd) properties.

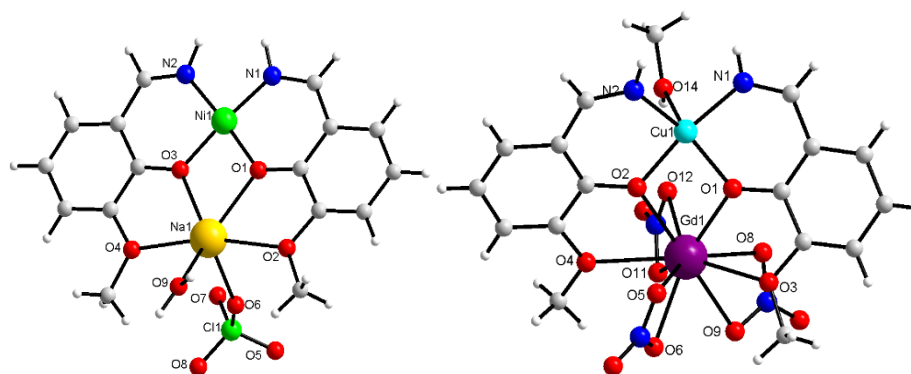


Figure 1.13. Molecular structures of $[Ni(L^3)_2Na(ClO_4)(H_2O)]$ (left) and $[Cu(CH_3OH)(L^3)_2Gd(NO_3)_3]$ (right)^{49,51}.

Thus, summarizing the results of the literature data, it is possible to highlight some features of the coordination behavior of H_2L^1 , H_2L^2 and HL^3 :

- The oxygen atom of the methoxy group ($-OCH_3$) either forms a single coordination bond providing chelates or does not participate in coordination at all. No examples with a bridging function of the methoxy group have been reported.
- The oxygen atom of the phenolic group ($-OH_{ph}$) is always involved in coordination in the deprotonated form. The oxygen atom is involved in a chelate mode of coordination or can exhibit μ_2 - or μ_3 -bridging functions.
- The nitrogen atom of the imino group is more often involved in chelating modes of coordination with other donor atoms. There are no examples of bridging coordination.
- The greatest variability is shown by the hydroxyl group of the alcohol arm ($-OH_{alk}$). The probability that it will be coordinated or uncoordinated, protonated or deprotonated is the same. The oxygen atom may exhibit μ_2 - or μ_3 -bridging functions.
- Coordination of neutral ligands is not typical, except in some cases where the ligands are coordinated in zwitterionic forms.

1.3. Heterometallic *d-s* coordination compounds

It is known that heterometallic coordination compounds can exhibit properties different from the properties of similar monometallic compounds. Therefore, to strengthen the corresponding properties of the coordination compound, it is vital to choose the right combination of metal centers. Most currently investigated heterometallic complexes contain combinations of *d-d'* or *d-f* elements, which is associated with the study of exchange interactions between paramagnetic centers and the prospects of their use as new magnetic materials. However, in recent years there has been a growing interest in the study of heterometallic complexes involving *s*-metals. Until recently, studies of the coordination properties of *s*-metals were mostly as individual reports, and the first systematic review of such coordination compounds appeared only in 2008 and can be considered the beginning of systematic research in this direction^{55,56}. Coordination properties ions of *s*-metals, in contrast to *d*-metals, are characterized by the following features: a) absence of rigid coordination geometry, b) ion-covalent nature of the chemical bond, c) non-toxicity, except for heavy *s*-elements, d) biological role as macronutrients (Na, K, Mg, Ca). In addition, most alkali and alkaline earth metal compounds are commercially available. Typically,

s-metal complexes are readily soluble in water and are often used to make pharmaceuticals. The *s*-metal complexes are convenient models for studying similar but more expensive lanthanide complexes, due to the similarity of radius sizes, coordination and chemical properties. Moreover, the inclusion of diamagnetic ions of *s*-metals in molecular structures with magnetic properties can deepen the understanding of the nature of magnetism arising in these structures.

Among known heterometallic *d-s* coordination compounds, complexes containing Mn/Ca pair are the most actively studied today. This is due to the discovery of the presence of a cluster fragment $\text{Mn}_4\text{O}_5\text{Ca}$ in plant cells and its fundamental role in the process of photosynthesis (Fig. 1.14)^{57,58}. According to X-ray diffraction analysis, the active center ($\text{Mn}_4\text{O}_5\text{Ca}$ cofactor) of Photosystem II is cube-shaped, containing three manganese atoms and one calcium atom bound by four oxygen atoms. One manganese atom is in a distant outer position^{57,59,60}. Cluster cofactor effectively catalyzes the oxidation of water to oxygen with TON (turnover frequency is ratio of moles of product to number of moles of catalyst) 106 and TOF (turnover number is rate of conversion of substrate into product) $\approx 500 \text{ s}^{-1}$. The proposed mechanisms of water oxidation, which take place during photosynthesis, indicate that the calcium atom is involved in the catalytic process⁶¹.

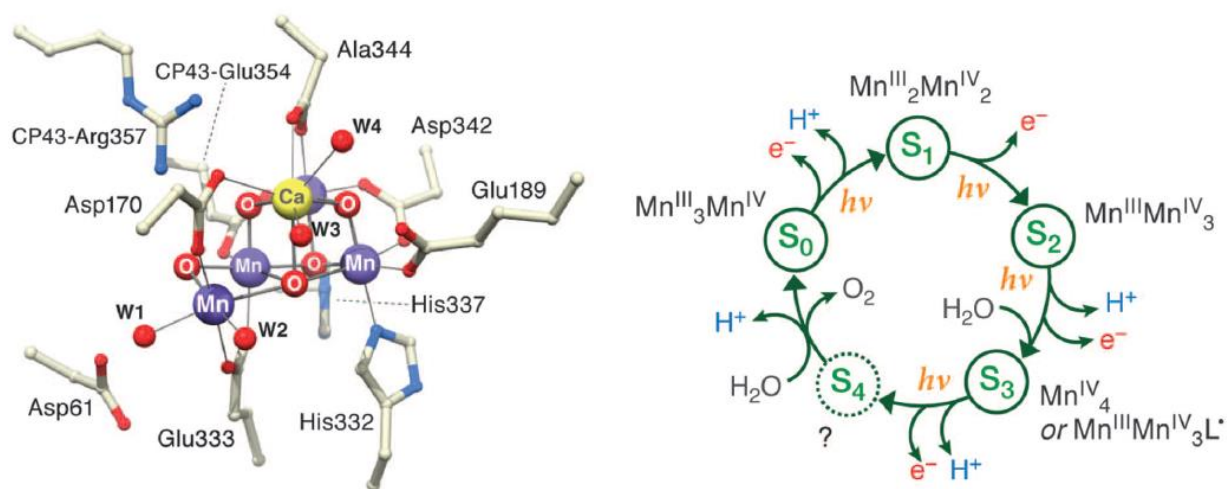


Figure 1.14. Crystal structure of the cofactor $\text{Mn}_4\text{O}_5\text{Ca}$ (left) and the proposed mechanism of water oxidation (right)⁵⁸.

Modeling of Mn/Ca cofactor has led to sudden increase in the number of scientific papers on the synthesis of such structures and the study of the mechanism of one of the most important catalytic reactions occurring in nature^{61–63}. However, many aspects of the photocatalytic reaction remain unclear: the detailed mechanism of the reaction, the nature of structural changes during the reaction, and perhaps one of the important issues is the specific role of calcium, as calcium ion is not active in redox reactions, but its presence is necessary both for the photo-assembly of the cluster and for the manifestation of its catalytic properties. A number of studies have shown the

importance of the presence of calcium, as attempts to replace calcium with other metals have not led to the desired results⁶⁴. Only the replacement of calcium with strontium, which has relatively similar size and alkalinity, in the cluster fragment also catalyzes the decomposition of water, but the rate of reaction is much lower⁶². Therefore, it is assumed that the calcium atom to some extent stabilizes the high valence states of manganese.

In the work of Y. Park⁶⁵ the effect of redox-inactive metal ions (Ca and Ba) on the facilitation of dioxygen activation has been studied, which in turn can increase the reactivity of heterometallic transition metal complexes.

Isolated octa-core complexes $[\text{Mn}_6\text{M}_2\text{O}_9(\text{L}^4)_{10}(\text{HL}^4)_5]$ ($\text{M} = \text{Ca}, \text{Sr}; \text{HL}^4 = 4\text{-tBuC}_6\text{H}_4\text{COOH}$)⁶⁶ contain a cluster $\{\text{Mn}^{\text{IV}}_6\}$ having the structure of a flat ring. The atoms of which are connected by bridged oxygens and two alkaline earth metal ions are located outside the plane of this ring. Magnetochemical studies demonstrate antiferromagnetic interaction in these complexes (Fig. 1.15). The effect of diamagnetic Ca^{2+} and Sr^{2+} ions on the magnetic behavior of the complexes was confirmed by quantum chemical calculations and was correlated with their polarizing action⁶⁶.

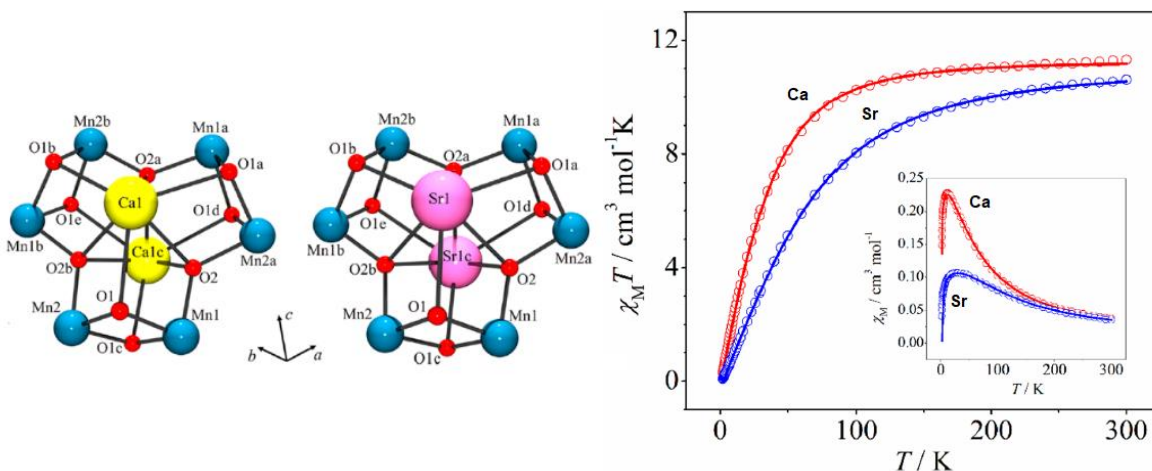


Figure 1.15. Crystal structure of $[\text{Mn}^{\text{IV}}_6\text{Ca}_2\text{O}_9]^{10+}$ (left) i $[\text{Mn}^{\text{IV}}_6\text{Sr}_2\text{O}_9]^{10+}$ fragments (right) and temperature dependences $\chi_M T(T)$ and $\chi_M(T)$ for their complexes⁶⁶.

Another pair of metals that attracts attention is the combination of *s*-metals with a copper atom. The choice of Cu is due to the specific redox properties and "plasticity" of copper complexes. That is the centers of Cu(II) form a wide range of coordination polyhedra – from a flat square (D_{4h}) to an almost perfect octahedron (O_h) with relatively small changes in the thermodynamic stability. The combination of these factors causes a number of unique physicochemical and biological processes involving copper complexes. Like *s*-metals, copper plays an important biological role, which makes this pair more attractive for the research.

At the beginning of this thesis, about 300 reports were found with crystal structures of complexes containing Cu/M (M = Ca, Sr, Ba). In most cases, such complexes have a polymeric or ionic structure (copper ion is part of the anion and the M^{2+} ion acts as a cation). The number of complexes consisting of a heterometallic cation, the inner sphere of which includes both M^{2+} and Cu^{2+} , and a simple extrasphere anion is much smaller. The obtained complexes are used for modeling and development of antitumor drugs⁶⁷, can be used in catalysis⁶⁸⁻⁷⁰, exhibit magnetic^{71,72}, sorption⁷³, luminescent^{74,75} properties and biological activity^{70,76}. Heterometallic Cu-Ca/Sr/Ba complexes with SB ligands were synthesized by the salt method⁷⁷⁻⁸⁰ or by the "building block method"^{72,81-85}. The majority of the complexes are formed with the participation of Salen type SBs.

1.4. Coordination compounds with ligands based on 2,1,3-benzothiadiazole

2,1,3-Benzothiadiazole (BTD) belongs to the class of the heterocyclic aromatic compounds containing a benzene ring fused to a thiadiazole ring. BTD system has pronounced electron-withdrawing capacity and luminescent efficiency (Fig. 1.16). BTD is widely used as "building block" in organic electronics for the synthesis of organic light-emitting diodes (OLEDs), dyes, solar cells, liquid crystals, organic conductors, working elements in photovoltaic cells, fluorescent probes and polymer thermometers⁸⁶. BTD derivatives often form well-organized structures due to π - π interactions and non-covalent bonds between heteroatoms.

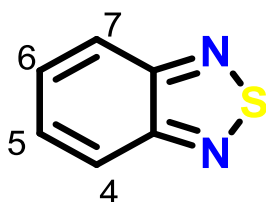


Figure 1.16. 2,1,3-Benzothiadiazole (BTD) moiety.

Coordination chemistry of the unsubstituted BTD is limited to individual reports, which are devoted mainly to the study of synthesis and crystal structure of complexes with Co, Ni, Cu, Ag, Ga, Ru, Ir⁸⁷⁻⁹⁴.

Interesting examples are the dimeric $[Cu_2(OAc)_4(BTD)_2]$ and polymeric $\{[Cu_6(OAc)_8(OCH_3)_4(BTD)_2]\}_n$ complexes with BTD. Their formation depends on the reaction conditions, namely, the ratio of starting materials and the use of solvents of different nature. Both complexes were obtained by the salt method. For the polymeric complex, an alternative method of synthesis using the copper dimer complex has been additionally developed⁹². X-ray

crystallographic analysis revealed that BTD behaves as monodentate ligand in the $[\text{Cu}_2(\text{OAc})_4(\text{BTD})_2]$ complex and as bidentate bridging ligand in the polymer complex (Fig. 1.17). In the 2D coordination polymer, antiferromagnetic exchange interactions were observed between the copper (II) ions.

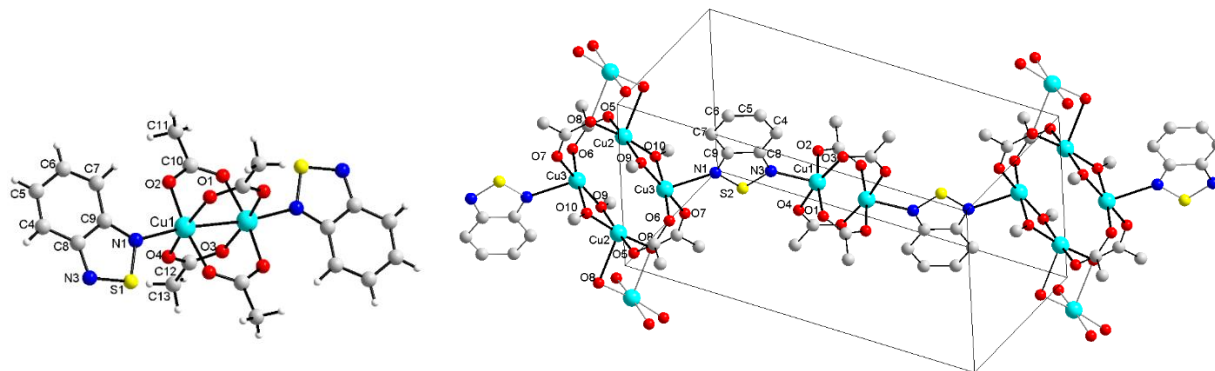


Figure 1.17. Crystal structure of the complex $[\text{Cu}_2(\text{OAc})_4(\text{BTD})_2]$ (left) and $\{[\text{Cu}_6(\text{OAc})_8(\text{OCH}_3)_4(\text{BTD})_2]\}_n$ (right)⁹².

The coordination properties of BTD derived ligands have only been actively studied in the last 10 years. The six main types of BTD-ligands can be distinguished by the number and position of substituents on the fused benzene ring (Fig. 1.18).

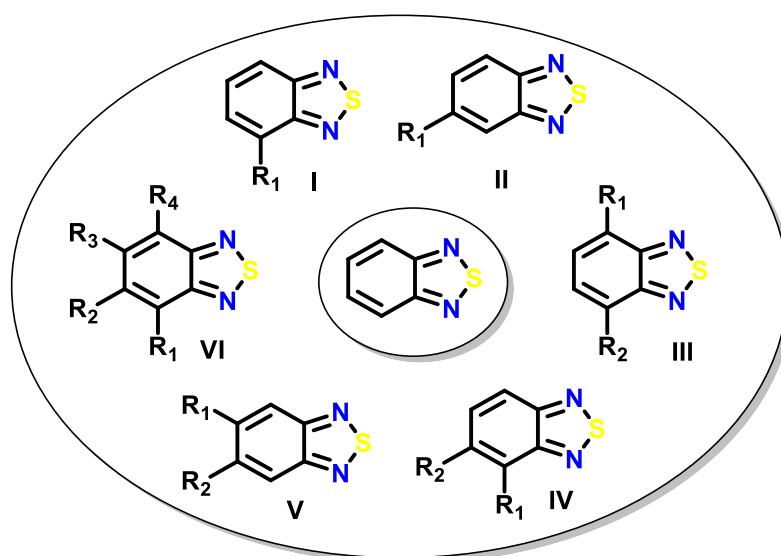


Figure 1.18. Types of BTD ligands.

The ligands of type **I**, where BTD is monosubstituted in the fourth position (Fig. 1.16) are the most studied. Involvement of a labile substituent with a given number and arrangement of donor atoms makes possible to increase the coordination potential of the ligand due to the additional chelating function. The simplest representatives of type **I** ligands are the *N*-donor ligand L^5 (4-amino-BTD) and the *O,N*-donor ligand HL^6 (4-hydroxy-BTD).

For L^5 complexes with copper, zinc, silver and iridium were obtained. In these complexes the following types of coordination are observed: (a) N^1 -monodentate, the ligand is coordinated through the N^1 atom of the BTD ring (for example, $[\text{Cu}_2(L^5)_2(\text{CH}_3\text{CN})_4](\text{PF}_6)_2$, $[\text{Ir}(L^5)_2\text{Cp}^*\text{Cl}_2]$, $[\text{Cd}(L^5)_2(\text{H}_2\text{O})_2(\text{NO}_3)_2]$, $[\text{Cd}L^5\text{Cl}_2]_n$, $[\text{Cd}(L^5)_2\text{Hal}_2]_n$ (Hal = Cl, Br)); (b) N^4 -monodentate, coordination occurs through the N^4 atom of the amino group (for example, $[\text{Zn}(L^5)_2\text{Cl}_2]$ and $[\text{Zn}L^5(\text{H}_2\text{O})\text{Cl}_2]$); (c) N,N -bidentate-bridging, the ligand performs a bridge function through atoms N^1 and N^4 (for example, $[\text{Cd}L^5\text{Cl}_2]_n$, $[\text{Ag}L^5(\text{NO}_3)]_n$, $[\text{Ag}(L^5)_2(\text{NO}_3)]_n$) (Fig. 1.19)^{93,95-99}. In the complex $[\text{Ag}(L^5)_3(\text{NO}_3)]_2$ all three types of coordination (a-c) occur simultaneously⁹⁷.

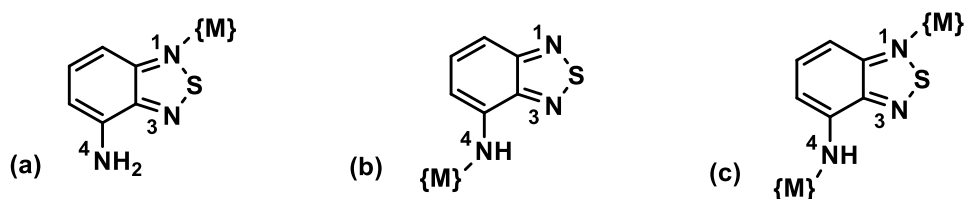


Figure 1.19. Known coordination modes of L^5 ¹⁰⁰.

In the work of S.N. Konchenko and coworkers⁹⁸ quantum chemical calculations were performed on the model complexes $[\text{M}(L^5)\text{Cl}_n]$ ($\text{M} = \text{Zn}, \text{Cd}, n = 2$; $\text{M} = \text{Cu}, \text{Ag}, n = 1$) in order to determine the most efficient mode of coordination. Coordination of type (a) was found to be more thermodynamically advantageous than type (b). However, it should be noted that the values of the Gibbs free energy in both cases are quite similar and reach the maximum of about $30 \text{ kJ}\cdot\text{mol}^{-1}$. Thus, it can be assumed that intermolecular interactions play a crucial role.

In the solid state, Zn ⁹⁶, Ag ⁹⁷, Cd ⁹⁵ complexes with L^5 have luminescent properties with a slight shift of the bands depending on the nature of the metal and the type of coordination of the ligand¹⁰⁰.

Replacement of the amino group in L^5 with a hydroxyl group in HL^6 allowed to obtain a series of multi-ligand polynuclear complexes of lanthanides $[\text{Ln}_4(\text{dbm})_6(L^6)_4(\text{OH})_2]$ and $[\text{Ln}_4(\text{dbm})_4(L^6)_6(\text{OH})_2]$, where dbm = dibenzoylmethane and Ln = Er, Yb, Dy¹⁰¹⁻¹⁰³. These complexes have been synthesized using LnCl_3 salts or $[\text{Ln}_5(\text{dbm})_{10}(\text{OH})_5]$ complexes as precursors. The HL^6 ligand is coordinated in deprotonated form, having both chelating (via O - and N -donor atoms) and bridging (via μ - O atom) functions. In all complexes, the cluster fragment $\{\text{Ln}_4(\mu\text{-OH})_2\}$ has the same structure (Fig. 1.20). The obtained coordination compounds have luminescent properties in dichloromethane solution. The deprotonated ligand exhibits an "antenna effect" for the emission of lanthanide ions in the near infrared region. Magnetochemical studies have shown that, depending on the nature of the Ln (III) ion, the complexes show different temperature dependences of the effective magnetic moment in the range 80–300 K. After

decreasing the temperature, complexes with Dy show weak ferromagnetic interactions, whereas weak antiferromagnetic interactions have been observed for both types of complexes with Yb and Er.

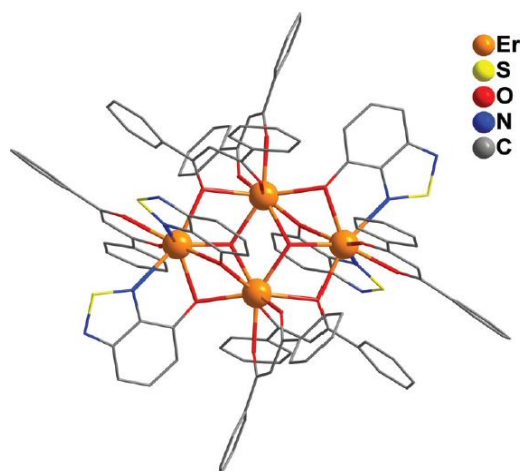


Figure 1.20. Crystal structure of $[\text{Er}_4(\text{dbm})_6(\text{L}^6)_4(\text{OH})_2]^{102}$.

Additional representatives of type I are ligands L^7 and L^8 , which were obtained by the condensation of L^5 with the corresponding ketones (Fig. 1.21)^{99,104,105}.

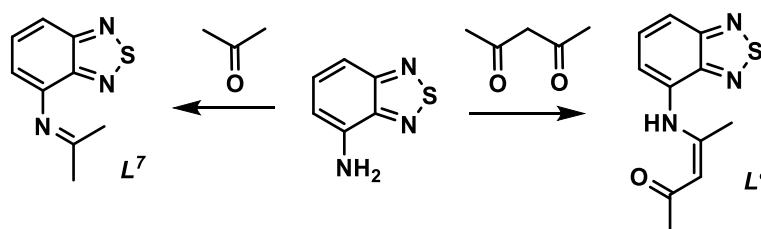


Figure 1.21. Scheme of formation of the ligands L^7 and L^8 .

For L^7 , the complexes $[\text{Cu}_2(\text{L}^7)_2(\text{CH}_3\text{CN})_4](\text{PF}_6)_2$ and $[\text{Cu}_2(\text{L}^7)_2](\text{ClO}_4)_2$ ⁹⁹ were obtained, in which two types of N,N' -bidentate-bridging function of the ligand involve one substituent nitrogen atom and one of the two nitrogen atoms of the thiaziazole ring (Fig. 1.22).

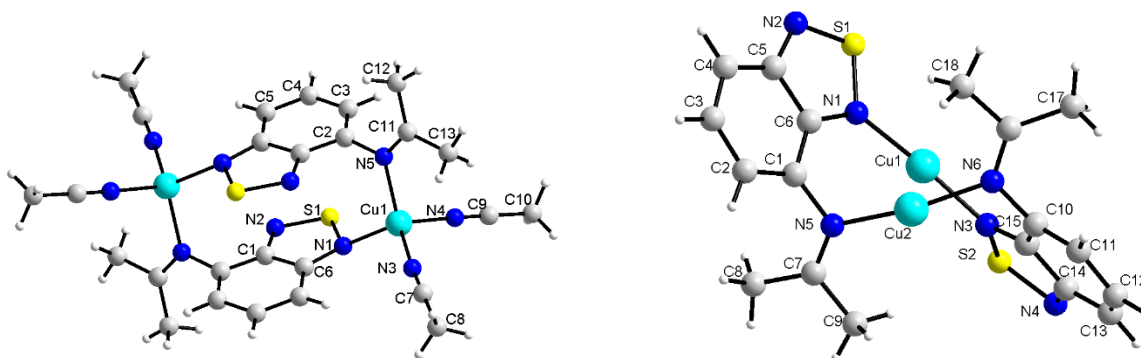


Figure 1.22. Crystal structure of $[\text{Cu}_2(\text{L}^7)_2(\text{CH}_3\text{CN})_4](\text{PF}_6)_2$ (left) and $[\text{Cu}_2(\text{L}^7)_2](\text{ClO}_4)_2$ (right)⁹⁹ (anions are omitted for clarity).

Ligand L^8 has been used to obtain complexes $[\text{Zn}(L^8)_2]$ and $[\text{Ln}(L^8)_3]$, $\text{Ln} = \text{Eu}, \text{Sm}, \text{Gd}$ ^{104,105}. Various types of its coordination have been determined: N,O -binuclear chelate type in the complexes with zinc and N,N,O -tridentate chelate type in the lanthanide complexes (Fig. 1.23). In the solid state, the obtained compounds demonstrate luminescent properties with $\lambda_{\text{max}} = 530 \text{ nm}$ for the zinc complex and $\lambda_{\text{max}} = 625 \text{ nm}$ for the samarium complex ($\lambda_{\text{max}} = 593 \text{ nm}$ for the free ligand). Studying the solution of $[\text{Zn}(L^8)_2]$ in dichloromethane, luminescence quenching is observed.

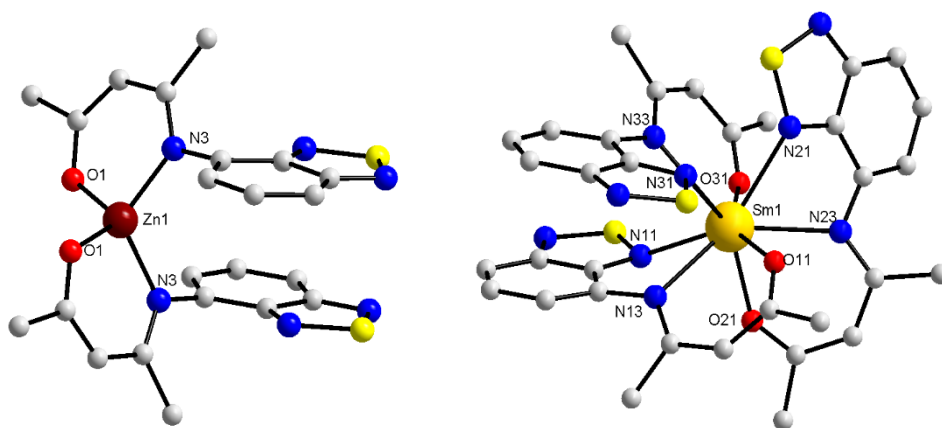


Figure 1.23. The crystal structure of $[\text{Zn}(L^8)_2]$ (left) and $[\text{Sm}(L^8)_3]$ (right)^{104,105}.

BTD-derived ligands of type **II** consist of monosubstituted derivatives in the fifth position of the benzene ring (Fig. 1.16). An example is the ligand $L^9 = 5$ -(3-thiophene)-2,1,3-benzothiadiazole used for the synthesis of the complex $[\text{Ru}(\text{C}_2\text{H}_2\text{R})\text{Cl}(\text{CO})(L^9)(\text{PPh}_3)_2]$ ¹⁰⁶. The coordination mode of the ligand L^9 is monodentate due to one nitrogen atom of the BTD ring (Fig. 1.24). The obtained ruthenium complex is promising for the development of highly sensitive and selective probes for CO.

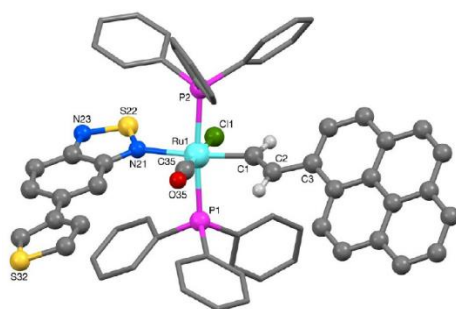


Figure 1.24. The crystal structure of $[\text{Ru}(\text{C}_2\text{H}_2\text{R})\text{Cl}(\text{CO})(L^9)(\text{PPh}_3)_2]$ ¹⁰⁶.

BTD ligands of **III-V** types belong to disubstituted derivatives (Fig. 1.18).

Type **III** ligands are used for the synthesis of metal-organic frameworks (MOFs)^{107–109}, metal-organic compounds^{110–112} and coordination polymers¹¹³. As an example of MOFs compounds based on type **III** BTD-ligand one can cite the cadmium complex with $H_2L^{10} = 4,7$ -dicarboxylic acid-2,1,3-benzothiadiazole (analogue of terephthalic acid), which has been obtained as two porous isomers (MOFs structure $\{[S@Cd_6L^{10}_6]H_2O\}_n\}$)¹⁰⁷. Both isomers have 3D-porous lattices that differ in structure. The complexes demonstrate luminescent properties both in solid state and in solution, with two luminescence maxima present in the spectra. Only one peak of luminescence was recorded for the ligand in solution. The study of solvatochromic behavior revealed that with increasing polarity of the solvent or acidity of the medium there is a bathochromic shift of the luminescence maximum (Fig. 1.25).

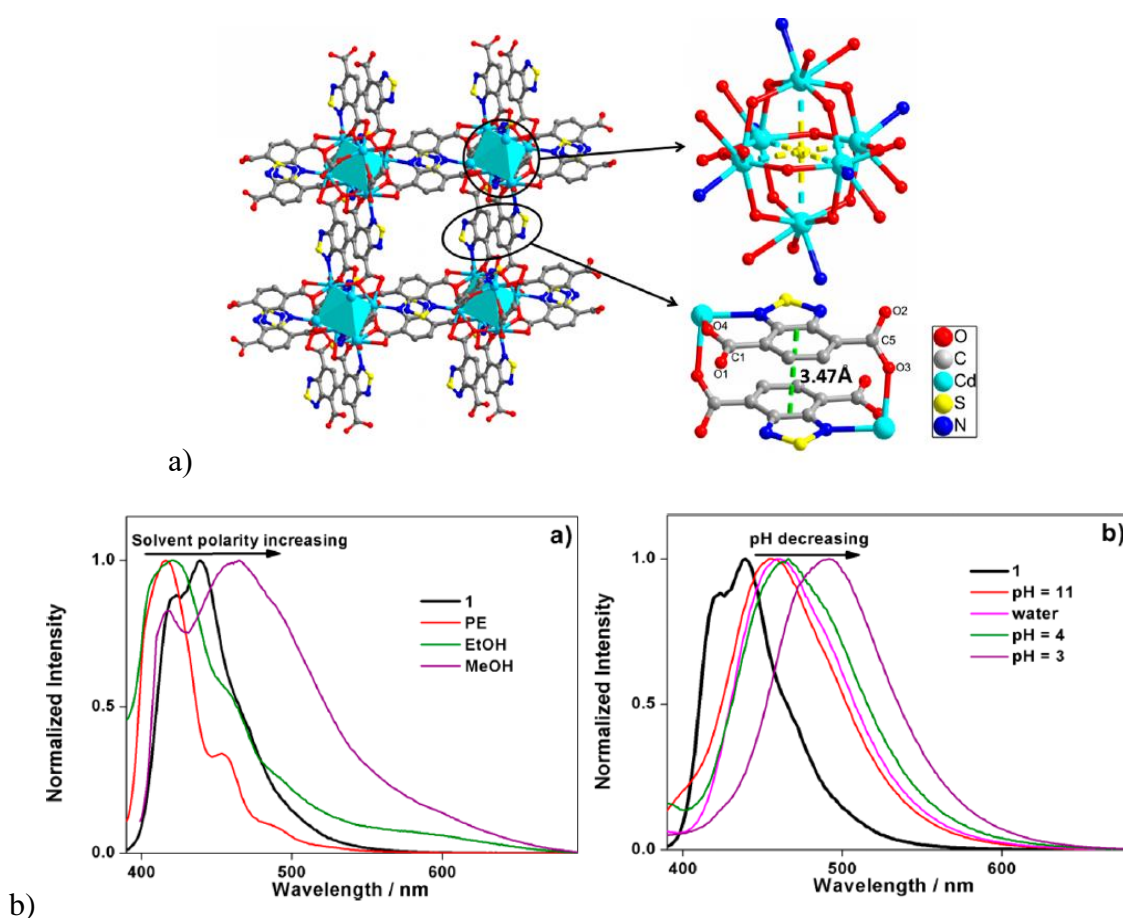


Figure 1.25. Complex $\{[S@Cd_6L^{10}_6]H_2O\}_n$: a) crystal structure, b) solvatochromic behavior¹⁰⁷.

Other examples of metal-organic compounds with a type **III** ligand are the palladium complexes in Fig. 1.26.¹¹¹ These complexes have fluorescent properties in solution at room temperature and show two emission bands. The peak located in the high energy range (~ 300 nm) refers to the emission of the ligand, and the peak (~ 500 nm) shifted in the low energy range is caused by the emission of the complex. The complexes show a solvatochromic effect.

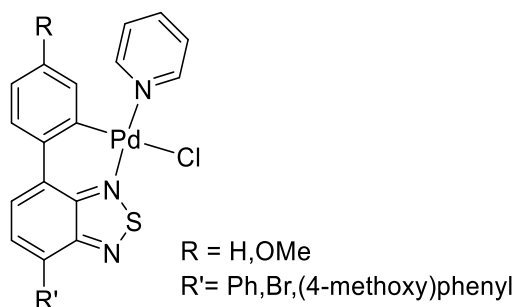


Figure 1.26. Structure of Pd metal-organic complexes with type **III** ligands¹¹¹.

A characteristic feature of BTD ligands of **IV-VI** types is the absence of participation in the coordination of donor atoms of 2,1,3-benzothiadiazole ring. This fragment is introduced into the coordination compound only to form or enhance the desired functional properties.

Thus, two multi-ligand complexes of ruthenium (Fig. 1.27) were obtained with the type **IV** ligand, which exhibit luminescent properties, and their interaction with DNA was studied¹¹⁴.

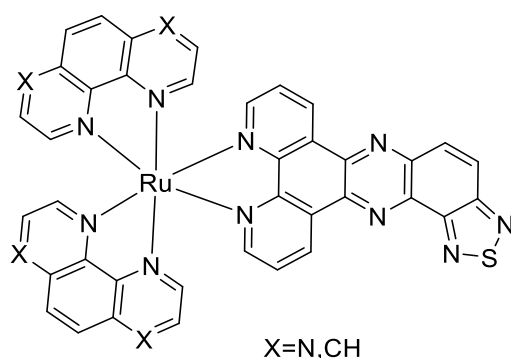


Figure 1.27. Structure of Ru complexes with type **IV** BTD-ligand¹¹⁴.

BTD-ligands of type **V** include a symmetrical SB H_2L^{11} , with which a zinc complex ZnL^{11} , exhibiting mechanochromic luminescent properties, has been obtained (Fig. 1.28)¹¹⁵. Thus, during mechanical grinding of the complex there is a change in luminescence from yellow ($\lambda_{\text{max}} = 545$ nm) to red ($\lambda_{\text{max}} = 645$ nm). This change is reversible and when the complex is treated with vapors of the corresponding solvent, a change in emission is observed. Applying of mechanical energy changes the morphology from crystalline to amorphous, destroying the lattice, which in turn affects the change in luminescent properties. After heat treatment the compound shows a maximum emission at 575 nm. The complex also exhibits the ability to form organic fluorescent gels.

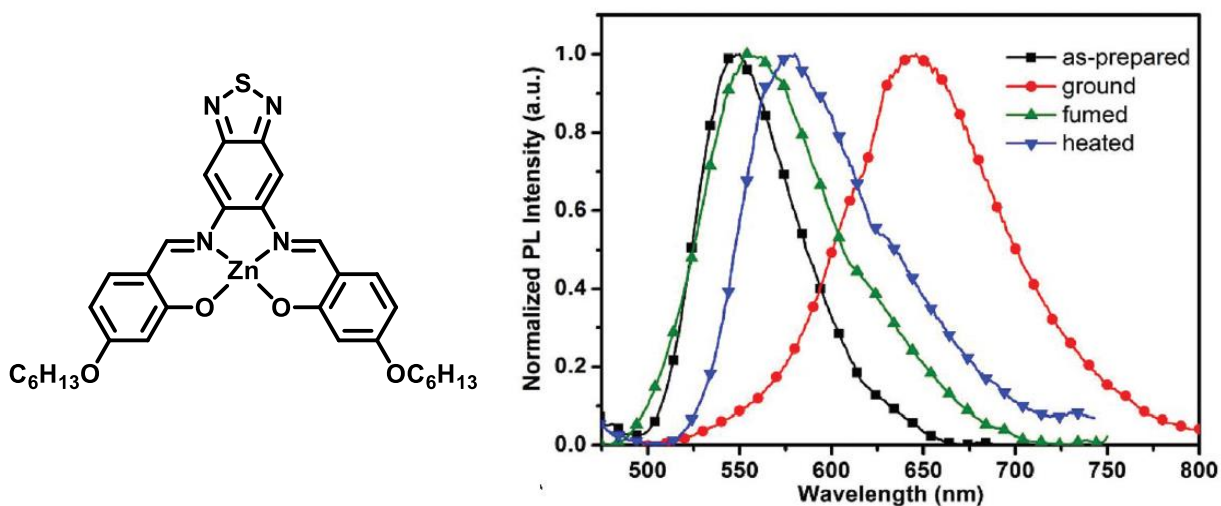


Figure 1.28. Structure of the ZnL^{11} complex and emission spectra (for the initial complex, after grinding into powder, after exposure to CH_2Cl_2 vapors and after keeping at $125^\circ C$)¹¹⁵.

Type VI includes ligand L^{12} , which is an analogue of 1,10-phenanthroline. Coordination in complexes with L^{12} occurs through nitrogen atoms from the phenanthroline moiety^{116,117}. The structure of the complex $[Fe(L^{12})_2(NCS)_2]$ is shown in Figure 1.29. This complex has a 3D crystal structure with $S \cdots S$ contacts between thiadiazole rings and thiocyanate groups. For the complex $[Fe(L^{12})_2(NCS)_2]$ the phenomenon of spin-crossover between high-spin and low-spin state above room temperature without hysteresis is observed¹¹⁶.

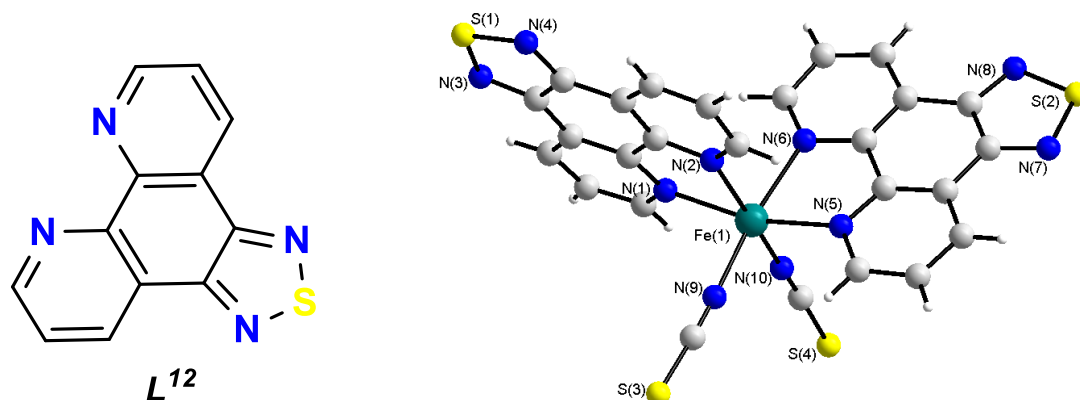


Figure 1.29. Structure of the ligand L^{12} (left) and the complex $[Fe(L^{12})_2(NCS)_2]$ (right)¹¹⁶.

Analyzing the literature, we can retrieve the main task of modern coordination chemistry, as design and synthesis of functional materials of given structure and properties. This task can be performed by establishing correlations between the structure and properties of compounds. Since complexation reactions are sensitive to both interacting substances and reaction conditions, the formation of target coordination compounds can potentially be controlled by selecting or changing

one of the factors, the nature of the central atom(s), the structure of the ligands, or the synthesis conditions.

Considering the results from the literature reviews, the coordination compounds based on *3d*-metals with *N*- or *N,O*-donor polydentate ligands have been selected as objects of the study. The use of polydentate Schiff bases as ligands is due to the relative ease of their design, synthesis and modification, predictable coordination behavior, as well as a number of functional properties.

Synthesis of new ligands derived from 2,1,3-benzothiadiazole has been going on for the last decade. The obtained results, namely a number of complexes with electro- and photophysical properties, give reason to consider them as one of the most promising types of functional ligands.

Coordination chemistry of *s*-metals is a relatively new branch of coordination chemistry, which is still in its infancy. Synthesis and study of both monometallic and heterometallic compounds of *s*-metals are of great importance, not only practical but also theoretical.

References

1. Vigato, P. A.; Peruzzo, V.; Tamburini, S. *Coord. Chem. Rev.* **2012**, *256* (11), 953–1114.
2. Lochenie, C.; Schötz, K.; Panzer, F.; Kurz, H.; Maier, B.; Puchtler, F.; Agarwal, S.; Köhler, A.; Weber, B. *J. Am. Chem. Soc.* **2018**, *140* (2), 700–709.
3. Golbedaghi, R.; Fausto, R. *Polyhedron* **2018**, *155*, 1–12.
4. Da Silva, C. M.; Da Silva, D. L.; Modolo, L. V.; Alves, R. B.; de Resende, M. A.; Martins, C. V. B.; de Fátima, Â. *J. Adv. Res.* **2011**, *2* (1), 1–8.
5. Malik, M. A.; Dar, O. A.; Gull, P.; Wani, M. Y.; Hashmi, A. A. *MedChemComm* **2018**, *9* (3), 409–436.
6. Kaczmarek, M. T.; Zabiszak, M.; Nowak, M.; Jastrzab, R. *Coord. Chem. Rev.* **2018**, *370*, 42–54.
7. Liu, X.; Manzur, C.; Novoa, N.; Celedón, S.; Carrillo, D.; Hamon, J.-R. *Coord. Chem. Rev.* **2018**, *357*, 144–172.
8. Zhu, H.; Fan, J.; Wang, B.; Peng, X. *Chem. Soc. Rev.* **2015**, *44* (13), 4337–4366.
9. Zhang, J.; Xu, L.; Wong, W.-Y. *Coord. Chem. Rev.* **2018**, *355*, 180–198.
10. De Fátima, Â.; Pereira, C. de P.; Olímpio, C. R. S. D. G.; de Freitas Oliveira, B. G.; Franco, L. L.; da Silva, P. H. C. *J. Adv. Res.* **2018**, *13*, 113–126.
11. Shaw, S.; White, J. D. *Chem. Rev.* **2019**, *119* (16), 9381–9426.
12. Andruh, M. *Dalton Trans.* **2015**, *44* (38), 16633–16653.
13. Coxall, R. A.; Harris, S. G.; Henderson, D. K.; Parsons, S.; Tasker, P. A.; Winpenny, R. E. P. *J. Chem. Soc. Dalton Trans.* **2000**, *14*, 2349–2356.
14. Li, L. Z.; Zhao, C.; Xu, T.; Ji, H. W.; Yu, Y. H.; Guo, G. Q.; Chao, H. *J. Inorg. Biochem.* **2005**, *99* (5), 1076–1082.
15. Dong, J.-F.; Li, L.-Z.; Yu, W.-J.; Cui, H.; Wang, D.-Q. *Acta Crystallogr., Sect. E* **2007**, *63* (7), 1992–1992.
16. Saha, D.; Maity, T.; Bera, R.; Koner, S. *Polyhedron* **2013**, *56*, 230–236.
17. Mitra, M.; Raghavaiah, P.; Ghosh, R. *New J. Chem.* **2014**, *39* (1), 200–205.
18. Hazra, S.; Koner, R.; Lemoine, P.; Sañudo, E. C.; Mohanta, S. *Eur. J. Inorg. Chem.* **2009**, *2009* (23), 3458–3466.
19. Tsave, O.; Halevas, E.; Yavropoulou, M. P.; Kosmidis Papadimitriou, A.; Yovos, J. G.; Hatzidimitriou, A.; Gabriel, C.; Psycharis, V.; Salifoglou, A. *J. Inorg. Biochem.* **2015**, *152*, 123–137.
20. Shen, S.; Xue, S.; Lin, S.-Y.; Zhao, L.; Tang, J. *Dalton Trans.* **2013**, *42* (29), 10413–10416.
21. Petrusenko, S. R.; Stetsyuk, O. M.; Omelchenko, I. V. *Acta Crystallogr., Sect. E* **2013**, *69* (6), 326–327.

22. Xue, L.-W.; Zhao, G.-Q.; Han, Y.-J.; Feng, Y.-X. *Acta Crystallogr., Sect. E* **2010**, *66* (9), 1172–1173.
23. Koner, R.; Hazra, S.; Fleck, M.; Jana, A.; Lucas, C. R.; Mohanta, S. *Eur. J. Inorg. Chem.* **2009**, *2009* (33), 4982–4988.
24. Manna, S. C.; Manna, S.; Mistri, S.; Patra, A.; Zangrando, E.; Puschmann, H.; Goddard, P. A.; Ghannadzadeh, S. *ChemistrySelect* **2018**, *3* (34), 9885–9891.
25. Zhang, Y.; Zhang, X.-M.; Liu, T.-F.; Xu, W.-G. *Transit. Met. Chem.* **2010**, *35* (7), 851–858.
26. Zheng, Y.-Z.; Lan, Y.; Anson, C. E.; Powell, A. K. *Inorg. Chem.* **2008**, *47* (23), 10813–10815.
27. Bhowmik, P.; Aliaga-Alcalde, N.; Gómez, V.; Corbella, M.; Chattopadhyay, S. *Polyhedron* **2013**, *49* (1), 269–276.
28. Zhang, Y.; Wu, J.; Shen, S.; Liu, Z.; Tang, J. *Polyhedron* **2018**, *150*, 40–46.
29. Cindrić, M.; Strukan, N.; Vrdoljak, V.; Kajfež, T.; Kamenar, B. *Z. Anorg. Allg. Chem.* **2002**, *628* (9–10), 2113–2117.
30. Halevas, E.; Tsave, O.; Yavropoulou, M. P.; Hatzidimitriou, A.; Yovos, J. G.; Psycharis, V.; Gabriel, C.; Salifoglou, A. *J. Inorg. Biochem.* **2015**, *147*, 99–115.
31. Oshio, H.; Hoshino, N.; Ito, T.; Nakano, M.; Renz, F.; Gütllich, P. *Angew. Chem. Int. Ed.* **2003**, *42* (2), 223–225.
32. Hazra, S.; Majumder, S.; Fleck, M.; Mohanta, S. *Polyhedron* **2008**, *27* (5), 1408–1414.
33. Yang, P.-P.; Wang, X.-L.; Li, L.-C.; Liao, D.-Z. *Dalton Trans.* **2011**, *40* (16), 4155–4161.
34. Gungor, E.; Coban, M. B.; Kara, H.; Acar, Y. *J. Clust. Sci.* **2018**, *29* (3), 533–540.
35. Modak, R.; Sikdar, Y.; Cosquer, G.; Chatterjee, S.; Yamashita, M.; Goswami, S. *Inorg. Chem.* **2016**, *55* (2), 691–699.
36. Gungor, E.; Kara, H.; Colacio, E.; Mota, A. *J. Eur. J. Inorg. Chem.* **2014**, *2014* (9), 1552–1560.
37. Lu, Z.; Fan, T.; Guo, W.; Lu, J.; Fan, C. *Inorg. Chim. Acta* **2013**, *400*, 191–196.
38. Li, Y.-M.; Kuang, W.-W.; Zhu, L.-L.; Xu, Y.; Yang, P.-P. *Eur. J. Inorg. Chem.* **2016**, *2016* (31), 4996–5003.
39. Tian, C.-B.; Yuan, D.-Q.; Han, Y.-H.; Li, Z.-H.; Lin, P.; Du, S.-W. *Inorg. Chem. Front.* **2014**, *1* (9), 695–704.
40. Tercero, J.; Ruiz, E.; Alvarez, S.; Rodríguez-Forteza, A.; Alemany, P. *J. Mater. Chem.* **2006**, *16* (26), 2729–2735.
41. Ahmed, N.; Das, C.; Vaidya, S.; Langley, S. K.; Murray, K. S.; Shanmugam, M. *Chem. Eur. J.* **2014**, *20* (44), 14235–14239.
42. Ahmed, N.; Das, C.; Vaidya, S.; Kumar Srivastava, A.; K. Langley, S.; S. Murray, K.; Shanmugam, M. *Dalton Trans.* **2014**, *43* (46), 17375–17384.

43. Modak, R.; Sikdar, Y.; Thuijs, A. E.; Christou, G.; Goswami, S. *Inorg. Chem.* **2016**, *55* (20), 10192–10202.
44. Ahmed, N.; Upadhyay, A.; Rajeshkumar, T.; Vaidya, S.; Schnack, J.; *Dalton Trans.* **2015**, *44* (43), 18743–18747.
45. Karmakar, S.; Khanra, S. *CrystEngComm* **2014**, *16* (12), 2371–2383.
46. Lu, J.-W.; Huang, Y.-H.; Lo, S.-I.; Wei, H.-H. *Inorg. Chem. Commun.* **2007**, *10* (10), 1210–1213.
47. Zhang, H.; Zhang, J.; Liu, R.; Li, Y.; Liu, W.; Li, W. *Eur. J. Inorg. Chem.* **2016**, *26*, 4134–4143.
48. Salehi, M.; Hasanzadeh, M. *Inorg. Chim. Acta* **2015**, *426*, 6–14.
49. Costes, J.-P.; Dahan, F.; Laurent, J.-P. *Inorg. Chem.* **1994**, *33* (13), 2738–2742.
50. Meally, S. T.; Taylor, S. M.; Brechin, E. K.; Piligkos, S.; Jones, L. F. *Dalton Trans.* **2013**, *42* (28), 10315–10325.
51. Costes, J.-P.; Dahan, F.; Dupuis, A.; Laurent, J.-P. *Inorg. Chem.* **1997**, *36* (16), 3429–3433.
52. Wei, L.-Q.; Zhang, K.; Feng, Y.-C.; Wang, Y.-H.; Zeng, M.-H.; Kurmoo, M. *Inorg. Chem.* **2011**, *50* (15), 7274–7283.
53. Zhang, S.-H.; Song, Y.; Liang, H.; Zeng, M.-H. *CrystEngComm* **2009**, *11* (5), 865–872.
54. Sobola, A. O.; Watkins, G. M.; Brecht, B. V. *South Afr. J. Chem.* **2014**, *67*, 45–51.
55. Fromm, K. M. *Coord. Chem. Rev.* **2008**, *252* (8), 856–885.
56. Fromm, K. M. *Coord. Chem. Rev.* **2020**, *408*, 213193.
57. Rutherford, A. W.; Boussac, A. *Science* **2004**, *303* (5665), 1782–1784.
58. Cox, N.; Retegan, M.; Neese, F.; Pantazis, D. A.; Boussac, A.; Lubitz, W. *Science* **2014**, *345* (6198), 804–808.
59. Zouni, A.; Witt, H.-T.; Kern, J.; Fromme, P.; Krauss, N.; Saenger, W.; Orth, P. *Nature* **2001**, *409* (6821), 739–743.
60. Loll, B.; Kern, J.; Saenger, W.; Zouni, A.; Biesiadka, J. *Nature* **2005**, *438* (7070), 1040–1044.
61. Najafpour, M. M.; Renger, G.; Hołyńska, M.; Moghaddam, A. N.; Aro, E.-M.; Carpentier, R.; Nishihara, H.; Eaton-Rye, J. J.; Shen, J.-R.; Allakhverdiev, S. I. *Chem. Rev.* **2016**, *116* (5), 2886–2936.
62. Gerey, B.; Gouré, E.; Fortage, J.; Pécaut, J.; Collomb, M.-N. *Coord. Chem. Rev.* **2016**, *319*, 1–24.
63. Gagrani, A.; Tsuzuki, T. *Chem. Eng. Sci.* **2019**, *194*, 116–126.
64. Najafpour, M. M.; Ehrenberg, T.; Wiechen, M.; Kurz, P. *Angew. Chem. Int. Ed.* **2010**, *49* (12), 2233–2237.
65. Park, Y. J.; Ziller, J. W.; Borovik, A. S. *J. Am. Chem. Soc.* **2011**, *133* (24), 9258–9261.

66. Escriche-Tur, L.; Jover, J.; Font-Bardia, M.; Aullón, G.; Corbella, M. *Inorg. Chem.* **2015**, *54* (24), 11596–11605.
67. Mangani, S.; Orioli, P. *J. Chem. Soc. Dalton Trans.* **1987**, *12*, 2999–3002.
68. Saha, D.; Hazra, D. K.; Maity, T.; Koner, S. *Inorg. Chem.* **2016**, *55* (12), 5729–5731.
69. Liu, Q.-F.; Liu, W.; Cao, Y.-P.; Dong, Y.-L.; Liu, H.-M. *Inorg. Nano-Met. Chem.* **2017**, *47* (1), 153–157.
70. Grancha, T.; Ferrando-Soria, J.; Cano, J.; Amorós, P.; Seoane, B.; Gascon, J.; Bazaga-García, M.; Losilla, E. R.; Cabeza, A.; Armentano, D.; Pardo, E. *Chem. Mater.* **2016**, *28* (13), 4608–4615.
71. Sanchis, M. J.; Gomez-Romero, P.; Folgado, J. V.; Sapina, F.; Ibanez, R.; Beltran, A.; Garcia, J.; Beltran, D. *Inorg. Chem.* **1992**, *31* (13), 2915–2919.
72. Zhang, J.; Cheng, S.; Wang, X.; Yuan, L.; Xue, M.; Wang, Y.; Liu, W. *CrystEngComm* **2013**, *15* (30), 6074–6082.
73. Grancha, T.; Mon, M.; Ferrando-Soria, J.; Gascon, J.; Seoane, B.; Ramos-Fernandez, E. V.; Armentano, D.; Pardo, E. *J. Mater. Chem. A* **2017**, *5* (22), 11032–11039.
74. Zou, G.-H.; Gao, J. *Synth. React. Inorg. Met.-Org. Nano-Met. Chem.* **2016**, *46* (11), 1721–1724.
75. Chang, X.; Jiang, L.-T.; Chen, S.-C.; He, M.-Y.; Chen, Q. *J. Coord. Chem.* **2020**, *73* (3), 439–452.
76. Mon, M.; Bruno, R.; Ferrando-Soria, J.; Bartella, L.; Donna, L. D.; Talia, M.; Lappano, R.; Maggiolini, M.; Armentano, D.; Pardo, E. *Mater. Horiz.* **2018**, *5* (4), 683–690.
77. Constable, E. C.; Zhang, G.; Housecroft, C. E.; Neuburger, M.; Zampese, J. A. *CrystEngComm* **2010**, *12* (6), 1764–1773.
78. Datta, A.; Das, K.; Massera, C.; Clegg, J. K.; Sinha, C.; Huang, J.-H.; Garribba, E. *Dalton Trans.* **2014**, *43* (14), 5558–5563.
79. Chandrasekhar, V.; Senapati, T.; Dey, A.; Das, S.; Kalisz, M.; Clérac, R. *Inorg. Chem.* **2012**, *51* (4), 2031–2038.
80. Zhao, Q.; Wei, Z.-L.; Kang, Q.-P.; Zhang, H.; Dong, W.-K. *Spectrochim. Acta. A. Mol. Biomol. Spectrosc.* **2018**, *203*, 472–480.
81. Hazra, S.; Sasmal, S.; Nayak, M.; A. Sparkes, H.; K. Howard, J. A.; Mohanta, S. *CrystEngComm* **2010**, *12* (2), 470–477.
82. Finelli, A.; Héroult, N.; Crochet, A.; Fromm, K. M. *ACS Omega* **2019**, *4* (6), 10231–10242.
83. Mandal, S.; Roy, S.; Mondal, S.; Sparkes, H. A.; Mohanta, S. *Inorg. Chim. Acta* **2018**, *482*, 612–620.

84. Chiboub Fellah, F. Z.; Costes, J.-P.; Dahan, F.; Duhayon, C.; Tuchagues, J.-P. *Polyhedron* **2007**, *26* (15), 4209–4215.
85. Liu, W.-L.; Zou, Y.; Lu, C.-S.; Dang, D.-B.; Li, Y.-Z.; Yao, Y.-G.; Meng, Q.-J. *Polyhedron* **2004**, *23* (13), 2125–2134.
86. Neto, B. A. D.; Lapis, A. A. M.; Júnior, E. N. da S.; Dupont, J. *Eur. J. Org. Chem.* **2013**, *2*, 228–255.
87. Alcock, N. W.; Hill, A. F.; Roe, M. S. Notes. *J. Chem. Soc. Dalton Trans.* **1990**, *5*, 1737–1740.
88. Munakata, M.; Kuroda-Sowa, T.; Maekawa, M.; Nakamura, M.; Akiyama, S.; Kitagawa, S. *Inorg. Chem.* **1994**, *33* (7), 1284–1291.
89. Renner, M. W.; Barkigia, K. M.; Melamed, D.; Smith, K. M.; Fajer, J. *Inorg. Chem.* **1996**, *35* (18), 5120–5121.
90. Papaefstathiou, G. S.; Perlepes, S. P.; Escuer, A.; Vicente, R.; Gantis, A.; Raptopoulou, C. P.; Tsohos, A.; Psycharis, V.; Terzis, A.; Bakalbassis, E. G. *J. Solid State Chem.* **2001**, *159* (2), 371–378.
91. Papaefstathiou, G. S.; Tsohos, A.; Raptopoulou, C. P.; Terzis, A.; Psycharis, V.; Gatteschi, D.; Perlepes, S. P. *Cryst. Growth Des.* **2001**, *1* (3), 191–194.
92. Skorda, K.; Papaefstathiou, G. S.; Vafiadis, A.; Lithoxidou, A.; Raptopoulou, C. P.; Terzis, A.; Psycharis, V.; Bakalbassis, E.; Tangoulis, V.; Perlepes, S. P. *Inorg. Chim. Acta* **2001**, *326* (1), 53–64.
93. Bashirov, D. A.; Sukhikh, T. S.; Kuratieva, N. V.; Naumov, D. Yu.; Konchenko, S. N.; Semenov, N. A.; Zibarev, A. V. *Polyhedron* **2012**, *42* (1), 168–174.
94. Zanias, S.; Papaefstathiou, G. S.; Raptopoulou, C. P.; Papazisis, K. T.; Vala, V.; Zambouli, D.; Kortsaris, A. H.; Kyriakidis, D. A.; Zafiroopoulos, T. F. *Bioinorg. Chem. and Appl.* **2010**, 1–10.
95. Sukhikh, T. S.; Ogienko, D. S.; Bashirov, D. A.; Kuratieva, N. V.; Komarov, V. Y.; Rakhmanova, M. I.; Konchenko, S. N. *J. Coord. Chem.* **2016**, *69* (21), 3284–3293.
96. Bashirov, D. A.; Sukhikh, T. S.; Kuratieva, N. V.; Chulanova, E. A.; Yushina, I. V.; Gritsan, N. P.; Konchenko, S. N.; Zibarev, A. V. *RSC Adv.* **2014**, *4* (54), 28309–28316.
97. Sukhikh, T. S.; Bashirov, D. A.; Shuvaev, S.; Komarov, V. Yu.; Kuratieva, N. V.; Konchenko, S. N.; Benassi, E. N. *Polyhedron* **2018**, *141*, 77–86.
98. Sukhikh, T. S.; Komarov, V. Yu.; Konchenko, S. N.; Benassi, E. *Polyhedron* **2018**, *139*, 33–43.
99. Munakata, M.; He, H.; Kuroda-Sowa, T.; Maekawa, M.; Suenaga, Y. *J. Chem. Soc. Dalton Trans.* **1998**, *9*, 1499–1502.
100. Sukhikh, T. S.; Ogienko, D. S.; Bashirov, D. A.; Konchenko, S. N. *Russ. Chem. Bull.* **2019**, *68* (4), 651–661.

101. Sukhikh, T. S.; Bashirov, D. A.; Kolybalov, D. S.; Andreeva, A. Y.; Smolentsev, A. I.; Kuratieva, N. V.; Burirov, V. A.; Mustafina, A. R.; Kozlova, S. G.; Konchenko, S. N. *Polyhedron* **2017**, *124*, 139–144.
102. Sukhikh, T. S.; Bashirov, D. A.; Kuratieva, N. V.; Smolentsev, A. I.; Bogomyakov, A. S.; Burirov, V. A.; Mustafina, A. R.; Zibarev, A. V.; Konchenko, S. N. *Dalton Trans.* **2015**, *44* (12), 5727–5734.
103. Andreeva, A. Y.; Sukhikh, T. S.; Kozlova, S. G.; Konchenko, S. N. *J. Mol. Struct.* **2018**, *1166*, 190–194.
104. Sukhikh, T. S.; Bashirov, D. A.; Ogienko, D. S.; Kuratieva, N. V.; Sherin, P. S.; Rakhmanova, M. I.; Chulanova, E. A.; Gritsan, N. P.; Konchenko, S. N.; Zibarev, A. V. *RSC Adv.* **2016**, *6* (50), 43901–43910.
105. Sukhikh, T. S.; Ogienko, D. S.; Bashirov, D. A.; Kurat'eva, N. V.; Smolentsev, A. I.; Konchenko, S. N. *Russ. J. Coord. Chem.* **2019**, *45* (1), 30–35.
106. Toscani, A.; Marín-Hernández, C.; Robson, J. A.; Chua, E.; Dingwall, P.; White, A. J. P.; Sancenón, F.; de la Torre, C.; Martínez-Mañez, R.; Wilton-Ely, J. D. E. T. *Chem. Eur. J.* **2019**, *25* (8), 2069–2081.
107. Cheng, Q.; Han, X.; Tong, Y.; Huang, C.; Ding, J.; Hou, H. *Inorg. Chem.* **2017**, *56* (3), 1696–1705.
108. Han, X.; Cheng, Q.; Meng, X.; Shao, Z.; Ma, K.; Wei, D.; Ding, J.; Hou, H. *Chem. Commun.* **2017**, *53* (74), 10314–10317.
109. Marshall, R. J.; Kalinovsky, Y.; Griffin, S. L.; Wilson, C.; Blight, B. A.; Forgan, R. S. *J. Am. Chem. Soc.* **2017**, *139* (17), 6253–6260.
110. Dai, F.-R.; Zhan, H.-M.; Liu, Q.; Fu, Y.-Y.; Li, J.-H.; Wang, Q.-W.; Xie, Z.; Wang, L.; Yan, F.; Wong, W.-Y. *Chem. Eur. J.* **2012**, *18* (5), 1502–1511.
111. Mancilha, F. S.; Barloy, L.; Rodembusch, F. S.; Dupont, J.; Pfeffer, M. *Dalton Trans.* **2011**, *40* (40), 10535–10544.
112. Zhang, Y.-M.; Meng, F.; Tang, J.-H.; Wang, Y.; You, C.; Tan, H.; Liu, Y.; Zhong, Y.-W.; Su, S.; Zhu, W. *Dalton Trans.* **2016**, *45* (12), 5071–5080.
113. Song, W.-C.; Liang, L.; Cui, X.-Z.; Wang, X.-G.; Yang, E.-C.; Zhao, X.-J. *CrystEngComm* **2018**, *20* (5), 668–678.
114. Poulsen, B. C.; Estalayo-Adrián, S.; Blasco, S.; Bright, S. A.; Kelly, J. M.; Williams, D. C.; Gunnlaugsson, T. *Dalton Trans.* **2016**, *45* (45), 18208–18220.
115. Song, X.; Yu, H.; Yan, X.; Zhang, Y.; Miao, Y.; Ye, K.; Wang, Y. *Dalton Trans.* **2018**, *47* (17), 6146–6155.
116. Shuku, Y.; Suizu, R.; Awaga, K.; Sato, O. *CrystEngComm* **2009**, *11* (10), 2065–2068.

117. Souza, B. de; Xavier, F. R.; Peralta, R. A.; Bortoluzzi, A. J.; Conte, G.; Gallardo, H.; Fischer, F. L.; Bussi, G.; Terenzi, H.; Neves, A. *Chem. Commun.* **2010**, 46 (19), 3375–3377.

Chapter 2

COORDINATION COMPOUNDS WITH HYDROXYLATED SCHIFF BASES

2.1. Introduction

Coordination compounds of *3d*-metals with polydentate ligands attract the attention of researchers thanks to a wide range of functional properties (magnetic, electro- and photophysical, optical, catalytic, biological) and are suitable for search and development of new materials. To a certain extent, it is possible to predict the structure of coordination compounds using: 1) modeling the ligand structure by changing its geometric shape, set and location of donor centers and substituents; 2) selection of a metal pair (for heterometallic complexes) of a given electronic configuration, with the necessary redox properties, size, stiffness/softness and geometry of the coordination polyhedron; 3) changing the synthesis conditions.

As previously described in § 1.3, the coordination compounds with *s*-metal have practical and fundamental importance. But no detailed study of "synthesis-structure-properties" of heterometallic *d-s* complexes has been undertaken up to date. Two main approaches to the preparation of polynuclear complexes are known: the method "building block"¹ and "serendipitous assembly"², which are widely used for the synthesis *d-s* complexes³⁻⁹.

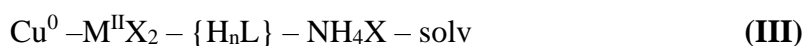
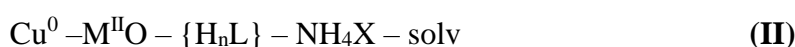
But the formation of heterometallic compounds based on *s*- and *d*-metals is more difficult comparing with other complexes with *d-d* combinations, because in these systems there is a competitive of coordination between two metals with different coordination opportunities. Since the transition metal complexes are more stable thermodynamically than the coordination compounds with *s*-elements, the possibility of forming monometallic complexes is higher.

In our group in Kyiv in the course of systematic work on the development of the "direct synthesis" (DS) approach we have been successful in the preparation of different homo- and heterometallic complexes with transition metals¹⁰. This synthetic strategy is based on the one-pot self-assembly of coordination fragments formed in situ starting from zerovalent metals or metal oxides. One of the advantages of this technique is the slow dissolution powder of transition metals, that is creating a concentration gradient and slow down the reaction of mononuclear complex formation. For example, for the synthesis of heterometallic complexes, one can use powder of transition metals and oxide or salt of alkaline earth metals, which creates favorable conditions for the formation of complexes with *s*-metals.

With the aim of synthesizing polynuclear *d-s* coordination compounds by the “direct synthesis” approach, we have chosen classical Schiff base ligands. They have several important advantages: 1) relative simplicity of preparation and modification; 2) they usually form stable complexes; 3) they possess high chelating-bridging potential, which increases the possibility of formation of complexes with different nuclearities.

2.2. Heterometallic *d-s* complexes

The following systems were chosen to investigate the peculiarities of the formation of heterometallic Cu – alkaline earth metal complexes with hydroxylated Schiff bases:



where M = Ca, Sr, Ba; X = Cl, Br, I, SCN, OAc, BF₄, SO₄, NO₃; solv = CH₃OH, DMF, DMSO; H_nL = **H₂L¹**, **H₂L²**, **HL³**, **H₂L⁴** (Fig. 2.1).

The ligand is formed *in situ* by condensation of amino alcohols or ammonia with *o*-vanillin or salicylaldehyde. The asymmetric *N, O*-donor Schiff base **H₂L¹**, **H₂L²**, **HL³**, **H₂L⁴** possess both chelating and bridging capabilities.

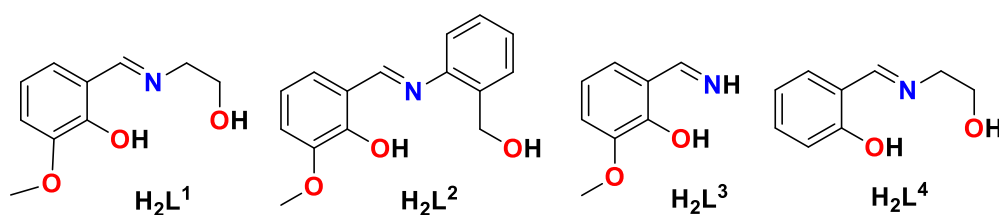


Figure 2.1. Schiff base ligands.

The system **I** involves *s*-metals oxides and copper (II) salts with the appropriate ligand. In this system conversion of the starting materials takes place within 40-60 minutes. Crystals of the products were the best obtained in methanol. From other solvents the product of the reaction crystallizes after adding isopropanol or diethyl ether. However, in the system **I** it was possible to isolate only the already known complex Cu(HL¹)₂¹¹.

Using copper powder in the systems **II** and **III**, the reaction rate slowed down to 4-5 h. Complexes [Cu₄(L¹)₄(CH₃OH)₄]·2,2CH₃OH (1), [Ca{Cu(HL¹)₂}₂]Br₂ (2),

[Ca{Cu(HL¹)₂}₂]I₂·0.4H₂O (**3**), [Ca{Cu(HL¹)₂}₂(CH₃OH)]I₂ (**3a**), [Ca{Cu(HL¹)₂}₂](SCN)₂ (**4**), [Sr{Cu(HL¹)₂}₂(CH₃OH)]I₂ (**5**), [Sr{Cu(HL¹)₂}₂(H₂O)₂](SCN)₂·0,65CH₃OH (**6**) and [Ba{Cu(HL¹)₂}₂(CH₃OH)₂]I₂ (**8**) were obtained from the system **II**. The individual compounds were isolated from methanol. The complex [Ca{Cu(HL¹)₂}₂CH₃OH]I₂ (**3a**) is formed in mixture with [Ca{Cu(HL¹)₂}₂]I₂·0.4H₂O (**3**) from the system **II** when the reaction is carried out at room temperature. The complex **3** was isolated individually when heated at 60 °C. The tetranuclear complex [Cu₄(L¹)₄(CH₃OH)₄]·2,2CH₃OH (**1**) was formed through the reaction of copper powder, calcium oxide, ammonium chloride and SB in methanol. However, compound **1** is unstable in air. Probably, the small size of the chloride anion does not favour the formation of the heterometallic complex. [Sr{Cu(HL¹)₂}₂NO₃]NO₃·CH₃OH (**7**) was obtained from the system **III** with copper powder, strontium nitrate and **H₂L¹** in methanol. Mixtures containing Cu(HL¹)₂ are formed in other solvents or by using NH₄OAc, NH₄BF₄ or (NH₄)₂SO₄.

The almost coplanar geometry and coordination unsaturation of the metal ion motivated the use of the complex Cu(HL¹)₂ as potential metallo-ligand in system **IV**. Thus, the reaction of Cu(HL¹)₂ with BaO in methanol afforded crystals of [Cu₄(HL¹)₂(L¹)₂(NCS)₂(CH₃OH)₂]·2CH₃OH (**10**). In other cases, only mixtures were obtained from this system.

The formation of the complex [Ba{Cu(HL¹)₂}₂(CH₃OH)₂](SCN)₂ (**9**) has not been observed in the systems **I-IV**. Therefore, to obtain complex **9** we have used CuSCN and Ba(SCN)₂·2H₂O with **H₂L¹** in methanol.

To summarize, the most straightforward for the synthesis of *d-s* heterometallic complexes with **H₂L¹** is the system **II** in which there is a dependence of the interaction time and product composition on the ratio Cu : M. Thus, at the stoichiometric ratio of metals 2:1 it was not possible to obtain heterometallic complexes and the formation of the known Cu(HL¹)₂ complex was observed. Formation of the heterometallic complexes were observed in the system with the ratio Cu : M = 1:1 or 1:2. In the latter case, the reaction is faster. The main factors that influence the formation of heterometallic complexes with **H₂L¹** can be identified as: a) the molar ratio of Cu – M (M = Ca, Sr, Ba); b) the rate of copper dissolution; c) the nature of the ammonium salt (anion radii); d) the temperature.

In the case of **H₂L²** from the system **II** it was isolated the discrete complex [Ca{Cu(HL²)₂}₂]I₂ (**11**), while with **HL³** – [Cu(L³)₂Ca(NCS)₂(H₂O)] (**12**).

The synthetic procedures are presented in Appendix 1.

The IR spectra of the complexes **2-12** are quite similar and the characteristic absorption bands are presented in Table 2.1.

Table 2.1. Characteristic infrared absorption bands (cm^{-1}) of complexes **2-12**.

No	$\nu(\text{OH})^*$	$\nu(\text{CN})_{\text{SCN}}$	$\nu(\text{NO})_{\text{NO}_3}$	$\nu(\text{C}=\text{N})$	$\nu(\text{C}-\text{O})$	$\nu(\text{C}-\text{S})$
2	3260	-	-	1622	1227	-
3	3321	-	-	1625	1224	-
4	3360	2069	-	1625	1241	853
5	3357	-	-	1625	1224	-
6	3366	2056	-	1626	1222	855
7	3338	-	1380	1627	1220	-
8	3382	-	-	1628	1242	-
9	3375	2055	-	1626	1248	845
10	3357	2054	-	1627	1222	854
11	3400	-	-	1620	1221	-
12	3340	2076	-	1617	1225	853

* maximum for the broad band

The broad band at $3450\text{-}3200\text{ cm}^{-1}$ is assigned to the non-deprotonated hydroxyl groups of the ligands establishing hydrogen bonds in the solid state. The characteristic $\nu(\text{C}=\text{N})$ stretching vibration for imino group appears as very strong bands in the range $1617\text{-}1628\text{ cm}^{-1}$ for the complexes and in the range $1640\text{-}1650\text{ cm}^{-1}$ for the free ligands. The shift of the absorption band to the low-frequency region indicates the creation of the M-N coordination bond. A similar shift of the $\nu(\text{C}-\text{O})$ vibration in the low-frequency region ($1220\text{-}1248\text{ cm}^{-1}$ for the complexes and $\sim 1270\text{ cm}^{-1}$ for the free ligands) confirms the coordination of the metal. In the IR spectrum of the complex **7** the peaks of the coordinated and uncoordinated nitrate group overlap, forming a wide band with a maximum at 1380 cm^{-1} . Coordinated and non-coordinated thiocyanate groups in **4, 6, 9, 10, 12** are confirmed by the presence of a very intense peak $\nu(\text{CN})$ at $2054\text{-}2076\text{ cm}^{-1}$ and weak peak $\nu(\text{C}-\text{S})$ at $845\text{-}855\text{ cm}^{-1}$. The other vibrations are found in the fingerprint region for these types of ligands.

Crystallographic data, selected distances and angles are presented in Appendix 2.

The complex $[\text{Cu}(\text{L}^3)_2\text{Ca}(\text{NCS})_2(\text{H}_2\text{O})]$ (**12**) contains the Cu(II) and Ca(II) ions linked by two μ -phenoxido-bridges from the ligands to form a binuclear $\{\text{Cu}(\mu\text{-O})_2\text{Ca}\}$ core, with a distance $\text{Cu}\cdots\text{Ca}$ of 3.427 \AA and CuOCa angles of *ca* 106° (Fig. 2.2). The copper atom is surrounded by two nitrogen and by two oxygen atoms from the SB ligands. The CuN_2O_2 unit has a slightly distorted square planar geometry. The Cu-O/N bond distances are in the range $1.918(2)\text{-}1.936(3)\text{ \AA}$ and the *cis*- and *trans*-angles deviate from ideal symmetry by less than 8° ($\tau_4 = 0.112$). The copper atom is away from the N_2O_2 plane by *ca* 0.01 \AA .

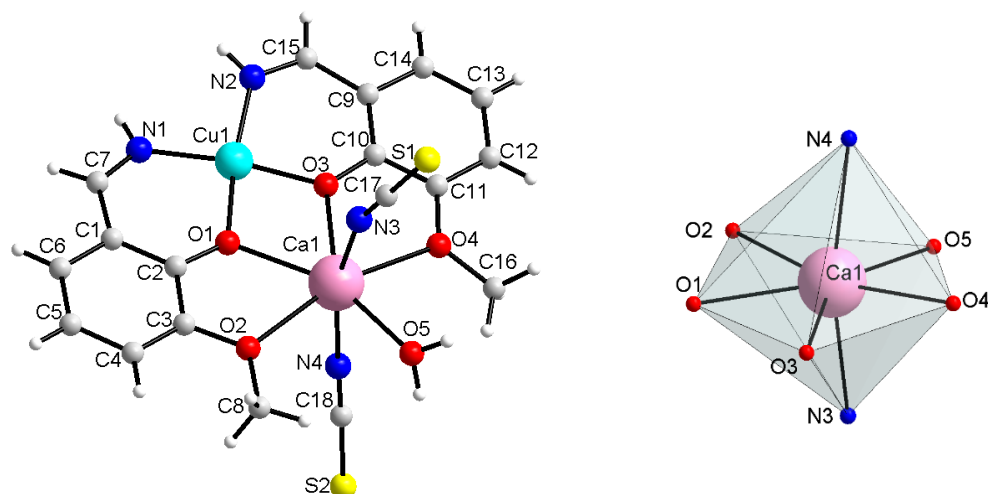


Figure 2.2. Molecular structure (left) and coordination polyhedron of the Ca(II) in the complex **12** (right) ¹².

The calcium ion is seven coordinated with a N_2O_5 coordination environment. The $\{Cu(L^3)_2\}$ fragment chelates the Ca(II) atom in a tetradentate manner by the four oxygen atoms. Two sites are occupied by nitrogen atoms of two SCN groups and the remaining one is completed by oxygen from the one water molecule. The geometry of CaN_2O_5 motif is best described as a distorted pentagonal bipyramid. The pentagon base on five oxygen atoms with nitrogen in the axial position (Fig. 2.2). The Ca-O bond distances are the longest for the coordinating methoxy groups [2.511(2) and 2.521(2) Å] and the shortest for the coordinating phenoxide groups and the water molecule [2.339(2) - 2.356(2) Å]. The bond valence sum (BVS) method confirms to the +2 oxidation state for copper [2.07] and calcium [2.11]^{13,14}. In this complex the ligand shows O,O',O',N -tetradentate coordination mode or $[2.1_12_12_12]$ ¹⁵, which is characteristic for the similar compounds (Table 1.3)^{16,17}.

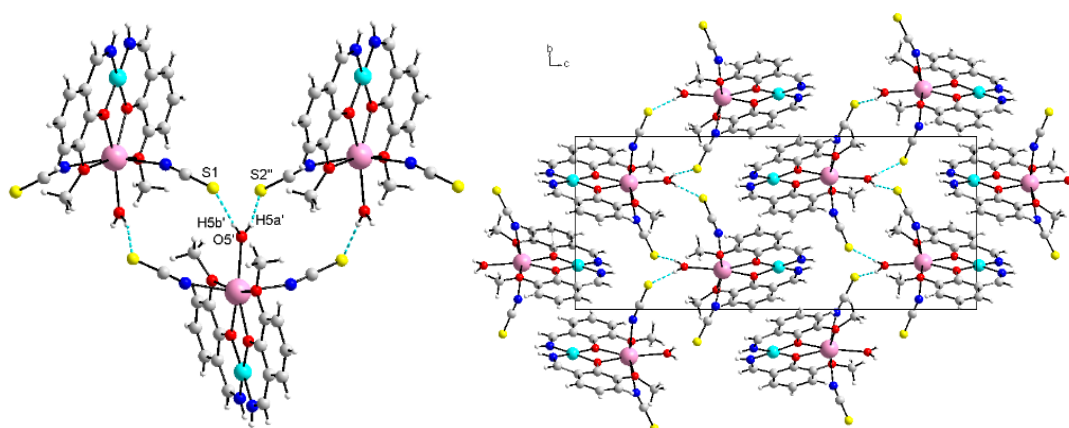
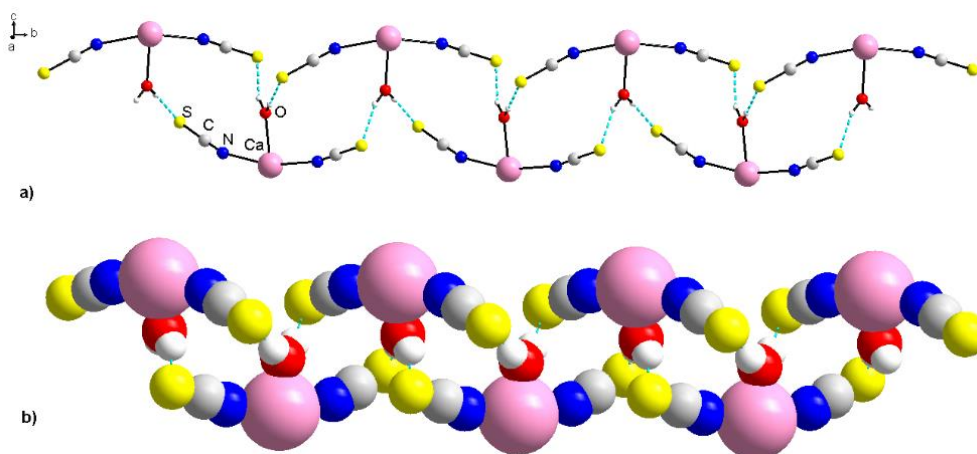


Figure 2.3. Complex **12**: fragment of the crystal chain (left) and crystal packing along the a axis (right) showing hydrogen bonds¹².

Table 2.2. Hydrogen bonds parameters (Å, °) **12**¹².

D-H...A	d(D-H)	d(D...A)	d(H...A)	angles (D-H...A)
O5'-H5b'...S1	0.894	3.228	2.338	173.94
O5'-H5a'...S2	0.894	3.294	2.432	162.44

Each binuclear complex forms four O-H...S hydrogen bonds with the two adjacent molecules of complex involving the coordinated water molecules and SCN ions (Fig. 2.3, Table 2.2). The hydrogen bonded repeat units are forming chains based on a double twelve-membered $[R_2^2(12)]_2$ synthon¹⁸ (Fig. 2.4). The calcium atoms in the chains are arranged in zigzag fashion. The shortest Ca...Ca contact amounts at 7.792(7) Å and Ca-Ca-Ca angle measures 85.093(7) °. The 1D supramolecular chains run parallel to the *b*-axis.

**Figure 2.4.** Fragment of the crystal structure of **12**, demonstrating the chain skeleton based on the $[R_2^2(12)]_2$ synthon¹².

The heterometallic complexes $[\text{Ca}\{\text{Cu}(\text{HL}^1)_2\}_2]\text{I}_2 \cdot 0.4\text{H}_2\text{O}$ (**3**), $[\text{Ca}\{\text{Cu}(\text{HL}^1)_2\}_2(\text{CH}_3\text{OH})]\text{I}_2$ (**3a**), $[\text{Ca}\{\text{Cu}(\text{HL}^1)_2\}_2(\text{SCN})_2]$ (**4**), $[\text{Sr}\{\text{Cu}(\text{HL}^1)_2\}_2(\text{CH}_3\text{OH})]\text{I}_2$ (**5**), $[\text{Sr}\{\text{Cu}(\text{HL}^1)_2\}_2(\text{H}_2\text{O})_2](\text{SCN})_2 \cdot 0.65\text{CH}_3\text{OH}$ (**6**), $[\text{Sr}\{\text{Cu}(\text{HL}^1)_2\}_2\text{NO}_3]\text{NO}_3 \cdot \text{CH}_3\text{OH}$ (**7**), $[\text{Ba}\{\text{Cu}(\text{HL}^1)_2\}_2(\text{CH}_3\text{OH})_2]\text{I}_2$ (**8**), $[\text{Ba}\{\text{Cu}(\text{HL}^1)_2\}_2(\text{CH}_3\text{OH})_2](\text{SCN})_2$ (**9**) have similar crystal structures, but only the complexes **8** and **9** are isostructural. Their crystal structure is based on the heterometallic trinuclear $[\text{M}\{\text{Cu}(\text{HL}^1)_2\}_2]^{2+}$ ($\text{M} = \text{Ca}, \text{Sr}, \text{Ba}$) dication and single-charge anions X^- ($\text{X} = \text{Br}, \text{I}, \text{SCN}, \text{NO}_3$). The oxygen donor atoms of the $\{\text{Cu}(\text{HL}^1)_2\}$ moiety chelate the *s*-metal in a tetradentate chelating manner (by two phenoxo and two methoxy oxygen atoms) (Fig. 2.5).

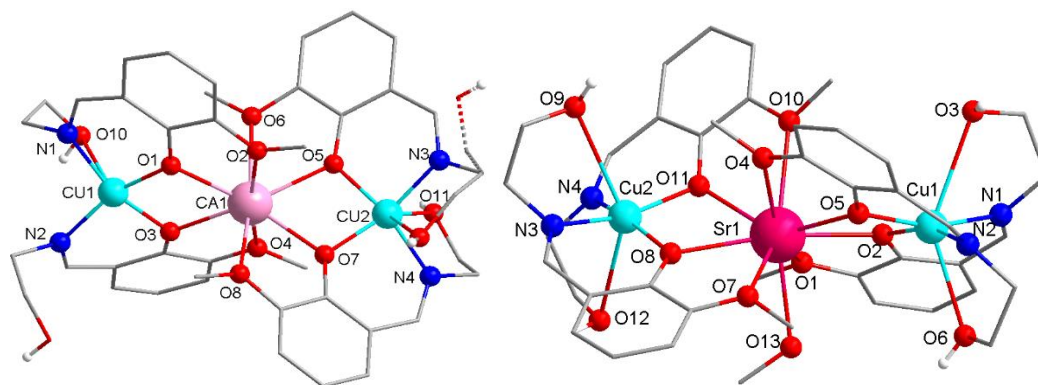


Figure 2.5. Crystal structure of coordination cations $[\text{Ca}\{\text{Cu}(\text{HL}^1)_2\}_2]^{2+}$ (**3**) (left) and $[\text{Sr}\{\text{Cu}(\text{HL}^1)_2\}_2(\text{CH}_3\text{OH})]^{2+}$ (**5**) (right).

The ligand displays pentadentate ($OO'O'NO''$) or tetradentate ($OO'O'N$) coordination mode ($[2.1_12_{12}01_2]$ or $[2.1_12_{12}1_21_2]^{15}$). Due to the increase of the metal radius in the row $\text{Ca}^{2+} < \text{Sr}^{2+} < \text{Ba}^{2+}$ there is an increase in its coordination number from 8 to 10. This is fulfilled through four oxygen atoms of the ligands and additional coordination of the nitrate ion, water or methanol molecules.

In the complex **7** the cationic unit $[\text{Sr}\{\text{Cu}(\text{HL}^1)_2\}_2\text{NO}_3]^+$ was formed by two $\{\text{Cu}(\text{HL}^1)_2\}$ moieties and one bidentate NO_3^- group forming the SrO_{10} unit.

Only oxygen atoms were involved in the coordination of *s*-metals. In order to describe more precisely the geometry, SHAPE analyses have been used^{19,20}. The results of SHAPE analyses show the values that are a measure of the deviation of the geometry from the idealized polyhedron (zero is the value for an ideal polyhedron). The eight-coordinated polyhedra of the calcium atoms have a geometry of triangular dodecahedron (4.416 for complex **3**) and distorted cube (4.945 for **4**). SHAPE analysis reveals that the most appropriate geometry for the nine-coordinated calcium atom in the complex **3a** is muffin with deviation value of 3.816 and spherical-relaxed capped cube with a value of 4.242 for the strontium atom, in the case of the complex **5**. The best polyhedron for the ten-coordinated atoms are described as distorted sphenocorona with deviation values 3.951 (for complex **6**), 4.939 (for **7**), 4.028 (for **8**) and 3.823 (for **9**).

The three metal atoms locate in a nearly linear fashion. The value of the CuMCu ($\text{M} = \text{Ca}, \text{Sr}, \text{Ba}$) angles varies from 156.51° to 177.26° , the largest angle deviation from 180° being in complex **8** and the smallest in **3**.

The copper atoms are coordinated exclusively by the donor atoms of the two monodeprotonated ligands. The hexa-coordinated $\text{Cu}(\text{II})$ atoms have a N_2O_4 coordination environment within distorted elongated bipyramid geometry $[4+2]$, with four short bonds and two

long semi-coordinated bonds (Fig. 2.5). In the basal plane the Cu–O bond lengths are 1.949–1.984 Å and the Cu–N bond lengths are 1.906–1.939 Å. The values of the axial Cu–O bonds lie in the 2.429–2.998 Å range, which is within the allowed limits for Cu(II)–O²¹. The *trans*-angles OCuO vary from 134.18 to 144.15 °. The equatorial plane N₂O₂ is distorted and the values of the angular parameter τ_4 ²² (parameter confirms the significant deviation of the geometry of the equatorial plane from the flat square) are within the values 0.26–0.40 (Table 2.3).

In the complexes **3**, **6** and **7** one copper atom is penta-coordinated within slightly distorted square-pyramidal [4+1] configuration N₂O₃ (Fig. 2.5 as example **3**). The τ_5 values are equal to 0.02 (for **3**), 0.12 (for **6**) and 0.20 (for **7**)²³. The equatorial Cu–N and Cu–O bond lengths vary from 1.945 to 1.980 Å and from 1.908 to 1.936 Å, respectively. The axial Cu–O bond involves the OH group from an alcohol arm (2.432, 2.653 and 2.975 Å, respectively for **3**, **6** and **7**). It should be noted that one of the copper atoms is five-coordinated only in the complexes containing non-coordinated molecules of solvent. BVS analysis¹³ is presented in Table 2.3.

Table 2.3. Selected geometrical parameters, the BVS and index τ values for complexes **3–9**.

№	angles (Cu–M–Cu), °	[CN] – BVS			τ_4/τ_5^*	
		Cu1 ^{24,25}	Cu2 ^{24,25}	M (Ca,Sr,Ba) ^{14,26}	Cu1	Cu2
3	177.260(2)	[4+1] – 2.06	[4+2] – 2.09	[8] – 2.16	0.022*	0.348
3a	172.35(5)	[4+2] – 2.07	[4+2] – 2.09	[9] – 2.11	0.291	0.277
4	176.72(2)	[4+2] – 2.04	[4+2] – 2.08	[8] – 2.12	0.348	0.334
5	170.314(38)	[4+2] – 2.08	[4+2] – 2.07	[9] – 2.21	0.275	0.275
6	162.376(13)	[4+2] – 2.06	[4+1] – 2.08	[10] – 2.19	0.259	0.204*
7	165.961(24)	[4+2] – 2.07	[4+1] – 2.04	[10] – 2.19	0.289	0.115*
8	156.51(2)	[4+2] – 2.04	[4+2] – 2.04	[10] – 2.37	0.396	0.396
9	157.450(14)	[4+2] – 2.09	[4+2] – 2.09	[10] – 2.39	0.367	0.367

* τ_4/τ_5 for the four- or five-coordinated copper atom

The copper-calcium iodide complexes **3** and **3a** are pseudo-polymorphic compounds that differ by the presence of an additional molecule of methanol in the coordination environment of calcium. As a result, the coordination number of the calcium changes from eight in complex **3** to nine in **3a**.

Complexes **8** and **9** are isostructural and crystallize in the monoclinic *C2/c* space group. The crystal structure of the complex cation [Ba{Cu(HL¹)₂}(CH₃OH)₂]²⁺ in **8–9** is depicted in the Figure 2.6. The complexes consist of one Ba^{II} ion, two Cu^{II} ions, four monodeprotonated ligands and two molecules of methanol. The copper and the barium atoms are six-coordinated and ten-coordinated, respectively.

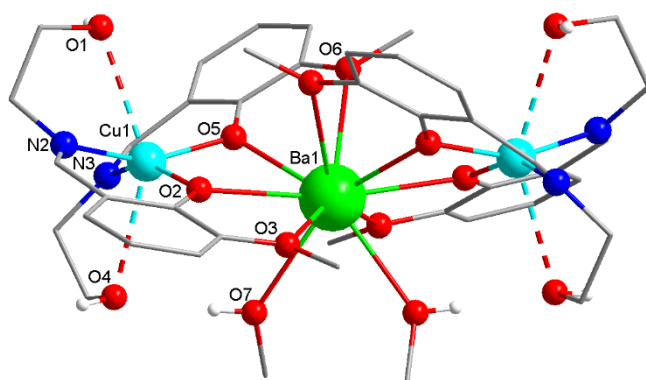


Figure 2.6. Crystal structure of complex cation $[\text{Ba}\{\text{Cu}(\text{HL}^1)_2\}_2(\text{CH}_3\text{OH})_2]^{2+}$ in **8-9**.

In the crystal packing of complexes **8** and **9**, the coordinated molecules of methanol form intramolecular hydrogen bonds with the hydroxyl group of the ligand, which, in turn, forms intermolecular hydrogen bonds with uncoordinated anions. The anions ensure a bridging function, they link the adjacent molecules of complexes forming a hydrogen network in the *ab* plane (Fig. 2.7).

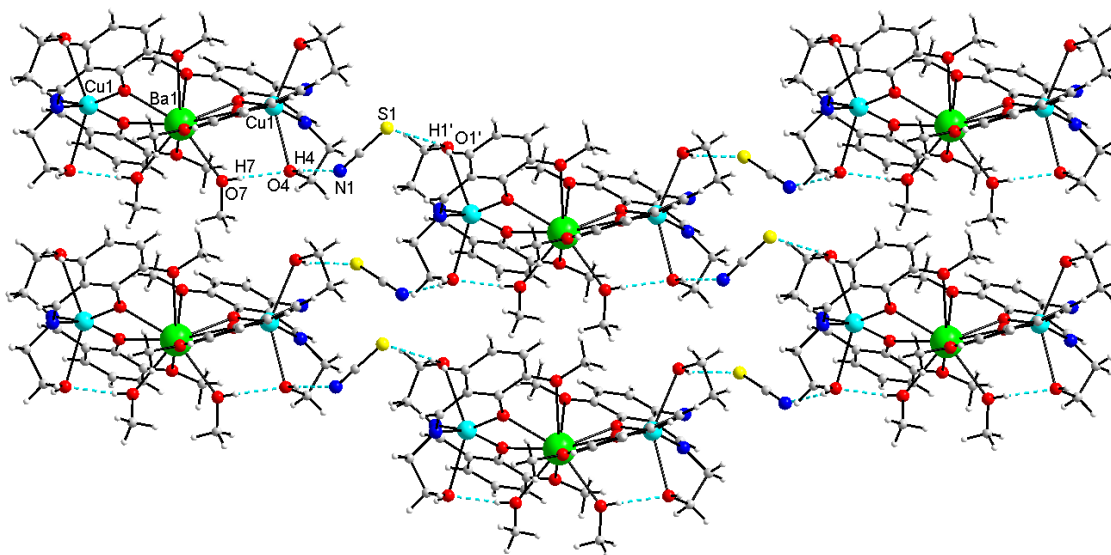


Figure 2.7. Fragment of the crystal structure of **9**, showing hydrogen bonds.

The crystal lattices of all complexes contain a number of hydrogen bonds formed by I^- , SCN^- , NO_3^- , hydroxyl groups of SB and the molecules of solvent. For example, in complex **5** the formation of five types of hydrogen bonds was recorded. The iodide ions act as bridges between adjacent molecules of complex forming hydrogen bonds with OH groups of the ligand and coordinated methanol molecules. As a result, parallel 1D chains are formed along the *a* axis (Fig. 2.8).

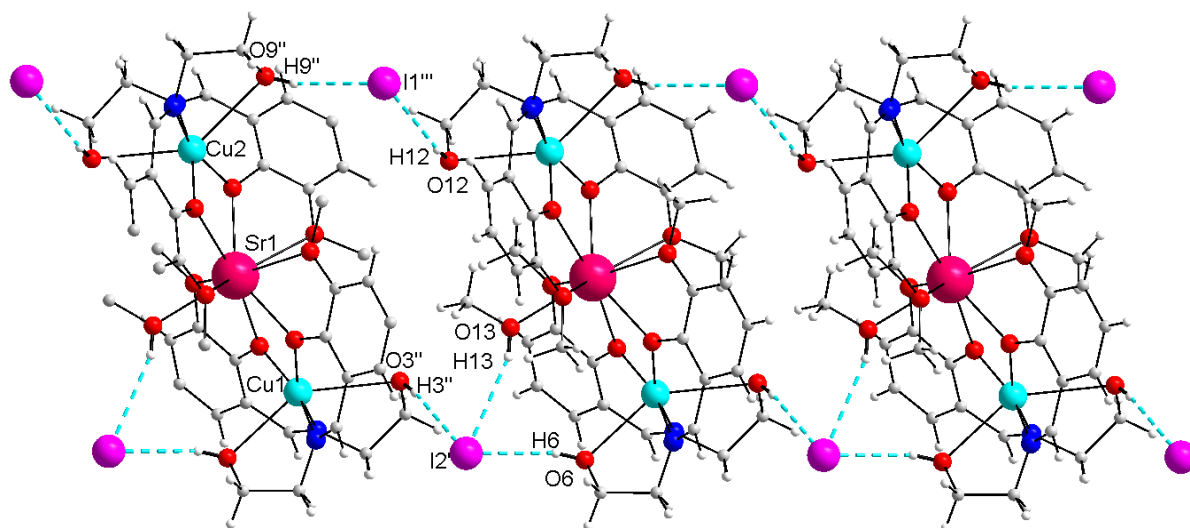


Figure 2.8. Fragment of crystal structure of **5** viewed along the *a* axis.

In the complex **6**, the number of noncovalent interactions almost doubles (Fig. 2.9) comparing with the complex **5**. The SCN^- anions, the coordinated and uncoordinated hydroxyl groups of the ligand, the coordinated water molecules and molecule of methanol are involved in the formation of the hydrogen bonds.

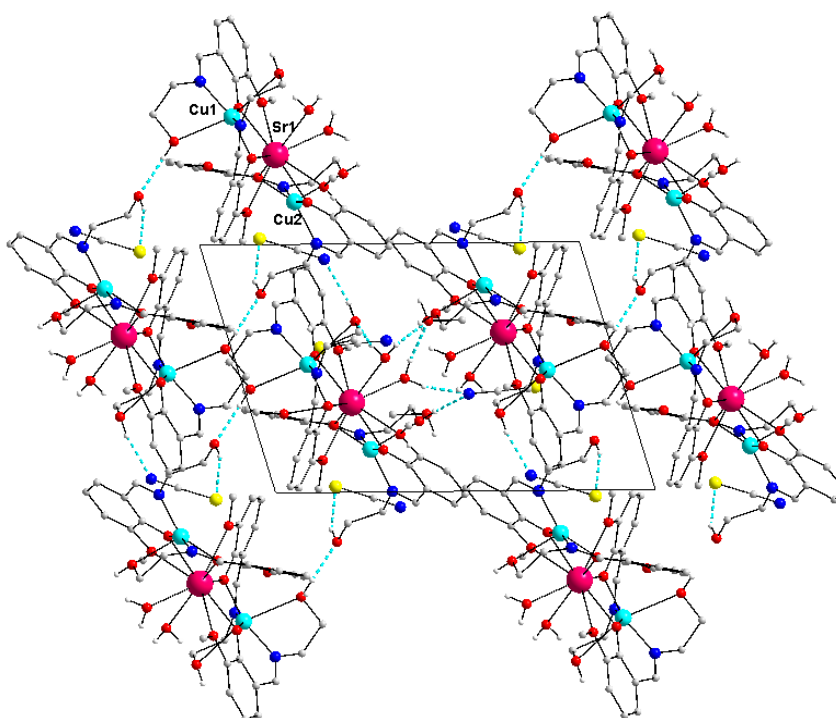


Figure 2.9. Crystal packing of **6** with the hydrogen bonds viewed along the *a* axis.

In complex **7** the nitrate ions, OH-groups of ligands and non-coordinated methanol molecules are involved in intermolecular hydrogen bonds forming a 2D supramolecular structure in the plane *ac* (Fig. 2.10).

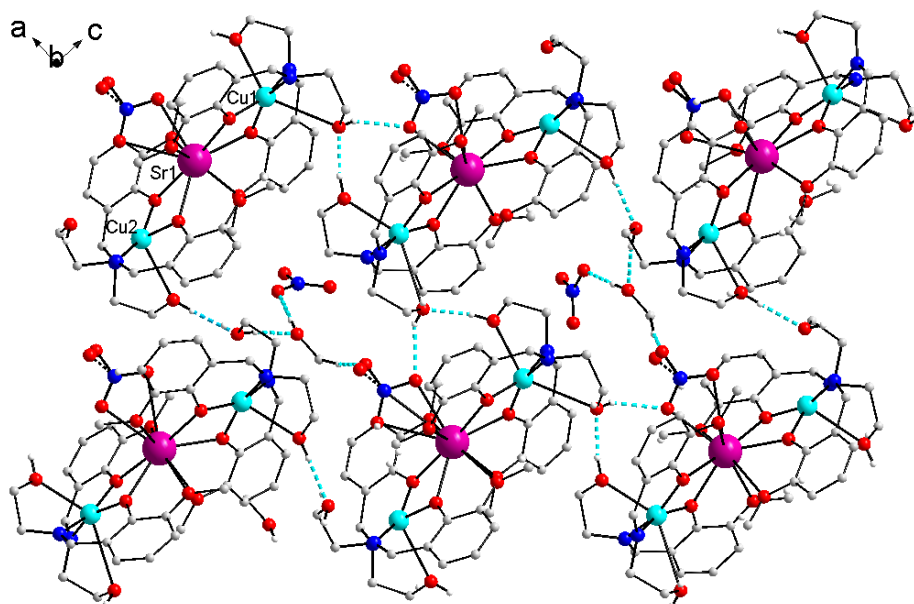


Figure 2.10. Fragment of crystal structure of 7 showing hydrogen bonds.

The arm of hydroxyl group of the SB is very flexible. Depending on the composition of the complex the formation of the different types of contacts can be observed with the participation of the OH group. When uncoordinated solvent molecules are present in the crystal packing one of the OH group does not participate in the Cu-O bond but is more involved in the formation of an intermolecular hydrogen bond. As a result, the coordination number of copper is reduced from six to five.

These heterometallic complexes have been investigated in polymer composite films based on polyvinyl butyral for photovoltaic properties properties, in collaboration with group of N. A. Davidenko in Taras Shevchenko National University of Kyiv²⁷⁻²⁹ and for antimicrobial activity in collaboration with O.V. Pocas in Institute of Epidemiology and Infectious Diseases of the Academy of Medical Sciences of Ukraine³⁰.

2.3. Tetranuclear Cu(II) complexes

Complex $[\text{Cu}_4(\text{L}^1)_4(\text{CH}_3\text{OH})_4] \cdot 2,2\text{CH}_3\text{OH}$ (**1**) crystallizes in the centrosymmetric monoclinic $P2_1/c$ space group and has a tetranuclear structure (Fig. 2.11). The molecule contains a distorted Cu_4O_4 cubane-like core. The copper atoms are linked by four μ -phenoxido-bridging of the hydroxyl groups of the four ligands.

Each copper ion has distorted octahedral environment O_5N , with four oxygen and one nitrogen atoms from the ligand and one oxygen atom from the coordinated methanol molecule. The coordination geometry of copper(II) is distorted elongated bipyramid (4+1+1) within the

CuO₅N unit. In the equatorial plane the values of the Cu-N/O bond lengths are in the range 1.917(3)-1.978(3) Å and are significantly elongated in the axial positions – 2.450(3)-2.863(20) Å. The longest contact is between the copper and oxygen atoms of the coordinated methanol molecule. Using the Cu···Cu distances (Table 2.4) the Cu₄O₄ complex **1** can be classified into [4+2] cubane type^{31,32}.

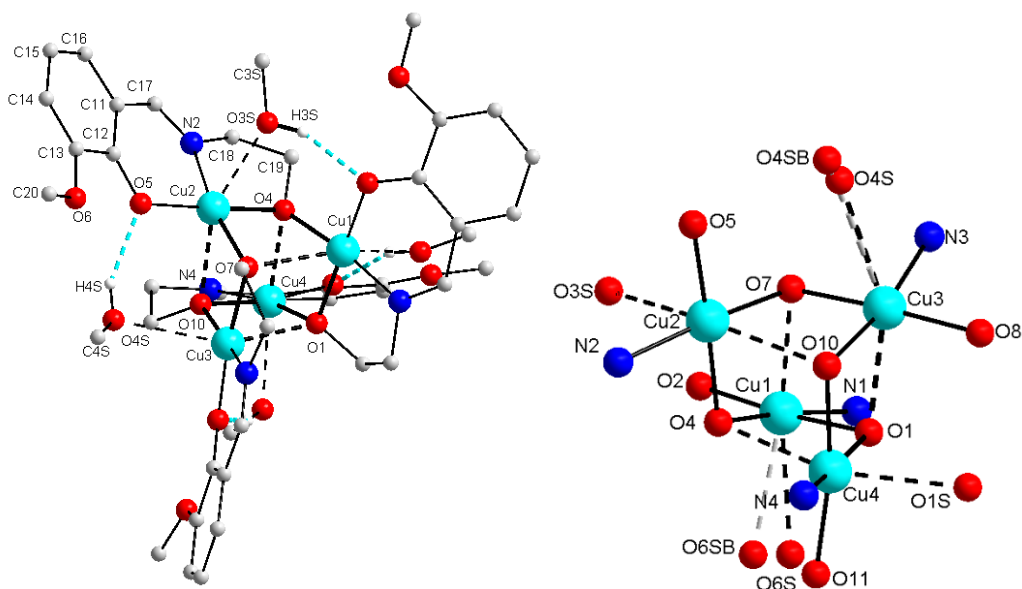


Figure 2.11. Molecular structure (left) and cubane Cu₄O₄ core (right) of **1**.

Table 2.4. The Cu···Cu distances (Å) for **1**.

Cu1···Cu2	3.138	Cu1···Cu4	3.146	Cu2···Cu4	3.473
Cu1···Cu3	3.421	Cu2···Cu3	3.147	Cu3···Cu4	3.109

The deprotonated hydroxyl groups and the coordinated methanol molecules take part in the formation of intramolecular O-H···O hydrogen bonds (Fig. 2.11, Table 2.5).

Table 2.5. Intramolecular hydrogen bonds (Å,°) for **1**.

D-H···A	d(D···A)	d(H···A)	angle (D-H···A)
O4S-H4S···O5	2.776	1.998	153.36
O3S-H3S···O2	2.743	1.980	150.59
O1S-H1S···O8	2.786	1.976	155.85
O6S-H6S···O11	2.767	1.979	161.41

The complex [Cu₄(HL¹)₂(L¹)₂(NCS)₂(CH₃OH)₂]**2**·2CH₃OH (**10**) crystallizes in the centrosymmetric C2/c space group and has a tetranuclear structure (Fig. 2.12). The Cu₄O₄ core is located on a two-fold crystallographic axis. The asymmetric unit consists of two crystallographically independent copper atoms coordinated by monodeprotonated and bis-

deprotonated ligands, one SCN group and one methanol molecule. It should be noted that in the structure two different coordination modes of the ligand $\mathbf{H}_2\mathbf{L}^1$ were obtained (O, N, O', O', O' -pentadentated or $[3.01_13_{123}1_1]$ for $(\mathbf{HL}^1)^-$ and O, O', O', N -tetradentated $(\mathbf{L}^1)^{2-}$ or $[2.1_12_{12}01_2]$ ¹⁵).

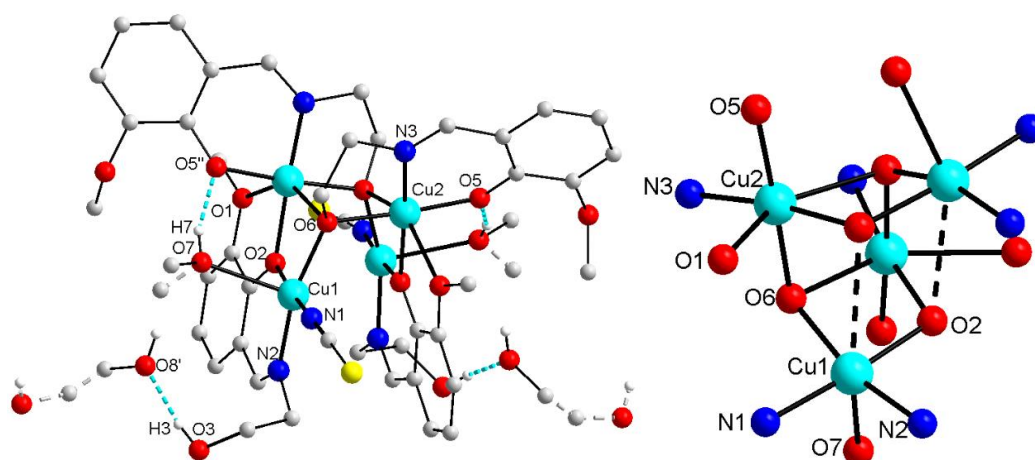


Figure 2.12. Molecular structure (left) and pseudo-cubane core (right) of **10**.

The coordination environment $\text{Cu}(1)\text{N}_2\text{O}_3$ is formed by donor atoms of two ligands, one molecule of methanol and a thiocyanate group. In the equatorial plane the bond lengths vary between 1.94-1.98 Å and the axial $\text{Cu}(1)\text{-O}(7)$ distance is equal to 2.43 Å. The coordination polyhedron has a square-pyramidal geometry and the structural parameter τ_5 is equal to 0.21²³. The $\text{Cu}(1)$ atom is displaced from the basal plane by 0.13 Å. The $\text{Cu}(2)$ atom has six-coordinated environment formed exclusively by donor atoms from the three ligands. The polyhedron $\text{Cu}(2)\text{NO}_5$ has a tetragonally elongated octahedron (4+2) geometry. The difference between the bond lengths in the equatorial plane is about 0.08 Å, the axial distances of octahedron are almost equal [2.35 and 2.37 Å]. The *cis*-angles at the atom $\text{Cu}(2)$ vary from 71.94 to 112.66 ° and the minimum and maximum *trans*-angles values are 144.7 and 176.0 °.

The geometry of the Cu_4O_4 fragment can be interpreted as pseudo-cuban type. The linear and angular distortions are very large. For example, the $\text{Cu}\cdots\text{Cu}$ distances in the tetranuclear core are 3.195, 3.220, 3.368 and 3.948 Å.

The molecules of solvent are involved in an intramolecular and an intermolecular hydrogen bond with the SCN-group, hydroxyl and methoxy group of the ligand (Table 2.6).

Table 2.6. Hydrogen bond parameters (Å, °) of **10**.

D-H...A	d (D...A)	d (H...A)	angles (D-H...A)
O3-H3...O8'	2.671	1.877	162.36
O7-H7...O5''	2.735	1.917	160.59
O9-H9...S1	3.315	2.541	157.88

2.4. Mn(II) and Mn(III) complexes

Since the discovery of the crystal structure and important role of the $\text{Mn}_4\text{O}_5\text{Ca}$ cluster in the Photosystem II numerous investigations of Mn-Ca complexes have been reported^{33,34}. Given that Mn-Ca complexes catalyze the photochemical oxidation of water and have magnetic properties, various synthetic methods were used. We decided to test first the previously studied systems **I-III**, by replacing copper with manganese. Unfortunately, these systems were not effective for the synthesis of heterometallic complexes. At the same time, the polymeric manganese (III) complexes $\{[\text{Mn}(\text{HL}^1)_2]\text{Cl}\}_n$ (**13**), $\{[\text{Mn}(\text{HL}^1)_2]\text{Br}\}_n$ (**14**), $[\text{Mn}(\text{HL}^1)_2(\text{NCS})]_n$ (**15**), $\{[\text{Mn}(\text{HL}^4)_2]\text{Br}\}_n$ (**16**), $\{[\text{Mn}(\text{HL}^4)_2]\text{I}\}_n$ (**17**) and $\{[\text{Mn}(\text{HL}^4)_2]\text{NCS}\}_n$ (**18**) were obtained from the systems **I-II** with H_2L^1 and H_2L^4 . The binuclear complex $[\text{Mn}^{\text{II}}_2(\text{HL}^2)_2(\text{NCS})_2] \cdot 2\text{C}_2\text{H}_5\text{OH}$ (**19**) was isolated from the system **II** in ethanol.

IR spectra of the complexes **13-18** have similar absorption bands confirming the presence of the ligand. The very strong intensity absorption band in the region $1599\text{--}1649\text{ cm}^{-1}$ corresponds to the $\nu(\text{C}=\text{N})$ bond vibration. The broad band around $3400\text{--}3100\text{ cm}^{-1}$ is due to hydroxo groups of ligands. The very strong peaks $\nu(\text{CN})$ at 2071 and 2055 cm^{-1} and weak $\nu(\text{CS})$ vibrations at 784 and 760 cm^{-1} correspond to coordinated and non-coordinated thiocyanide group in complexes **15** and **16**, respectively.

In the IR spectrum of **19**, a broad absorption band at $3670\text{--}3130\text{ cm}^{-1}$ is due to the O-H stretching frequency of ligands and ethanol molecules. The strong band $\nu(\text{C}=\text{N})$ at 1630 cm^{-1} indicates the imino group. The characteristic frequency of coordinated SCN group appears at 2044 cm^{-1} .

The thermal investigations of complex **19** were carried out in the temperature range $0\text{--}600^\circ$. A weight loss occurs in stages. The first mass loss starting at 100°C is equal to two molecules of $\text{C}_2\text{H}_5\text{OH}$ ($11,20\%_{\text{ex}}$ versus $11,08\%_{\text{calc}}$). On the DTA curve a well-defined exo-effect probably due to the decomposition of the complex was observed at 495°C . At the same time there is a sharp loss of mass and its output at a constant value, which is retained when further heated to 600°C . The total weight loss is 87% .

2.4.1. $[\text{Mn}^{\text{II}}_2(\text{HL}^2)_2(\text{NCS})_2] \cdot 2\text{C}_2\text{H}_5\text{OH}$

The complex $[\text{Mn}^{\text{II}}_2(\text{HL}^2)_2(\text{NCS})_2] \cdot 2\text{C}_2\text{H}_5\text{OH}$ (**19**) possesses a binuclear structure consisting of two Mn(II) ions, two SCN-groups and two mono-deprotonated ligands. The O, O', O', N, O'' -pentadentate bridging coordinated mode of the HL is observed (Fig. 2.13). The

manganese atoms are linked through two μ -O bridges from phenol groups of the SB, giving the $\{\text{Mn}(\mu\text{-O})_2\text{Mn}\}$ core with a $\text{Mn}\cdots\text{Mn}$ distance of 3.3820(4) Å and MnOMn angles around 105°.

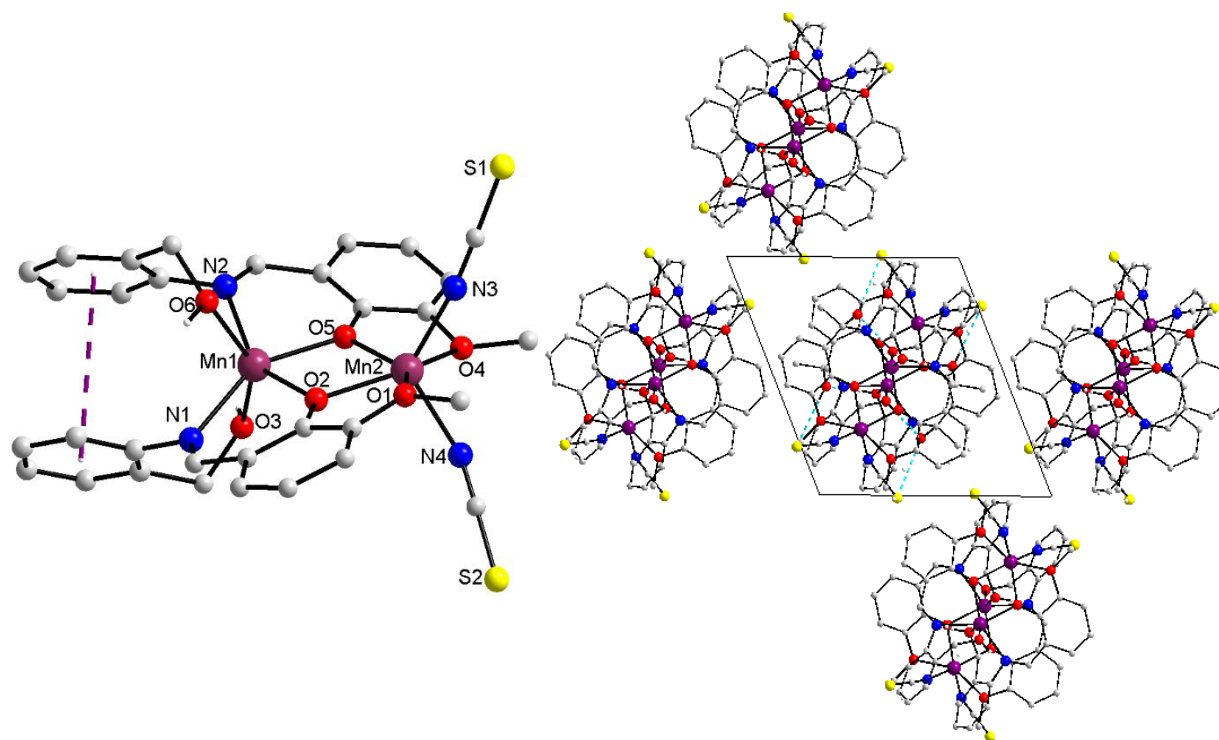


Figure 2.13. The molecular structure (left) and the fragment of the crystal structure along c axis (right) of complex **19**.

The coordination environment of the Mn1 atom is built exclusively by donor atoms of two ligands. The values of the Mn-O/N bond lengths cover the range 2.110-2.241 Å and values of the *cis*-angles and *trans*-angles range from 74.69 to 125.36° and from 146.06 to 149.09°, respectively. Four oxygen atoms from two ligands and two nitrogen atoms of SCN groups are coordinated to the Mn2 atom. The shortest are the Mn-N bonds [2.092-2.099 Å] and the longest connections [2.423-2.431 Å] are formed with the oxygen atom of the methoxy group. The *cis*-angles range from 68.46 to 138.32° and *trans*-angles from 125.64 to 152.64°. The coordination polyhedron for the metal atoms is distorted. The BVS analysis applied to the appropriate bond lengths leads to the +2 oxidation state for Mn1 (1.98) and Mn2 (2.00)¹³. In the complex **19**, between the two benzene rings of ligands it exists π - π stacking interactions with a distance of 3.9 Å.

The uncoordinated molecules of ethanol establish hydrogen bonds with hydroxy group of ligands from one molecule of complex and with coordinated NCS groups from adjacent molecules of complex. The ethanol molecules connect adjacent molecules of complexes by hydrogen bonds forming 1D chains along the c axis (Fig. 2.14, Table 2.7).

The uncoordinated molecules of ethanol establish hydrogen bonds with hydroxy group of ligands from one molecule of complex and with coordinated NCS groups from adjacent molecules of complex. The ethanol molecules connect adjacent molecules of complexes by hydrogen bonds forming 1D chains along the *c* axis (Fig. 2.14, Table 2.7).

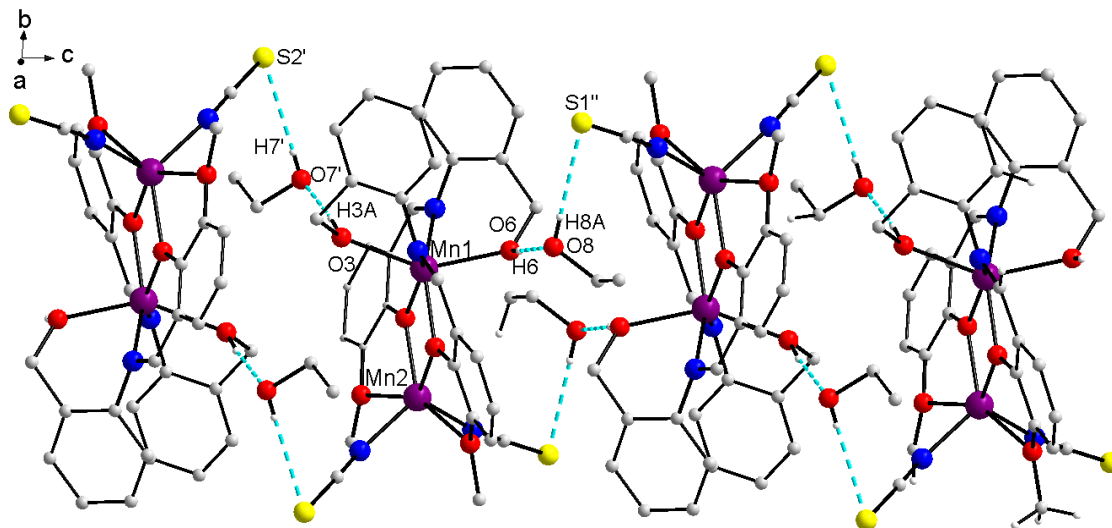


Figure 2.14. Fragment of the crystal structure of the complex **19** showing the hydrogen bonds.

Table 2.7. Hydrogen bond parameters (Å, °) of **19**.

D-H...A	d(D...A)	d(H...A)	angle (D-H...A)
O7-H7...S1	3.321	2.514	177.12
O3-H3A...O7'	2.678	1.852	174.09
O6-H6...O8	2.717	1.857	167.51
O8-H8A...S1''	3.292	2.562	178.71

2.4.2. Manganese (III) coordination polymers

The complexes $[\text{Mn}(\text{HL}^1)_2(\text{NCS})]_n$ (**15**), $\{[\text{Mn}(\text{HL}^4)_2\text{Br}]_n$ (**16**), $\{[\text{Mn}(\text{HL}^4)_2\text{I}]_n$ (**17**), $\{[\text{Mn}(\text{HL}^4)_2\text{NCS}]_n$ (**18**) have one-dimensional polymeric structure. The Mn(III) centers form the bricks of the polymer chains (Fig. 2.17). The crystal lattice of the complexes **16-18** consist of cationic polymeric chains $[\text{Mn}(\text{HL}^{1,4})_2]_n^+$ and counterions X^- (Br, I, SCN). In the case of **15** the crystal packing consists of polymeric chains and it was built out of neutral $[\text{Mn}(\text{HL}^4)_2(\text{NCS})]_n$ units.

The manganese atom is six-coordinated within N_2O_4 and N_3O_3 coordination environments in the complexes **16-18** and **15**, respectively. The pseudo-octahedral (4+2) geometry of the central atom is typical for Mn(III). The deviation from ideal octahedral (O_h) symmetry is minute for the angular parameters (the largest value observed for the **15**) and is mainly observed for the linear parameters (Table 2.8). The differences in the bond lengths of the metal coordination polyhedra are more than 0.4 Å.

Table 2.8. Comparison of geometrical parameters and BVS values for the complexes **15-18**³⁵.

	H₂L¹		H₂L⁴	
	15	16	17	18
Mn—O (short), Å	1.844(2)	1.873(1)	1.871(1)	1.861(3)
Mn—O (long), Å	1.864(2)	2.287(2)	2.288(1)	1.876(3)
	2.340(2)			2.242(3)
Mn—N, Å	2.031(2)	2.029(2)	2.026(2)	2.282(3)
	2.053(2)			2.037(4)
	2.231(2)			2.049(4)
Δ_{\max}^* , Å	0.496(2)	0.414(2)	0.417(2)	0.421(4)
BVS ^{13,36}	3.13	3.00	3.02	3.01
<i>trans</i> -angles, °	178.43(7)	180	180	177.9(2)
	173.02(7)			178.9(1)
	178.39(7)			179.1(2)
Δ_{\max}^* , °	5.41(7)	0	0	2.1(2)
<i>cis</i> -angles, °	84.78(6)–93.89(7)	86.97(6)–93.03(6)	87.33(5)–92.67(5)	87.5(1)–93.6(1)
Δ_{\max}^* , °	9.11(7)	6.06(6)	5.34(5)	6.1(1)

Δ_{\max}^* – the difference between a max and min bond length or angles

The +3 oxidation state for the manganese atom in all complexes has been confirmed by comparison of the bond distances and existence of Jahn–Teller elongation. This is also supported by a bond valence sum analysis (Table 2.8).

In the crystal lattice, the ligands display chelated-bridging function ([2.1₁1₂1₁]¹⁵) creating one dimensional polymeric structure. The anions within the cationic chains are involved in the formation of layers in the *ab* plane. The parallel layers are linked by C–H··· π interactions resulting in formation of 3D supramolecular architecture (Table 2.9, 2.10, Fig. 2.16).

Table 2.9. Hydrogen bond parameters (Å, °) of **15-18**³⁵.

D—H···A	H···A	D···A	D—H···A
15			
O5—H29···S1'	2.66(3)	3.426(2)	155(3)
O6'—H15'···S1'	2.60(3)	3.347(2)	167(3)
16			
O2—H10···Br1'	2.42(1)	3.265(2)	173(3)
17			
O2—H5···I1'	2.66(1)	3.508(1)	172(3)
18			
O3—H5···N3	1.88(4)	2.706(5)	162(8)
O4'—H6'···S1	2.31(6)	3.154(3)	175(9)

Table 2.10. Mn···Mn distances and C–H··· π interactions (Å) for **15-18**³⁵.

	H₂L¹		H₂L⁴	
	15 (NCS)	16 (Br)	17 (I)	18 (NCS)
C–H··· π	–	3.2020(2)	3.3206(1)	2.5930(1)
Mn···Mn	6.6950(4)	5.7196(3)	5.7552(2)	5.7247(9)

The crystal structures of the halide complexes **16** and **17** and $\{[\text{Mn}(\text{HL}^4)_2\text{Cl}]_n\}^{37}$ with H_2L^4 are very similar but not isostructural. We can observe the correlation between the size of the halogen atom and the Mn \cdots Mn distances. Thus, the increase in the radius of the anions in the sequence $\text{Cl}^- (1.81\text{\AA}) < \text{Br}^- (1.97\text{\AA}) < \text{I}^- (2.23\text{\AA})$ leads to an increase in the Mn \cdots Mn distances by *ca* 0.02 \AA . Despite the fact that the size of the SCN group is larger than halogen ions, in complex **18** the distance Mn \cdots Mn is slightly smaller than expected. That can be explained by the difference of the crystal structures, namely the C-H \cdots π interactions (Fig. 2.16).

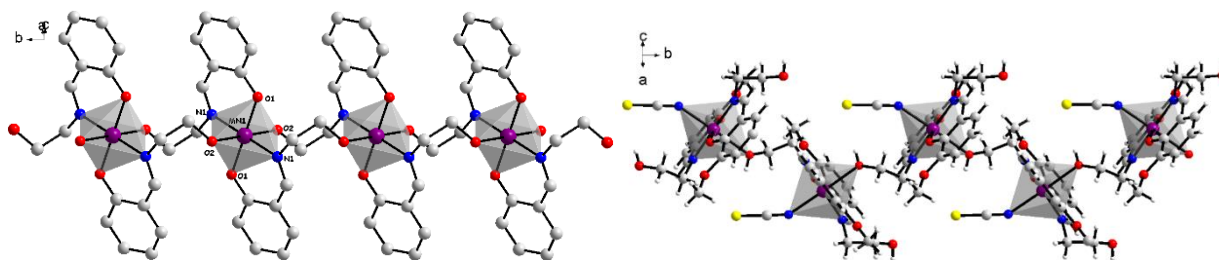


Figure 2.15. Fragment of the polymeric cation $[\text{Mn}(\text{HL}^4)_2]^+_n$ in the complexes **16-18** (left) and fragment of the polymeric chain $[\text{Mn}(\text{HL}^1)_2(\text{NCS})]_n$ in the complex **15** (right) ³⁵.

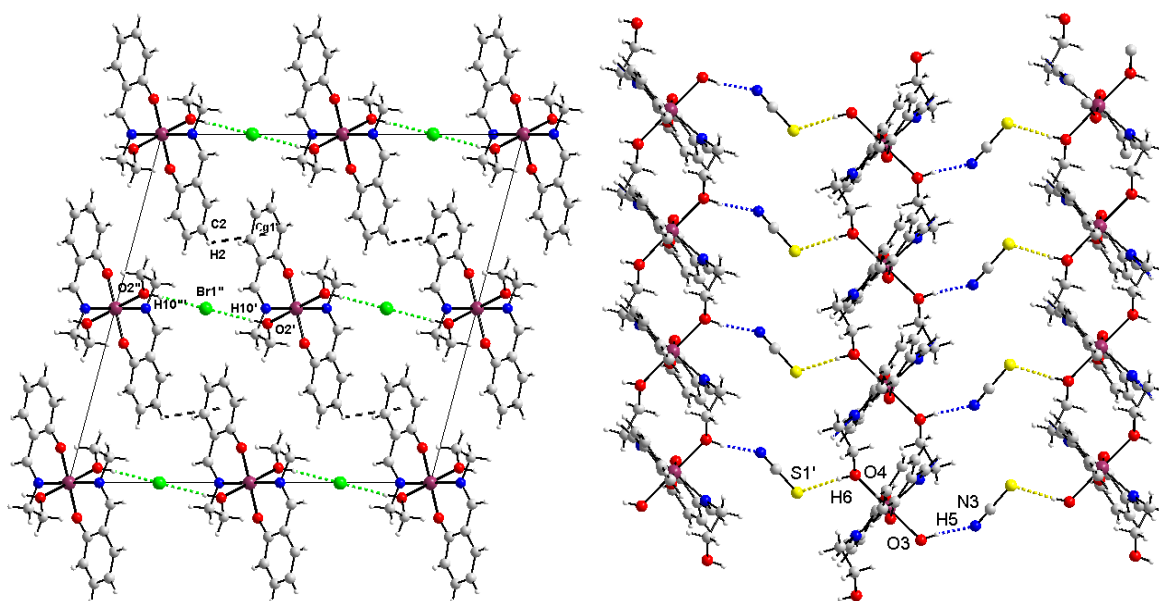


Figure 2.16. Fragment of the crystal structure of the complex **16** (left) and **18** (right) ³⁵.

In the case of the thiocyanate complexes the replacement of H_2L^4 to H_2L^1 leads to the formation of the neutral complex $[\text{Mn}(\text{HL}^1)_2(\text{NCS})]$ (**15**) with a molecular structure different from the complex $\{[\text{Mn}(\text{HL}^4)_2]\text{SCN}\}_n$ (**18**) which has a cationic structure. In complex **15**, the Mn(III) atom forms the $\{\text{MnN}_3\text{O}_3\}$ unit with the two SCN groups and the two SB ligands with *N,O*-bidentate and *O,N,O'*-tridentated bridging coordination mode. The metal atom is displaced from the equatorial plane by 0.07 \AA toward N_{NCS} . The arrangement of manganese atoms within the chain

has a zigzag shape with Mn···Mn distance of 6.7 Å and the angle formed by three nearest atoms being 121.3°. Intra- and intermolecular hydrogen bonds are formed by non-coordinated S_{NCS} atom with OH groups from the aminoalcohol arms of the ligand (Fig. 2.17).

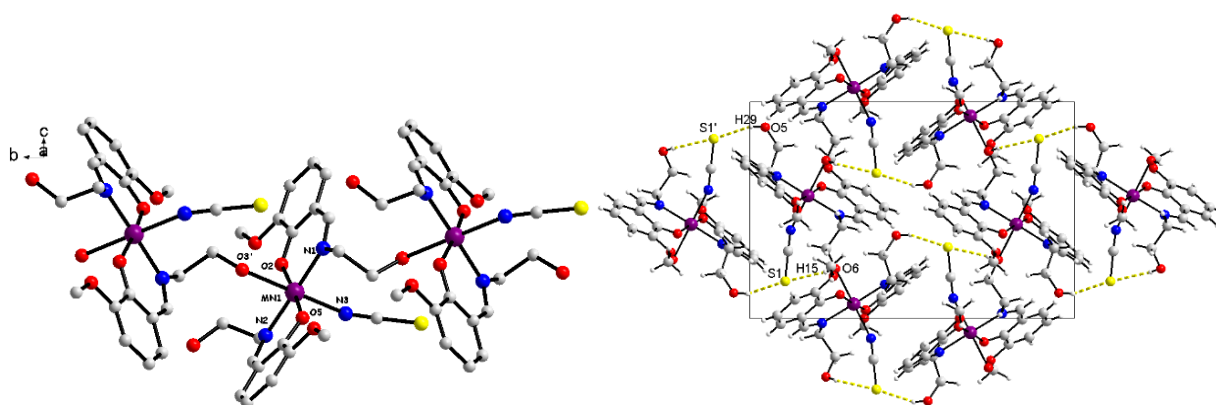


Figure 2.17. Complex **15**: fragment of the polymeric chain (left) and crystal packing view along the *b* axis (right) ³⁵.

2.4.3. EPR spectral studies

It is known that the ground state of the Mn(III) is the even-spin $S = 2$ state. The Mn(III) complexes show typically large zero-field splitting (the *D* parameter of the spin Hamiltonian (1) of a few cm^{-1}). The $M_S = 2$ and $M_S = -2$ levels of the $S = 2$ state are split very little in the absence of the magnetic field (approximately $3E^2/D$) and a nominally “forbidden” $\Delta M_S = 4$ transition sometimes appears in X-Band EPR at an effective $g \sim 8$. A high-field electron paramagnetic resonance (HFEP, ~ 600 GHz) spectroscopy is an effective technique to record all possible transitions in the manganese (III) complexes (Fig. 2.20). To accurately determine the spin Hamiltonian parameters:

$$\hat{H} = \mu_B \mathbf{B} \{ \mathbf{g} \} \hat{\mathbf{S}} + D \left\{ \hat{S}_z^2 - \frac{1}{3} S(S+1) \right\} + E (\hat{S}_x^2 - \hat{S}_y^2) + B_4^0 \mathcal{O}_4^0 + B_4^4 \mathcal{O}_4^4 \quad (1) \quad ^{35},$$

a number of spectra were recorded and the resonance fields were plotted versus the microwave frequency. The spin Hamiltonian parameters which were found from fitted the obtained dependencies are shown in Table 2.11.

A high-field electron paramagnetic resonance (HFEP) methods was used for the complexes **13-18** and for the previously reported complexes $\{[\text{Mn}(\text{HL}^1)_2]\text{I}\}_n$ ³⁸ and $\{[\text{Mn}(\text{HL}^4)_2]\text{Cl}\}_n$ ³⁷ with similar structures.

In contrast to other compounds, complex $[\text{Mn}(\text{HL}^1)_2(\text{NCS})]_n$ (**15**) contains a coordinated SCN group in the coordination sphere Mn (III). Therefore, we were interested to compare it's the

spin Hamiltonian parameters to those of the other compounds that contain uncoordinated anion. The value of D parameter for the complexes ranges from 3.197 to -3.44 cm^{-1} and is the largest for **15** (Table 2.11). A larger range was observed for the E parameter (from -0.525 to -0.77 cm^{-1}). The complexes with H_2L^2 have more distorted structures compared to those of H_2L^1 ligand thanks it the E parameter tends to be larger.

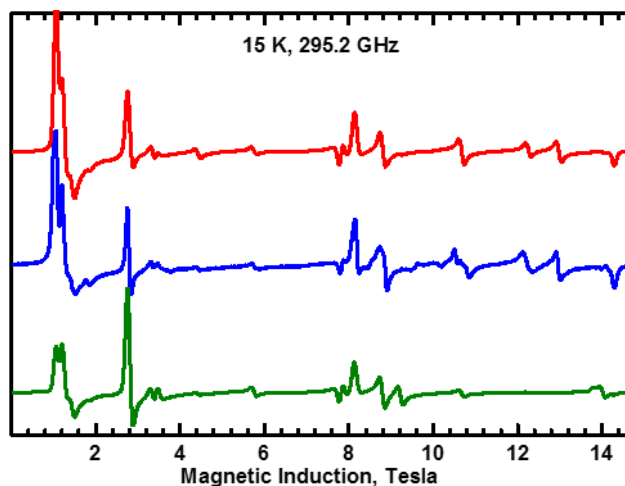


Figure 2.18. HFEPR spectrum of **18**. Medium – experimental; top – simulated using parameters from Table 2.11; down – simulated with the signs of D and E inverted ³⁵.

Table 2.11. Experimental spin Hamiltonian parameters³⁵.

Complex	g_x	g_y	g_z	D, cm^{-1}	E, cm^{-1}
13	2.001(2)	1.997(1)	1.998(2)	$-3.271(2)$	$-0.663(1)$
14	1.999(1)	1.997(1)	2.000(1)	$-3.290(2)$	$-0.699(2)$
$\{[\text{Mn}(\text{HL}^1)_2\text{I}]_n\}$	1.999(9)	1.961(4)	1.990(6)	$-3.34(1)$	$-0.76(1)$
15	2.00 (1)	1.97(1)	1.96 (1)	$-3.44(1)$	$-0.77(1)$
$\{[\text{Mn}(\text{HL}^4)_2\text{Cl}]_n\}$	1.982(4)	1.985(4)	1.998(2)	$-3.231(2)$	$-0.578(2)$
16	1.980(2)	1.974(2)	1.988(3)	$-3.223(3)$	$-0.548(2)$
17	1.984(4)	1.963(3)	1.998(5)	$-3.197(3)$	$-0.525(3)$
18	1.998(1)	1.986(1)	1.992(2)	$-3.296(3)$	$-0.662(2)$

The Density functional theory (DFT) and *ab initio* methods have been performed to get the zero-field splitting contribution. The spin-orbit coupling contribution to D and E was calculated using the state-averaged complete active space self-consistent field (CASSCF) approach, with four electrons in 5 orbitals (5 quintet and lowest 35 triplet states were taken into account)³⁹⁻⁴¹. Functional B3LYP in the ORCA software package^{14,42} was employed with TZVPP basis set for Mn and all coordinated atoms and SVP^{43,44} bases set for all remaining atoms. The “coupled-perturbed” scheme implementing in ORCA was used to calculate the spin-spin contribution. The calculated dates coincide well with the experimental values (Table 2.12).

Table 2.12. Experimental and calculated zero-field splitting parameters³⁵.

	13	15	16	17	18
$D_{\text{exp}}, \text{cm}^{-1}$	-3.271	-3.44	-3.223	-3.197	-3.296
$D_{\text{calc}}, \text{cm}^{-1}$	-3.458	-3.507	-3.419	-3.453	-3.431
$E_{\text{exp}}/D_{\text{exp}}$	0.20	0.21	0.17	0.16	0.20
$E_{\text{calc}}/D_{\text{calc}}$	0.16	0.18	0.13	0.13	0.15
$D_{\text{so}}^{\text{a}}, \text{cm}^{-1}$	-3.005	-3.064	-2.958	-2.991	-2.978
$E_{\text{so}}^{\text{a}}, \text{cm}^{-1}$	-0.493	-0.576	-0.393	-0.401	-0.482
$D_{\text{ss}}^{\text{b}}, \text{cm}^{-1}$	-0.453	-0.443	-0.461	-0.462	-0.453
$E_{\text{ss}}^{\text{b}}, \text{cm}^{-1}$	-0.046	-0.042	-0.038	-0.039	-0.046

^aSpin-orbit coupling contribution. ^bSpin-spin contribution.

It is interesting to compare the complexes **15** to **18**, which contain a coordinated and uncoordinated thiocyanate group, respectively. Thus, for **15** the calculated values of $D = -3.507 \text{ cm}^{-1}$ and $E = -0.578 \text{ cm}^{-1}$ correlate well with the experimental ones (Table 2.12). The spin-spin contributions to D and E was -3.064 cm^{-1} and -0.576 cm^{-1} , respectively, while the spin-orbit coupling related contribution were -0.443 cm^{-1} and -0.042 cm^{-1} , respectively. For **18** the calculations produced $D = -3.432 \text{ cm}^{-1}$ and $E = -0.528 \text{ cm}^{-1}$ (the spin-orbit contribution to D and E are -0.453 cm^{-1} and -0.046 cm^{-1} , respectively, and spin-spin contributions are -2.978 cm^{-1} and -0.482 cm^{-1}). Thus, changing the composition of the coordination sphere from N_3O_3 (**15**) to N_2O_4 (**18**) does not lead to significant changes in the value of parameter D .

To verify the presence of exchange interactions between Mn (III) centres DFT calculation was performed in the ORCA program using similarly as in the calculations of D above, functional and basis sets. A fragment containing two Mn ions was cut out of the chain of **18** and a broken-symmetry calculation was carried out. An exchange integral value J of just 0.02 cm^{-1} (antiferromagnetic, using the Heisenberg-Dirac-Van Vleck Hamiltonian, $H = JS_1S_2$) was obtained. The same value is obtained when calculating exchange interactions through the hydrogen bridges involving the SCN^- ion in **18**. For complex **15**, the calculated value of J is 0.04 cm^{-1} , although the distance $\text{Mn}\cdots\text{Mn}$ in the chain 6.695 \AA is longer than in **18** (5.725 \AA). It should be mentioned here that the magnitude of the exchange interactions depends less on the interatomic distance than on the nature of a bridge between the metal atoms.

2.5. Tautomerism in H_2L^2

Recently, a number of works have been published on the study of the keto-enol tautomerism in salicylidene type of SB⁴⁵⁻⁴⁹. This research has shown that the OH form is in general more stable than the NH form. The stability of the NH form can be increased at low temperatures in the presence of aggregate forces or donor solvents. Also, the formation of a certain OH/NH

form may be partially influenced by internal (the nature and position of substituent groups in the structure of SB^{46,47}) and external (packing forces, temperature and solvent) factors⁴⁸⁻⁵⁰.

In the investigation of systems with H_2L^2 it was observed formation of mixtures that include a crystalline precipitate of pure ligand. The colour of the precipitate varies from bright orange to red depending on the selected solvent. Therefore, the condensation of 2-aminobenzyl alcohol and *o*-vanillin in different solvents was investigated. It has been found that unsolvated H_2L^2 (**20**) is formed from ethanol, DMF, DMSO or acetonitrile solutions. Its pseudo-polymorphs $\text{H}_2\text{L}^2 \cdot \text{CH}_3\text{OH}$ (**20a**) and $\text{H}_2\text{L}^2 \cdot \text{H}_2\text{O}$ (**20b**) were obtained from methanol and water, respectively (Fig. 2.19).

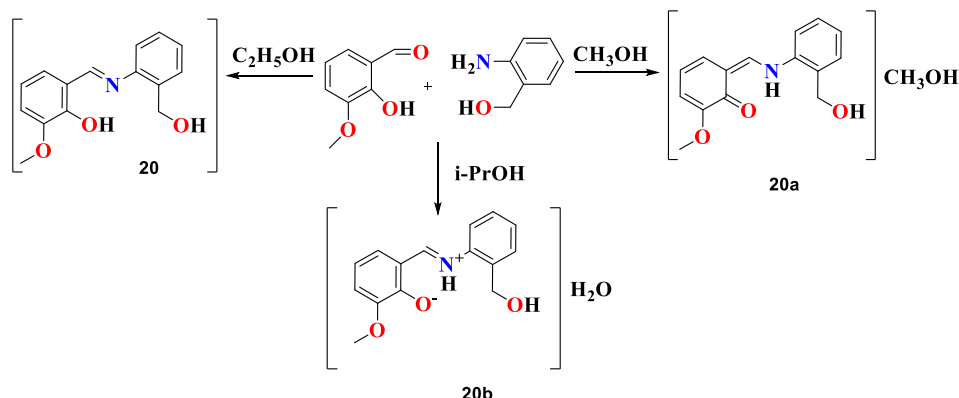


Figure 2.19. Syntheses of **20-22b**⁵¹.

For the assignment of the tautomeric form in the salicylidene SBs commonly used are the crystallographic criteria with the following geometrical parameters: (1) the values of the C8-N and C7-O bond lengths (atoms numbering are shown in Figure 2.20) should be close to 1.362 Å (single bond) and 1.222 Å (double bond) for the keto form and vice versa for the enol forms; (2) the C6-C8 bond length is longer than the C6-C7 in the keto form and shorter than the C6-C7 for enol form; (3) the lengths of all C-C bonds of the benzaldehyde ring are approximately the same for the enol form, whereas in the keto form, the long and short bonds usually alternate; (4) intramolecular N-H \cdots O in the keto form is weaker than OH \cdots N hydrogen bond in the enol form.

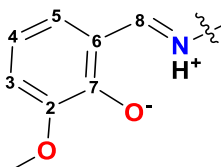


Figure 2.20. Fragment of the SB with atom numbering⁵¹.

Table 2.13. Selected bond distances (Å) for **20-20b** ⁵¹.

	20	20a	20b
C(8) - N(1)	1.2806(16)	1.308(2)	1.296(2)
C(7) - O(2)	1.3446(14)	1.292(2)	1.320(2)
C(9) - N(1)	1.4142(16)	1.416(2)	1.412(2)
C(1) - O(1)	1.4251(15)	1.427(2)	1.431(2)
C(2) - O(1)	1.3586(15)	1.362(2)	1.370(2)
C(15) - O(3)	1.4215(16)	1.415(2)	1.417(2)
Aldehyde part			
C(6) - C(8)	1.4492(17)	1.417(2)	1.434(2)
C(6) - C(7)	1.4047(17)	1.429(3)	1.418(2)
C(6) - C(5)	1.4077(17)	1.418(3)	1.410(2)
C(5) - C(4)	1.3729(19)	1.366(3)	1.372(3)
C(4) - C(3)	1.3992(19)	1.413(3)	1.406(2)
C(3) - C(2)	1.3833(17)	3.373(3)	1.374(2)
C(2) - C(7)	1.4113(17)	1.443(3)	1.420(2)
Amine part			
C(9) - C(10)	1.4015(17)	1.391(3)	1.398(2)
C(9) - C(14)	1.4029(18)	1.397(3)	1.400(2)
C(10) - C(11)	1.3849(19)	1.383(3)	1.385(3)
C(11) - C(12)	1.383(2)	1.386(3)	1.387(3)
C(12) - C(13)	1.388(2)	1.380(3)	1.384(3)
C(13) - C(14)	1.3931(18)	1.396(3)	1.394(2)
C(14) - C(15)	1.5092(17)	1.514(3)	1.515(2)
N(1) - H(1)	-	0.93(3)	0.98(7)

The corresponding C-O, C-N, C-C bond lengths in the **20-20b** are typical for SB (Table 2.13). According to the crystallographic criteria (1)-(3) **H₂L²** has an enol, keto and keto-enol form in **20**, **20a** and **20b**, respectively. But an intramolecular N-H...O hydrogen bond in **20a** is noticeably shorter than the corresponding O-H...N hydrogen bond in **20** (Table 2.13.), which does not correspond to the criterion (4). If assumed that the NH-keto tautomer is in resonance with the zwitterionic form having an ionic (N⁺-H...O⁻) character, it may explain such a strong hydrogen bond in the compound **20a**. So the crystal structure **20b** can be interpreted as a mixture of OH-enol and NH-zwitterionic forms.

Thus, the analyzed crystallographic data strongly suggest that the keto-enol tautomerism of **H₂L²** in solid state is a complex system resulting from different NH-OH equilibria (Fig. 2.21).

According to the results of X-ray diffraction analysis the unsolvated **H₂L²** (**20**) crystallizes in the enol form, while its methanol solvent **H₂L²·CH₃OH** (**20a**) and monohydrate solvent **H₂L²·H₂O** (**20b**) are possessing keto or mixed enol-zwitterionic (~ 1:1) forms respectively.

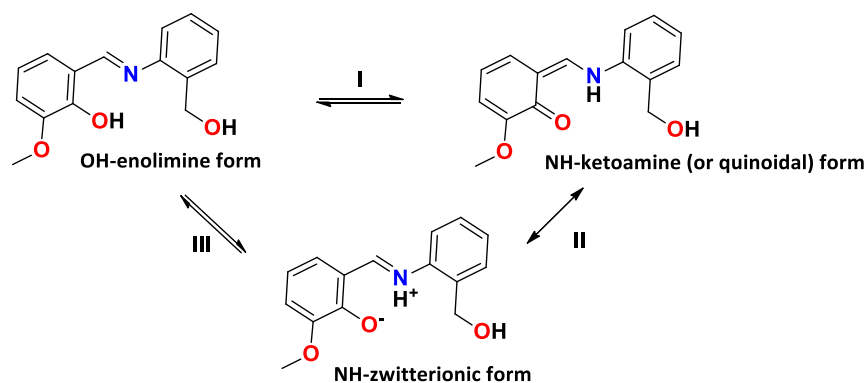


Figure 2.21. Keto-enol tautomerism in $\mathbf{H}_2\mathbf{L}^{251}$.

The parameters of intra- and intermolecular H-bonds are given in Table 2.14. Due to intermolecular H-bonds in the crystal lattice of **20** and **20a** helical structures were generated. In the case of **20b** the double chains form a 1D supramolecular architecture (Fig. 2.23-25).

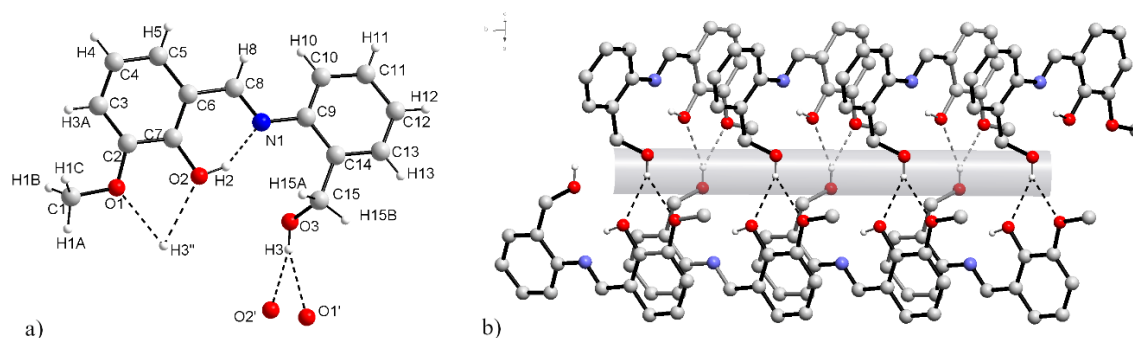


Figure 2.23. Molecular structure (a) and fragment of the helical structure based on intermolecular H-bonds (b) of the compound **20**⁵¹.

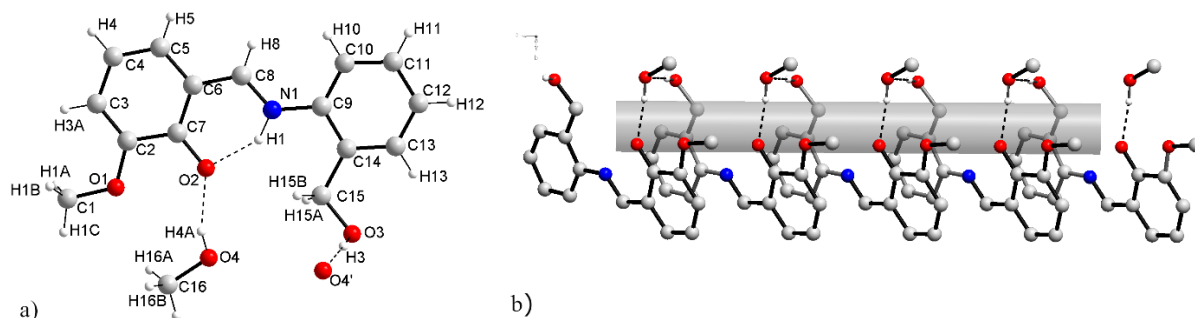


Figure 2.24. Molecular structure (a) and fragment of the helical structure based on intermolecular H-bonds (b) of the compound **20a**⁵¹.

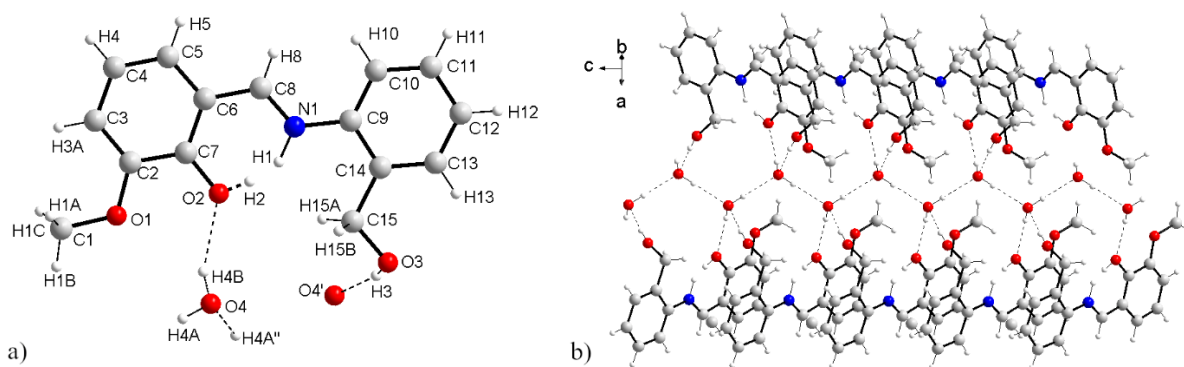


Figure 2.25. Molecular structure (a) and fragment of the double chain (b) of the compound **20b**⁵¹.

Table 2.14. Hydrogen bond parameters (Å, °) of **20**, **20a** and **20b**⁵¹.

	D – H...A	H...A	D...A	< D – H...A
Intramolecular H-bonds				
20	O2 – H2...N1	1.76(2)	2.581	150(2)
20a	N1 – H1...O2	1.71(3)	2.510	143(3)
20b	N1 – H1...O2	1.68	2.518	141.0
	O2 – H2...N1	1.76	2.518	149.4
Intermolecular H-bonds				
20	O3 – H3...O1'	2.22	2.844	133.3
	O3 – H3...O2'	2.32	3.087	155.55
20a	O3 – H3...O4'	1.91(4)	2.716	176(3)
	O4 – H4A...O2	1.85(2)	2.661	159(3)
20b	O4 – H4B...O2	1.99	2.775	153.4
	O3 – H3...O4'	2.03	2.835	167.0
	O4 – H4A...O4'	2.00	2.847	175.6

The aim of performed DFT calculations was to compare the relative stability of the keto and enol forms for the compounds **20-20b**. All calculation were performed by means of the Gaussian 09 software at the PBE0/6-311++G(2df,2pd) level of theory⁵²⁻⁵⁵. Keto and enol tautomers were generated from the X-ray structures by moving the H position. When the structure includes a second molecule involved in a hydrogen bond with the SB, this second molecule was removed to isolate the role of this interaction.

The compound **20** demonstrates a clear stability of the enol isomer, the keto isomer did not converge. The X-ray data for **20** confirmed this result. For the compound **20a** two isomers have practically the same the stability, the small difference in total energies (0.2 kcal·mol⁻¹) being in favour of the enol form. However, the keto form is more stable (by 0.3 kcal·mol⁻¹) when the Gibbs free energies was used. In the solid state, the compound **20a** contains a keto form of ligand and methanol molecule. The results of the calculations confirm the strong effect of the HB since without methanol the energy differences are larger than 4 kcal·mol⁻¹. For compound **20b**, the enol form is more stable regardless of the presence or absence the molecule of water. Thus, the calculations show a significant effect of HB on the stabilization of tautomers. Comparing the

Hirshfeld charges we can note the N atom are positive in the keto form and negative in the enol form. The O charges are more negative in the keto form than in the enol form (Table 2.15).

Table 2.15. Total molecular energies, Gibbs free energies, Hirshfeld charges ⁵¹.

	form	ΔE (0 K) keto/enol	ΔG (RT) keto/enol	ΔG (RT)	N charge	O charge
20	enol			1.1	-0.14	-0.08
20a	keto	0.2	0		0.04	-0.25
20a	enol	0	0.3		-0.19	-0.06
20a (no CH ₃ OH)	keto	0	0	0	0.03	-0.28
20a (no CH ₃ OH)	enol	4.7	4.0	4.0	-0.14	-0.07
20b	keto	0.4	1.6		0.04	-0.25
20b	enol	0	0		-0.13	-0.06
20b (no H ₂ O)	keto	4.1	2.9	2.9	0.03	-0.28
20b (no H ₂ O)	enol	0	0	0.1	-0.14	-0.07

The absorption spectra of all compounds have identical shape. In Figure 2.25, the calculated absorption spectra of **20b** for the keto and enol forms are compared to the experimental one measured in acetonitrile. Electron density difference (EDD) plots corresponding to the transition from the ground state to the excited state are represented in Figure 2.26. According to the calculations, a clear difference between the two isomers is expected in the 400-500 nm range (Fig. 2.25). For the optimized enol isomer the first band form around 340 nm is a combination of two transitions S_1 (HOMO-1 \rightarrow LUMO) and S_2 (mainly of HOMO-1 \rightarrow LUMO). For the keto form the band at 441 nm correspond to S_1 , while the next intense transition is S_3 at 329 nm results predominantly from the HOMO-1 \rightarrow LUMO excitation. The experimental spectrum shows no band above 400 nm, therefore it mostly corresponds to the enol form.

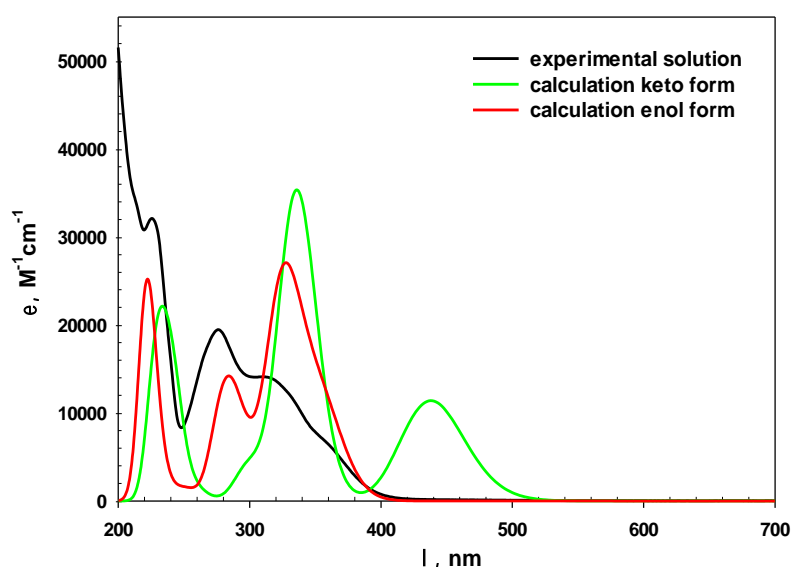


Figure 2.25. UV-vis spectra of **20b**: experimental ($3.5 \cdot 10^{-5}$ M in acetonitrile), calculated keto and enol form⁵¹.

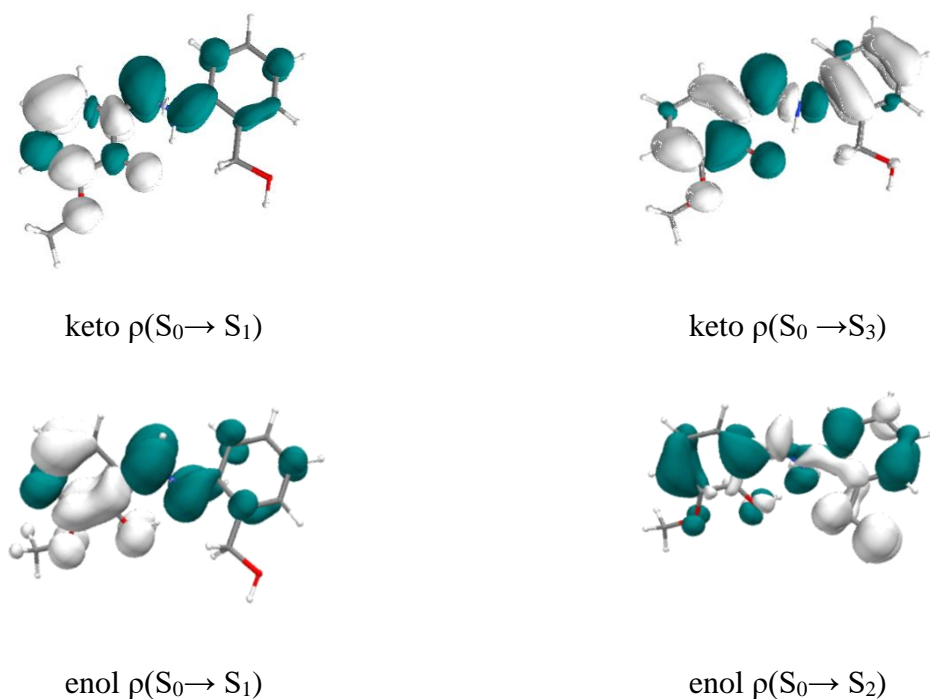


Figure 2.26. Density difference plots for enol and keto forms for compound **20b** (blue regions correspond to the excited electron density whereas the white region correspond to the hole)⁵¹.

The compounds **20-20b** exhibit luminescence in the solid state (Fig. 2.27). As an example, the calculated and experimental spectra of **20b** are presented in Figure 2.27. The calculated emission maximum at 573 nm is in good accordance with the experimental spectra at 590 nm after excitation at 490 nm. In contrast to the solid state, all compounds are not luminescent in solution.

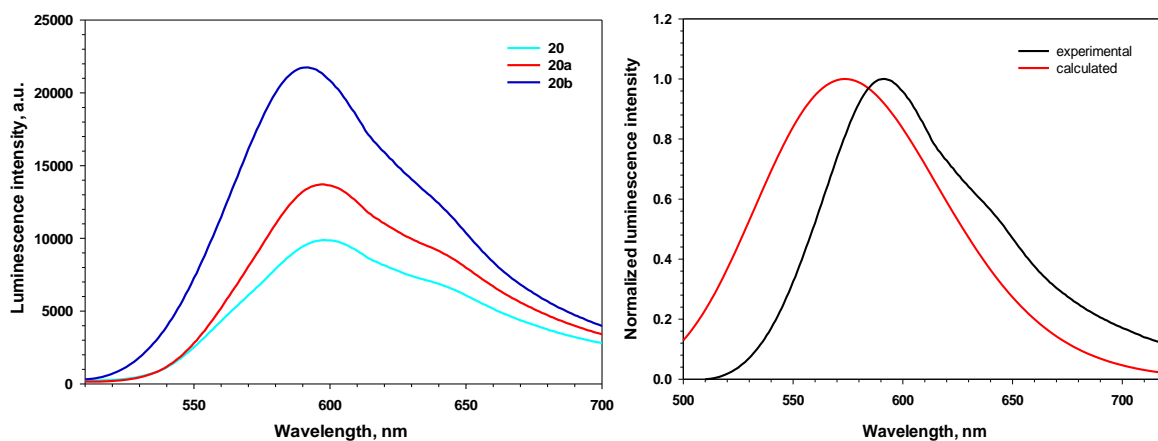


Figure 2.27. Luminescence emission spectra of **20-20b** (left) in the solid state and normalized experimental and calculated emission spectra of **20b** (right)⁵¹.

2.6. Conclusion

It was found that the most appropriate system to produce heterometallic *d-s* complexes was the system **II** using metallic copper and alkaline earth metal oxides. A series of *d-s* heterometallic Cu/M (M = Ca, Sr, Ba) complexes with the SB derivatives of *o*-vanillin was obtained. The

complexes **2-9** have similar structures. The basis of their structure consists of trinuclear double-charged complex cations $[M\{Cu(HL^1)_2\}_2]^{2+}$ ($M = Ca, Sr, Ba$), the formation of which can be considered as a result of coordination of two neutral $Cu(HL^1)_2$ molecules to the central *s*-metal. The molecules of $Cu(HL^1)_2$ act as four-dentate ligands of the chelate type. The structure of the complex $[Cu(L^3)_2Ca(NCS)_2(H_2O)]$ (**12**) is based on the binuclear fragment $\{Cu(\mu-O)_2Ca\}$. The fragment $\{Cu(L^3)_2\}$ acts as a chelating tetradentate ligand, which coordinates to the calcium atom. The crystal lattices of the analyzed compounds are characterized by different types of intermolecular and intramolecular hydrogen bonds with the participation of solvent molecules, uncoordinated anions and hydroxyl groups of SB.

A number of trivalent manganese compounds with the general formula $Mn(HL^{1,4})_2X$ ($X = Cl, Br, I, NCS$) (**13-18**) and a divalent manganese complex $[Mn^{II}_2(HL^2)_2(NCS)_2] \cdot 2C_2H_5OH$ (**19**) which contains a binuclear fragment $\{Mn(\mu-O)_2Mn\}$ have been isolated. The structure of halide complexes of trivalent manganese is based on the cationic chains $[Mn(HL^{1,4})_2]^{+n}$, while thiocyanate complexes (**15, 18**) contain both cationic and neutral chains depending on the structure of the ligand.

By comparing the spin-Hamiltonian parameters, it was noted that complex **15**, which unlike similar ones contains in the coordination sphere both the SB and the coordinated thiocyanate group, shows the largest values of the parameters E and D. In this case, greater distortion of the complex structure leads to an increase of value of the parameter E. The presence of weak antiferromagnetic exchange interactions between Mn(III) atoms through $\{-NCCO-\}$ bridges is supported by quantum chemical calculations.

It was shown that the ligand H_2L^2 in the solid state exists in the enol (**20**), keto (**20a**) and mixed enol-zwitterionic (**20b**) tautomeric forms depending by the nature of the solvent or the absence of the latter. Quantum chemical calculations of this ligand are in the good correlation with the results of X-ray structural data and reveal significant influence of hydrogen bonds on the stability of tautomeric forms. The ligand and its solvate forms show luminescent properties.

References

1. Fujita, M.; Umemoto, K.; Yoshizawa, M.; Fujita, N.; Kusukawa, T.; Biradha, K. *Chem. Commun.* **2001**, *6*, 509–518.
2. Winpenny, R. E. P. *J. Chem. Soc. Dalton Trans.* **2002**, *1*, 1–10.
3. Escriche-Tur, L.; Jover, J.; Font-Bardia, M.; Aullón, G.; Corbella, M. *Inorg. Chem.* **2015**, *54* (24), 11596–11605.
4. Hewitt, I. J.; Tang, J.-K.; Madhu, N. T.; Clérac, R.; Buth, G.; Anson, C. E.; Powell, A. K. *Chem. Commun.* **2006**, *25*, 2650–2652.
5. Alaimo, A. A.; Koumoussi, E. S.; Cunha-Silva, L.; McCormick, L. J.; Teat, S. J.; Psycharis, V.; Raptopoulou, C. P.; Mukherjee, S.; Li, C.; Gupta, S. D.; Escuer, A.; Christou, G.; Stamatatos, T. C. *Inorg. Chem.* **2017**, *56* (17), 10760–10774.
6. Datta, A.; Das, K.; Massera, C.; Clegg, J. K.; Sinha, C.; Huang, J.-H.; Garribba, E. *Dalton Trans.* **2014**, *43* (14), 5558–5563.
7. Zhang, J.; Cheng, S.; Wang, X.; Yuan, L.; Xue, M.; Wang, Y.; Liu, W. *CrystEngComm* **2013**, *15* (30), 6074–6082.
8. Chang, X.; Jiang, L.-T.; Chen, S.-C.; He, M.-Y.; Chen, Q. *J. Coord. Chem.* **2020**, *73* (3), 439–452.
9. Chiboub Fellah, F. Z.; Costes, J.-P.; Dahan, F.; Duhayon, C.; Tuchagues, J.-P. *Polyhedron* **2007**, *26* (15), 4209–4215.
10. Kokozay, V. N.; Vassilyeva, O. Yu.; Makhankova, V. G.; Kharisov, B., Ed.; Elsevier, **2018**; 183–237.
11. Li, L. Z.; Zhao, C.; Xu, T.; Ji, H. W.; Yu, Y. H.; Guo, G. Q.; Chao, H. *J. Inorg. Biochem.* **2005**, *99* (5), 1076–1082.
12. Plyuta, N.; Vassilyeva, O. Y.; Kokozay, V. N.; Omelchenko, I.; Petrusenko, S. *Acta Crystallogr. Sect. E.* **2020**, *76* (3), 423–426.
13. Brown, I. D.; Altermatt, D. *Acta Crystallogr., Sect B* **1985**, *41* (4), 244–247.
14. Chen, H.; Adams, S. *IUCrJ* **2017**, *4* (5), 614–625.
15. Coxall, R. A.; Harris, S. G.; Henderson, D. K.; Parsons, S.; Tasker, P. A.; Winpenny, R. E. P. *J. Chem. Soc. Dalton Trans.* **2000**, *14*, 2349–2356.
16. Mondal, S.; Hazra, S.; Sarkar, S.; Sasmal, S.; Mohanta, S. *J. Mol. Struct.* **2011**, *1004* (1), 204–214.
17. Chandrasekhar, V.; Senapati, T.; Dey, A.; Das, S.; Kalisz, M.; Clérac, R. *Inorg. Chem.* **2012**, *51* (4), 2031–2038.
18. Bernstein, J.; Davis, R. E.; Shimoni, L.; Chang, N.-L. *Angew. Chem. Int. Ed. Engl.* **1995**, *34* (15), 1555–1573.

19. Lluell, M.; Casanova, D.; Girera, J.; Alemany, P.; Alvarez, S. SHAPE, version 2.1; Universitat de Barcelona: Barcelona, Spain.
20. Alvarez, S.; Alemany, P.; Casanova, D.; Cirera, J.; Lluell, M.; Avnir, D. *Coord. Chem. Rev.* **2005**, *249*, 1693–1708.
21. Alvarez, S. *Dalton Trans.* **2013**, *42* (24), 8617–8636.
22. Yang, L.; Powell, D. R.; Houser, R. P. *Dalton Trans.* **2007**, *9*, 955–964.
23. Addison, A. W.; Rao, T. N.; Reedijk, J.; Rijn, J. van; Verschoor, G. C. *J. Chem. Soc. Dalton Trans.* **1984**, *7*, 1349–1356.
24. Liu, W.; Thorp, H. H. *Inorg. Chem.* **1993**, *32* (19), 4102–4105.
25. Wood, R. M.; Palenik, G. J. *Inorg. Chem.* **1998**, *37* (16), 4149–4151.
26. Gagné, O. C.; Hawthorne, F. C. *Sci. Cryst. Eng. Mater.* **2015**, *71* (5), 562–578.
27. Davidenko, N. A.; Davidenko, I. I.; Kokozay, V. N.; Studzinsky, S. L.; Petrusenko, S. R.; Plyuta, N. I. *J. Appl. Spectrosc.* **2015**, *82* (5), 750–754.
28. Davidenko, N. A.; Kokozay, V. N.; Studzinsky, S. L.; Petrusenko, S. R.; Plyuta, N. I.; Davidenko, I. I. *J. Appl. Spectrosc.* **2018**, *84* (6), 1056–1060.
29. Davidenko, N.; Kokozay, V.; Studzinsky, S.; Petrusenko, S.; Plyuta, N. *Visnyk Kyivskoho Natsionalnoho Universytetu Im. Tarasa Shevchenk* **2015**, *51*, 5–8.
30. Kokozay, V.; Pocas, O.; Petrusenko, S.; Plyuta, N. Patent Patent of Ukraine № 121713, **2020**.
31. Tercero, J.; Ruiz, E.; Alvarez, S.; Rodríguez-Forteza, A.; Alemany, P. *J. Mater. Chem.* **2006**, *16* (26), 2729–2735.
32. Ruiz, E.; Rodríguez-Forteza, A.; Alemany, P.; Alvarez, S. *Polyhedron* **2001**, *20* (11), 1323–1327.
33. Rutherford, A. W.; Boussac, A. *Science* **2004**, *303* (5665), 1782–1784.
34. Zouni, A.; Witt, H.-T.; Kern, J.; Fromme, P.; Krauss, N.; Saenger, W.; Orth, P. *Nature* **2001**, *409* (6821), 739–743.
35. Stetsiuk, O.; Plyuta, N.; Avarvari, N.; Goreshnik, E.; Kokozay, V.; Petrusenko, S.; Ozarowski, A. *Cryst. Growth Des.* **2020**, *20* (3), 1491–1502.
36. Thorp, H. H. *Inorg. Chem.* **1992**, *31* (9), 1585–1588.
37. Zhang, L.-F.; Ni, Z.-H.; Zong, Z.-M.; Wei, X.-Y.; Ge, C.-H.; Kou, H.-Z. *Acta Crystallogr., Sect. C* **2005**, *61* (12), 542–544.
38. Petrusenko, S. R.; Stetsyuk, O. M.; Omelchenko, I. V. *Acta Crystallogr. Sect. E* **2013**, *69* (6), 326–327.
39. Shova, S.; Vlad, A.; Cazacu, M.; Krzystek, J.; Bucinsky, L.; Breza, M.; Darvasiová, D.; Rapta, P.; Cano, J.; Telsler, J.; Arion, V. B. *Dalton Trans.* **2017**, *46* (35), 11817–11829.

40. Duboc, C.; Ganyushin, D.; Sivalingam, K.; Collomb, M.-N.; Neese, F. *J. Phys. Chem. A* **2010**, *114* (39), 10750–10758.
41. Pascual-Álvarez, A.; Vallejo, J.; Pardo, E.; Julve, M.; Lloret, F.; Krzystek, J.; Armentano, D.; Wernsdorfer, W.; Cano, J. *Chem. Eur. J.* **2015**, *21* (48), 17299–17307.
42. Neese, F. *Comput. Mol. Sci.* **2012**, *2* (1), 73–78.
43. Schäfer, A.; Horn, H.; Ahlrichs, R. *J. Chem. Phys.* **1992**, *97* (4), 2571–2577.
44. Eichkorn, K.; Weigend, F.; Treutler, O.; Ahlrichs, R. *Theor. Chem. Acc.* **1997**, *97* (1), 119–124.
45. Hadjoudis, E.; Mavridis, I. M. *Chem. Soc. Rev.* **2004**, *33* (9), 579–588.
46. Chatziefthimiou, S. D.; Lazarou, Y. G.; Hadjoudis, E.; Dziembowska, T.; Mavridis, I. M. *J. Phys. Chem. B* **2006**, *110* (47), 23701–23709.
47. Galić, N.; Cimerman, Z.; Tomisić, V. *Spectrochim. Acta. A. Mol. Biomol. Spectrosc.* **2008**, *71* (4), 1274–1280.
48. Minkin, V. I.; Tsukanov, A. V.; Dubonosov, A. D.; Bren, V. A. *J. Mol. Struct.* **2011**, *998* (1), 179–191.
49. Pis-Diez, R.; Echeverría, G. A.; Piro, O. E.; Jios, J. L.; Parajón-Costa, B. S. *A New J. Chem.* **2016**, *40* (3), 2730–2740.
50. Ogawa, K.; Harada, J. *J. Mol. Struct.* **2003**, *647* (1), 211–216.
51. Plyuta, N.; Kokozay, V.; Cauchy, T.; Avarvari, N.; Goresnik, E.; Petrusenko, S. *ChemistrySelect* **2019**, *4* (27), 7858–7865.
52. Frisch, M. J.; Trucks, G. W.; Schlegel, H. B.; Scuseria, G. E.; Robb, M. A.; Cheeseman, J. R.; Scalmani, G.; Barone, V.; Mennucci, B.; Petersson, G. A.; Nakatsuji, H.; Caricato, M.; Li, X.; Hratchian, H. P.; Izmaylov, A. F.; Bloino, J.; Zheng, G.; Sonnenberg, J. L.; Hada, M.; Ehara, M.; Toyota, K.; Fukuda, R.; Hasegawa, J.; Ishida, M.; Nakajima, T.; Honda, Y.; Kitao, O.; Nakai, H.; Vreven, T.; Montgomery, J. A., Jr.; Peralta, J. E.; Ogliaro, F.; Bearpark, M.; Heyd, J. J.; Brothers, E.; Kudin, K. N.; Staroverov, V. N.; Kobayashi, R.; Normand, J.; Raghavachari, K.; Rendell, A.; Burant, J. C.; Iyengar, S. S.; Tomasi, J.; Cossi, M.; Rega, N.; Millam, J. M.; Klene, M.; Knox, J. E.; Cross, J. B.; Bakken, V.; Adamo, C.; Jaramillo, J.; Gomperts, R.; Stratmann, R. E.; Yazyev, O.; Austin, A. J.; Cammi, R.; Pomelli, C.; Ochterski, J. W.; Martin, R. L.; Morokuma, K.; Zakrzewski, V. G.; Voth, G. A.; Salvador, P.; Dannenberg, J. J.; Dapprich, S.; Daniels, A. D.; Farkas, Ö.; Foresman, J. B.; Ortiz, J. V.; Cioslowski, J.; Fox, D. J. *Gaussian~09 Revision E.01*.
53. Adamo, C.; Barone, V. *J. Chem. Phys.* **1999**, *110* (13), 6158–6170.
54. Krishnan, R.; Binkley, J. S.; Seeger, R.; Pople, J. A. *J. Chem. Phys.* **1980**, *72* (1), 650–654.
55. Frisch, M. J.; Pople, J. A.; Binkley, J. S. *J. Chem. Phys.* **1984**, *80* (7), 3265–3269.

COORDINATION COMPOUNDS WITH SCHIFF BASE LIGANDS BASED ON
2,1,3-BENZOTHIADIAZOLE**3.1. Introduction**

The modification of ligands by addition of different substituents is one of the ways to influence the properties of complexes. Therefore, the search for new ligands is a very active area in the molecular design of coordination compounds. For this purpose, Schiff base ligands are attractive for researchers in coordination chemistry, since they allow easy variation of the functions and coordination properties.

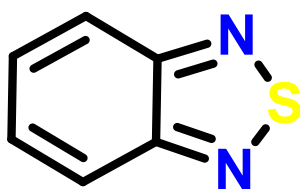


Figure 3.1. 2,1,3-Benzothiazole (BTD) moiety.

2,1,3-Benzothiadiazole (BTD) is one of the most important rings of π -conjugated systems (Fig. 3.1). This heterocycle possesses several desirable characteristics like strong electron-withdrawing capacity, efficient fluorophore, relatively high electron affinity, which are very important for organic light technology¹.

Organic and polymeric compounds containing a BTD unit have a wide range of potential applications as fluorescent materials (fluorescent probes^{2,3} and polymeric thermometers⁴), electron-transporting layers in organic light-emitting diodes¹, chemosensors⁵, dyes⁶ and organic conductors⁷. However, as described in Chapter 1.4 the coordination properties of ligands which include BTD are relatively limited. Up to now only two Schiff base ligands bearing BTD fragment are known. Complexes with these ligands shown interesting crystal arrangement (copper complexes⁸) and mechanochromic properties (zinc complex⁹).

With this view we were interested to design new Schiff base ligands, containing 2,1,3-benzothiadiazole fragment and *N,O*-chelating moiety. The location of the substituents should allow the donor atoms of the BTD fragment to be involved in the coordination of transition metals.

3.2. Synthesis and crystal structure of Schiff base ligands

For the preparation of Schiff base ligands we decided to use the precursor 4-amino-2,1,3-benzothiadiazole (**d**)^{10,11} (Fig. 3.2). The synthesis of 4-amino-2,1,3-benzothiadiazole was previously described, therefore we chose the most efficient strategy, the easiest to apply and with good yields (Fig. 3.2). The precursor was obtained in three steps starting from the commercially available 1,2-diaminobenzene (**a**). The first step is the formation of benzothiadiazole (**b**) (BTD)

using thionyl chloride in the presence of base, the second one is a classical nitration reaction to obtain the nitro-BTD (**c**) and the last one is reduction by zero valent iron powder to amino group.

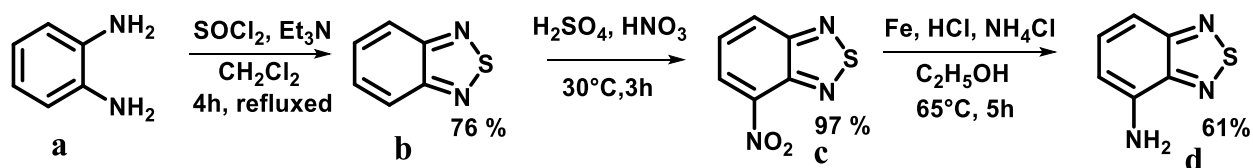


Figure 3.2. Synthesis of 4-amino-2,1,3-benzothiadiazole.

The Schiff base ligands **HL**⁵ and **HL**⁶ were prepared by condensation of 4-amino-2,1,3-benzothiadiazole (**d**) with salicyl aldehyde or *o*-vanillin in ethanol (Fig. 3.3). The new ligands were characterized by ¹H and ¹³C NMR, IR spectroscopy and high resolution mass spectrometry. The synthetic procedures are presented in Appendix 1.

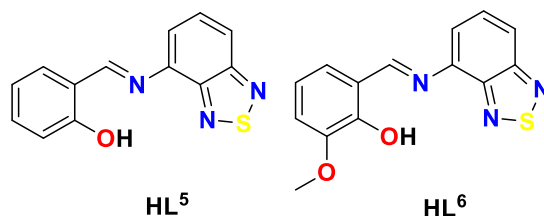


Figure 3.3. Schiff base ligands based on 2,1,3-benzothiadiazole.

HL⁵ and **HL**⁶ crystallize in the centrosymmetric orthorhombic *Pbcn* and monoclinic *P2*₁/*c* space groups, respectively. The torsion angles C(7)-N(3)-C(6)-C(1) between the BTD and phenyl rings are 26.89 ° and 10.68 °, respectively, in **HL**⁵ and **HL**⁶. As shown in Fig. 3.4-5, an intramolecular hydrogen bond between the OH group and the N atom of the imino group exists in the two ligands, together with a C7-H4···N1 hydrogen bond involving the BTD unit in **HL**⁶ (Table 3.1). In the crystal packing, each two adjacent **HL**⁶ molecules are coupled by intermolecular hydrogen bonds.

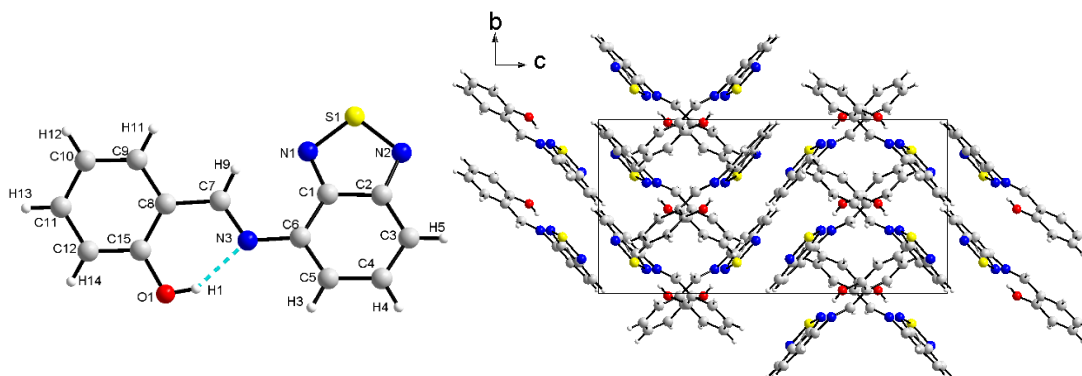
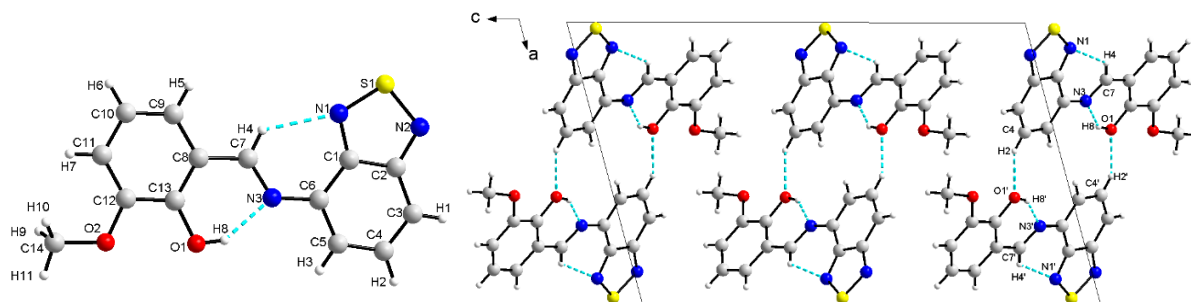


Figure 3.4. Crystal structure of **HL**⁵ with intramolecular H-bond interaction (left) and crystal packing along the axis *a* (right).

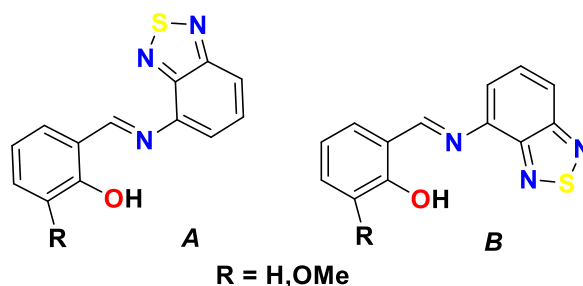
Table 3.1. Hydrogen bonds parameters (\AA , $^\circ$) of ligands **HL**⁵ and **HL**⁶.

	A...H-D	d(A...H), \AA	d(A...D), \AA	\angle (D-H...A), $^\circ$
HL ⁵	N(3) ... H(1) - O(1)	1.889	2.615	146.89
	N(1) ... H(4) - C(7)	2.242	2.929	130.12
HL ⁶	N(3) ... H(8) - O(1)	1.871	2.597	146.91
	O'(1) ... H(2) - C(4)	2.578	3.245	129.03

**Figure 3.5.** Molecular structure of ligand **HL**⁶ (left) and fragment of crystal structure with intra- and intermolecular interactions (right).

Next, we have performed DFT calculations on both ligands in order to compare the experimental conformations with the optimized ones in the gas phase. Theoretical calculations have been done using Gaussian 09 package¹², with the PBE0 functional¹³ and TZVP^{14,15} basis set. Optimized geometries were then confirmed as global minima by frequency calculations. Starting geometries for **HL**⁵ and **HL**⁶ were derived from the X-ray structures.

After optimization, we observe that the calculated bond lengths and angles are in good agreement with the experimental geometry of A-conformer of Schiff base (Fig. 3.6).

**Figure 3.6.** A- and B-conformer for Schiff base ligands.

A slight deviation from planarity between the salicylidene and BTD moieties was observed. In the calculated geometry, the C(7)N(3)C(6)C(1) dihedral angle is equal to 2.93 $^\circ$ (**HL**⁵) and 0 $^\circ$ (**HL**⁶) (atom numbering in Figure 3.4a-5a). The B-conformer of the Schiff base was created by changing the dihedral angle. In the resulting B-conformer of **HL**⁵ the C(7)N(3)C(6)C(1) dihedral angle is equal to 143.81 $^\circ$ and 142.64 $^\circ$ for **HL**⁶. Calculations show that the A-conformer

of **HL**⁵ and **HL**⁶ is more stable in the gas phase, which was in agreement with the SCXRD analysis. The difference in Gibbs free energies is 2.7 kcal·mol⁻¹ (**HL**⁵) and 5.3 kcal·mol⁻¹ (**HL**⁶).

The UV-vis absorption spectra of the Schiff base ligands were recorded at room temperature in DCM (Fig. 3.7). The spectra have intense bands in the region 263 – 326 nm and 338 – 435 nm, which can be assigned to n- π^* and π - π^* transitions. In the case of **HL**⁵ were observed in the spectrum two peaks: the first band is a combination of two peak appear at λ_{max} = 288 nm (34722 cm⁻¹) with ϵ = 12364 M⁻¹ cm⁻¹ and at 310 nm (32258 cm⁻¹) with ϵ = 13857 M⁻¹ cm⁻¹; the second one with ϵ = 11621 M⁻¹ cm⁻¹ appear at 381 nm (26246 cm⁻¹). The spectrum of **HL**⁶ presents two bands at 304 nm (32895 cm⁻¹) and 376 nm (26595 cm⁻¹) with molar absorption coefficients of 10792 and 10792 M⁻¹ cm⁻¹, respectively.

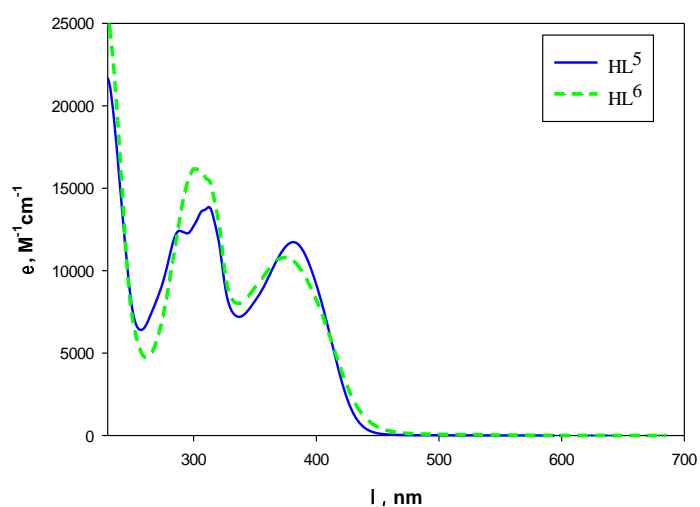


Figure 3.7. UV-vis spectra of **HL**⁵ and **HL**⁶ in DCM.

In Figure 3.8, the experimental spectrum of **HL**⁵ in DCM is plotted along with the calculated transition energies for *A*- and *B*-conformers were shown. We can see a clear difference between the two conformers. Clearly, the experimental spectrum mainly corresponds to the calculated *B*-conformer. Taken note of this we discuss then the calculated spectrum and EDD plots corresponding to the main transitions from the ground state to the excited states of the *B*-conformer (Fig. 3.8, Table 3.2). The first band is a combination of two transitions S_1 (a vertical absorption at 390 nm, $f = 0.269$) and S_2 (at 344 nm, $f = 0.069$), which correspond to HOMO \rightarrow LUMO (98%) and HOMO-1 \rightarrow LUMO (95%), respectively. The second band correspond to a first peak (S_3 state at 317 nm, $f = 0.142$) and second peak which is a combination of S_5 (at 286 nm, $f = 0.093$) and S_6 (at 274 nm, $f = 0.137$).

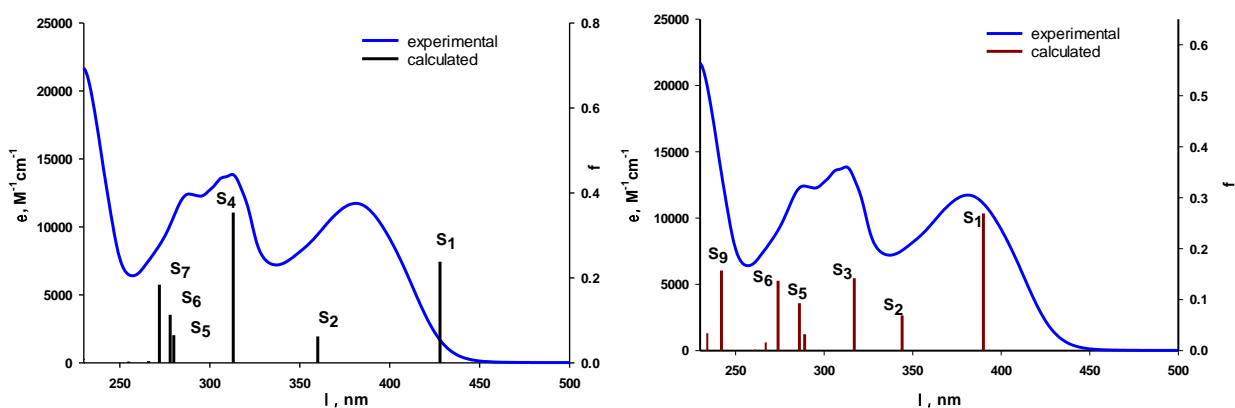
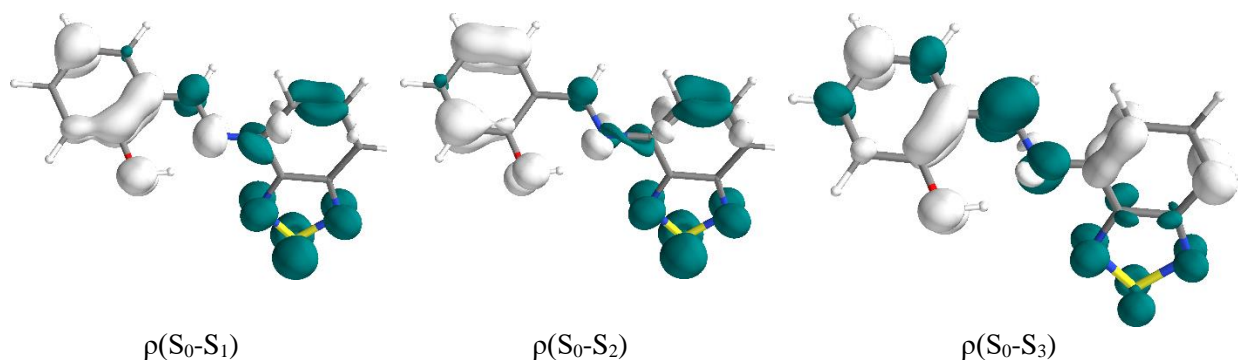


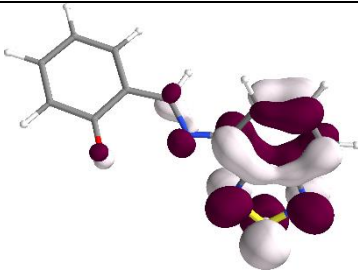
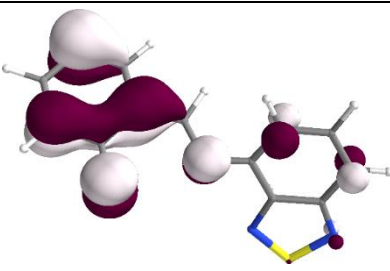
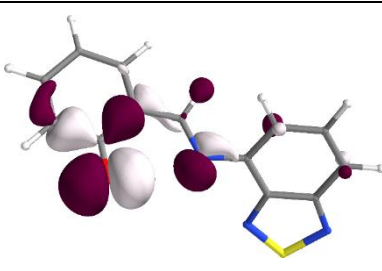
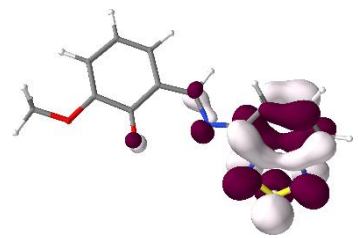
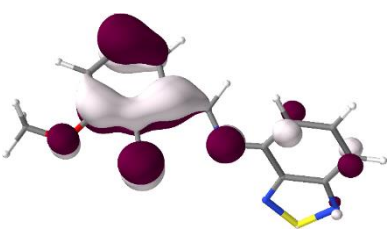
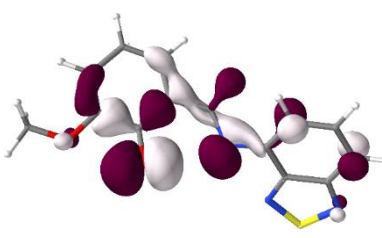
Figure 3.8. Experimental and calculated absorption spectra of the *A*- (left) and *B*-conformers (right) of ligand **HL⁵**.

Table 3.2. Density difference plots between the excited states and the ground state for the *B*-conformer of ligand **HL⁵** (the excited electron and the hole regions are indicated by respectively blue and white surfaces).



Furthermore, DFT calculations were performed for the deprotonated ligands to determine the coordination possibilities. HOMO and HOMO-1 for the deprotonated ligands (**L⁵⁻**) and (**L⁶⁻**) are shown in Table 3.3. It should be noted that the contribution of the molecular orbitals is similar for (**L⁵⁻**) and (**L⁶⁻**). HOMO and HOMO-1 are mainly located on the phenol ring, oxygen and nitrogen atoms. For the coordination properties of the ligands we will focus on the N- and O-donor atoms. The π type HOMO and n type HOMO-1 are located on phenolic O and imine N. The BTD ring does not have any participation in the HOMO and HOMO-1, therefore we can hypothesize that its coordination to metal centers will be much weaker compared to the Schiff base unit. We can assume as well that HOMO-1 corresponds to the orbital taking part in coordination, considering the symmetry and high energy. The main coordination should be by the O_{phen} and the N_{im} atoms. The LUMO's are essentially localized on the benzothiadiazole ring, confirming that this fragment has acceptor properties. Coordination by N from BTD is not favored, the $M-N_{\text{BTD}}$ bonds being expected to be weak, with long distances. LUMO topology is in favor of a π back-bonding interaction with the metal atom.

Table 3.3. LUMO, HOMO and HOMO-1 for (\mathbf{L}^5)⁻ and (\mathbf{L}^6)⁻.

	LUMO	HOMO	HOMO-1
(\mathbf{L}^5) ⁻	 0.67 eV	 -1.68 eV	 -2.39 eV
(\mathbf{L}^6) ⁻	 0.72 eV	 -1.54 eV	 -2.47 eV

Hirshfeld charges for the oxygen and nitrogen atoms of the deprotonated ligands are presented in Table 3.4. The most negative charges correspond to oxygen of the phenyl group and nitrogen of the imino group. The N_{BTD} atoms have the lowest negative charges. That confirms the electron deficiency of the BTD. The molecular electrostatic potential mapped on the electron density at the van der Waals radii for (\mathbf{L}^5)⁻ and (\mathbf{L}^6)⁻ are represented in Figure 3.9. The red color illustrates the most negative potentials (electron-rich regions), while the blue one corresponds to the most positive potentials (electron-poor regions). Near the O_{ph} and the N_{im} atoms we can observe the most negative potentials and the most positive near the S atom of BTD unit.

Table 3.4. Hirshfeld charges for (\mathbf{L}^5)⁻ and (\mathbf{L}^6)⁻.

	$O(2)_{met}$	$O(1)_{ph}$	$N(3)_{im}$	$N(1)_{BTD}$	$N(2)_{BTD}$
(\mathbf{L}^5) ⁻	-	-0.419	-0.378	-0.218	-0.269
(\mathbf{L}^6) ⁻	-0.236	-0.395	-0.380	-0.218	-0.270

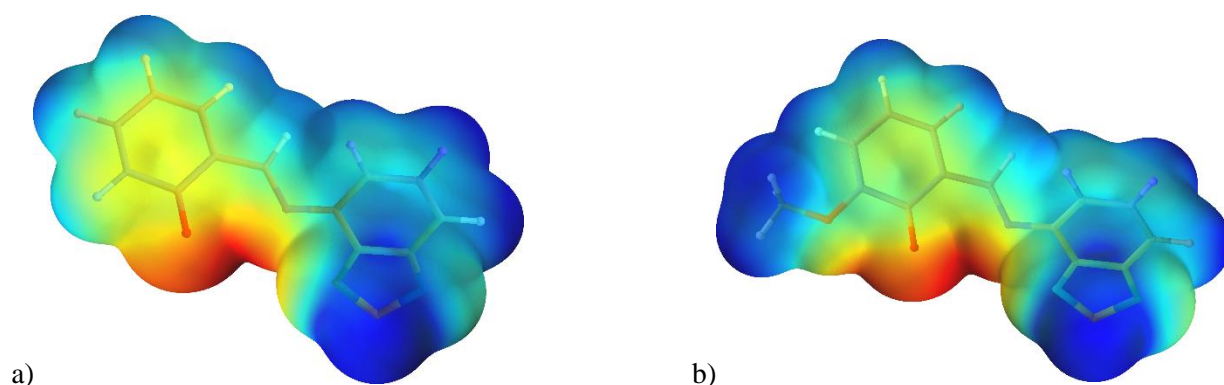
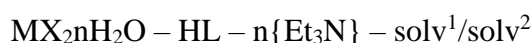


Figure 3.9. Representation of the molecular electrostatic potential mapped on the electron density: a) (L^5); b) (L^6)⁻ (cutoff value of $0.002 e^-/\text{bohr}^3$). Red, blue and green regions correspond to the most negative, the most positive potentials and intermediate values respectively.

3.3. Synthesis and crystal structures of coordination compounds with HL^5 and HL^6

To study the coordination chemistry of HL^5 and HL^6 the following metal centers and conditions were used:



where $M = \text{Co, Ni, Cu, Zn}$; $X = \text{Cl, OAc, Hfac}$; $HL = HL^5, HL^6$; $\text{solv}^1 = \text{CH}_3\text{OH, MeCN}$;
 $\text{solv}^2 = \text{CH}_2\text{Cl}_2, \text{CHCl}_3$.

The ligand HL^5 was reacted with $\text{Cu}(\text{OAc})_2 \cdot \text{H}_2\text{O}$ in a mixture of methanol and dichloromethane to form a mononuclear complex $\text{Cu}(L^5)_2$ (**21**). Using chloride or acetate precursors of other metals proved to be unsuccessful to isolate complexes. However, a series of complexes $\text{Co}(L^5)_2$ (**22**), $\text{Ni}(L^5)_2$ (**23**), $\text{Zn}(L^5)_2$ (**24**) were obtained by reaction with $\text{M}(\text{Hfac})_2 \cdot n\text{H}_2\text{O}$ (Fig. 3.10). It should be noted that the complex $[\text{Cu}(L^5)(\text{Hfac})]$ (**25**) was synthesized by reacting $\text{Cu}(\text{Hfac})_2 \cdot \text{H}_2\text{O}$ with HL^5 , regardless of the ratio of the starting materials. Slow evaporation of the solvents afforded single crystals.

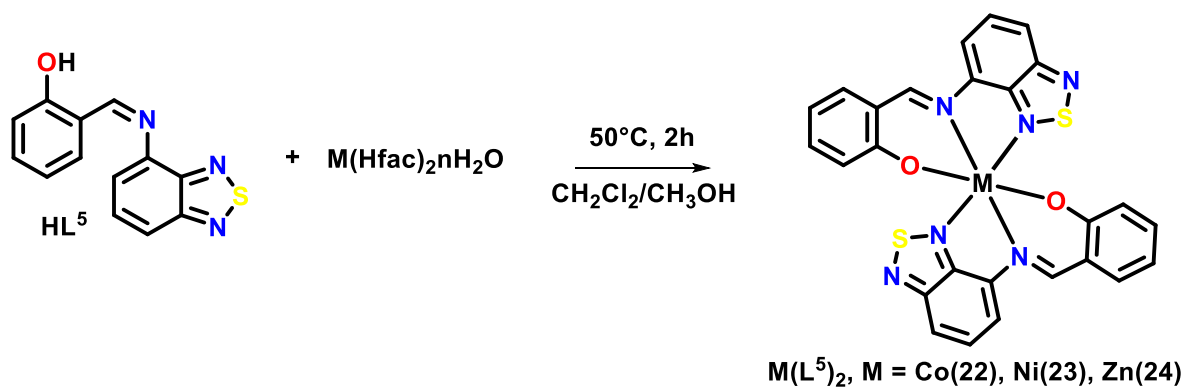


Figure 3.10. Synthesis of the complexes **22-24**.

The complex $\text{Cu}(\text{L}^6)_2$ (**26**) was synthesized similarly as complex **25** by using HL^6 . In these conditions, the complexes $\text{Zn}(\text{L}^6)_2$ (**27**) and $[\text{Co}(\text{L}^6)_2] \cdot \text{CH}_2\text{Cl}_2$ (**28**) were obtained as well from the corresponding acetate salts in the presence of triethylamine.

The infrared spectra of the complexes are similar. The characteristic $\nu(\text{C}=\text{N}_{im})$ stretching frequencies appear at 1609 (**21**), 1606 (**22**), 1610 (**23**), 1610 (**24**) and 1610 cm^{-1} (**25**). In the case of complexes **26-28** with the HL^6 ligand, the band $\nu(\text{C}=\text{N}_{im})$ is in the range $1605 - 1600 \text{ cm}^{-1}$. The difference between the position of the $\nu(\text{CO})$ absorption band for the ligands and the complexes does not exceed 20 cm^{-1} . The shift of the valence vibrations ($\text{C}=\text{N}_{im}$) and (CO) for the complexes in comparison with the spectra of the free ligand into the low-energy region confirms the coordination of the metal in the complexes **21-28**.

UV-Vis spectra of complexes $\text{Zn}(\text{L}^5)_2$ (**24**) and $\text{Zn}(\text{L}^6)_2$ (**27**) in DMSO at room temperature are presented in Figure 3.9. The spectra do not change over a period of four hours, indicating their stability in this solvent. Three bands in the region 250-410 nm correspond to those previously described for the ligands in Figure 3.5. A weak shoulder at 448 nm (22321 cm^{-1}) and $\epsilon = 8814.29 \text{ M}^{-1} \text{ cm}^{-1}$ for complex **24** and at 459 nm (21786 cm^{-1}) and $\epsilon = 6992.82 \text{ M}^{-1} \text{ cm}^{-1}$ for **27** is observed, probably corresponding to deprotonated ligand, which can be assigned to $n-\pi^*$ transitions.

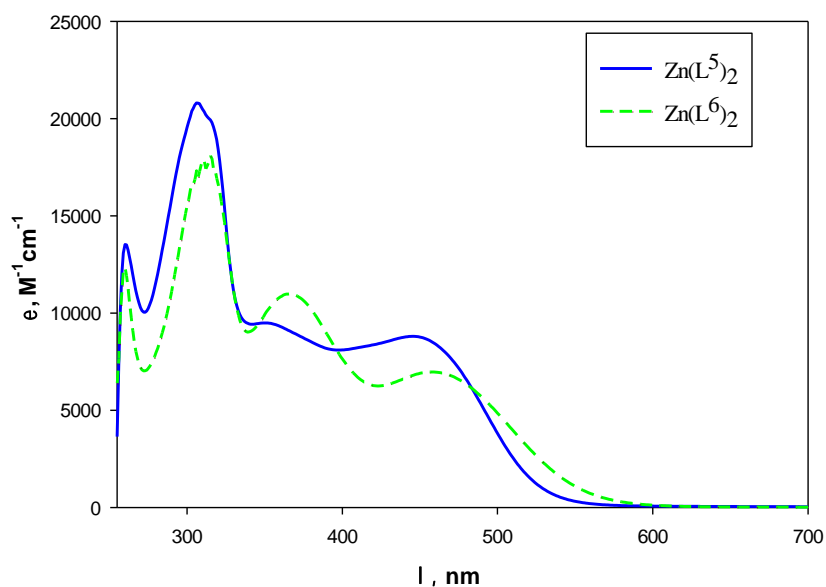


Figure 3.11. UV-vis spectra of **24** and **27** in DMSO ($c = 2 \cdot 10^{-4} \text{ M}$).

Complexes $\text{Cu}(\text{L}^5)_2$ (**21**), $\text{Co}(\text{L}^5)_2$ (**22**), $\text{Ni}(\text{L}^5)_2$ (**23**), $\text{Zn}(\text{L}^5)_2$ (**24**) crystallize in the centrosymmetric orthorhombic $Pbcn$ space group (Fig. 3.12). The crystal structures are quite similar and based on coordination of two deprotonated ligands to the metal atom. The ligand displays O,N,N' -tridentate coordination modes, i.e. [1.111] by Harris notation¹⁶.

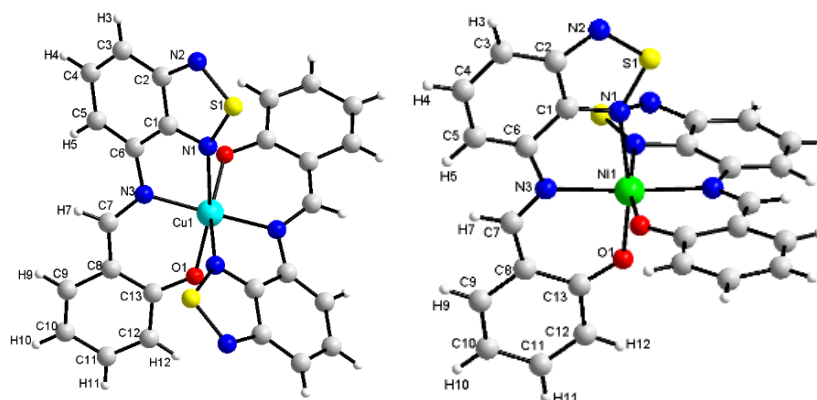


Figure 3.12. The molecular structure of complexes **21** (left) and **23** (right).

The coordination environment of the metals is formed only by the donor atoms of the two ligands, that is the MN_4O_2 chromophores. The geometry of the polyhedron is rather distorted; such deformation may be due to the rigid ligand geometry, which ensures a chelating function. The ligands are oriented around the central atom in the *mer*-configuration. Selected bond lengths and bond angles are given in Table 3.5. The value of the bond lengths and angles for the complexes **22-24** are not very different. The $M-N_{BTD}$ bonds are elongated in all complexes. In complex **21** the value of $Cu-N_{BTD}$ (2.7821(41) Å) is the longest in the series, the angles also having large deviations from the ideal octahedral geometry. SHAPE analysis for the coordination environment $\{N_4O_2\}$ of the metal ion has been performed^{17,18}. Thus, the least deformed six-coordinated polyhedron is in the complexes **22** and **23**, having a geometry of slightly distorted octahedron, with SHAPE analysis values 0.880 and 1.880, respectively. In the complex **24** more pronounced deformation, with a SHAPE value 2.080, has been observed. In the case of complex **21** the deviation from the value of the ideal geometry is the largest – 4.129 (distorted octahedron). The bond valence sum (BVS)¹⁹ analysis applied to the corresponding bond lengths leads to the +2 oxidation state for the metal ions of all complexes (Table 3.5).

Table 3.5. Selected geometrical parameters for the complexes **21-24**.

	Cu(L ⁵) ₂ (21)	Co(L ⁵) ₂ (22)	Ni(L ⁵) ₂ (23)	Zn(L ⁵) ₂ (24)
M—O, Å	1.930(3)	1.9979(16)	1.9977(13)	1.9878(17)
M—N, Å	1.970(4)	2.1138(18)	2.0587(15)	2.0783(18)
M—N _{thias} , Å	2.7821(41)	2.2856(18)	2.2208(16)	2.5104(19)
<i>trans</i> -angles, °	134.4(2) – 162.7(2)	161.68(7) – 179.17(10)	168.05(5) – 176.32(8)	158.93(7) – 169.12(10)
<i>cis</i> -angles, °	92.66(15) – 94.03(15)	77.16(7) – 104.6(1)	79.42(6) – 97.88(6)	74.46(7) – 111.13(10)
M···M, Å	7.325	7.391	7.226	7.333
π - π , Å	3.551	I 3.527 II 3.886	I 3.528 II 3.783	3.536
BVS	2.06 ²⁰	1.98 ^{20,21}	1.92 ²²	2.07 ^{19,23}

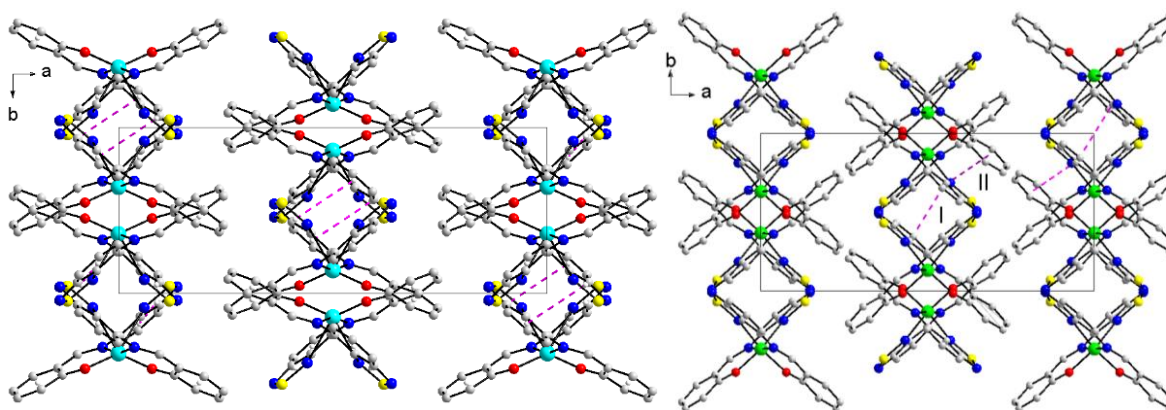


Figure 3.13. Crystal packing of complexes **21** (left) and **23** (right).

Though all complexes have similar molecular structures, their crystal lattices present some slight differences. In the packing, the complexes form chains along the *b*-axis connected by π - π stacking interactions (Fig. 3.13, Table 3.5). In the complexes **21-24**, the benzothiadiazole electron acceptor moiety forms M- N_{BTD} bonds and establish π - π stacking interactions with benzene rings of the BTD moieties. In the case of complex **21** the Cu- N_{BTD} distance is rather long (~ 2.8 Å) and thus the coordinated benzothiadiazole ring is more flexible, taking part in π - π stacking interactions (Fig. 3.14). In complexes **22** and **23** another type of π - π interactions between salicyl and benzene rings of the ligands was found (Fig. 3.14a, Table 3.5), the corresponding distances being comparatively much longer in **21** [4.548 Å] and **24** [4.114 Å].

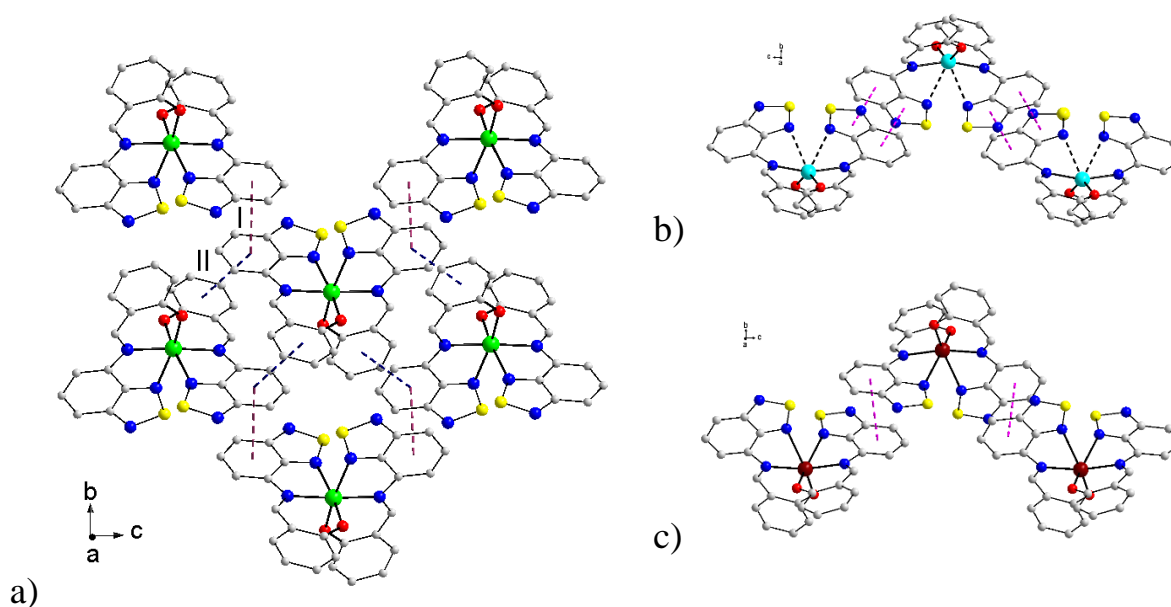


Figure 3.14. Fragment of the crystal structures with π - π stacking interactions highlighted (dotted): a) **23**, b) **21**, c) **24**.

Complex [Cu(L⁵)(Hfac)] (**25**) crystallizes in the monoclinic $P2_1/c$ space group. The copper ion is coordinated by the deprotonated ligand and a Hfac ligand. The coordination environment of

Cu(II) is formed by the N₂O₃ motif with square pyramid geometry, the deformation from ideal symmetry being small, $\tau = 0.05$ ²⁴. The BVS analysis applied to the corresponding bond lengths leads to the +2 oxidation state for the copper ion (BVS = 2.112)^{19,22} (Fig. 3.15). The molecules of complex form chains through π - π stacking: I – between benzothiadiazole’s parts [3.552 Å] and II – salicylidene moieties [3.564 Å] of the neighbor complexes.

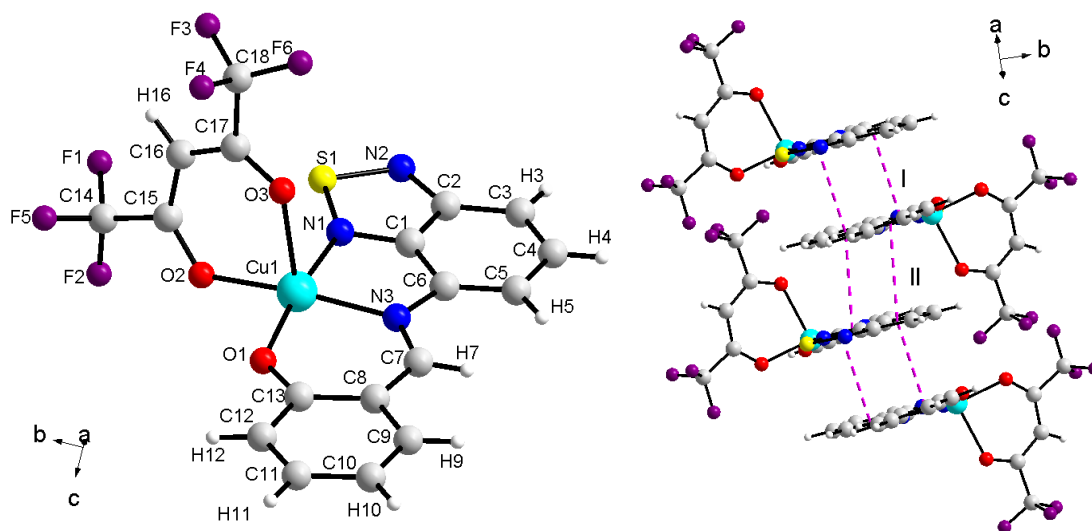


Figure 3.15. The molecular structure (left) and fragment of the crystal packing showing the π - π interactions (right) of the complex **25**.

With ligand **HL**⁶ the complexes Cu(L⁶)₂ (**26**), Zn(L⁶)₂ (**27**), [Co(L⁶)₂] \cdot CH₂Cl₂ (**28**) have been obtained. They consist of the metal ion, two deprotonated molecules of ligand and one molecule of non-coordinated solvent in the case of complex **28**. The ligand displays *O,N*-bidentate or *O,N,N*-tridentate coordination mode ([1.0110] or [1.0111]¹⁶).

Complexes **26** and **27** crystallize in the monoclinic *P*2₁/*c* space group. The crystal structures are quite similar, consisting in a central metal atom and two deprotonated ligands (L⁶). In the complex **26** the copper atom has a square-planar coordination geometry, with a $\tau_4 = 0$ ²⁵ thanks to the N₂O₂ coordinating motif. The value of the *trans*-angles is 180.00°, while the *cis*-angles deviate from 90° less than 0.44°. The bond length distances vary from 1.888 to 2.010 Å. Intermolecular Cu \cdots H contacts [2.715 Å] are established along the axial coordination positions of the copper ion (Fig. 3.16)^{26,27}.

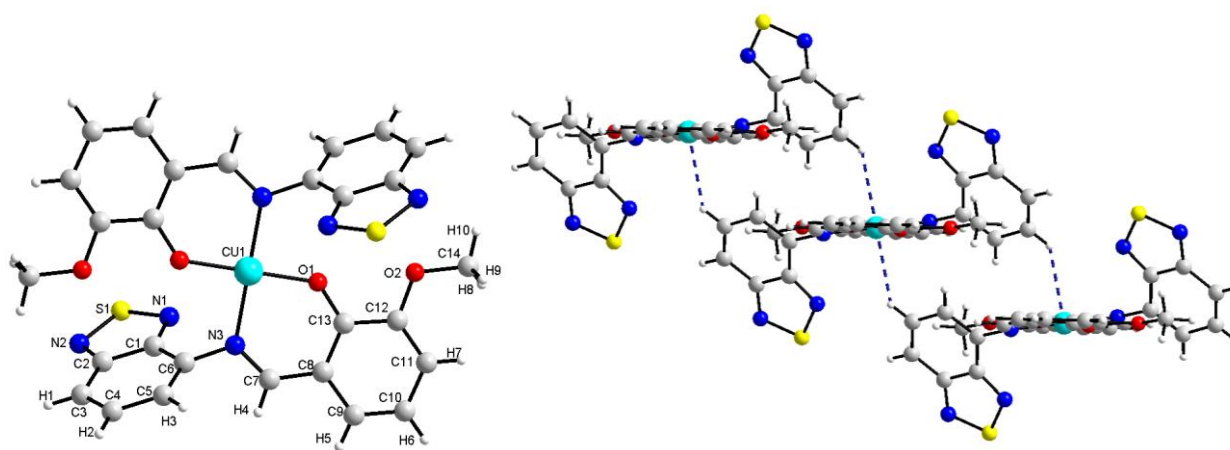


Figure 3.16. Complex **26**: molecular structure (left) and fragment of the crystal packing (right).

In the crystal, π - π stacking [3.632 Å] between benzothiadiazole rings of the adjacent molecules of ligand is observed (Fig. 3.17).

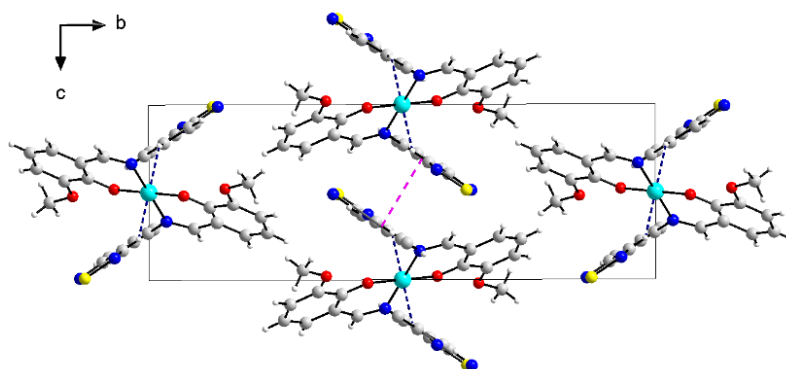


Figure 3.17. Crystal structure of the complex **26** along the axis a .

Unlike the complex $\text{Zn}(\text{L}^5)_2$ (**24**), the zinc atom is five-coordinated in the complex $\text{Zn}(\text{L}^6)_2$ (**27**). The N_3O_2 motif is best described as a slightly distorted square pyramid, as confirmed by the Addison parameter $\tau_5 = 0.112$ ²⁴. In the equatorial plane, the Zn-N/O bond lengths vary in the range 1.968(2) to 2.058(2) Å, while the axial Zn-N bond distance is 2.425(2) Å. The corresponding *cis*- and *trans*-angles are 75.953(93) – 117.204(82) ° and 155.434(85) – 162.141(94) °, respectively. The zinc atom is displaced from the N_2O_2 plane by 0.349 Å. Molecules of complexes connected by π - π stacking interactions make chains parallel to the b -axis [I – 3.521 Å, II – 3.725 Å] (Fig. 3.18).

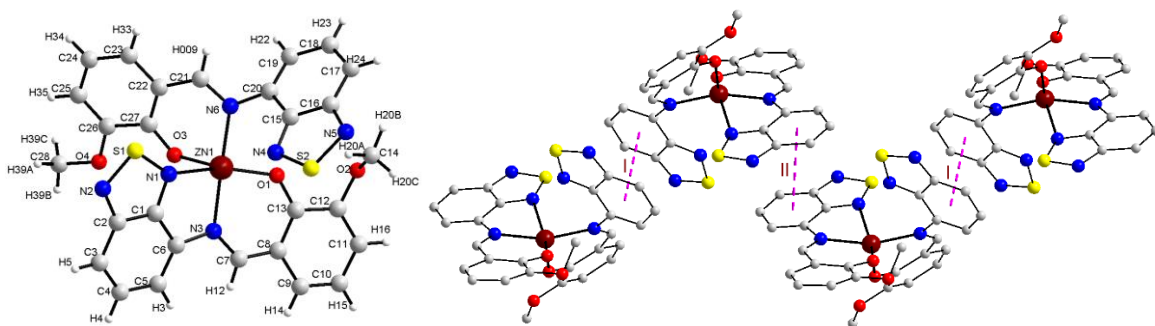


Figure 3.18. Complex **27**: molecular structure (left) and fragment of crystal packing (right).

The complex $[\text{Co}(\text{L}^6)_2] \cdot \text{CH}_2\text{Cl}_2$ (**28**) crystallizes in the triclinic $P-1$ space group. The asymmetric unit consists in a molecule of complex and one non-coordinated molecule of dichloromethane. The coordination environment of the cobalt atom is a distorted octahedron. The Co – N bond lengths are 2.088(4)-2.248(4) Å and Co – O are 1.997(3)-2.004(3) Å. The *cis*-angles vary in the range 77.64(15)–105.46(14)° and the *trans*-angles from 159.13(15) to 167.54(14)°. The bond-valence-sum analysis indicates for the cobalt ion (BVS = 2.08) a +2 oxidation state.

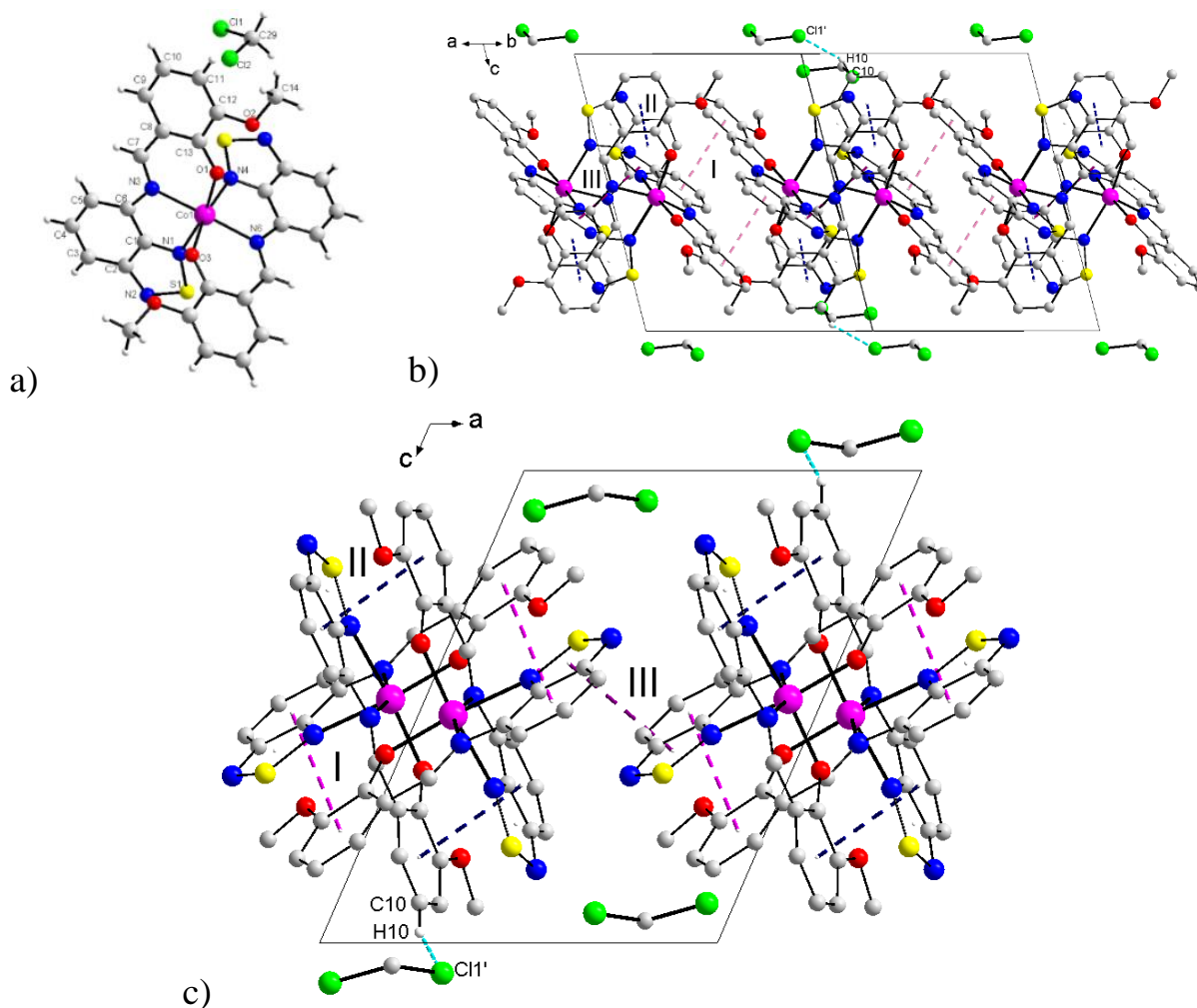


Figure 3.19. Complex **28**: molecular structure (a) and crystal packing with intermolecular interactions (b, c), H atoms have been omitted for clarity.

The adjacent complexes are connected by three types of π - π interactions: I between phenol-benzothiadiazole rings 3.55 Å; II phenol-benzothiadiazole rings 3.52 Å; III thiadiazol-thiadiazol rings 3.67 Å. The molecules of solvent and complex are linked by C-H \cdots Cl hydrogen bond (Table 3.6, Fig. 3.19).

Table 3.6. Hydrogen bond parameters (Å, °) of **28**.

D-H \cdots A	d(D \cdots A)	d(H \cdots A)	angle (D-H \cdots A)
C(10)-H(10) \cdots Cl'(1)	3.828	3.033	144.40

3.4. Magnetic properties

The magnetic properties of complexes [Cu(L⁵)(Hfac)] (**25**), Cu(L⁶)₂ (**26**), [Co(L⁶)₂] \cdot CH₂Cl₂ (**28**) have been investigated in collaboration with Prof. Miguel Julve and Prof. Francisco Lloret, ICMol, University of Valencia, Spain.

The magnetic properties of **25** and **26** in the form of $\chi_M T$ versus T plot [χ_M is the magnetic susceptibility per one mol of copper(II) ions] are shown in Figure 3.20. The magnetic properties of both compounds are very similar. At room temperature, the values of $\chi_M T$ is are 0.401 (**25**) and 0.409 cm³ mol⁻¹ K (**26**). They are as expected for magnetically isolated spin doublets. Upon cooling down, these values remain constant until 50 (**25**) and 40 (**26**) K and they further decrease slightly to 0.385 (**25**) and 0.397 cm³ mol⁻¹ K (**26**). The shape of these plots is typical of the occurrence of very weak antiferromagnetic interactions between spin doublets.

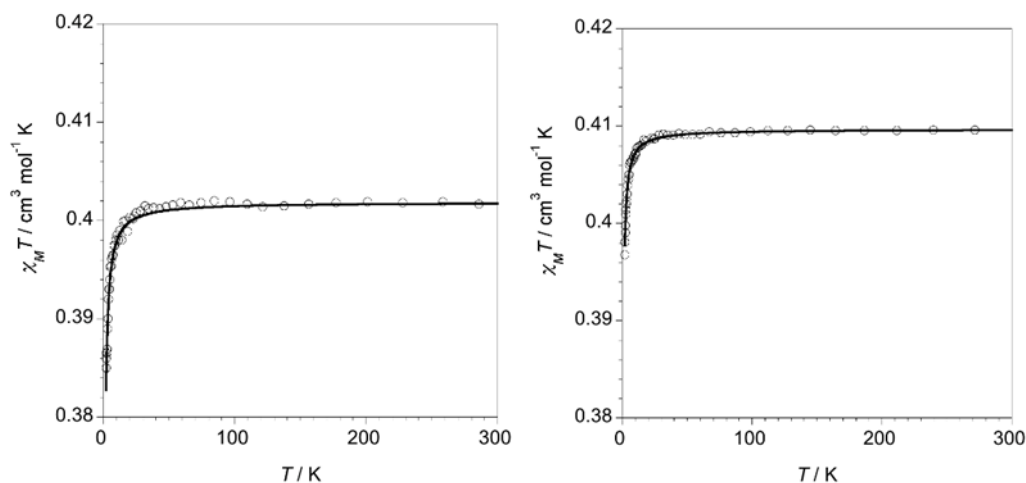


Figure 3.20. Thermal dependence of $\chi_M T$ for **25** (left) and **26** (right): (o) experimental; (—) best-fit curve through eq (1).

The analysis of the magnetic data of **25** and **26** by the Curie law for a spin doublet have been made through following equation:

$$\chi_M T = N\beta^2 g^2 / 4(T - \theta) \quad (1)$$

where θ is a Curie-Weiss term that takes into account the intermolecular magnetic interactions, led to the following best-fit parameters: $g = 2.07$ and $\theta = -0.10$ K for **25** and $g = 2.09$ and $\theta = -0.06$ K for **26**. The weakness of the antiferromagnetic interaction in the two cases is as expected because of the degree of magnetic isolation between the spin doublets in the two crystal structures [the shortest values of the intermolecular Cu...Cu separation in them 6.225 (**25**) and 7.286 Å (**26**)].

The direct current (dc) magnetic properties of complex $[\text{Co}(\text{L}^6)_2] \cdot \text{CH}_2\text{Cl}_2$ (**28**) in the form of $\chi_M T$ against T plot are shown in Figure 3.21. At room temperature, the value of $\chi_M T$ is equal to $2.27 \text{ cm}^3 \text{ mol}^{-1} \text{ K}$. The fact that this value is larger than that calculated for a high spin cobalt(II) ion ($S_{\text{Co}} = 3/2$) with $g_{\text{Co}} = 2.0$ using the spin formula [$\chi_M T = g_{\text{Co}}^2 \times S_{\text{Co}}(S_{\text{Co}} + 1) = 1.874 \text{ cm}^3 \text{ mol}^{-1} \text{ K}$] is indicative of the existence of a significant orbital contribution in the magnetic moment²⁸. Upon cooling down, $\chi_M T$ continuously decreases until it reaches a minimum value of $0.96 \text{ cm}^3 \text{ mol}^{-1} \text{ K}$ at 1.9 K. No maximum χ_M is observed over the entire temperature range explored. The decrease of $\chi_M T$ on cooling can be attributed to the depopulation of the higher-energy Kramers doublets from the cobalt(II) centers and/or an antiferromagnetic interaction between the high-spin cobalt(II) ions. The occurrence in the structure of **28** of π - π stacking interactions involving benzothiadiazole, phenol and thiadiazol rings (values of the inter-ring distances in the range 3.52-3.67 Å) would provide a possible pathway for weak intermolecular magnetic interactions, the shortest Co...Co separation being 6.321 Å.

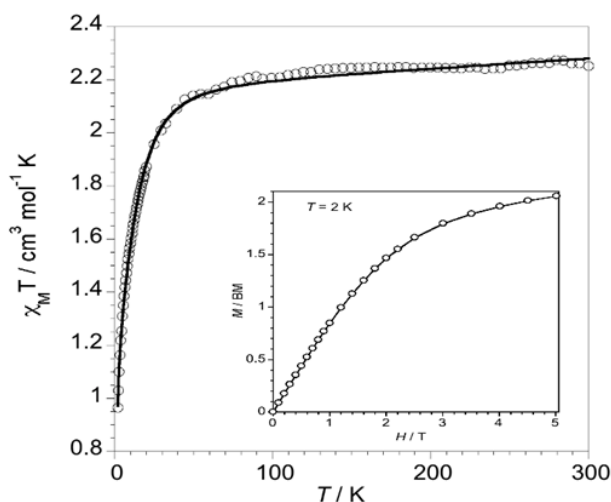


Figure 3.19. Temperature dependence of the $\chi_M T$ for **28**: (o) experimental; (—) theoretical curve with the best fit through eq. (2). The inset shows the M versus H/T plots at 2.0 K.

The magnetic susceptibility data of **28** were analyzed with the Hamiltonian (2)²⁹:

$$H = -\alpha\lambda L_{Co}S_{Co} + \Delta[L_{z,Co}^2 - L(L+1)/3] + \beta H(-\alpha L_{Co} + g_e S_{Co}) \quad (2)$$

where λ is the spin-orbit coupling constant and α is an orbital reduction factor defined as $\alpha = A\kappa$. The parameter κ represents the reduction of the orbital momentum due to the delocalization of the unpaired electrons while A accounts for the mixing of the term ${}^4T_{1g}(P)$ with the fundamental ${}^4T_{1g}({}^4F)$ in the context of the splitting by the crystal field of the terms 4F and 4P of the free ion Co(II) with a $3d^7$ electron configuration. It should be noted that A takes values between 1.5 and 1, which correspond to the limits of the weak and strong crystalline field, respectively. Finally, Δ is the energy difference between the singlet 4A_2 and the doublet 4E levels that come from the splitting of the ground state triplet orbital ${}^4T_{1g}$ under an axial distortion of the ideal symmetry environment O_h of the cobalt(II) ion. The 4A_2 and 4E levels are in turn split by second-order spin-orbit coupling, resulting into two and four Kramers doublets, respectively.

Since there is no analytical expression for the magnetic susceptibility as a function of the parameters α , Δ and λ , their values have been determined by using numerical techniques of matrix diagonalization³⁰. Best-fit parameters of the magnetic data of **28** in the whole temperature range explored are $\alpha = 1.154$, $\Delta = 1224 \text{ cm}^{-1}$, $\lambda = -120.1 \text{ cm}^{-1}$ and $\theta = -0.921 \text{ K}$ with $R = 1.4 \times 10^{-6}$ (R is the agreement factor defined as $\sum[(\chi_M T)_{\text{exp}} - (\chi_M T)_{\text{calcd}}]^2 / \sum(\chi_M T)_{\text{exp}}^2$). θ is a Curie-Weiss term that was also added to equation (2) to account for the intermolecular magnetic interactions. The theoretical curve (Fig. 3.19) reproduces well the experimental values from room temperature to 1.9 K. The fact the value of **28** is smaller than that of the free ion ($\lambda_0 = -180 \text{ cm}^{-1}$) is due to covalency effects. Anyway, the values of the fitted parameters are of order of those reported for other six-coordinate high-spin cobalt(II) complexes^{29,31–35}.

The field dependence of the magnetization at 2.0 K shows a quasi-saturation value of $M_S = 2.04 \text{ BM}$ at 5 T (Fig. 3.19). This value is smaller than expected for $S_{Co} = 3/2$ with $g = 2.0$ (that is 3.0 MB). This difference is due to the fact that for cobalt(II) complexes in O_h symmetry at $T < 30 \text{ K}$, only the low-lying Kramers doublet is thermally populated and then, the magnetic susceptibility data below this temperature can be interpreted through a model where an effective spin $S_{\text{eff}} = 1/2$ is assumed for this low-lying doublet³⁶. Precisely, an effective spin $S_{\text{eff}} = 1/2$ with a value of g equal to 4.10 [according to equation (3)]

$$g = (10 + 2\alpha)/3 \quad (3)$$

characterize this state ($\alpha = 1.154$ and $M_S = 2.05 \text{ MB}$) in agreement with the experimental data.

In order to explore the possible occurrence of slow magnetic relaxation in **28** (Single-Ion Magnet behavior, SIM), alternating current (ac) magnetic susceptibility measurements were carried out as a function of the frequency in the temperature range 2.0-7.0 K under applied H_{dc} fields of 0, 1000 and 2500 G with an oscillating field of ± 5.0 G. These measurements under $H_{dc} = 0$ G show the absence of out-of-phase signals (χ_M''), suggesting the presence of quantum tunneling magnetization effects (QTM). The application of a dc magnetic fields of 1000 and 2500 G cancels this effect and causes the appearance of frequency-dependent χ_M'' signals as shown in Figures 3.20 for $H_{dc} = 1000$ and 2500 G, respectively.

The relaxation times (τ) obtained from the maxima of χ_M'' [$\tau(T) = 1/2\pi\nu_{max}$] follow an Arrhenius law:

$$\tau = \tau_0 \exp(E_a/kT) \quad (4)$$

where τ_0 is the pre-exponential coefficient and E_a is the energy barrier. As can be seen in Figure 3.20, the graphical representation $\ln(\tau)$ as a function of $1/T$ obeys this law in the highest temperature interval with values of 2.0×10^{-9} s and 27.7 cm^{-1} (1000 G) and 9.4×10^{-10} s and 29.5 cm^{-1} (2500 G). These τ_0 and E_a values are of the same order than those obtained in previous works with other mononuclear six-coordinate high-spin cobalt(II) compounds³⁷.

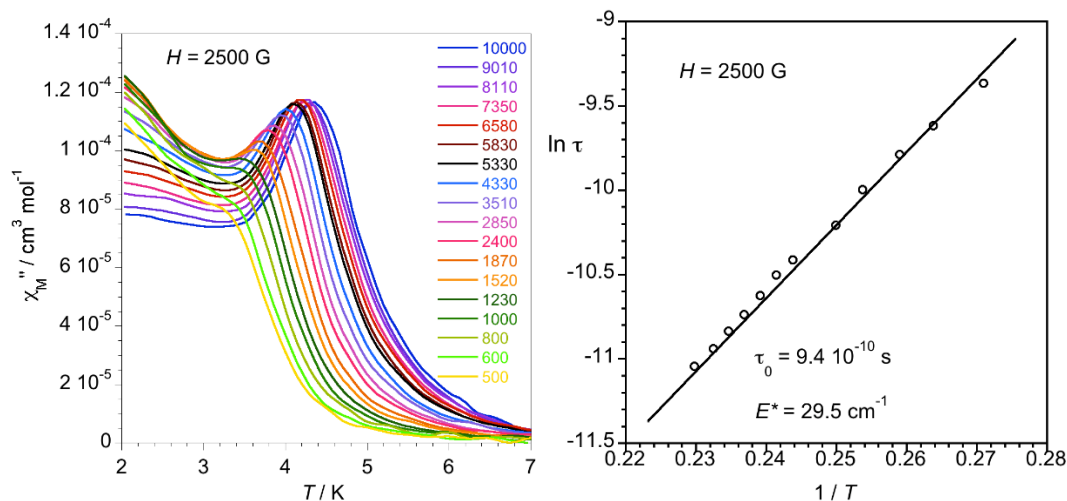


Figure 3.20. Frequency dependence of the out-of-phase components of the magnetic susceptibility of **28** under a static magnetic field $H_{dc} = 2500$ G with an oscillating field ± 0.5 G and at the indicated frequencies. Arrhenius plots in the form of $\ln(\tau)$ as a function of $1/T$ for **28** under static magnetic field of 2500 (right): (o) experimental data; (--) fit by eq. (3).

The deviation of law Arrhenius in the region of lower temperatures not visualized here, has its origin in the possible intervention of other relaxation processes that will be subject of a further analysis.

3.5. Conclusion

The ligands **HL**⁵ and **HL**⁶ have been synthesized by condensation of 4-amino-2,1,3-benzothiadiazole with salicyl aldehyde or *o*-vanillin and have been fully characterized. There is an intramolecular hydrogen bond between OH groups and N atom of the imino groups in the both ligands. Furthermore, each two adjacent **HL**⁶ molecules are coupled by an intermolecular hydrogen bond.

Complexes with general formula $[M(L^{5,6})_2] \cdot nCH_2Cl_2$ (M = Cu, Ni, Co, Zn) and the heteroleptic complex $[Cu(L^5)(Hfac)]$ were obtained. The ligands **HL**⁵ and **HL**⁶ show *O,N* - bidentate and *O,N,N'*-tridentate coordination modes. In the crystal packing the complexes are connected by π - π stacking interactions.

The magnetic behavior for the complexes $[Cu(L^5)(Hfac)]$ (**25**), $Cu(L^6)_2$ (**26**), $[Co(L^6)_2] \cdot CH_2Cl_2$ (**28**) has been studied. Slow relaxation of magnetization of complex **28** in the low temperature range 2.0-7.0 K has been investigated.

References

1. Neto, B. A. D.; Lapis, A. A. M.; Júnior, E. N. da S.; Dupont, J. *Eur. J. Org. Chem.* **2013** (2), 228–255.
2. Cruz, E. H. G. da; Carvalho, P. H. P. R.; Corrêa, J. R.; Silva, D. A. C.; Diogo, E. B. T.; Filho, J. D. de S.; Cavalcanti, B. C.; Pessoa, C.; Oliveira, H. C. B. de; Guido, B. C.; Filho, D. A. da S.; Neto, B. A. D.; Júnior, E. N. da S. *New J. Chem.* **2014**, 38 (6), 2569–2580.
3. Neto, B. A. D.; Carvalho, P. H. P. R.; Correa, J. R. *Acc. Chem. Res.* **2015**, 48 (6), 1560–1569.
4. Uchiyama, S.; Kimura, K.; Gota, C.; Okabe, K.; Kawamoto, K.; Inada, N.; Yoshihara, T.; Tobita, S. *Chem. Eur. J* **2012**, 18 (31), 9552–9563.
5. Moro, A. V.; Ferreira, P. C.; Migowski, P.; Rodembusch, F. S.; Dupont, J.; Lüdtke, D. S. *Tetrahedron* **2013**, 69 (1), 201–206.
6. Fernandes, S. S. M.; Pereira, A.; Ivanou, D.; Mendes, A.; Raposo, M. M. M. *Dyes Pigm.* **2018**, 151, 89–94.
7. Pop, F.; Amacher, A.; Avarvari, N.; Ding, J.; Daku, L. M. L.; Hauser, A.; Koch, M.; Hauser, J.; Liu, S.-X.; Decurtins, S. *Chem. Eur. J* **2013**, 19 (7), 2504–2514.
8. Munakata, M.; He, H.; Kuroda-Sowa, T.; Maekawa, M.; Suenaga, Y. *J. Chem. Soc., Dalton Trans.* **1998**, 9, 1499–1502.
9. Song, X.; Yu, H.; Yan, X.; Zhang, Y.; Miao, Y.; Ye, K.; Wang, Y. *Dalton Trans.* **2018**, 47 (17), 6146–6155.
10. Da Silva Miranda, F.; Signori, A. M.; Vicente, J.; de Souza, B.; Priebe, J. P.; Szpoganicz, B.; Gonçalves, N. S.; Neves, A. *Tetrahedron* **2008**, 64 (22), 5410–5415.
11. Liu, Y.; Lu, Y.; Prashad, M.; Repič, O.; Blacklock, T. *J. Adv. Synth. Catal.* **2005**, 347 (2–3), 217–219.
12. Frisch, M. J.; Trucks, G. W.; Schlegel, H. B.; Scuseria, G. E.; Robb, M. A.; Cheeseman, J. R.; Scalmani, G.; Barone, V.; Mennucci, B.; Petersson, G. A.; Nakatsuji, H.; Caricato, M.; Li, X.; Hratchian, H. P.; Izmaylov, A. F.; Bloino, J.; Zheng, G.; Sonnenberg, J. L.; Hada, M.; Ehara, M.; Toyota, K.; Fukuda, R.; Hasegawa, J.; Ishida, M.; Nakajima, T.; Honda, Y.; Kitao, O.; Nakai, H.; Vreven, T.; Montgomery, J. A., Jr.; Peralta, J. E.; Ogliaro, F.; Bearpark, M.; Heyd, J. J.; Brothers, E.; Kudin, K. N.; Staroverov, V. N.; Kobayashi, R.; Normand, J.; Raghavachari, K.; Rendell, A.; Burant, J. C.; Iyengar, S. S.; Tomasi, J.; Cossi, M.; Rega, N.; Millam, J. M.; Klene, M.; Knox, J. E.; Cross, J. B.; Bakken, V.; Adamo, C.; Jaramillo, J.; Gomperts, R.; Stratmann, R. E.; Yazyev, O.; Austin, A. J.; Cammi, R.; Pomelli, C.; Ochterski, J. W.; Martin, R. L.; Morokuma, K.; Zakrzewski, V. G.; Voth, G. A.; Salvador, P.; Dannenberg, J. J.; Dapprich, S.; Daniels, A. D.; Farkas, Ö.; Foresman, J. B.; Ortiz, J. V.; Cioslowski, J.; Fox, D. J. Gaussian~09 Revision E.01.

13. Adamo, C.; Barone, V. *J. Chem. Phys.* **1999**, *110* (13), 6158–6170.
14. Schäfer, A.; Horn, H.; Ahlrichs, R. *J. Chem. Phys.* **1992**, *97* (4), 2571–2577.
15. Schäfer, A.; Huber, C.; Ahlrichs, R. *J. Chem. Phys.* **1994**, *100* (8), 5829–5835.
16. Coxall, R. A.; Harris, S. G.; Henderson, D. K.; Parsons, S.; Tasker, P. A.; Winpenny, R. E. P. *J. Chem. Soc. Dalton Trans.* **2000**, *14*, 2349–2356.
17. Llunell, M.; Casanova, D.; Girera, J.; Alemany, P.; Alvarez, S. SHAPE, version 2.1; Universitat de Barcelona: Barcelona, Spain.
18. Alvarez, S.; Alemany, P.; Casanova, D.; Cirera, J.; Llunell, M.; Avnir, D. *Coord. Chem. Rev.* **2005**, *249*, 1693–1708.
19. Brown, I. D.; Altermatt, D. *Acta Crystallogr., Sect B* **1985**, *41* (4), 244–247.
20. Wood, R. M.; Palenik, G. J. *Inorg. Chem.* **1998**, *37* (16), 4149–4151.
21. (IUCr) Bond valence parameters <https://www.iucr.org/resources/data/datasets/bond-valence-parameters> (accessed Feb 26, 2020).
22. Liu, W.; Thorp, H. H. *Inorg. Chem.* **1993**, *32* (19), 4102–4105.
23. Brese, N. E.; O’Keeffe, M. *Acta Crystallogr., Sect. B* **1991**, *47* (2), 192–197.
24. Addison, A. W.; Rao, T. N.; Reedijk, J.; Rijn, J. van; Verschoor, G. C. *J. Chem. Soc. Dalton Trans.* **1984**, *7*, 1349–1356.
25. Yang, L.; Powell, D. R.; Houser, R. P. *Dalton Trans.* **2007**, *9*, 955–964.
26. Thakur, T. S.; Desiraju, G. R. *Chem. Commun.* **2006**, *5*, 552–554.
27. Çolak, A. T.; Yeşilel, O. Z.; Büyükgüngör, O. *J. Mol. Struct.* **2011**, *991* (1), 68–72.
28. Carlin, R. L. *Magnetochemistry*, Springer-Verlag.; Berlin, **1986**.
29. Lloret, F.; Julve, M.; Cano, J.; Ruiz-García, R.; Pardo, E. *Inorg. Chim. Acta* **2008**, *361* (12), 3432–3445.
30. Cano, J. VPMAG Package; University of Valencia, Valencia, Spain, **2003**.
31. Munno, G. D.; Julve, M.; Lloret, F.; Faus, J.; Caneschi, A. *J. Chem. Soc., Dalton Trans.* **1994**, *8*, 1175–1183.
32. Sakiyama, H.; Ito, R.; Kumagai, H.; Inoue, K.; Sakamoto, M.; Nishida, Y.; Yamasaki, M. *Eur. J. Inorg. Chem.* **2001**, *2001* (8), 2027–2032.
33. Mishra, V.; Lloret, F.; Mukherjee, R. *Inorg. Chim. Acta* **2006**, *359* (12), 4053–4062.
34. Fabelo, O.; Pasán, J.; Lloret, F.; Julve, M.; Ruiz-Pérez, C. *Inorg. Chem.* **2008**, *47* (9), 3568–3576.
35. Świtlicka-Olszewska, A.; Palion-Gazda, J.; Klemens, T.; Machura, B.; Vallejo, J.; Cano, J.; Lloret, F.; Julve, M. *Dalton Trans.* **2016**, *45* (25), 10181–10193.
36. Lines, M. E. *J. Chem. Phys.* **1971**, *55* (6), 2977–2984.

37. Świtlicka, A.; Palion-Gazda, J.; Machura, B.; Cano, J.; Lloret, F.; Julve, M. *Dalton Trans.* **2019**, 48 (4), 1404–1417.

Chapter 4

COORDINATION COMPOUNDS WITH 2,1,3-BENZOTHIADIAZOLE BASED PYRIDINE AND 2,2'-BIPYRIDINE LIGANDS

4.1. Introduction

Schiff base ligands containing 2,1,3-benzothiadiazole (BTD) unit were described in Chapter 3. The next step in our work was to synthesize BTD based chelating ligands consisting of two different organic coordinating moieties to be explored in coordination chemistry to produce novel functional complexes.

In 2004 Y. Yamashita and co-workers¹ reported on the synthesis of new ligands containing benzothiadiazole and pyridine units (Fig. 4.1). The compounds were obtained through Stille coupling. The molecules have non-planar geometry and form stacks in the solid state thanks to π - π stacking interactions. These compounds are efficient fluorophores with high electron affinity, making them very promising for coordination with various metal centers. For example, compound I (hereafter **L**⁸) showing luminescent properties, has two N-donor coordination pockets.

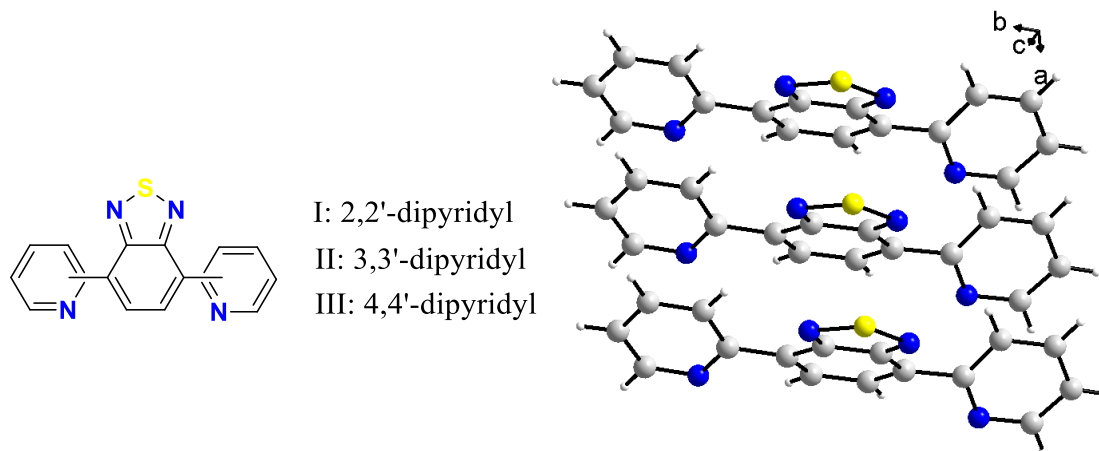


Figure 4.1. Compounds I-III (left) and fragment of crystal packing of compound I (right).

With the aim of designing and studying new functional ligands, we combined the BTD moiety with ones of the most popular units in coordination chemistry, namely pyridine and 2,2'-bipyridine.

4.2. Synthesis, DFT calculations and crystal structure of ligands **L**⁷- **L**¹⁰

We chose for this project mono- and ditopic ligands containing one 2,1,3-benzothiadiazole (BTD) unit and one or two pyridine (*py*) or 2,2'-bipyridine (*bipy*) fragments. The arrangement of

donor atoms creates one (**L**⁷ and **L**⁹) or two (**L**⁸ and **L**¹⁰) chelating "pockets" for potential coordination of metal ions (Fig. 4.2).

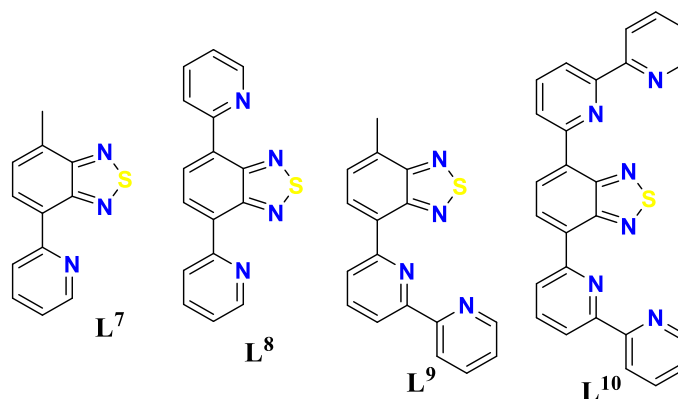


Figure 4.2. Ligands **L**⁷-**L**¹⁰ based on 2,1,3-benzothiadiazole.

The synthesis and crystal structure of ligand **L**⁸ are known¹. This compound shows luminescent properties ($\lambda_{em,max} = 469$ nm), but mentions about coordination properties were not found in the literature.

The ligands **L**⁷, **L**⁹, **L**¹⁰ were synthesized by Suzuki reaction using BTD derivatives of dioxaborolane and bromine derivatives of *py* in the presence of a palladium catalyst and a base (Fig. 4.3).

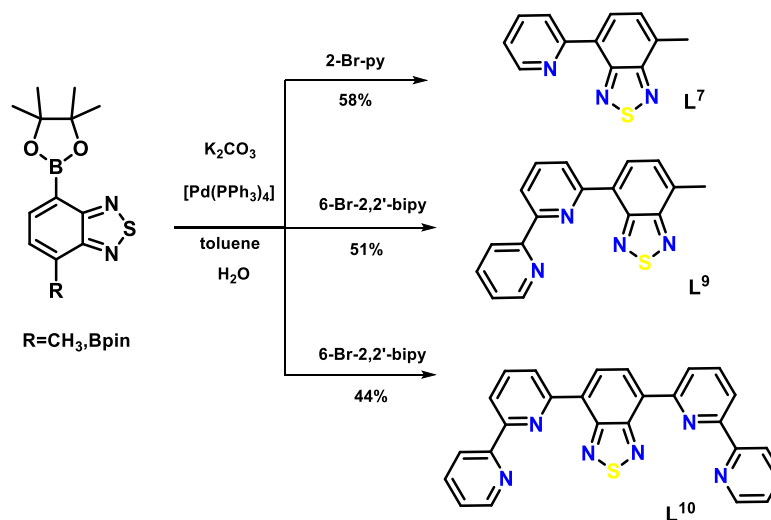


Figure 4.3. Synthesis of the new ligands **L**⁷, **L**⁹ and **L**¹⁰.

The precursor (**e**) in Figure 4.4, obtained in four steps starting from 2-amino-5-nitrotoluene, was used for the synthesis of **L**⁷ and **L**⁹. The first two steps are reduction of the nitro group of (**a**) and then formation of the BTD ring (**c**); the next one is the bromination of 4-methyl-BTD (**c**) to 4-methyl-7-bromo-BTD (**d**)². The last step is the production of the dioxaborolane derivative (**e**)³. Similar reactions were used for the synthesis of the precursor (**i**) for the bis-ligands from 1,2-diaminobenzene (**f**) as starting material⁴⁻⁶.

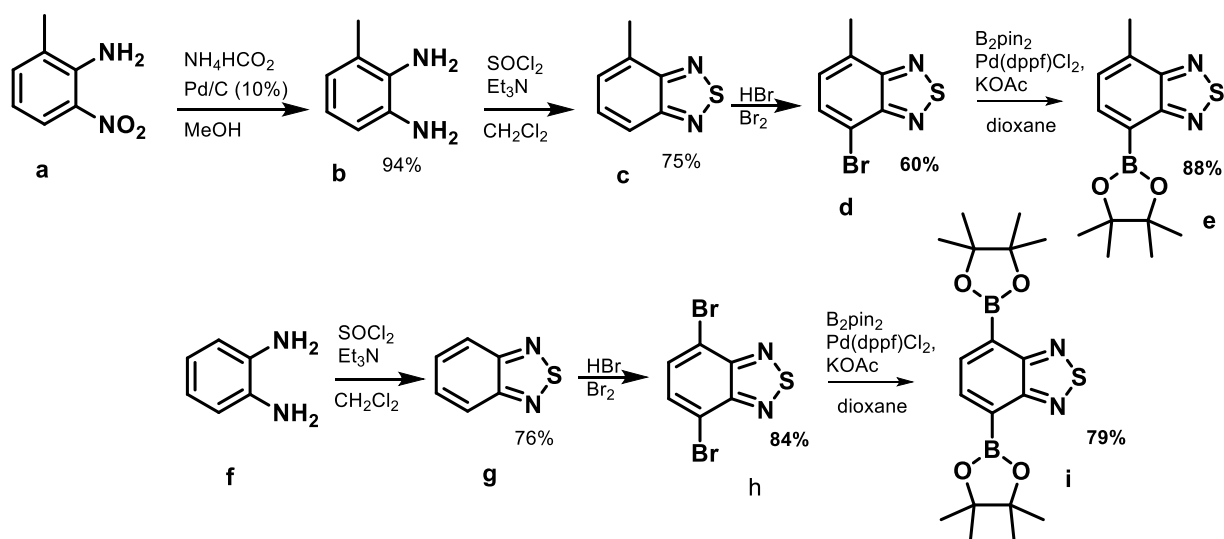


Figure 4.4. Synthesis of the precursors.

The new ligands **L**⁷, **L**⁹, **L**¹⁰ were characterized by ¹H and ¹³C NMR, IR spectroscopy and high resolution mass spectrometry. The synthetic procedures are presented in Appendix 1.

Crystals of **L**⁷ and **L**⁹, suitable for X-ray diffraction analysis, were grown from dichloromethane/methanol solution (1/1), while in the case of **L**¹⁰ polycrystalline powders were obtained. **L**⁷ and **L**⁹ crystallize in the monoclinic *P*2₁/*n* space group. The BTD part adopts an *anti*-conformation with respect to pyridine or bipyridine rings, with torsion angles N3C8C6C1 of 174.33 ° and 172.96 ° for **L**⁷ and **L**⁹, respectively (Fig. 4.5). The adjacent molecules of ligands are connected by π - π stacking interactions [3.834 and 3.829 Å] and S...S contacts of 3.649 Å and 3.322 Å for ligands **L**⁷ and **L**⁹, respectively.

Density Functional Theory (DFT) calculations were performed for geometry optimizations and electronic parameters. DFT method implemented in the Gaussian 09 package⁷, the PBE0 functional⁸ and 6-311++G(2df, 2pd) basis sets^{9,10} were used. Starting geometries for the ligands **L**⁷ and **L**⁹ were derived from the experimentally observed X-ray structures. The calculated bond lengths and angles are in good agreement with the experimental geometries. Upon optimization only modifications in the planarity of the ligands were observed. The value of the angle N3C8C6C1 is close to 180 ° (exp. 174.33 °) for **L**⁷ and amounts at 163.1 ° (exp. 172.96 °) in the case of **L**⁹.

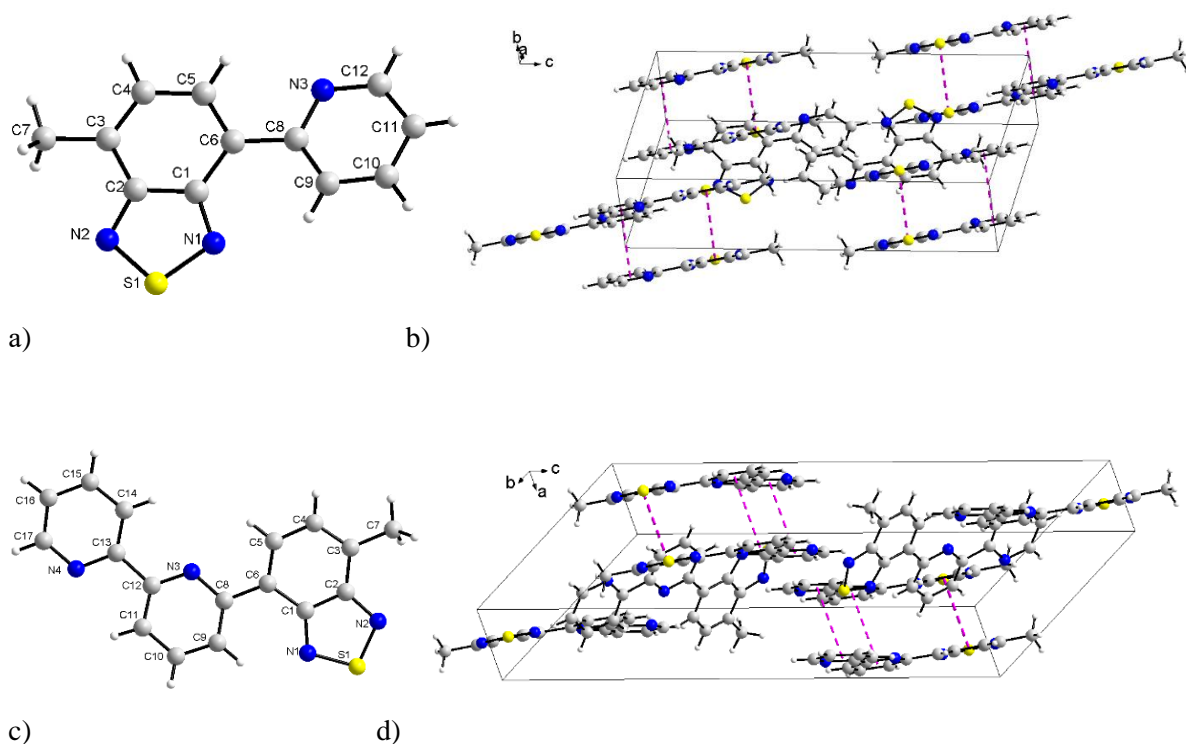
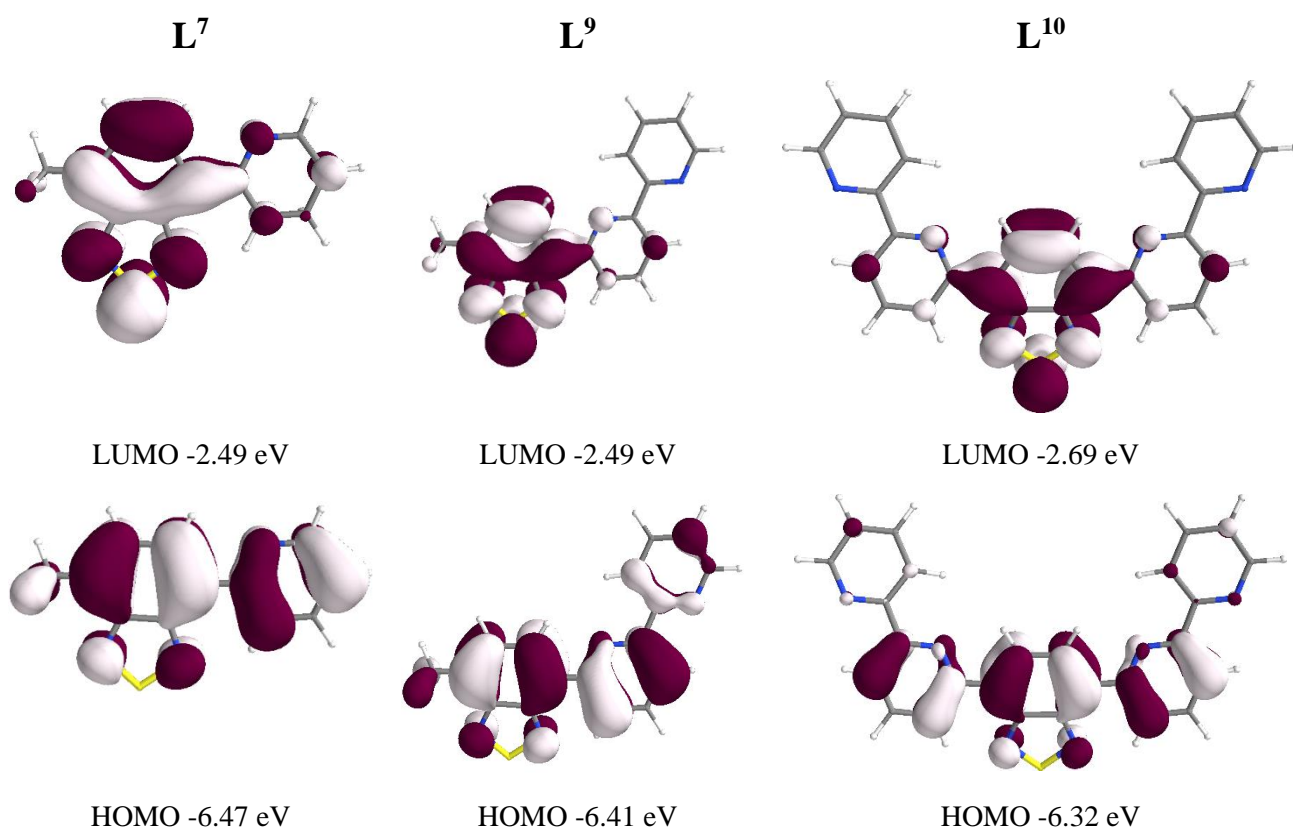


Figure 4.5. Molecular structure and fragment of the crystal packing with highlighted π - π interactions (dotted line) for L^7 (a and b) and L^9 (c and d).

Table 4.1. HOMO's and LUMO's of L^7 , L^9 and L^{10} .



The HOMO and LUMO pictures for \mathbf{L}^7 , \mathbf{L}^9 and \mathbf{L}^{10} are presented in Table 4.1. The values of the LUMO energies for all ligands are quite low and at the same time the largest contributions are localized on the BTD moiety, in agreement with the electron-withdrawing properties of the BTD unit. The topologies and energies of the frontier molecular orbital for \mathbf{L}^7 and \mathbf{L}^9 are quite the same. Replacing one *py* with *bipy* seems to have a small effect on the electronic properties of the ligand. The HOMO delocalizes on the whole molecule in \mathbf{L}^7 and mostly on BTD and adjacent *py* rings in \mathbf{L}^9 and \mathbf{L}^{10} .

The electrochemical behavior of the ligands was studied by cyclic voltammetry in CH_2Cl_2 . The graphics for the ligands \mathbf{L}^7 , \mathbf{L}^9 and \mathbf{L}^{10} , showing oxidation-reduction processes are represented in Figure 4.5. \mathbf{L}^7 and \mathbf{L}^9 show a similar behavior with a reversible reduction-oxidation wave. This process is located at $E_{1/2} = -1.65$ and -1.68 V for \mathbf{L}^7 and \mathbf{L}^9 , respectively. Very likely this reduction process can be attributed to the one-electron reduction of the BTD moiety, which is further proved by DFT calculations (Fig. 4.6). In contrast to \mathbf{L}^7 and \mathbf{L}^9 , the ditopic ligand \mathbf{L}^{10} presents two reduction waves. The first one located at $E_{1/2} = -1.30$ V is reversible and the irreversible reduction step is located at $E_{\text{red}} = -1.93$ V. Comparing the oxidation-reduction progress of the ligands a positive shift can be observed for the reduction potential of \mathbf{L}^{10} . The LUMO of the ligands shows contribution mainly from BTD part and a weak contribution from *py* or *bipy* parts. DFT calculations indicate a difference of LUMO energies between \mathbf{L}^9 and \mathbf{L}^{10} of 0.20 eV, thus correlating with the anodic shift of potential in the case of \mathbf{L}^{10} .

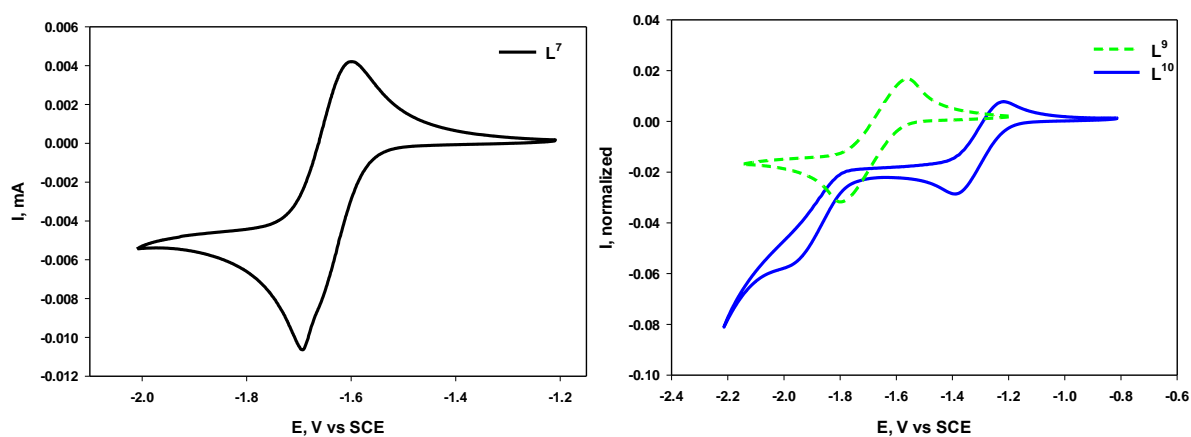
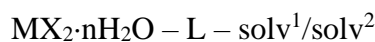


Figure 4.6. Cyclic voltammograms of \mathbf{L}^7 , \mathbf{L}^9 and \mathbf{L}^{10} V vs SCE ($c = 10^{-4}$ M, CH_2Cl_2 , 0.1 M NBu_4PF_6 , 100 $\text{mV}\cdot\text{s}^{-1}$, Pt).

4.3. Coordination compounds with ligands based on 2,1,3-benzothiadiazole

The following metal centers and conditions were used for studying the coordination chemistry of L^7 , L^8 , L^9 and L^{10} :



where $M = Mn, Co, Ni, Cu, Zn, Pt$; $X = Cl, Hfac$; $L = L^7, L^8, L^9, L^{10}$; $solv^1 = CH_3OH, CH_3CN, n\text{-heptan}$; $solv^2 = CH_2Cl_2, CHCl_3$.

Complexes $[Co_2(L^7)_2Cl_4(CH_3OH)_2]$ (**29a**), $[Cu_2(L^7)_2Cl_4]$ (**30**), $[ZnL^7Cl_2]$ (**31**) were obtained using L^7 with chloride salts (in the molar ratio 1:1) in a mixture of methanol and dichloromethane. The crystals of $[Co_2(L^7)_2Cl_4(CH_3OH)_2]$ (**29a**) have red color, while green crystals with a composition $[Co_2(L^7)_2Cl_4]$ (**29b**) were formed in the same mixture as **29a** after one week, from the mother liquor left at air. The complex $[PtL^7Cl_2]$ (**32**) was prepared by reaction of $PtCl_2$ and L^7 in acetonitrile and dichloromethane. The reaction of the ligand in dichloromethane with $[M(Hfac)_2] \cdot nH_2O$ in methanol produced the series of complexes $[MnL^7(Hfac)_2]$ (**33**), $[CoL^7(Hfac)_2]$ (**34**), $[NiL^7(Hfac)_2]$ (**35**), $[CuL^7(Hfac)_2]$ (**36**) and $[ZnL^7(Hfac)_2]$ (**37**) (Fig. 4.7).

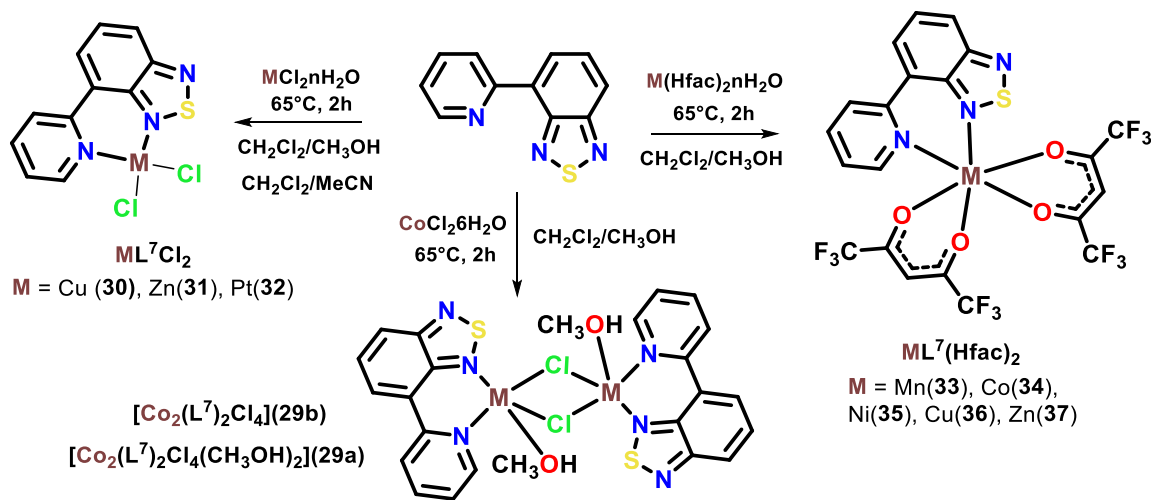


Figure 4.7. Synthesis of the complexes 29a-37.

A study of the coordination properties of L^8 was previously started in our group in Angers. Thus, several mononuclear $[ML^8(Hfac)_2]$ and binuclear $[M_2L^8(Hfac)_4]$ complexes with Co, Ni, Zn were obtained. Copper(II) complexes $[CuL^8(Hfac)_2]$ (**38**) and $[Cu_2L^8(Hfac)_4]$ (**39**) were synthesized during this work using $Cu(Hfac)_2 \cdot H_2O$ with L^8 in a mixture chloroform/methanol (for the complex **38**) and dichloromethane/*n*-heptane (for the complex **39**) (Fig. 4.8).

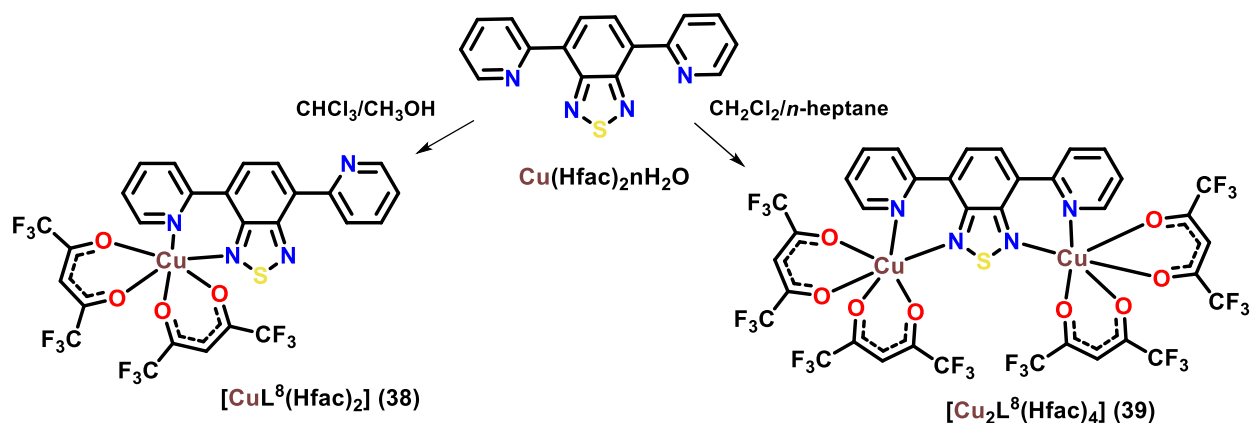


Figure 4.8. Synthesis of the complexes **38** and **39**.

Based on the results for **L⁷**, the same systems and conditions were used for the complexation with **L⁹**. The reaction of $\text{MX}_2 \cdot n\text{H}_2\text{O}$ with **L⁹** in dichloromethane/methanol results in the formation of the mononuclear complexes $[\text{MnL}^9\text{Cl}_2] \cdot 0.5\text{CH}_2\text{Cl}_2$ (**40**), $[\text{CuL}^9\text{Cl}_2] \cdot \text{H}_2\text{O}$ (**45**) and $[\text{ZnL}^9\text{Cl}_2]$ (**46**). The complexes $[\text{CoL}^9(\text{H}_2\text{O})_2\text{Cl}]\text{Cl} \cdot 3\text{H}_2\text{O}$ (**41**) and $[\text{NiL}^9(\text{H}_2\text{O})_3]\text{Cl} \cdot 2\text{H}_2\text{O}$ (**43**) have been obtained using cobalt(II) and nickel(II) chloride hexahydrate. At the same time, using anhydrous cobalt(II) chloride, the mononuclear complex $[\text{CoL}^9\text{Cl}_2] \cdot 0.25\text{CH}_2\text{Cl}_2$ (**42**) was isolated, while the binuclear complex $[\text{Ni}_2(\text{L}^9)_2\text{Cl}_4] \cdot 2\text{H}_2\text{O}$ (**44**) was prepared from anhydrous nickel(II) chloride (Fig. 4.9).

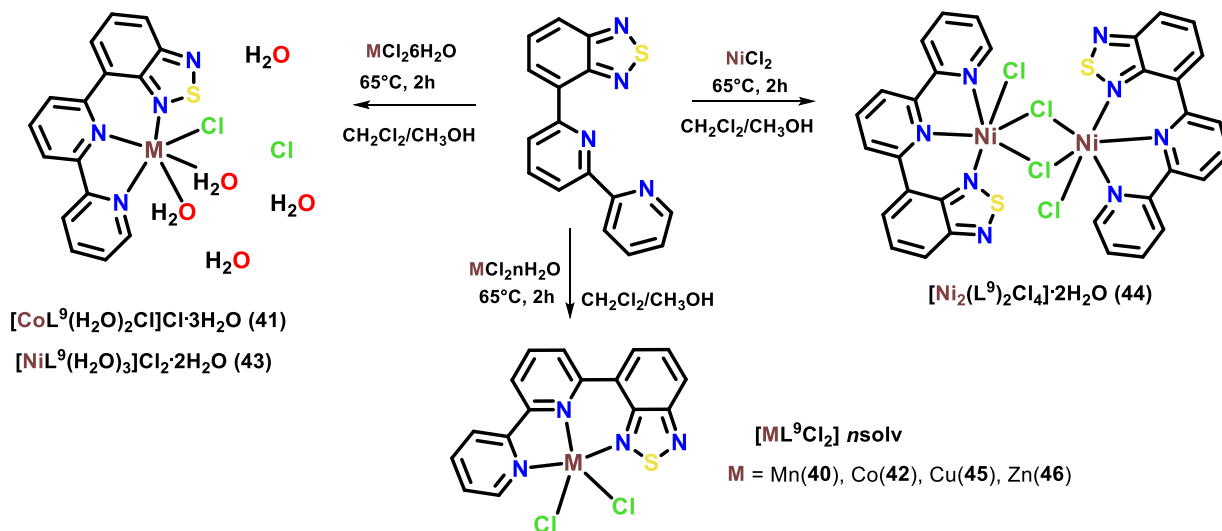


Figure 4.9. Synthesis of the complexes **40-46**.

The ligand **L⁹** reacted with $\text{M(Hfac)}_2 \cdot n\text{H}_2\text{O}$ ($\text{M} = \text{Ni}, \text{Cu}$) in a mixture of methanol and chloroform forming the mononuclear complexes $[\text{NiL}^9(\text{Hfac})(\text{H}_2\text{O})](\text{Hfac}) \cdot \text{H}_2\text{O}$ (**47**) and $[\text{CuL}^9(\text{Hfac})(\text{H}_2\text{O})](\text{Hfac}) \cdot \text{H}_2\text{O}$ (**48**). In the system with copper, by replacing methanol with ethanol the complex $[\text{CuL}^9(\text{Hfac})(\text{C}_2\text{H}_5\text{OH})](\text{Hfac})$ (**49**) was obtained (Fig. 4.10).

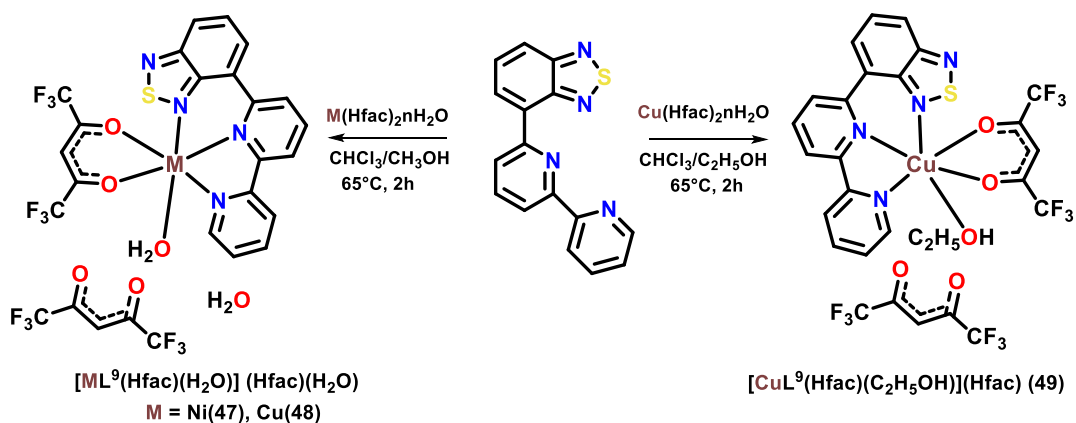


Figure 4.10. Synthesis of the complexes **47-49**.

Unfortunately, complexes with L^{10} could not be isolated and identified so far.

UV-vis spectra of **33-36** in dichloromethane at room temperature are shown in Figure 4.11. The ligand spectrum contains bands peaking at 236, 252, 315 and 363 nm. The spectra of the complexes are rather similar, containing a shoulder in the region 360-390 nm which is broadened and shifted to higher wavelength region compared to the ligand. It is probably due to the overlap of the $\pi-\pi^*$ transitions in the ligand with the $d-\pi^*$ metal to ligand charge transfer.

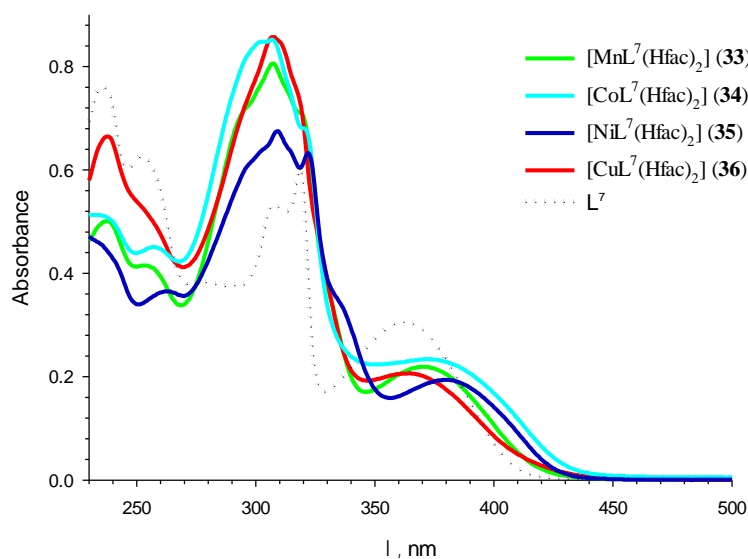


Figure 4.11. UV-vis spectra of the ligand L^7 and complexes **33-36** in DCM.

4.3.1. Crystal structures of coordination compounds with L^7

The complexes $[Co_2(L^7)_2Cl_4(CH_3OH)_2]$ (**29a**) and $[Co_2(L^7)_2Cl_4]$ (**29b**) have binuclear structures with a crystallographic inversion center between two cobalt atoms. These compounds crystallize in the centrosymmetric triclinic $P-1$ space group. The presence of coordinated methanol

molecules in the complex **29a** is the main difference in composition between these two complexes (Fig. 4.12).

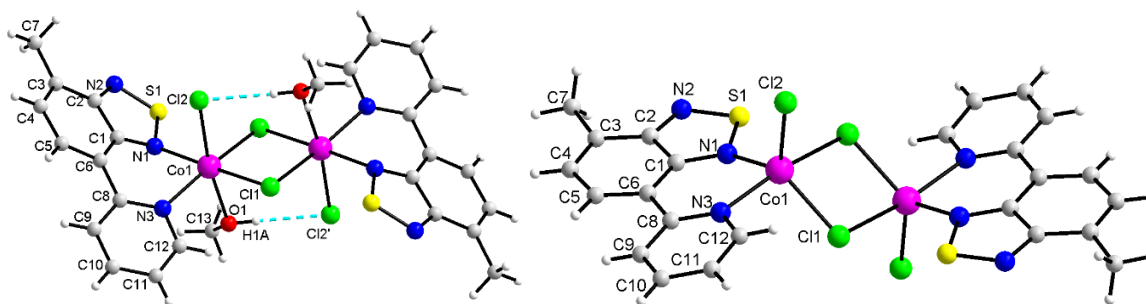


Figure 4.12. Molecular structure of complexes **29a** (left) and **29b** (right).

The complexes are based on the binuclear fragment $\{Co_2(\mu-Cl)_2\}$ with two bridging chloride ligands. The $Co \cdots Co$ contacts are 3.4650(5) and 3.7351(5) Å, while the $CoClCo$ angles are 89.42° and 98.61° for **29a** and **29b**, respectively. In the complex **29a**, the $Co(II)$ ions are coordinated by one *N,N*-bidentate chelating ligand, three chloride ions and one molecule of methanol forming a distorted N_2Cl_3O octahedral environment. The values of *trans*- and *cis*-angles are 167.44(5) – 177.45(5)° and 83.22(5) – 100.12(5)°, respectively. In the complex **29b**, the cobalt center is five-coordinated (N_2Cl_3) with the Addison parameter $\tau_5 = 0.62^{11}$. In addition, the bond lengths between the metal atom and the coordinated atoms are shorter than the similar bonds in the complex **29a** (Table 4.2).

Table 4.2. Selected geometrical parameters and the BVS values for the complexes **29-32**.

	29a	29b	30		31	32
			Cu1	Cu2		
M-Cl, Å	2.4090(6) 2.4538(6) 2.4713(6)	2.2724(6) 2.3205(5) 2.5748(5)	2.3351(13) 2.2736(14) 2.5997(13)	2.3191(14) 2.2824(14) 2.7277(14)	2.2115(11) 2.2076(12)	2.308(2) 2.3066(18)
M-N/O, Å	2.1371(19) 2.1604(16)	2.1505(16)	2.086(4)	2.096(4)	2.039(3)	1.990(6)
M-N _{BTD} , Å	2.1580(19)	2.0387(15)	2.011(4)	2.017(4)	2.047(3)	2.068(5)
angles,° XMY*	83.22(5)- 177.45(5)	81.393(18)- 167.21(5)	87.53(16)- 176.46(12)	83.88(12)- 170.36(12)	91.26(12)- 116.67(5)	88.01(17)- 175.6(6)
BVS	1.79 ^{12,13}	1.82 ^{14,15}	1.98 ^{14,15}	1.89 ^{14,15}	2.12 ^{13,14}	2.11 ^{12,14}
angles,° C1C6C8N3	23.51	8.49	5.62	16.32	17.94	25.82

*X,Y=Cl/O/N

The molecules of ligand have *syn*-conformation and the value of the dihedral angle between *py* and *BTD* fragments increases almost three times when changing the coordination number from 5 to 6 (Table 4.2).

In the complex **29a**, the chloride ion and the hydroxyl methanolic group form an intramolecular hydrogen bond, whereas, at the same time, the chloride ion is also involved in the formation of intermolecular $C-H \cdots Cl$ hydrogen bonds (Table 4.3). In addition, between adjacent

molecules of complexes there are weak π - π - and C7-H7b \cdots C_g interactions [3.623 Å and 2.321 Å, respectively]. In the complex **29b**, the adjacent molecules are coupled by π - π stacking [I – 3.575 Å, II – 3.552 Å] and C7-H7b \cdots C_g interactions [III – 2.951 Å] in the chains along the *a*-axis. The S \cdots N contacts [3.022 Å] link the neighboring chains in the supramolecular structure (Fig. 4.13).

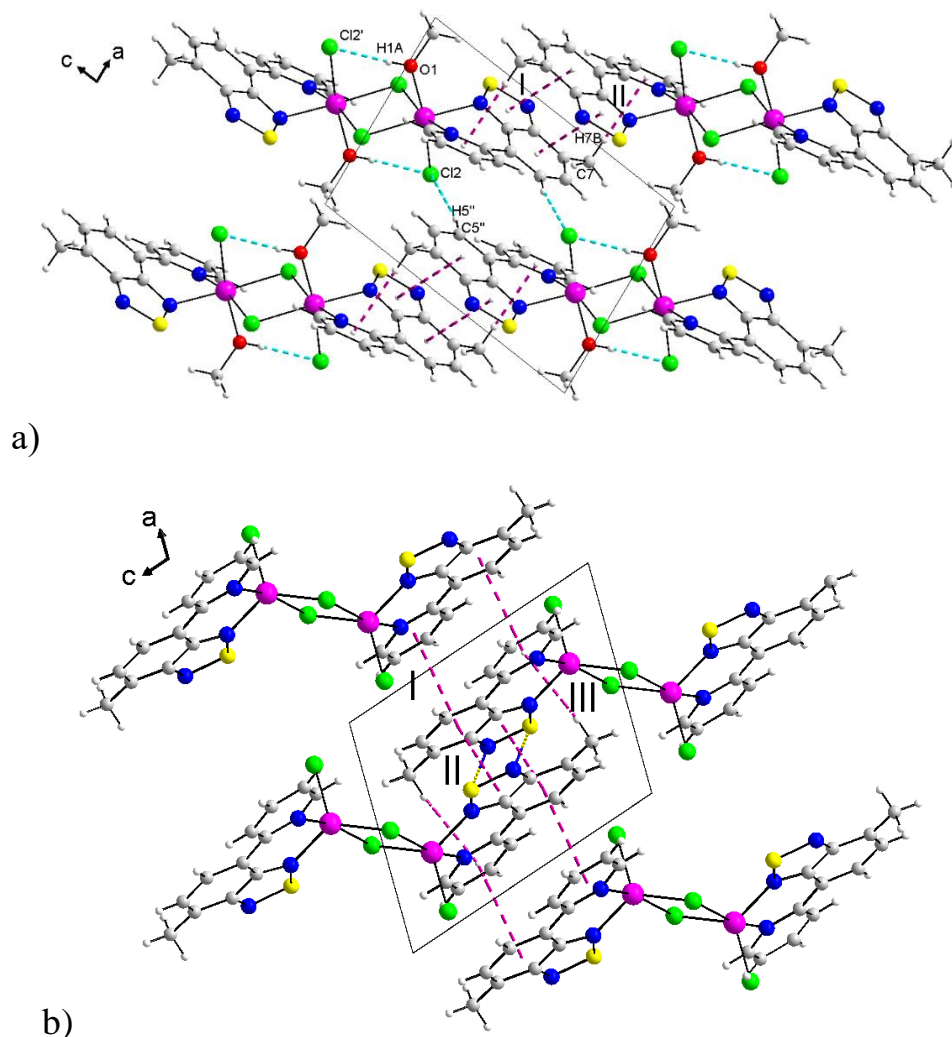


Figure 4.13. Crystal packing of complexes **29a** (a) and **29b** (b) with intramolecular and intermolecular interactions.

Table 4.3. Hydrogen bond parameters (Å, °) of **29a-32**.

D-H \cdots A	d(H \cdots A)	d(D \cdots A)	angles (D-H \cdots A)
29a			
O(1) – H(1A) \cdots Cl(2)	2.31	3.1555(18)	177
C(5) – H(5) \cdots Cl(2)	2.67	3.5831(3)	168
30			
C(4) – H(4) \cdots Cl(2)	2.75	3.6325	159
C(9) – H(9) \cdots Cl(2)	2.77	3.5539	142
C(17) – H(17) \cdots Cl(3)	2.78	3.6879	166
31			
C(7) – H(7B) \cdots Cl(2)	2.80	3.6841	154
C(12) – H(12) \cdots Cl(2)	2.79	3.5327	137
32			
C(11) – H(11) \cdots Cl(2)	2.78	3.6620	159

The results of the X-ray analysis show that the unit cell of the complex $[\text{CuL}^7\text{Cl}_2]$ (**30**) contains two independent molecules with binuclear $\{\text{Cu}_2(\text{L}^7)_2\text{Cl}_4\}$ and polymeric $\{\text{CuL}^7\text{Cl}_2\}_n$ structures (Fig. 4.14). The binuclear complex is based on the $\{\text{Cu}_2(\mu\text{-Cl})_2\}$ fragment with the $\text{Cu1}\cdots\text{Cu1}'$ distance 3.583 Å and the $\text{Cu1Cl1Cu1}'$ angle 92.94°. In the polymeric structure, the copper atoms also connect via chloride ions, with the $\text{Cu2}\cdots\text{Cu2}'$ distance 3.921 Å and the $\text{Cu2Cl4Cu2}'$ angle 102.62°. The copper ions have a N_2Cl_3 coordination environment with a square pyramidal geometry ($\tau_5 = 0.40$ for Cu1 and $\tau_5 = 0.26$ for Cu2). The structural parameters suggest that the polyhedron of Cu1 is more distorted than the one in the polymeric complex.

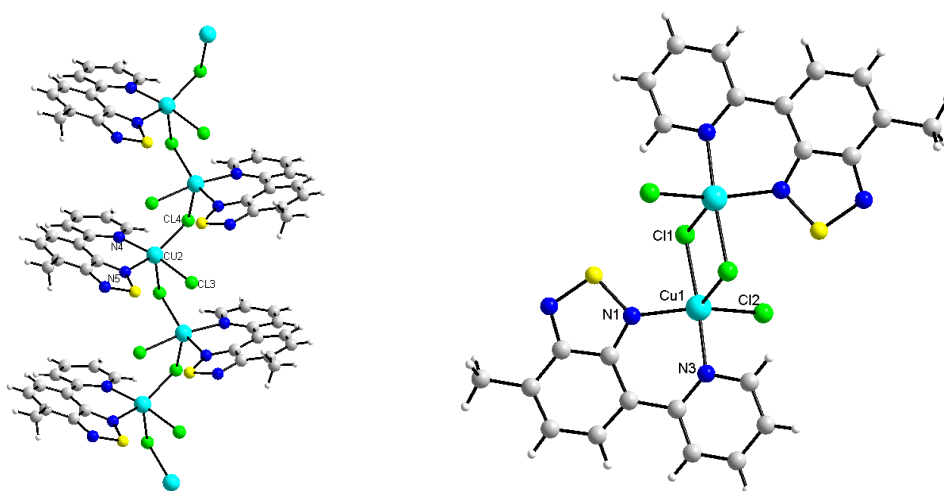


Figure 4.14. Polymeric (left) and binuclear (right) motifs in the crystal structure of complex **30**.

In complexes $[\text{ZnL}^7\text{Cl}_2]$ (**31**) and $[\text{PtL}^7\text{Cl}_2]$ (**32**), the metal atoms are four-coordinated within N_2Cl_2 environments (Fig. 4.15). The coordination geometry of Zn(II) is distorted tetrahedral with $\tau_4 = 0.93^{16}$. The platinum atom has a slightly distorted square planar geometry with a parameter $\tau_4 = 0.08$ thanks to the N_2Cl_2 coordination motif. The values of the *cis*-angles are 88.01(17)-93.39(18)° and the *trans*-angles are 173.24(17) and 175.6(6)°.

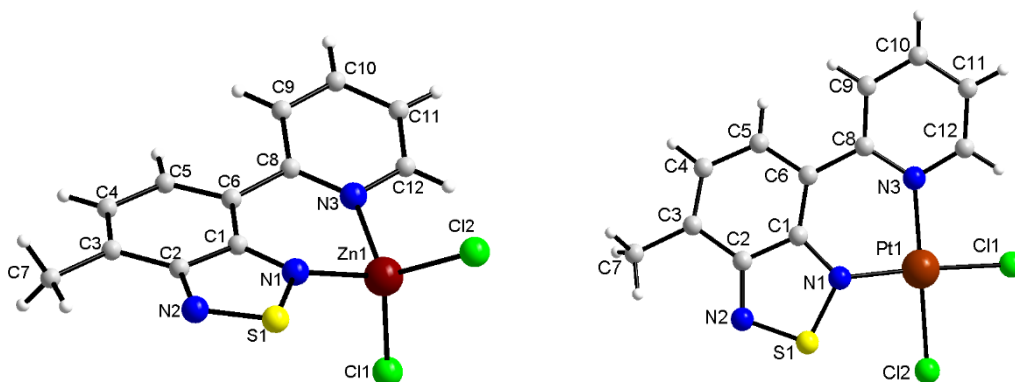


Figure 4.15. Molecular structure of complexes **31** (left) and **32** (right).

In the crystal packing **31** and **32** have an intermolecular C-H...Cl hydrogen bonds [3.831 (**31**) and 3.839 Å (**32**)] and π - π stacking interactions [4.062 (**31**) and 4.015 Å (**32**)] (Fig. 4.16-17, Table 4.3).

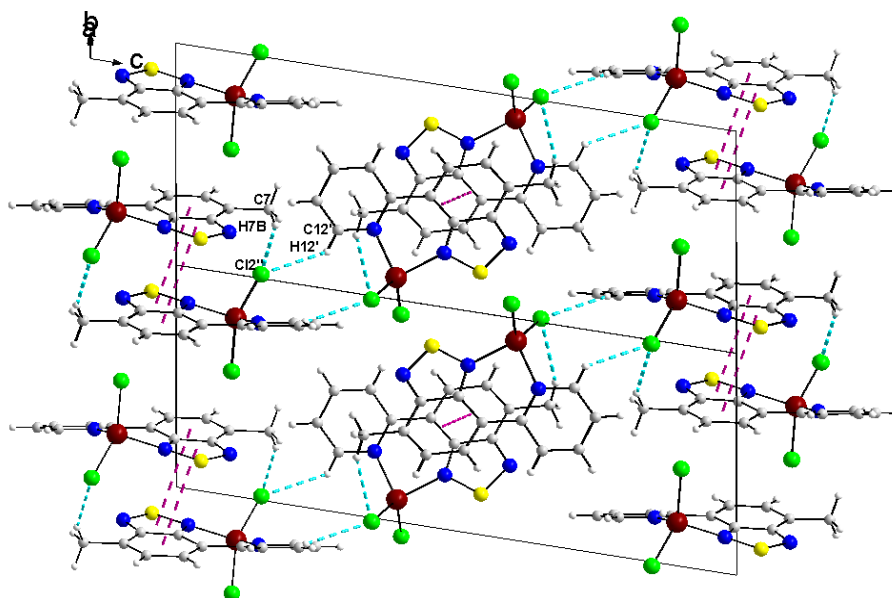


Figure 4.16. Crystal structure of complex **31**.

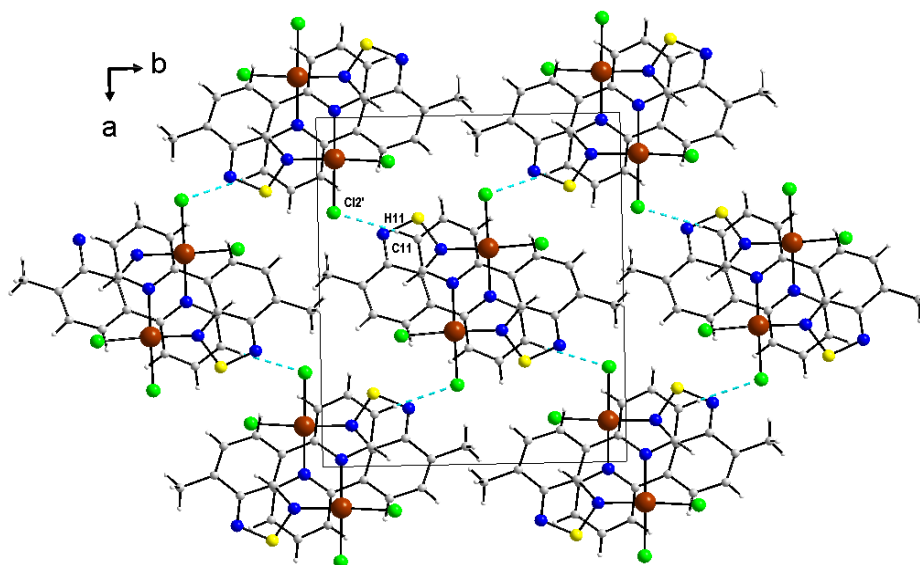


Figure 4.17. Crystal structure of complex **32**.

Complexes $[\text{MnL}^7(\text{Hfac})_2]$ (**33**), $[\text{CoL}^7(\text{Hfac})_2]$ (**34**), $[\text{NiL}^7(\text{Hfac})_2]$ (**35**), $[\text{CuL}^7(\text{Hfac})_2]$ (**36**), $[\text{ZnL}^7(\text{Hfac})_2]$ (**37**) crystallize in the centrosymmetric $P-1$ triclinic space group, the crystals having needle-shape. These complexes have similar molecular structures consisting of a metal atom, a molecule of ligand and two coordinated Hfac ions. Unfortunately, X-ray diffraction analysis was performed only for the complexes **34-36** because of the crystal quality.

Complex **36** contains one crystallographically independent molecule in the asymmetric unit cell, while complexes **34** and **35** contain two and four molecules of the same chemical type, respectively. The coordination environment of metals is formed by two N-donor atoms of **L7** and four O-donor atoms of Hfac, *i.e.* forming MN_2O_4 motifs (Fig. 4.18). In complexes **34-35**, the coordination geometry is a distorted octahedron, the main geometrical parameters and the BVS values being shown in Table 4.3. In the case of complex **36**, the copper ion may be in an axially elongated Jahn-Teller distorted octahedral geometry. The values of the axial Cu-O bond lengths are 2.246 and 2.318 Å, while the equatorial Cu-N/O bond lengths are in the range of 1.987-2.041 Å. The Cu(II) center is displaced from the plane O2O3N3N1 by 0.0244 Å.

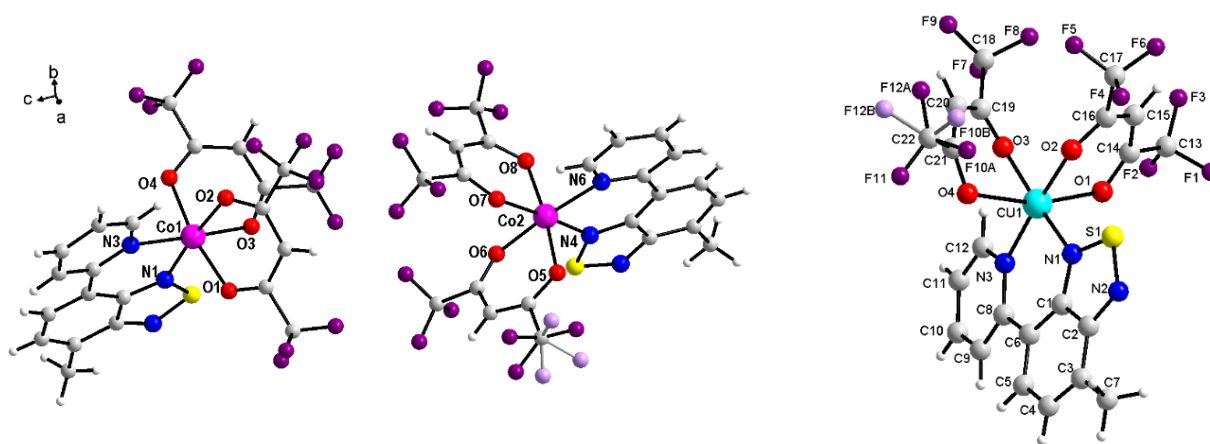


Figure 4.18. Crystal structures of complexes **34** (left) and **36** (right).

The molecules of ligand have *syn*-conformation in all complexes. The average values of the torsion angle between the BTD and *py* fragments of the ligand do not exceed 8.2° (angle C1C6C8N3 in the complex **36**). In the case of complex **35** the values of the angles vary in the range 0.182-22.140° (Table 4.4).

Table 4.4. Selected geometrical parameters and BVS values for the complexes **34-35**.

	34		35				36
	Co1	Co2	Ni1	Ni2	Ni3	Ni4	
M-N, Å	2.068(5)	2.073(5)	2.035(6)	2.015(7)	2.002(8)	2.033(8)	1.972(4)
	2.169(4)	2.141(5)	2.091(6)	2.081(6)	2.124(7)	2.062(9)	2.041(4)
	2.060(4)	2.052(4)	2.036(5)	2.023(5)	2.028(6)	2.022(8)	1.987(4)
M-O, Å	2.062(4)	2.065(4)	2.044(5)	2.028(6)	2.033(7)	2.032(7)	1.991(4)
	2.068(4)	2.078(4)	2.044(5)	2.050(5)	2.051(6)	2.047(7)	2.246(4)
	2.121(4)	2.083(4)	2.047(6)	2.060(6)	2.057(6)	2.051(8)	2.318(4)
<i>cis</i> -angles, °	83.88(15)-	86.65(17)-	86.1(2)-	85.8(2)-	84.5(3)-	86.5(3)-	82.97(16)-
	99.47(15)	98.71(18)	96.9(2)	96.7(3)	98.0(3)	98.5(3)	97.90(17)
<i>trans</i> -angles, °	169.00(15)	172.95(16)	174.2(2)	173.4(3)	169.2(2)	170.9(3)	165.29(13)
	174.59(17)	173.88(18)	174.4(2)	173.5(2)	173.9(3)	174.6(4)	173.24(17)
	175.96(17)	174.28(17)	176.9(2)	177.3(2)	174.9(3)	175.9(4)	175.59(17)
BVS	1.98 ^{12,13}	2.03 ^{12,13}	2.11 ¹⁵	2.15 ¹⁵	2.12 ¹⁵	2.16 ¹⁵	2.17 ¹⁵
angle, °							
<i>py</i> -BTD	7.081	5.29	7.024	2.762	0.182	22.140	8.165

In the crystal packing of complexes **34-36** there are π - π stacking interactions that connect adjacent molecules in parallel chains along the *a*-axis. In complex **34** two types of π - π interactions were found: between benzo rings of BTD fragment of the ligands [3.4896 Å] and between pyridine rings [3.5560 Å] (Fig. 4.19). At the same time, for complex **36**, in addition to the two types of π - π interactions [3.803 Å (I) and 3.793 Å (III)], there is a contact C17-H17B...centroid (II) with a distance of 2.832 Å and an angle 88.03 ° (Fig. 4.19). In the case of complex **35**, which contains four crystallographically independent molecules, several π - π stacking interactions of different nature were found [3.586-3.922 Å].

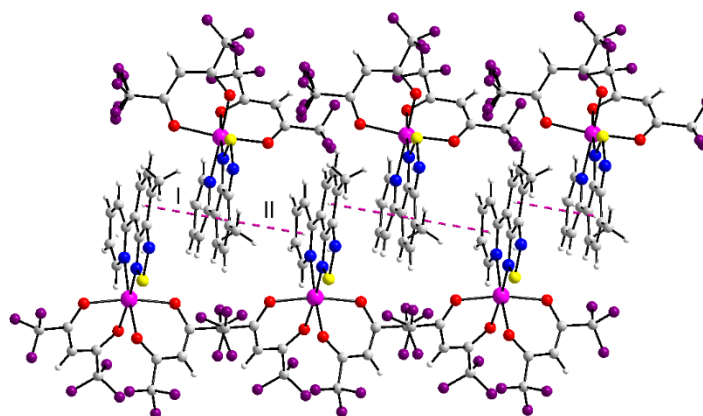


Figure 4.19. Fragment of the crystal structure of **34**.

As mentioned earlier, complexes **34-36** form parallel chains consisting of two rows of complexes. The octahedra of the complexes **34** and **35** contain only Δ or Λ isomers along one chain. In the case of **36**, each chain consists of one row of Δ and one row of Λ isomers linked by π - π stacking interactions (Fig. 4.20).

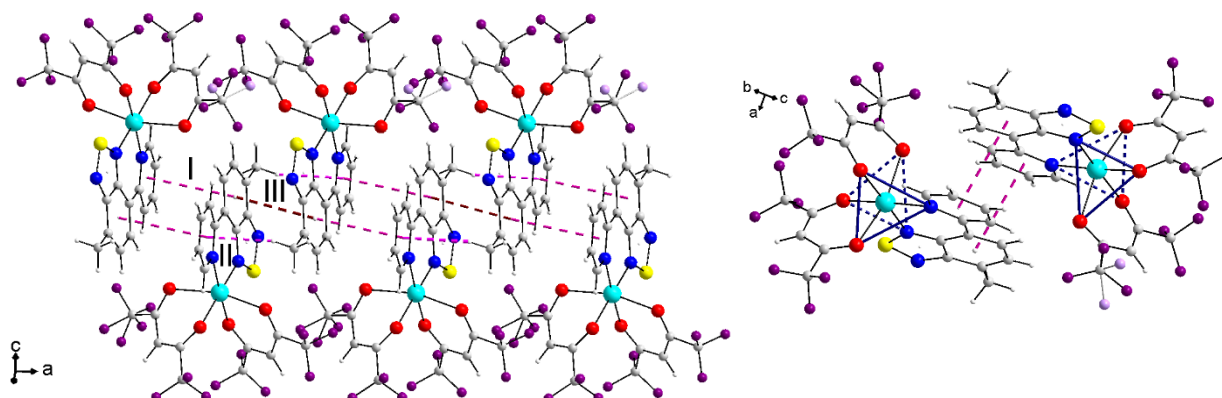


Figure 4.20. Complex **36**: left – fragment of crystal packing with intramolecular interactions; right – fragment of crystal packing showing Δ (left) and Λ (right) isomers.

4.3.2. Crystal structures of coordination compounds with L^8

The ligand L^8 has potentially two “coordination pockets” which are taking part in the formation of mono- and binuclear complexes $[CuL^8(Hfac)_2]$ (**38**) and $[Cu_2L^8(Hfac)_4]$ (**39**). They crystallize in the $P2_1/c$ and $C2/c$ space groups, respectively. *N,N*-bidentate-chelating and *N,N,N,N*-tetradentate-chelate bridging coordination mode were observed. The mononuclear complex contains one copper atom, two bidentate coordinated Hfac ions and one L^8 . In the binuclear complex, two coordination pockets of one ligand and four Hfac anions are involved in the coordination of the two copper ions (Fig. 4.21).

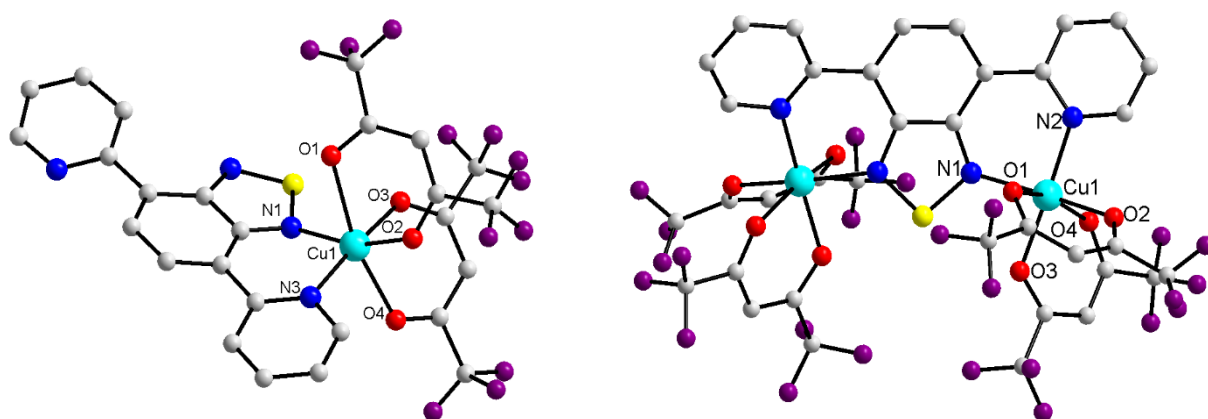


Figure 4.21. Molecular structures of complexes **38** (left) and **39** (right).

The copper atoms are in a distorted octahedral CuN_2O_4 geometry. Distortions are caused, on the one hand, by Jahn-Teller effect of copper ion, and on the other hand by the three chelating ligands. The axial Cu-O bonds are elongated and equal to 2.215(3)-2.402(3) Å and 2.267(6)-2.287(6) Å in **38** and **39**, respectively (Table 4.5).

Table 4.5. Selected geometrical parameters and the BVS values for complexes **38** and **39**.

	38	39
Cu-N, Å	2.007(3), 2.007(3)	2.032(6), 2.064(6)
Cu-O, Å	1.968(3)-2.402(3)	1.981(5)-2.287(6)
<i>cis</i> -angles, °	80.13(12)-108.41(12)	81.4(2)-107.2(2)
<i>trans</i> -angles, °	160.88(13), 166.86(10), 173.62(12)	169.9(2), 166.0(2), 164.9(2)
BVS	2.14 ¹⁵	2.06 ¹⁵
angles, ° (BTD- <i>py</i>)	15.04, 166.49	25.59
π - π , Å	3.866, 3.709, 3.669	3.731

In complex **38** the pyridine rings are in *syn*- and *anti*-configurations with respect to the BTD unit, the values of dihedral angles between BTD-*py* fragments being 15.04 and 166.49 °. In the binuclear complex **39** the dihedral angle is 25.59 ° and L^8 has only *syn*-configuration.

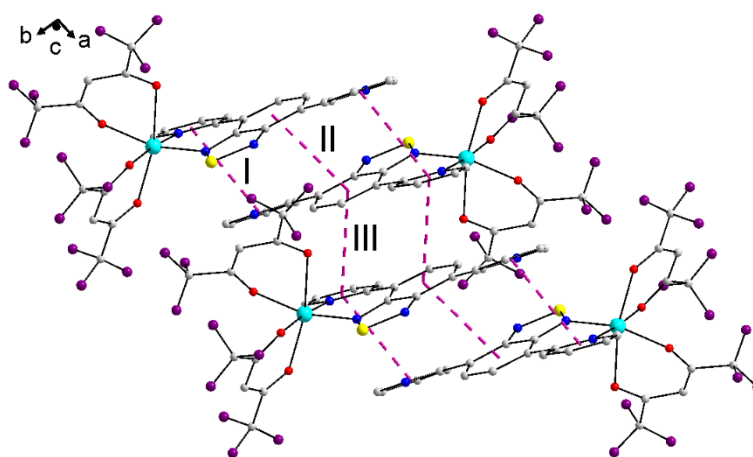


Figure 4.22. Fragment of the crystal packing showing π - π -interactions (I-3.866 Å, II-3.709 Å, III-3.669 Å) in complex **38**

Supramolecular chains are formed by π - π stacking interactions (Fig. 4.22-23, Table 4.5).

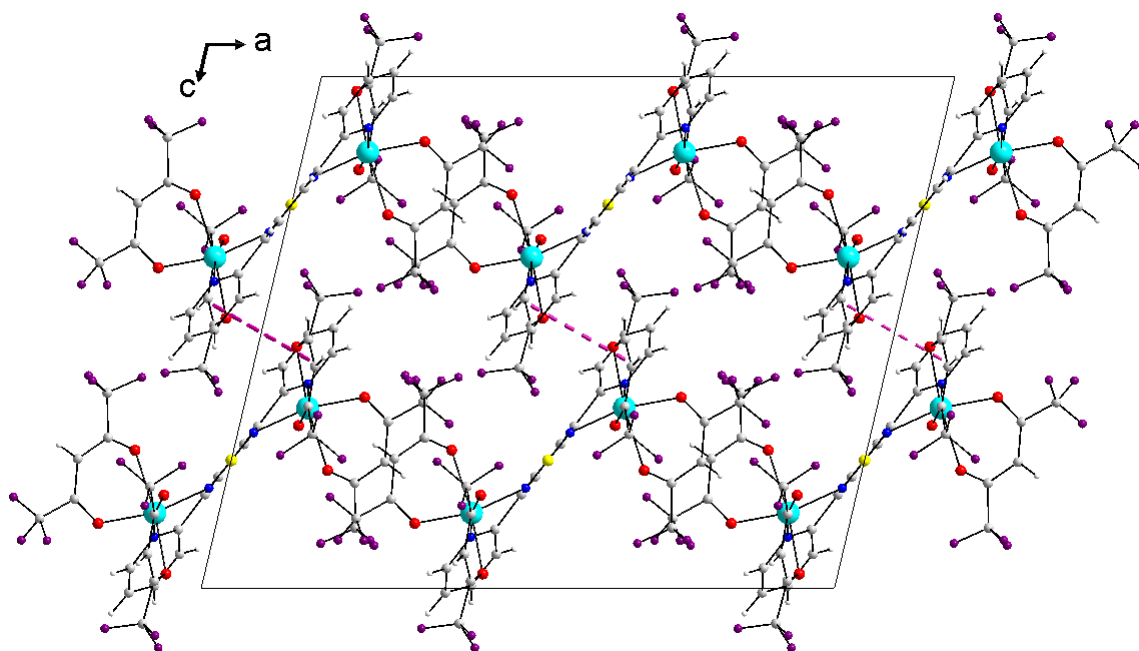


Figure 4.23. Crystal packing of the complex **39** with π - π interactions highlighted.

4.3.3. Crystal structures of coordination compounds with L^9

Complexes $[MnL^9Cl_2] \cdot 0.5CH_2Cl_2$ (**40**), $[CoL^9Cl_2] \cdot 0.25CH_2Cl_2$ (**42**), $[CuL^9Cl_2] \cdot H_2O$ (**45**), $[ZnL^9Cl_2]$ (**46**) crystallize in the centrosymmetric monoclinic $C2/c$ space group and the asymmetric unit is composed of one metal ion and the ligand L^9 , two chloride ions and molecules of solvent: dichloromethane (**40**, **42**) or water (**45**). The metal atoms are five-coordinated by two chloride ions and one molecule of tridentate (N,N,N) ligand. The metal atoms have a slightly

distorted N_3Cl_2 square pyramidal geometry (Fig. 4.24, Table 4.6). The largest deviations from this geometry are observed for complex **46** [$\tau_5 = 0.107$] and in the case of **45** the smallest ones [$\tau_5 = 0.003$]. The base of the pyramid is the plane $N1N3N4Cl2$ and the $Cl1$ atom is in axial position. The metal atom is displaced from the equatorial plane by 0.307 Å (Cu), 0.485 Å (Co), 0.544 Å (Zn) and 0.629 Å (Mn).

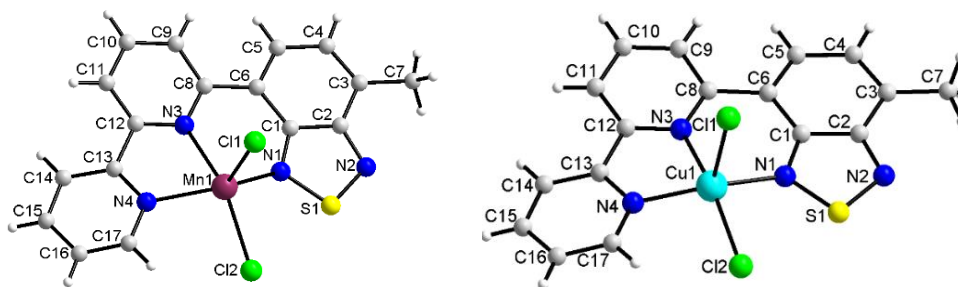


Figure 4.24. Molecular structure of complexes **40** (left) and **45** (right).

Table 4.6. Selected geometrical parameters and the BVS values for the complexes **40**, **42**, **45**, **46**.

	40	42	45	46
M-Cl, Å	2.3654(10)	2.3144(10)	2.2968(10)	2.2773(5)
M-N, Å	2.3966(10)	2.3460(11)	2.4699(11)	2.3261(5)
	2.170(3)	2.068(3)	1.992(4)	2.0614(18)
	2.318(3)	2.196(3)	2.070(3)	2.2592(16)
M-N _{BTD} , Å	2.183(3)	2.076(3)	1.979(3)	2.0919(17)
angles XMY, °	75.38(10)-	78.35(10)-	82.04(14)-	77.07(6)-
X, Y = Cl/N	148.77(8)	155.50(7)	162.91(10)	152.64(5)
τ_5	0.086	0.088	0.003	0.107
angles (C1C6C8N3), °	0.70	2.75	1.17	3.60
BVS	2.01 ^{12,13}	1.76 ^{12,13}	2.21 ^{14,15}	2.05 ¹⁴

The molecules assemble through the C-H \cdots Cl hydrogen bonds creating a two-dimensional supramolecular structure (Table 4.7). The fragments of the crystal structure of complexes **40** and **46** are shown as examples in Figure 4.25.

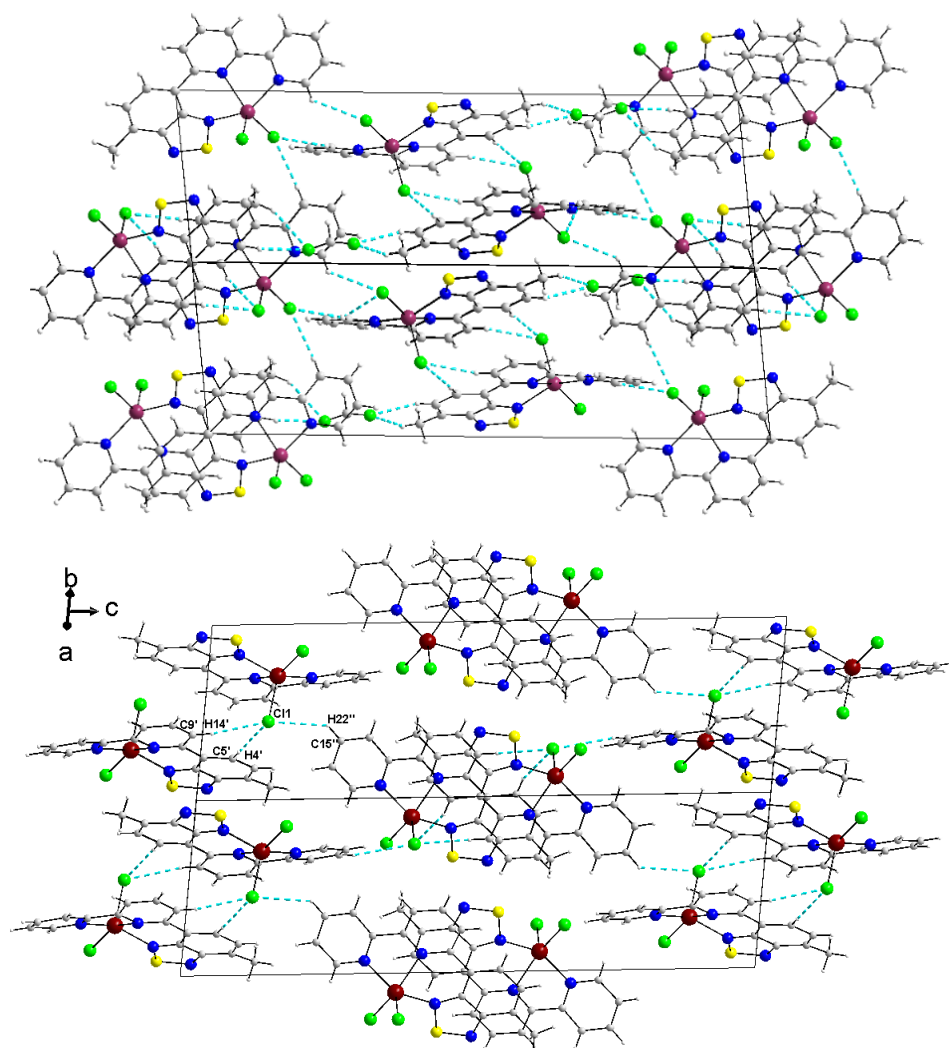


Figure 4.25. Fragments of the crystal packing showing hydrogen bonds of complexes **40** (top) and **46** (down).

Table 4.7. Hydrogen bond parameters (\AA , $^\circ$) of complexes **40**, **42**, **45**, **46** (without excluding solvent molecules).

D-H...A	d(H...A), \AA	d(D...A), \AA	angles (D-H...A), $^\circ$
40			
C(5)-H(5)...Cl(1)'	2.77	3.6703	163
C(9)-H(9)...Cl(1)'	2.82	3.7370	169
C(14)-H(14)...Cl(2)''	2.8738(13)	3.6367(44)	128.104(248)
C(17)-H(17)...Cl(2)'''	2.9573(12)	3.6654(43)	134.001(249)
42			
C(5)-H(5)...Cl(1)'	2.73	3.6195(7)	161
C(9)-H(9)...Cl(1)'	2.8784(10)	3.7888(39)	166.364(217)
C(15)-H(15)...Cl(1)''	2.9624(10)	3.6328(43)	130.179(254)
C(14)-H(14)...Cl(2)'''	2.9689(12)	3.7207(43)	138.955(251)
45			
C(5)-H(5)...Cl(1)'	2.63	3.5164(10)	159
C(9)-H(9)...Cl(1)'	2.78	3.7045(10)	170
C(15)-H(15)...Cl(1)''	2.65	3.4905(10)	130
46			
C(5)-H(4)...Cl(1)'	2.7242(6)	3.6107(24)	159.687(138)
C(9)-H(14)...Cl(1)'	2.7235(6)	3.6451(23)	171.035(130)
C(15)-H(22)...Cl(1)''	2.8585(6)	3.5286(25)	129.978(149)

Complexes $[\text{CoL}^9(\text{H}_2\text{O})_2\text{Cl}]\text{Cl}\cdot 3\text{H}_2\text{O}$ (**41**) and $[\text{NiL}^9(\text{H}_2\text{O})_3]\text{Cl}\cdot 2\text{H}_2\text{O}$ (**43**) crystallize in the centrosymmetric triclinic *P*-1 space group and consist of the metal atom, one molecule of ligand, coordinated or uncoordinated chloride ions and water molecules. The CoClN_3O_2 and NiN_3O_3 motifs have a distorted octahedral geometry formed by three nitrogen atoms of the ligand, two oxygen atoms of water and chloride ions (**41**) or by three nitrogen atoms of the ligand and three oxygen atoms of water (**43**) (Fig. 4.26-27). In complexes **41**, **43**, **44** with six coordinated central atom, the values of the torsion angle (C1C6C8N3) increases to almost 16° , comparing with values for the complexes **40**, **42**, **45**, **46** with five-coordinated metal [not exceeding 3.6°] (Table 4.6 and 4.8).

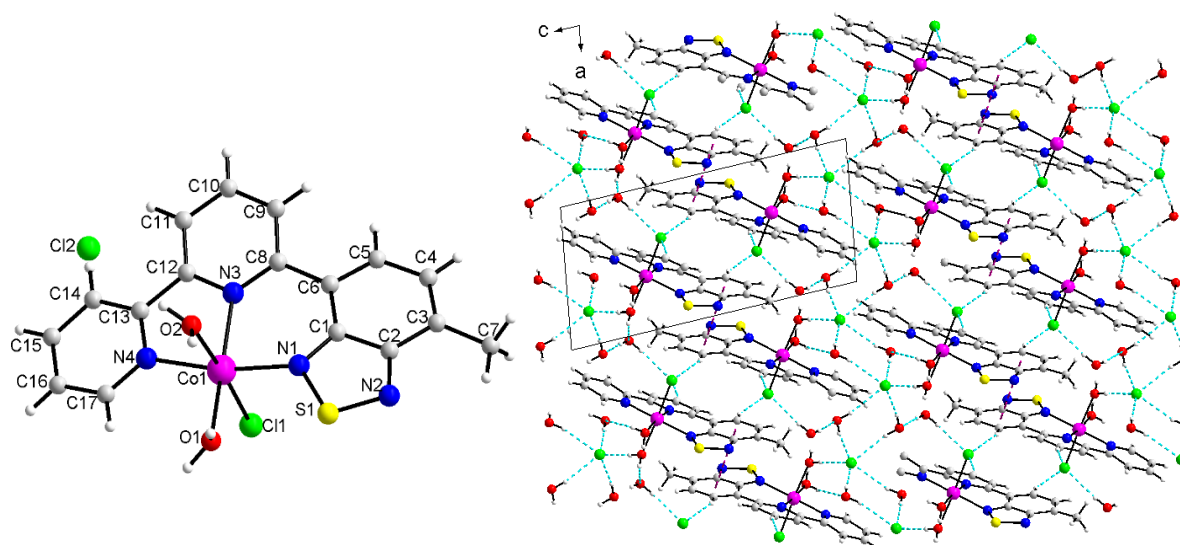


Figure 4.26. Complex **41**: molecular structure (left) and fragment of the crystal packing showing the H-bonds (right).

Table 4.8. Selected geometrical parameters and the BVS values for the complexes **41**, **43**, **44**.

	41	43	44
M-Cl, Å	2.4280(7)	-	2.3965(12), 2.4192(10), 2.5560(11)
M-N, Å	2.1299(16), 2.1299(16)	2.0963(14), 2.0362(14)	2.028(3), 2.087(3)
M-N _{BTD} , Å	2.0895(17)	2.0253(14)	2.013(3)
M-O, Å	2.1304(16), 2.2204	2.0604, 2.0622, 2.0897	-
<i>cis</i> -angles, °	79.94(7)- 102.67(7)	81.02(6)- 99.58(4)	81.35(13)- 97.82(9)
<i>trans</i> -angles, °	169.04(7), 172.36(7), 175.33(3)	171.16(6), 174.100, 178.49(4)	168.11(10), 171.83(13), 177.22(4)
BVS	1.79 ^{12,13}	2.02 ¹⁵	1.97 ^{14,15}
angle (C1C6C8N3), °	15.79	11.84	10.05

π - π -Stacking interactions exist between benzo rings of neighboring molecules of complex **41** [3.552 \AA] (Fig. 4.26). In the complex **43** the weak π - π stacking between benzo and pyridine rings involves two rings from each ligand [3.947 \AA] interacting in a parallel displaced mode (Fig. 4.27). The coordinated and uncoordinated molecules of water and chloride ions form several O-

H \cdots O and C-H \cdots Cl intermolecular hydrogen bonds resulting in creation of the supramolecular structure by non-covalent interactions in the crystal structure of **41** and **43**.

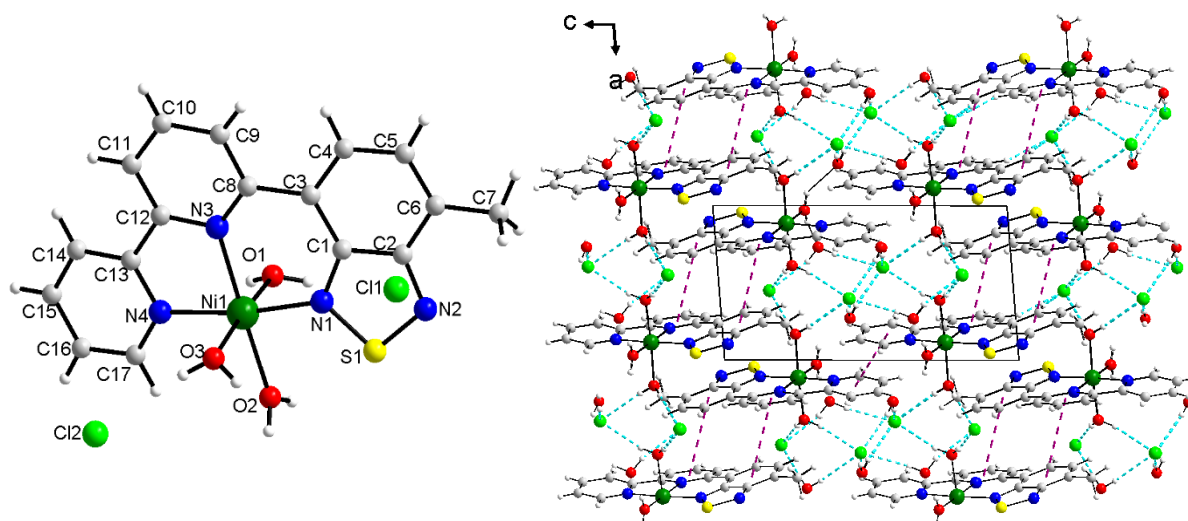


Figure 4.27. Complex **43**: molecular structure (left) and fragment of the crystal packing showing H-bonds (right).

The complex $[\text{Ni}_2(\text{L}^9)_2\text{Cl}_4] \cdot 2\text{H}_2\text{O}$ (**44**) crystallizes in the *P*-1 triclinic space group. The asymmetric unit consists of half of the binuclear complex, in which the center of inversion is in the middle of the Ni \cdots Ni distance. The crystal structure of **44** shows a binuclear $\{\text{Ni}_2(\mu\text{-Cl})_2\}$ fragment, where two chloride ions are bridging the Ni(II) atoms in an axial-equatorial manner. The Ni \cdots Ni distance is 3.7167(8) Å and the NiClNi angle is 96.63(4) ° (Fig. 4.28). The nickel (II) atom has a N₃Cl₃ coordination environment formed by three nitrogen atoms from the ligand and three chloride ions. The coordination geometry can be considered as a distorted octahedron (Table 4.8). In the crystal structure, π - π stacking interactions between the benzene and pyridine rings [3.815 Å] and a number of intermolecular hydrogen bonds were found.

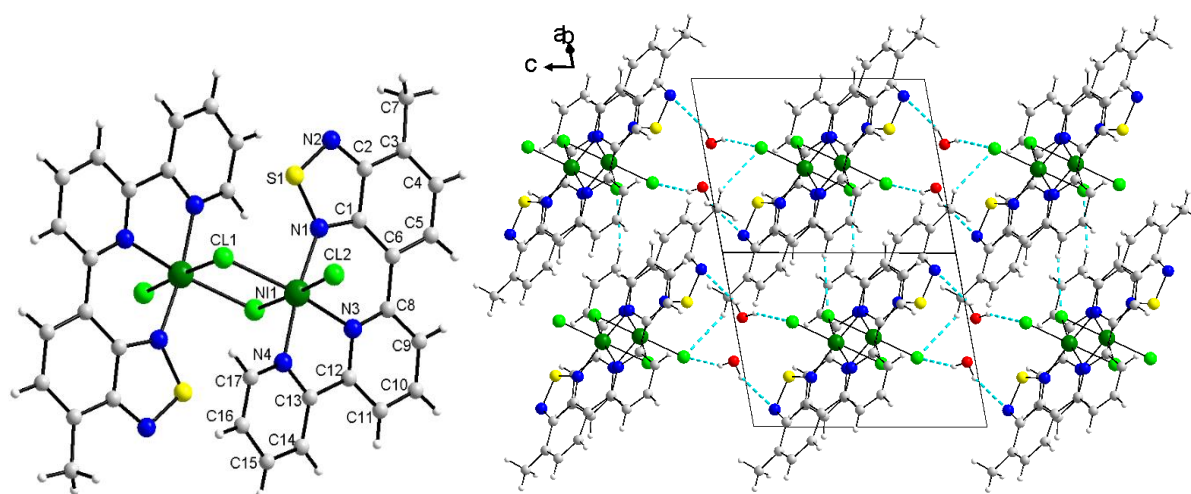


Figure 4.28. Complex **44**: molecular structure (left) and fragment of the crystal packing showing the hydrogen bonds (right).

Complexes $[\text{NiL}^9(\text{Hfac})(\text{H}_2\text{O})](\text{Hfac})\cdot\text{H}_2\text{O}$ (**47**), $[\text{CuL}^9(\text{Hfac})(\text{H}_2\text{O})](\text{Hfac})\cdot\text{H}_2\text{O}$ (**48**), $[\text{CuL}^9(\text{Hfac})(\text{C}_2\text{H}_5\text{OH})](\text{Hfac})$ (**49**) contain a metal atom, one molecule of L^9 , two Hfac anions and solvent molecules (two water molecules in **47** and **48** or one molecule of methanol in **49**). All metal atoms are six-coordinated (Fig. 4.29). In the complex **47**, the NiN_3O_3 chromophore has a distorted octahedral geometry (Table. 4.9). In the case of complexes **48** and **49**, the octahedron is distorted by elongation of the axial Cu-O bonds, leading to the formation of a tetragonal bipyramid (due to Jahn-Teller effect). The Cu-O_{ax} bond lengths are 2.2945(18) and 2.397(2) Å for complex **48**, or 2.3388(12) and 2.3982(12) Å for complex **49**.

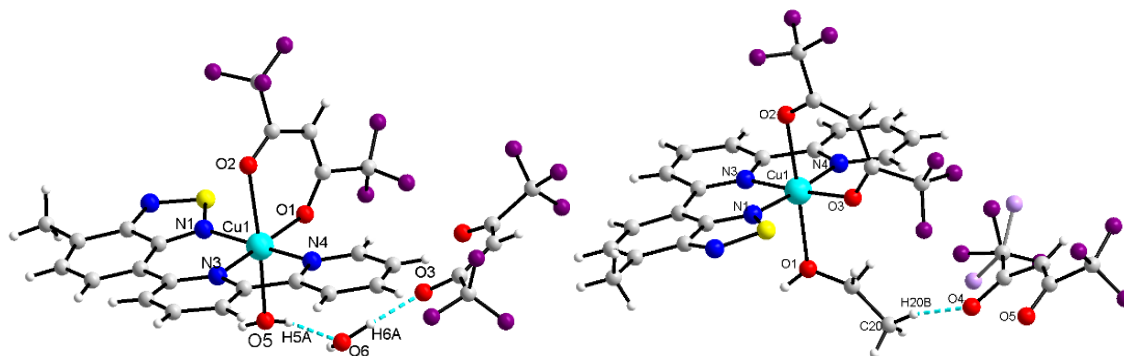


Figure 4.29. Crystal structures of complexes **48** (left) and **49** (right).

The ligand uses three N-donor atoms in the coordination, displaying *N,N,N*-tridentate chelating coordination mode. The value of dihedral angle (C1C6C8N3) does not differ significantly and is in the range of 8.32-9.69 ° (Table 4.9).

Table 4.9. Selected geometrical parameters and the BVS values for the complexes **47-49**.

	47	48	49
M-O, Å	2.0677(14)	2.0157(18)	2.0022
	2.0737(14)	2.2945(18)	2.3388(12)
	2.0927(14)	2.397(2)	2.3982(12)
M-N, Å	2.0144(18)	1.967(3)	1.966(3)
	2.0333(18)	1.970(3)	1.977(3)
	2.0657(17)	2.034(2)	2.028(3)
<i>cis</i> -angles, °	81.93(7)-93.29(7)	82.03(9)-94.25(9)	83.03(11)-94.38(8)
	172.79(7)	173.65(10)	174.74(12)
<i>trans</i> -angles, °	175.20(7)	172.91(7)	175.73(8)
	175.80(6)	175.37(10)	174.000
BVS	2.04 ¹⁵	2.10 ^{15,17}	2.09 ^{15,17}
angle(C1C6C8N3), °	9.27	9.39	8.69

Molecules of solvent take part in the formation of hydrogen bonds, linking two adjacent molecules of complex with coordinated and uncoordinated Hfac ions (Table. 4.10, Fig. 4.30).

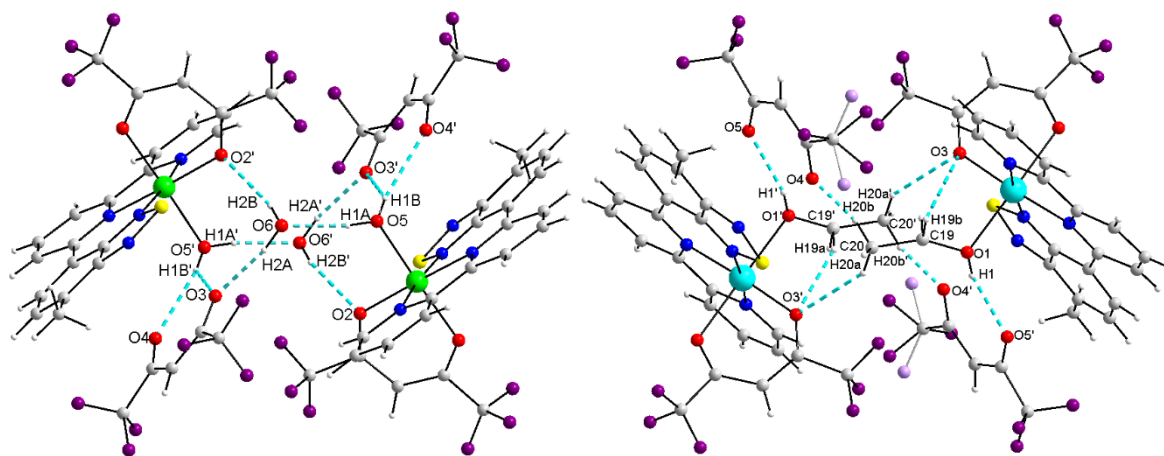


Figure 4.30. Fragment of the crystal packing showing hydrogen bonding in complexes **47** (left) and **49** (right).

In the crystal packing, in addition to a number of hydrogen bonds there are π - π and S \cdots N interactions. The S \cdots N distances are 3.062, 3.114 and 3.181 Å for **47**, **48** and **49**, respectively. Two types of π - π interactions were found: between the benzene and pyridine rings and between two pyridine rings [3.560 and 3.680 Å (**47**), 3.573 and 3.701 Å (**48**), 3.774 and 3.611 Å (**49**), respectively]. Such intermolecular interactions provide a 3D architecture (Fig. 4.31).

Table 4.10. Hydrogen bond parameters (Å, °) of **47** - **49**.

D-H \cdots A	d(H \cdots A), Å	d(D \cdots A), Å	angles (D-H \cdots A), °
47			
O(5) – H(5A) \cdots O(3)	2.28	2.9171(1)	140
O(5) – H(5A) \cdots O(4)	2.33	2.9691(1)	142'
O(5) – H(5B) \cdots O(6)	1.88	2.7009(1)	167
O(6) – H(6A) \cdots O(2)	2.38	3.1331(1)	163'
O(6) – H(6B) \cdots O(3)	2.02	2.7694(1)	165
48			
O(5) – H(5A) \cdots O(6)	1.95	2.7366(3)	166
O(5) – H(5B) \cdots O(3)	2.32	2.9375(3)	139
O(5) – H(5B) \cdots O(4)	2.29	2.9453(3)	144
O(6) – H(6A) \cdots O(3)	1.86	2.7865(3)	166
O(6) – H(6B) \cdots O(1)	2.38	3.2318(4)	156
49			
O(1) – H(1) \cdots O(5)'	2.08	2.8630(2)	152
C(20) – H(20A) \cdots O(3)'	2.52	3.3473 (2)	144'
C(19) – H(19A) \cdots O(3)	2.29	3.0681(2)	137
C(20) – H(20B) \cdots O(4)	1.74	2.6579(1)	158

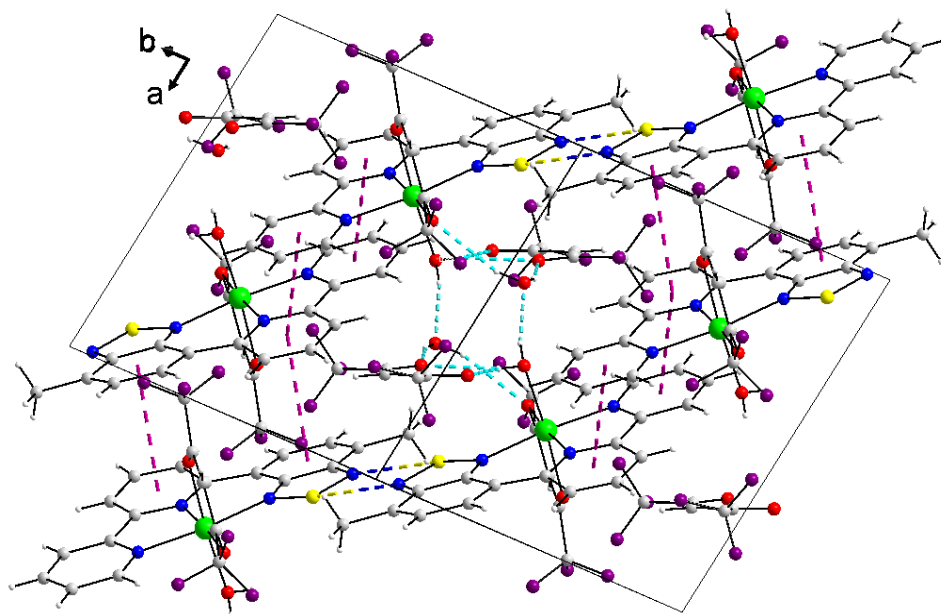


Figure 4.31. Crystal structure of the complex **47** showing hydrogen bonds, π - π -stacking and S \cdots N interactions.

4.4. Photophysical properties

The luminescent properties have been investigated in collaboration with Prof. A. Hauser, Department of Physical Chemistry Sciences II, University of Geneva, Switzerland. Absorption, emission and excitation spectra of the ligands **L**⁷, **L**⁹, **L**¹⁰ and complexes [Zn**L**⁷Cl₂] (**31**), [Pt**L**⁷Cl₂] (**32**), [Zn**L**⁹Cl₂] (**46**) were measured in CH₂Cl₂ ($\sim 1 \cdot 10^{-5}$ M).

UV-vis spectra of **L**⁷, **L**⁹, **L**¹⁰ show three maxima: the first peak at 250 and 240 nm (for **L**⁷ and **L**¹⁰, respectively), and a double peak at 240 and 263 nm for **L**⁹; the second peak is slightly doubled for all ligands (318 and 306 nm (**L**⁷), 311 and 318 nm (**L**⁹) and at 283 nm with shoulder at 315 nm for **L**¹⁰); the last intense peaks are at 362, 370 and 391 nm for **L**⁷, **L**⁹ and **L**¹⁰, respectively (Fig. 4.32 – 33). All ligands show luminescent properties with λ_{max} 460, 470 and 475 nm for **L**⁷, **L**⁹ and **L**¹⁰, respectively. Excitation and absorption spectra of ligands are identical, thus the luminescence is clearly due to the compounds and not to some impurity or decomposition product.

Time Dependent DFT (TD DFT) calculations were performed with the PBE0 functional⁸ and 6-311++G(2df,2pd)^{9,10} basis set, to reproduce the absorption and emission properties. For the emission, the first singlets were optimized. The calculated data for absorption and luminescence correlate well with the experimental ones (Fig. 4.32 – 33).

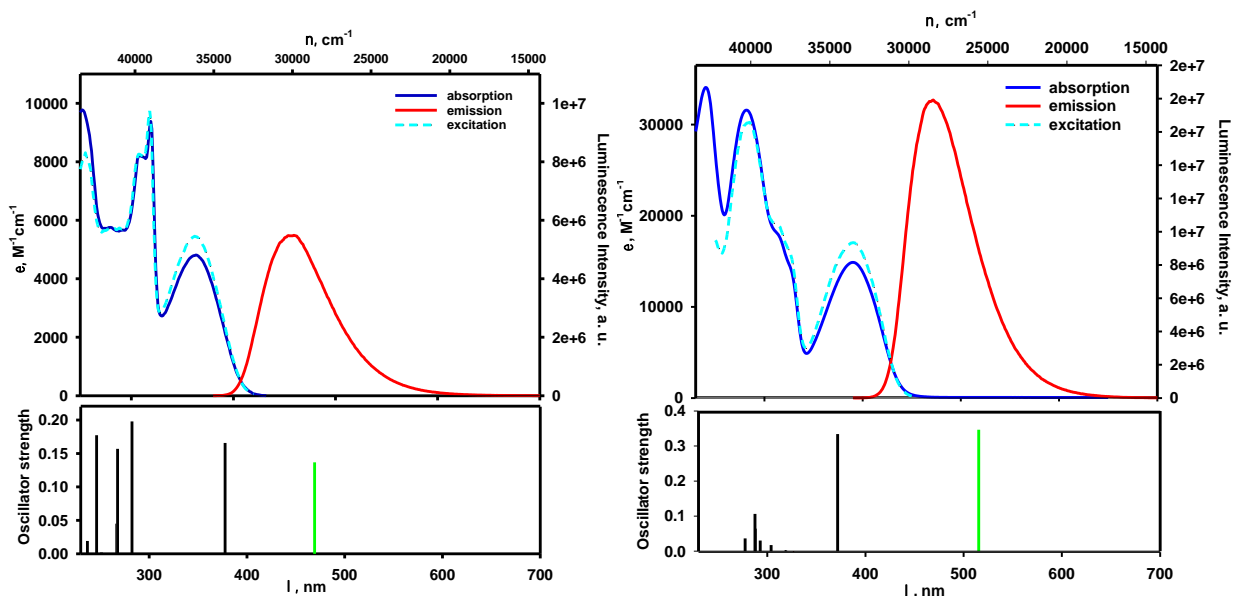


Figure 4.32. Comparison of the calculated (stick plot) and experimental (line graph) absorption, excitation and luminescence spectra of L^7 (left) and L^{10} (right), ($\lambda_{em}=460$ nm, $\lambda_{ex}=360$ nm and $\lambda_{em}=475$ nm, $\lambda_{ex}=380$ nm, respectively).

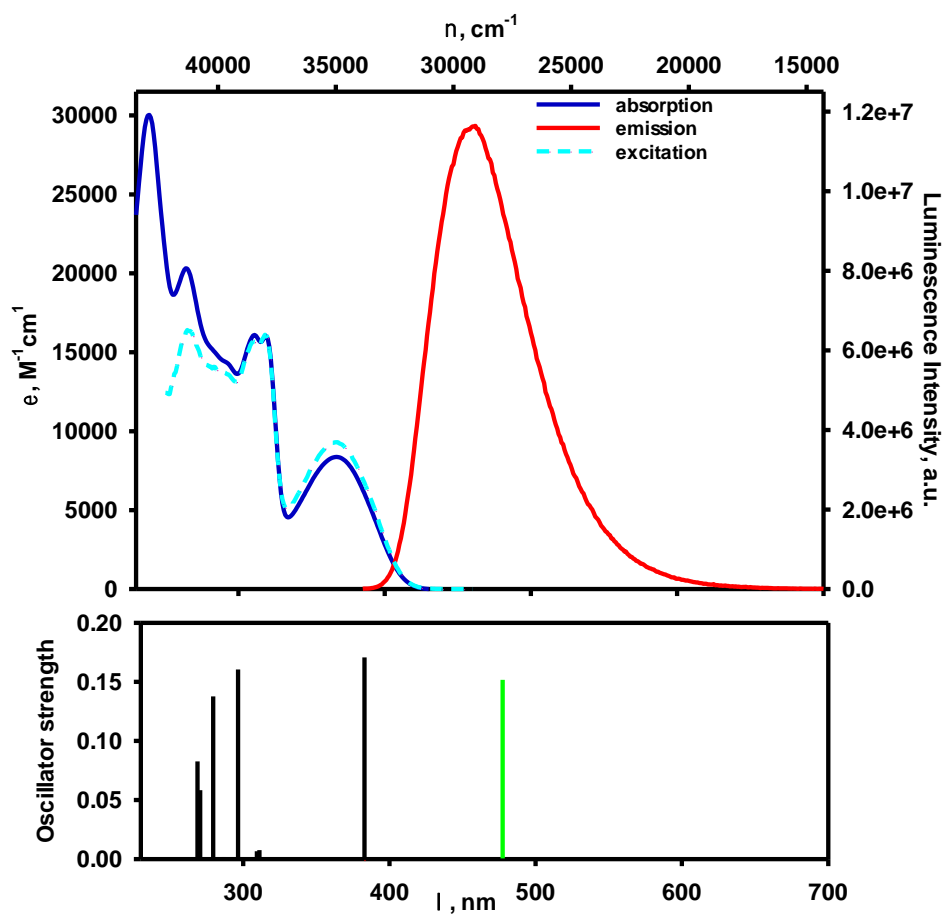
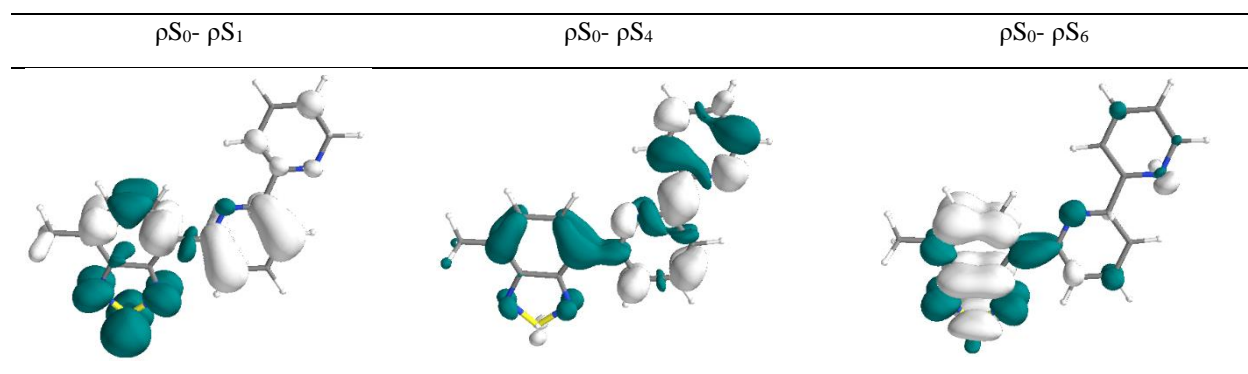


Figure 4.33. Comparison of the calculated (stick plot) and experimental (line graph) absorption, excitation and luminescence spectra of L^9 ($\lambda_{em}=470$ nm, $\lambda_{ex}=375$ nm).

For **L**⁹ the experimental and calculated photophysical properties have been compared by considering the electron density difference (EDD corresponds to the transition from the ground state to the excited state) (Fig. 4.33, Table 4.11). The experimental absorption band with a maximum at 370 nm corresponds to the calculated S₀ → S₁ transition with a maximum at 382 nm. This transition can be attributed to a π → π* transition, which is mainly the HOMO → LUMO excitation. The EDD of the S₀ → S₁ transition clearly shows electron density moving from benzene and pyridine ring to the thiazazole part of the ligand (from donor to acceptor). The second absorption band combines three transitions with a large contribution of S₀ → S₄: which is mainly a *py* π → π* transition. The third peak in the low-wavelengths region is dominated by the S₀ → S₆ and correspond to a BTD π → π* transition. The spectra of **L**⁷ and **L**¹⁰ look similar to **L**⁹ and caused mainly by analogous transitions.

The calculated emission spectra have maxima at 469, 477 and 515 nm for the ligands **L**⁷, **L**⁹ and **L**¹⁰, respectively, correlating well with the experimental ones at 460, 470 and 475 nm.

Table 4.11. Density difference plots for **L**⁹ (the blue region corresponds to the excited electron density whereas the white region corresponds to the hole).



The normalized absorption and luminescence spectra of [ZnL⁷Cl₂] (**31**), [PtL⁷Cl₂] (**32**) and [ZnL⁹Cl₂] (**46**) are shown in Figure 4.34. In the spectra of complexes **31** and **46** it exists a shift of bands in the low-wavelength region compared with the free ligands. The emission and excitation spectra of complex **32** look similar to the spectra for **L**⁷. Probably, it can be explained by the decomposition of the complex in solution or the compound contains some non-coordinated ligand. The absorption spectrum for complex **32** differs from the absorption spectrum of the ligand by the presence of the peak at 450 nm, corresponding probably to a metal to ligand charge transfer.

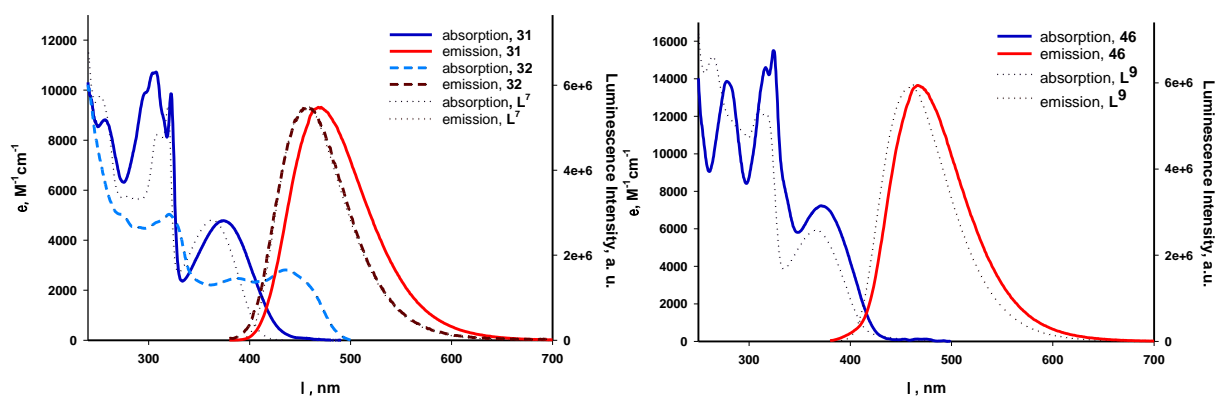


Figure 4.34. Normalized absorption and luminescence spectra of **31**, **32**, **L⁷** (left) and **46** and **L⁹** (right).

Normalized luminescence spectra of **L⁷**, **L⁹**, **L¹⁰** show a bathochromic shift with increasing number of heterocycles in the ligand (Fig. 4.35). A similar shift is observed in the emission spectra of the complexes, in comparison with the spectra of the free ligands.

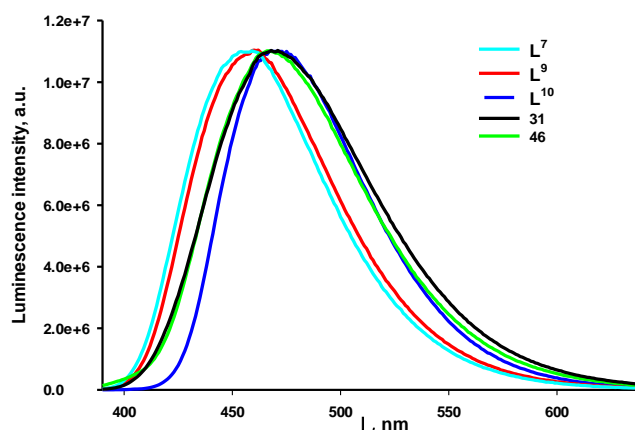


Figure 4.35. Normalized luminescence spectra of **L⁷**, **L⁹**, **L¹⁰**, **31** and **46**, in CH_2Cl_2 at room temperature ($\lambda_{\text{ex}} = 360 \text{ nm}$).

The luminescence quantum yields (η) were determined with diphenyl-anthracene as a standard reference with excitation at 360 nm having a luminescence quantum efficiency of 95% in n-heptane at room temperature, using the formula:

$$\eta = \frac{\int I_{\text{lum}}^{\text{sample}}(\lambda) d\lambda}{\int I_{\text{lum}}^{\text{ref}}(\lambda) d\lambda} \cdot \frac{OD_{\lambda_{\text{ex}}}^{\text{ref}}}{OD_{\lambda_{\text{ex}}}^{\text{sample}}} \cdot \left(\frac{n_{\text{solv}}^{\text{sample}}}{n_{\text{solv}}^{\text{ref}}} \right)^2$$

where $\int I_{\text{lum}}^{\text{sample}}(\lambda) d\lambda$ and $\int I_{\text{lum}}^{\text{ref}}(\lambda) d\lambda$ are the integrated luminescence intensities from the spectra corrected for the spectral response of the system, $OD_{\lambda_{\text{ex}}}^{\text{ref}}$ and $OD_{\lambda_{\text{ex}}}^{\text{sample}}$ the optical densities or absorbance at the excitation wavelength and $n_{\text{solv}}^{\text{sample}}$ and $n_{\text{solv}}^{\text{ref}}$ the refractive indices of the solvents for the sample and the reference, respectively.

The luminescence quantum efficiencies of **L⁷**, **L⁹**, **L⁹**, **L¹⁰**, **31** and **46** are given in Table 4.12. The highest luminescent quantum efficiency is found for ligand **L⁸** and the zinc complex **46**.

Table 4.12. Luminescence quantum efficiencies (η , %) of **L⁷**, **L⁹**, **L⁹**, **L¹⁰**, **31** and **46**.

	L⁷	L⁹	L¹⁰	31	46	L⁸ *1
η , %	76	74	80	61	83	86

4.5. Conclusion

Three new functionalized 2,1,3-benzothiadiazole ligands (**L⁷**, **L⁹**, **L¹⁰**) have been synthesized by Suzuki reaction and fully characterized. X-ray diffraction analysis for the ligands **L⁷** and **L⁹** showed that adjacent molecules of ligands are connected by π - π stacking interactions and rather weak S...S contacts. The electrochemical properties of these ligands have been studied.

The synthesis of mono- and binuclear complexes with Mn, Co, Ni, Cu, Zn, Pt have been described. Complexes with different composition were obtained depending on the use of cobalt and nickel anhydride or tetrahydrate. X-ray diffraction analysis showed that the $\{M_2(\mu-Cl)_2\}$ fragment containing bridging chlorine atoms provides binuclear complexes. The crystal structure of $[CuL^7Cl_2]$ (**30**) consists of binuclear molecular complexes $\{Cu_2(L^7)_2Cl_4\}$ and neutral polymer chains $\{Cu(L^7)Cl_2\}_n$. The **L⁸** ligand of multiligand complexes $[CuL^8(Hfac)_2]$ (**38**) and $[Cu_2L^8(Hfac)_4]$ (**39**), has *N,N*-bidentate-chelate and *N,N,N,N*-tetradentate-chelate bridging functions. In the crystal structures of all complexes due to intermolecular interactions such as hydrogen bonds, π - π stacking and S...N interactions, structures of different supramolecular architectures are observed.

It has been shown that the obtained ligands and zinc complexes have luminescent properties. The observed emission band centered at 460 - 475 nm. Excitation and absorption spectra of **L⁷**, **L⁹**, **L¹⁰** are identical, thus the luminescence is clearly due to the three chromophores. In the complex $[ZnL^9Cl_2]$ (**46**) coordination of **L⁹** to zinc atom increase the luminescence quantum efficiencies.

The crystallographic results, electrochemical and photophysical properties were supported by DFT and TD-DFT studies.

References

1. Akhtaruzzaman, Md.; Tomura, M.; Nishida, J.; Yamashita, Y. *J. Org. Chem.* **2004**, *69* (9), 2953–2958.
2. Agneeswari, R.; Tamilavan, V.; Song, M.; Hyun, M. H. *J. Mater. Chem. C* **2014**, *2* (40), 8515–8524.
3. Yamamoto, T.; Murakami, R.; Suginome, M. *J. Am. Chem. Soc.* **2017**, *139* (7), 2557–2560.
4. Paisley, N. R.; Tonge, C. M.; Sauv , E. R.; Halldorson, S. V.; Hudson, Z. M. *J. Polym. Sci. Part Polym. Chem.* **2018**, *56* (19), 2183–2191.
5. Yu, Y.; Bian, L.; Zhang, Y.; Liu, Z.; Li, Y.; Zhang, R.; Ju, R.; Yin, C.; Yang, L.; Yi, M.; Xie, L.; Huang, W. *ACS Omega* **2019**, *4* (3), 5863–5869.
6. Kumar, A.; Bawa, S.; Ganorkar, K.; Ghosh, S. K.; Bandyopadhyay A., *Inorg. Chem.* **2020**, *59* (3), 1746–1757.
7. Frisch, M. J.; Trucks, G. W.; Schlegel, H. B.; Scuseria, G. E.; Robb, M. A.; Cheeseman, J. R.; Scalmani, G.; Barone, V.; Mennucci, B.; Petersson, G. A.; Nakatsuji, H.; Caricato, M.; Li, X.; Hratchian, H. P.; Izmaylov, A. F.; Bloino, J.; Zheng, G.; Sonnenberg, J. L.; Hada, M.; Ehara, M.; Toyota, K.; Fukuda, R.; Hasegawa, J.; Ishida, M.; Nakajima, T.; Honda, Y.; Kitao, O.; Nakai, H.; Vreven, T.; Montgomery, J. A., Jr.; Peralta, J. E.; Ogliaro, F.; Bearpark, M.; Heyd, J. J.; Brothers, E.; Kudin, K. N.; Staroverov, V. N.; Kobayashi, R.; Normand, J.; Raghavachari, K.; Rendell, A.; Burant, J. C.; Iyengar, S. S.; Tomasi, J.; Cossi, M.; Rega, N.; Millam, J. M.; Klene, M.; Knox, J. E.; Cross, J. B.; Bakken, V.; Adamo, C.; Jaramillo, J.; Gomperts, R.; Stratmann, R. E.; Yazyev, O.; Austin, A. J.; Cammi, R.; Pomelli, C.; Ochterski, J. W.; Martin, R. L.; Morokuma, K.; Zakrzewski, V. G.; Voth, G. A.; Salvador, P.; Dannenberg, J. J.; Dapprich, S.; Daniels, A. D.; Farkas,  .; Foresman, J. B.; Ortiz, J. V.; Cioslowski, J.; Fox, D. J. Gaussian~09 Revision E.01.
8. Adamo, C.; Barone, V. *J. Chem. Phys.* **1999**, *110* (13), 6158–6170.
9. Krishnan, R.; Binkley, J. S.; Seeger, R.; Pople, J. A. *J. Chem. Phys.* **1980**, *72* (1), 650–654.
10. Frisch, M. J.; Pople, J. A.; Binkley, J. S. *J. Chem. Phys.* **1984**, *80* (7), 3265–3269.
11. Addison, A. W.; Rao, T. N.; Reedijk, J.; Rijn, J. van; Verschoor, G. C. *J. Chem. Soc. Dalton Trans.* **1984**, *7*, 1349–1356.
12. (IUCr) Bond valence parameters <https://www.iucr.org/resources/data/datasets/bond-valence-parameters> (accessed Feb 26, 2020).
13. Brown, I. D.; Altermatt, D. *Acta Crystallogr., Sect B* **1985**, *41* (4), 244–247.
14. Brese, N. E.; O’Keeffe, M. *Acta Crystallogr., Sect. B* **1991**, *47* (2), 192–197.
15. Liu, W.; Thorp, H. H. *Inorg. Chem.* **1993**, *32* (19), 4102–4105.
16. Yang, L.; Powell, D. R.; Houser, R. P. *Dalton Trans.* **2007**, *9*, 955–964.

17. Shields, G. P.; Raithby, P. R.; Allen, F. H.; Motherwell, W. D. S. *Acta Crystallogr., Sect.B* **2000**, 56 (3), 455–465.

GENERAL CONCLUSIONS AND PERSPECTIVES

In this thesis the synthesis, detailed X-ray structures analysis and physicochemical properties of new coordination compounds with multidentate *N*- and *N, O*-donor ligands have been explored. The development of methods for preparation of five new ligands **HL**⁵, **HL**⁶, **L**⁷, **L**⁹, **L**¹⁰ and forty five coordination compounds represents the major outcome of the thesis. All the new compounds were investigated by state-of-art physicochemical methods. Crystal structures of forty eight compounds (7 organic ligands and 41 coordination compounds) have been elucidated by X-ray crystallographic analysis. Quantum chemical calculations have been performed on certain compounds in order to offer a theoretical support to the corresponding experimental results.

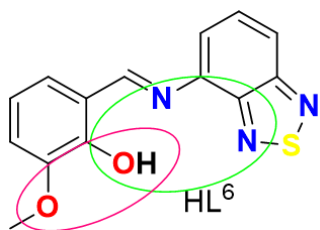
Based on comprehensive studies of the literature, three groups of organic compounds have been selected as promising polydentate ligands: 1) classical Schiff base ligands derivatives of *o*-vanillin and salicylic aldehyde (**H₂L**¹-**H₂L**⁴) (Chapter 2); 2) Schiff bases based on 2,1,3-benzothiadiazole (**HL**⁵-**HL**⁶) (Chapter 3); 3) functionalized 2,1,3-benzothiadiazole ligands (**L**⁷-**L**¹⁰) (Chapter 4).

The classical Schiff base ligands were successfully used to prepare polynuclear Cu, Mn, Cu/Ca, Cu/Sr, Cu/Ba complexes. The method of direct synthesis of a series of heterometallic *s-d* complexes (M/Cu, where M = Ca, Sr, Ba) with Schiff base derivatives of *o*-vanillin have been proposed. Polymeric manganese (III) complexes with the general formula Mn^{III}(HL^{1,4})₂X (X = Cl, Br, I, NCS) (**13-18**) were obtained by reaction between manganese powder, ammonium salt and organic ligands formed in situ in methanol solution. X-ray analysis shown that complexes possess cationic and neutral chain structures. In the coordination polymers very weak antiferromagnetic exchange interactions between Mn(III) ions through {–NCCO–} bridges have been found; the obtained data were supported by EPR spectroscopy and quantum chemical calculations.

It was shown that the ligand **H₂L**² in the solid state exists in different tautomeric forms triggered by the nature of the solvent or its absence. Quantum chemical calculations of this ligand reveal significant influence of hydrogen bonds on the stability of tautomeric forms. The ligand and its solvate forms show luminescent properties in the solid state. These features can be of paramount importance in the choice of the experimental conditions for further coordination chemistry studies with this type of ligands.

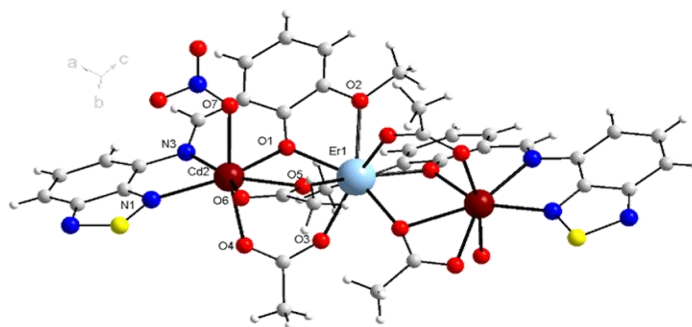
New *N, O*-polydentate Schiff base ligands (derivatives of 2,1,3-benzothiadiazole – **HL**⁵ and **HL**⁶) and their coordination compounds, namely, [M(L^{5,6})₂]_nCH₂Cl₂ (M = Cu, Co, Ni, Zn) (**21-24, 26-28**) have been prepared. DFT calculations were performed to determine the coordination possibilities for the deprotonated ligands **HL**⁵ and **HL**⁶. *N, O*-bidentate and *N, N, O*-

tridentate modes of coordination have been revealed. With the example of $[\text{Cu}(\text{L}^5)(\text{Hfac})]$ (**25**) the possibility of formation of heteroleptic complexes was shown. The magnetic behavior for the complex $[\text{Co}(\text{L}^6)_2] \cdot \text{CH}_2\text{Cl}_2$ (**28**) has been studied, showing a slow relaxation of magnetization in the low temperature regime 2.0-7.0 K.

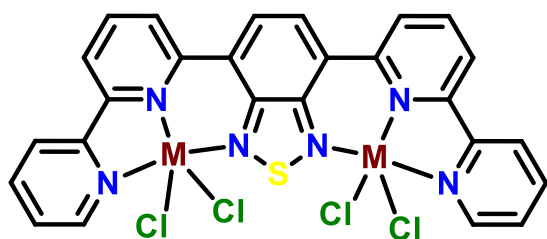


HL⁶ contains a $\{\text{N}_2\text{O}_2\}$ donor set with two distinct coordination pockets, which makes possible to synthesize binuclear complexes. Preliminary experiments have been performed to explore the possibility of preparing heterometallic d-f complexes.

With **HL**⁶ two heterometallic $[\text{ErCd}_2(\text{L}^6)_2(\text{AcO})_4(\text{NO}_3)(\text{H}_2\text{O})] \cdot 3\text{H}_2\text{O}$ and $[\text{NdCd}_2(\text{L}^6)_4\text{Cl}_2]\text{Cl} \cdot \text{CH}_2\text{Cl}_2$ complexes were obtained. According to the X-ray structure analysis data they have a trinuclear structure.

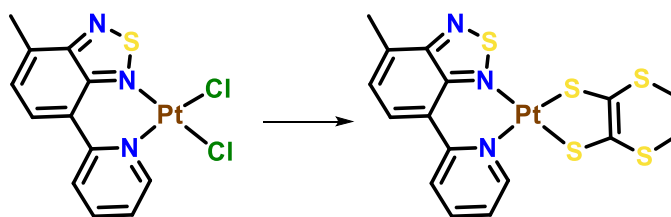


Three new *N*-polydentate ligands **L**⁷, **L**⁹ and **L**¹⁰, derivatives of 2,1,3-benzothiadiazole, have been obtained by Suzuki coupling. The crystallographic results, electrochemical and photophysical properties for ligands were supported by DFT and TD-DFT studies. Mono- and binuclear complexes with Mn, Co, Ni, Cu, Zn, Pt have been synthesized. The $\{\text{M}_2(\mu\text{-Cl})_2\}$ fragments containing bridging chlorine atoms form binuclear complexes with general formula $[\text{M}_2(\text{L}^{7,9})\text{Cl}_4(\text{solv})_n] \cdot \text{msolv}$ (M = Ni, Co, Cu; solv = CH₃OH, H₂O) (**29a-30, 44**). The crystal structure of CuL^7Cl_2 (**30**) consists of binuclear molecular complexes and neutral polymer chains. In the complex $[\text{Cu}_2\text{L}^8(\text{Hfac})_4]$ (**39**), two chelate "pockets" of **L**⁸ are involved in coordination. Ligands and zinc complexes $[\text{ZnL}^7\text{Cl}_2]$ (**31**), $[\text{ZnL}^9\text{Cl}_2]$ (**46**) are luminescent.



L⁸ and **L**¹⁰ are promising for the formation of binuclear complexes. It is expected that such complexes are likely to have interesting properties due to possible metal-metal intramolecular interactions

In further research the monometallic complexes with luminescent ligands can be used for the preparation of new multifunctional compounds. For example, in the Pt complex with **L**⁷, the



replacement of chloride ions with other organic ligands such as dithiolenes could provide multifunctional materials combining optical and conducting properties.

Experimental section

General information

Nuclear magnetic resonance (NMR) spectroscopy was performed with a Bruker Avance DRX 300 spectrometer operating at 300 MHz for ^1H and at 76 MHz for ^{13}C . The chemical shifts (δ) are measured along the x-axis in parts per million (ppm) from tetramethylsilane (TMS) as reference, to which is assigned a value of zero. The following abbreviations are used: singlet (s), doublet (d), triplet (t), doublet of doublets (dd), triplet of doublets (td), multiplet (m).

The ESI-MS spectra were performed with a Bruker MicrO-Tof-Q 2 or JEOL JMS 700 B/E spectrometer. MALDI-TOF MS were recorded with a Bruker Biflex III apparatus equipped with a N_2 laser ($\lambda = 337 \text{ nm}$).

Fourier transform infrared spectra (FTIR) were obtained using PerkinElmer Spectrum BX spectrometer for the samples pressed into pellets of KBr or ATR Bruker Vertex 70 spectrophotometer in the range $4000\text{--}400 \text{ cm}^{-1}$ (at 1 cm^{-1} resolution). Signal intensities (height) are denoted by the following abbreviations: vs-very strong, s-strong, m-medium, w-weak, br-broad.

Elemental analyses were recorded using Perkin-Elmer 2400 CHNS or Flash 2000 Fisher Scientific Thermo Electron analyzer.

The weight loss and thermal behaviour of compounds were investigated by Shimadzu simultaneous TGA/DTA analyzer DTG-60H.

UV-visible spectra were recorded with a Shimadzu UV-1800, Cary 5000 or Cary 5 Spectrophotometers. Luminescence and excitation spectra of samples were recorded with Shimadzu RF-6000 or Fluorolog 3 spectrofluorophotometer.

Cyclic voltammetry (CV) measurements were performed inside a glove box, by using a three-electrode cell that was equipped with Ag wire pseudo-reference electrode, Pt working electrode, and Pt counter electrode. Ferrocene was used as an internal reference and then the Fc/Fc^+ couple values have been adjusted to zero. The potentials were re-adjusted with respect to the saturated calomel electrode (SCE). The electrolyte was a 0.1 mol/L solution of (*n*-Bu₄N)PF₆ in DCM. All of the experiments were performed at RT at a scan rate of 100 mV/s. The voltammograms were recorded on a BioLogic SP-150 potentiostat.

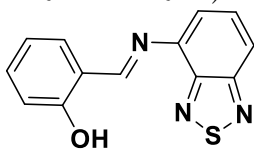
The high-field EPR spectra at temperatures ranging from *ca.* 3 K to 290 K were recorded on a home-built spectrometer at the EMR facility of the NHMFL. The instrument is equipped with a superconducting magnet (Oxford Instruments) capable of reaching a field of 17 T. Microwave frequencies over the range 52–630 GHz were generated by a phase-locked Virginia Diodes source,

producing a base frequency of 13 ± 1 GHz, which was multiplied by a cascade of frequency multipliers. The instrument is a transmission-type device and uses no resonance cavity.

Variable-temperature (300-1.9 K) direct current (dc) magnetic susceptibility measurements under applied fields of 0.1 ($T < 0$ K) and 1.0 kG ($T \geq 50$ K) and variable-field (0-5 T) magnetization measurements at 2.0 K for polycrystalline samples, were carried out with a Quantum Design SQUID magnetometer. Alternating current (ac) magnetic susceptibility measurements under different applied dc magnetic fields covering the 0-2500 G at low temperatures (2.0-7.0 K) were performed with a Quantum Design Physical Property Measurement System (PPMS). The magnetic susceptibility data were corrected for the diamagnetism of the constituent atoms and the sample holder (a plastic bag). Dc and ac measurements were done by crushing the crystals in order to prevent any displacement caused by the magnetic anisotropy.

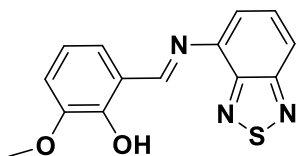
Synthetic procedures for the ligands

Synthesis of 2-[4-(2,1,3-benzothiadiazole)imino]methyl-phenol (**HL**⁵)



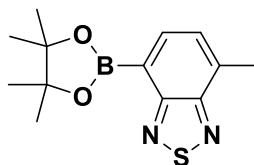
4-Amino-2,1,3-Benzothiadiazole (5 g, 33.07 mmol) and salicylaldehyde (3.53 ml, 33.07 mmol) were dissolved in ethanol (40 ml), forming a yellow-orange solution, which was magnetically stirred at 80 °C for 4 h. The yellow-orange solid was filtered and dried in air. Yield: 6.31 g (75%). Anal. Calc. for C₁₃H₉N₃OS (%): C, 61.16; H, 3.55; S, 12.56; N, 16.46. Found (%): C, 60.82; H, 3.57; S, 12.38; N, 16.47. IR (ATR, ν_{\max} cm⁻¹): 3072w, 1606s, 1568s, 1523s, 1479s, 1455s, 1411m, 1319s, 1284s, 1201s, 1152s, 1116s, 1071s, 1030m, 980m, 914s, 853s, 837s, 810vs, 760vs, 747vs, 667s, 616m, 597m, 550m, 522m, 504s, 471m, 454m, 445s. Exact mass, m/z 255.0459. ¹H RMN (300 MHz, CDCl₃) δ 13.38 (s, 1H), 9.51 (s, 1H), 7.92 (d, *J* = 8.8 Hz, 1H), 7.70 – 7.63 (m, 1H), 7.53 – 7.39 (m, 3H), 7.07 (d, *J* = 8.4 Hz, 1H), 6.98 (t, *J* = 7.5 Hz, 1H). ¹³C RMN (76 MHz, CDCl₃) δ 166.31, 161.31, 155.95, 149.52, 133.52, 132.64, 129.57, 121.17, 119.48, 118.96, 117.21.

Synthesis of 2-[4-(2,1,3-benzothiadiazole)imino]methyl-6-methoxy-phenol (**HL**⁶)



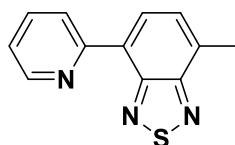
4-Amino-2,1,3-Benzothiadiazole (4.97 g, 32.86 mmol) and *o*-vanillin (4.97 mg, 32.86 mmol) were dissolved in ethanol (40 ml), forming a orange-red solution, which was magnetically stirred at 80 °C for 4 h. The orange-red solid was filtered and dried in air. Yield: 7.59 g (81%). Anal. Calc. for C₁₄H₁₁N₃OS (%): C, 58.93; H, 3.89; S, 11.24; N, 14.73. Found (%): C, 58.72; H, 3.93; S, 11.29; N, 14.96. IR (ATR, ν_{\max} cm⁻¹): 2933w, 1592s, 1570s, 1516s, 1463m, 1448vs, 1418vs, 1338m, 1320m, 1271vs, 1252s, 1211vs, 1169m, 1154m, 1066s, 1047s, 964s, 904s, 834vs, 808vs, 781vs, 741vs, 728vs, 652m, 622m, 600m, 557m, 511s, 492vs. Exact mass, m/z 285.0571. ¹H RMN (300 MHz, CDCl₃) δ 13.82 (s, 1H), 9.59 (s, 1H), 7.92 (d, *J* = 8.8 Hz, 1H), 7.70 – 7.63 (m, 1H), 7.49 (d, *J* = 8.0 Hz, 1H), 7.14 (d, *J* = 7.7 Hz, 1H), 7.05 (d, *J* = 8.0 Hz, 1H), 6.93 (t, *J* = 7.9 Hz, 1H), 3.97 (s, 3H). ¹³C RMN (76 MHz, CDCl₃) δ 166.98, 156.45, 152.05, 149.85, 148.75, 139.22, 130.02, 124.57, 122.24, 120.02, 119.57, 118.87, 115.51, 56.46.

Synthesis of 4-Methyl-7-(4,4,5,5-tetramethyl-1,3,2-dioxaborolan-2-yl)-2,1,3-benzothiadiazole



4-Bromo-7-methyl-2,1,3-benzothiadiazole (1 g, 4.37 mmol), bis(pinacolato)diboron (Bpin₂B₂) (1.67 g, 6.56 mmol) and potassium acetate (1.24 g, 12.63 mmol) were dissolved in dioxane (10 ml) in a Schlenk flask under argon. The resulting mixture was evacuated and backfilled with argon. It was stirred at 105 °C for 20 min and then [1,1'-bis(diphenylphosphino)ferrocene]palladium(II) dichloride (Pd(dppf)Cl₂, 0.18 g, 0.25 mmol) was added. The solution was stirred at 105 °C for 24 h. The completion of reaction was detected by TLC. After cooling, the solvent was removed under vacuum and the residue diluted with water and dichloromethane. The organic layer was separated, washed with water, brine and dried over MgSO₄. The solvent was evaporated under reduced pressure. The compound was purified by column chromatography (SiO₂, CH₂Cl₂) to give a light-yellow solid. Yield: 530 mg (87.93 %). The product was immediately used in the next step as starting material for synthesis of L⁷ and L⁹ in order to avoid the boronate decomposition.

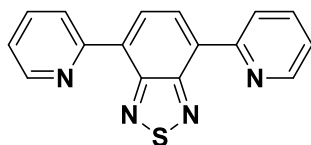
Synthesis of 4-(2-pyridine)-7-methyl-2,1,3-benzothiadiazole (L⁷)



4-Methyl-7-(4,4,5,5-tetramethyl-1,3,2-dioxaborolan-2-yl)-2,1,3-benzothiadiazole (600 mg, 2.17 mmol), 2-bromopyridine (0.21 ml, 2.17 mmol) and tetrakis(triphenylphosphine)palladium [Pd(PPh₃)₄] (109 mg, 108.63 μmol) were dissolved in degassed toluene (7 ml). The resulting mixture was evacuated and backfilled with argon in Schlenk flask. Potassium carbonate solution (1.8 g, 13.04 mmol in 1.8 ml water) was added and the solution was stirred at 80 °C for 48 h. After cooling, the solvent was removed under vacuum and the residue diluted with water and dichloromethane. The organic layer was separated, washed with water, brine and dried over MgSO₄. The solvent was evaporated under the reduced pressure. The compound was purified by column chromatography (SiO₂, CH₂Cl₂/EtOAc = 9 : 1) to give a white solid. Yield: 286 mg (57.96 %). Anal. Calc. for C₁₂H₉N₃S (%): C, 63.74; H, 3.99; N, 18.49; S, 14.11. Found: (%): C, 63.05; H, 3.94; N, 17.97; S, 13.73. IR (ATR, ν_{max} cm⁻¹): 2918w, 1738w, 1581s, 1548s, 1462s, 1433s, 1374s, 1324m, 1266s, 1095m, 1068s, 1050m, 992s, 947s, 884s, 861s, 844s, 795s, 772vs, 739s, 728s, 624s, 557s, 536s, 508s, 497s. Exact mass: 226.0449, 227.0516. ¹H RMN (300 MHz, CDCl₃) δ 8.77 (s, 1H), 8.61 (d, *J* = 7.8 Hz, 1H), 8.34 (d, *J* = 6.9 Hz, 1H), 7.86 (s, 1H), 7.51 (d, *J* = 6.6 Hz,

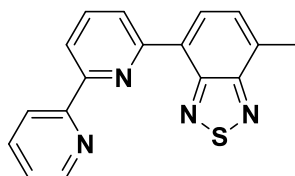
1H), 7.30 (s, 1H), 2.80 (s, 3H). ¹³C RMN (76 MHz, CDCl₃) δ 156.34, 154.55, 153.06, 149.80, 136.68, 135.09, 132.59, 129.82, 129.68, 124.74, 122.83, 18.37.

Synthesis of 4,7-bis(2-pyridine)-2,1,3-benzothiadiazole (L⁸)



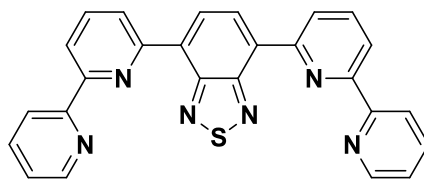
The ligand was synthesized according to the previously described procedure. Pochorovski I., Milic J., Kolarski D., Gropp C., Schweizer W. B., Diederich F. *J. Am. Chem. Soc.* **2014**, *136*, 10, 3852–3858.

Synthesis of 4-(2,2'-bipyridine)-7-methyl-2,1,3-benzothiadiazole (L⁹)



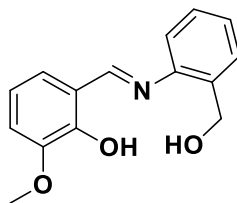
4-Methyl-7-(4,4,5,5-tetramethyl-1,3,2-dioxaborolan-2-yl)-2,1,3-benzothiadiazole (530 mg, 1.92 mmol), 6-bromo-2,2'-bipyridine (451 mg, 1.92 mmol) and tetrakis(triphenylphosphine)palladium [Pd(PPh₃)₄] (111 mg, 95.96 μmol) were dissolved in degased toluene (7 ml). The resulting mixture was evacuated and backfilled with argon in Schlenk flask. Potassium carbonate solution (1.59 g, 11.51 mmol in 1.7 ml water) was added and the solution was stirred at 80 °C for 48 h. After cooling, the solvent was removed under vacuum and the residue diluted with water and dichloromethane. The organic layer was separated, washed with water, brine and dried over MgSO₄. The solvent was evaporated under the reduced pressure. The compound was purified by column chromatography (SiO₂, CH₂Cl₂/EtOAc = 10: 0 → 9:1) to give a white solid. Yield: 300 mg (51.36 %). Anal. Calc. for C₁₇H₁₂N₄S (%): C, 67.08; H, 3.97; N, 18.41; S, 10.53. Found (%): C, 66.78; H, 3.94; N, 18.31; S, 10.50. IR (ATR, ν_{max} cm⁻¹): 2917w, 1578s, 1549s, 1492s, 1472m, 1455s, 1429s, 1370m, 1310m, 1277m, 1255s, 1169m, 1088s, 1044s, 993s, 965m, 892s, 865m, 850s, 825s, 793s, 773vs, 744s, 700s, 635s, 618s, 587s, 540s, 499s, 471m, 421m. Exact mass, m/z 303.0710, 304.0784. ¹H NMR (300 MHz, CDCl₃) δ 8.78 (d, *J* = 8.4 Hz, 1H), 8.71 (d, *J* = 5.7 Hz, 1H), 8.63 (d, *J* = 15.0 Hz, 2H), 8.44 (d, *J* = 7.8 Hz, 1H), 8.00 (t, *J* = 7.9 Hz, 1H), 7.87 (t, *J* = 7.7 Hz, 1H), 7.56 (d, *J* = 8.2 Hz, 1H), 7.37 – 7.30 (m, 1H), 2.83 (s, 3H). ¹³C NMR (76 MHz, CDCl₃) δ 156.50, 156.41, 155.85, 153.47, 153.20, 149.28, 139.75, 137.69, 137.02, 132.63, 129.75, 128.65, 124.71, 123.90, 121.39, 120.11, 18.35.

Synthesis of 4,7-bis(2,2'-bipyridine)-2,1,3-benzothiadiazole (**L¹⁰**)



4,7-Di(4,4,5,5-tetramethyl-1,3,2-dioxaborolan-2-yl)-2,1,3-benzothiadiazole (200 mg, 0.515 mmol), 6-bromo-2,2'-bipyridine (242 mg, 1.03 mmol) and tetrakis(triphenylphosphine)palladium [Pd(PPh₃)₄] (30 mg, 25.77 μmol) were dissolved in degassed toluene (2 ml). The resulting mixture was evacuated and backfilled with argon in Schlenk flask. Potassium carbonate solution (428 mg, 3.09 mmol in 0.46 ml water) was added and the solution was stirred at 80 °C for 48 h. After cooling, the solvent was removed under vacuum and the residue diluted with water and dichloromethane. The organic layer was separated, washed with water, brine and dried over MgSO₄. The solvent was evaporated under the reduced pressure. The compound was purified by column chromatography (SiO₂, cyclohexane/EtOAc = 8:2 → 1:1) to give a white solid. Yield: 100 mg (43.66 %). Anal. Calc. for C₂₆H₁₆N₆S (%): C, 70.25; H, 3.63; N, 18.91; S, 7.21. Found (%): C, 69.73; H, 3.70; N, 18.08; S, 6.87. IR (ATR, ν_{max} cm⁻¹): 1581s, 1564s, 1476w, 1454s, 1429s, 1294w, 1278w, 1257w, 1153w, 1097m, 1043m, 993m, 972m, 894m, 858m, 821m, 796w, 768vs, 741s, 697s, 673m, 657m, 634m, 619m, 594m, 584m, 563w, 532m, 508m, 449w, 418w, 401m. Exact mass, m/z 444.1152. ¹H NMR (300 MHz, CDCl₃) δ 8.93 (s, 1H), 8.88 (dd, *J* = 7.8, 1.0 Hz, 1H), 8.76 – 8.72 (m, 1H), 8.70 (d, *J* = 7.9 Hz, 1H), 8.51 (dd, *J* = 7.9, 1.0 Hz, 1H), 8.06 (t, *J* = 7.9 Hz, 1H), 7.89 (td, *J* = 7.7, 1.8 Hz, 1H), 7.37 (m, *J* = 7.5, 4.8, 1.2 Hz, 1H). ¹³C NMR (76 MHz, CDCl₃) δ 156.41, 155.99, 154.08, 153.13, 149.31, 137.75, 137.06, 132.36, 129.88, 125.26, 124.00, 121.44, 120.52.

Synthesis of 3-2-[(2-hydroxymethylbenzyl)imino]methyl}-6-methoxy-phenol (**H₂L²**)



H₂L². 2-Aminobenzyl alcohol (0.12 g, 1 mmol) and *o*-vanillin (0.15 g, 1 mmol) were dissolved in 10 ml of ethanol, forming a yellow solution, which was magnetically stirred at 50-60 °C for 15 minutes. Red crystals that precipitated after one day were collected by filtration and dried in air. Yield: 79% (0.20 g). Anal. Calc. for C₁₅H₁₅NO₃(%): C, 70.02; H, 5.88; N, 5.44. Found (%): C, 69.83; H, 5.36; N, 5.37. FTIR (KBr, ν_{max} cm⁻¹): 3531s, 3413m, 2933w, 2889w, 2842w, 1618vs, 1598m, 1573m, 1411w, 1257vs, 1205m, 1185m, 1112m, 1094w, 1016m, 967m, 857m, 781m, 765m, 732vs, 578w, 548w, 462w. (Ra:1616vs, 1596vs, 1570vs, 1492m, 1473s, 1453m, 1395w,

1343s, 1284w, 1200vs, 1167w, 1115w, 1074m, 1050m, 965w, 796m, 757w). H_2L^2 can be obtained using as solvent acetonitrile, DMF, DMSO.

$H_2L^2 \cdot CH_3OH$. 2-Aminobenzyl alcohol (0.12 g, 1 mmol) and *o*-vanillin (0.15 g, 1 mmol) were dissolved in 10 ml of methanol, forming a yellow solution, which was magnetically stirred at 50-60 °C for 15 minutes. Orange needle-shaped crystals that precipitated after 1-3 hours were collected by filtration and dried in air. Yield: 69% (0.20 g). Anal. Calc. for $C_{16}H_{19}NO_4$ (%): C, 66.42; H, 6.62; N, 4.84. Found (%): C, 65.63; H, 5.88; N, 4.83. FTIR (KBr, ν_{max} cm^{-1}): 3368s, 2930m, 2838m, 1614vs, 1598s, 1574m, 1460m, 1386w, 1360w, 1252vs, 1182m, 1104w, 1040m, 970m, 860w, 760m, 758m, 738s, 704w, 670w, 588w, 532w, 442w.

$H_2L^2 \cdot H_2O$. 2-Aminobenzyl alcohol (0.12 g, 1 mmol) and *o*-vanillin (0.15 g, 1 mmol) were dissolved in 10 ml of isopropanol, forming a yellow solution, which was magnetically stirred at 50-60 °C for 15 minutes. Orange needle-shaped crystals that precipitated after 1-3 hours were collected by filtration and dried in air. Yield: 62% (0.17 g). Anal. Calc. for $C_{15}H_{17}NO_4$ (%): C, 65.44; H, 6.22; N, 5.09. Found (%): C, 65.39; H, 6.06 ; N 5.37. FTIR (KBr, ν_{max} cm^{-1}): 3379s, 2934m, 2842m, 1614vs, 1596s, 1568m, 1459s, 1456m, 1252vs, 1185s, 1105m, 1040sm, 967s, 942w, 856w, 783m, 760m, 737s, 710w, 623w, 533w, 439w. (Ra:2875w, 1615m, 1600vs, 1572s, 1485m, 1456m, 1362s, 1286m, 1198s, 1151m, 1110w, 1045m, 934w, 834w, 787w, 763w, 734w, 664w, 599w, 540w, 499w, 441w).

Synthetic procedures for the complexes

[Cu₄(L¹)₄(CH₃OH)₄]·2,2CH₃OH (1)

Ethanolamine (0.24 ml, 4 mmol) and *o*-vanillin (0.6 g, 4 mmol) were dissolved in 30 ml of methanol, forming a yellow solution, which was magnetically stirred for 10 minutes. Then, copper powder (0.06 g, 1 mmol), CaO (0.11 g, 2 mmol) and NH₄Cl (0.11 g, 2 mmol) were added to the yellow solution. The reaction mixture was magnetically stirred at 50-60 °C until the dissolution of copper powder was observed (*ca* 4h). The solution was filtered and left for 1 day, then dark blue block-like crystals (unstable in air) were formed.

[Ca{Cu(HL¹)₂}₂]Br₂ (2)

Ethanolamine (0.24 ml, 4 mmol) and *o*-vanillin (0.6 g, 4 mmol) were dissolved in 30 ml of methanol, forming a yellow solution, which was magnetically stirred for 10 minutes. Then, copper powder (0.06 g, 1 mmol), CaO (0.11 g, 2 mmol) and NH₄Br (0.19 g, 2 mmol) were added to the yellow solution. The reaction mixture was magnetically stirred at 50-60 °C until the dissolution of copper powder was observed (*ca* 4 h). The solution was filtered and left for 1 day, then dark green crystals were formed. Yield: 0.3 g (58 %). Anal. Calc. for C₄₀H₄₈Br₂CaCu₂N₄O₁₂ (%): C, 43.53; H, 4.38; N, 5.08; Ca, 3.63; Cu, 11.51. Found (%): C, 42.4; H, 4.25; N, 5.03; Ca, 3.80; Cu, 12.24. IR (KBr, ν_{\max} cm⁻¹): 3260br, 2932w, 1622vs, 1559m, 1470vs, 1457vs, 1401m, 1299s, 1224vs, 1167m, 1076s, 1046s, 968m, 896w, 855m, 781w, 735s, 631w, 605w, 561w, 523w.

[Ca{Cu(HL¹)₂}₂]I₂·0,4H₂O (3)

Ethanolamine (0.24 ml, 4 mmol) and *o*-vanillin (0.6 g, 4 mmol) were dissolved in 30 ml of methanol, forming a yellow solution, which was magnetically stirred for 10 minutes. Then, copper powder (0.06 g, 1 mmol), CaO (0.11 g, 2 mmol) and NH₄I (0.29 g, 2 mmol) were added to the yellow solution. The reaction mixture was magnetically stirred at 50-60 °C until the dissolution of copper powder was observed (*ca* 4 h). The solution was filtered and left for 1 day, then dark green crystals were formed. Yield: 0.43 g (76 %). Anal. Calc. for C₄₀H_{48,8}N₄O_{12,4}Cu₂CaI₂ (%): C, 39.82; H, 4.05; N, 4.65; Ca, 3.32; Cu, 10.62. Found (%): C, 40.8; H, 4.7; N, 6.9; Ca, 3.9; Cu, 10.7. IR (KBr, ν_{\max} cm⁻¹): 3321s, 2934m, 1625vs, 1556m, 1473vs, 1403m, 1302m, 1224vs, 1168m, 1074m, 966m, 854m, 783m, 740m, 632m, 489w. ESI-MS (m/z): 471.93 [Ca{Cu(HL)₂}₂]²⁺, 1068.99 [Ca{Cu(HL)₂}₂]²⁺(I).

[Ca{Cu(HL¹)₂}₂](SCN)₂ (4)

Ethanolamine (0.24 ml, 4 mmol) and *o*-vanillin (0.6 g, 4 mmol) were dissolved in 30 ml of methanol, forming a yellow solution, which was magnetically stirred for 10 minutes. Then, copper powder (0.06 g, 1 mmol), CaO (0.11 g, 2 mmol) and NH₄SCN (0.15 g, 2 mmol) were added to the yellow solution. The reaction mixture was magnetically stirred at 50-60 °C until the dissolution of copper powder was observed (*ca* 4h). The solution was filtered and left for 1 day, then dark green crystals were formed. Yield: 0.35 g (66.03 %). Anal. Calc. for C₄₂H₄₈N₆O₁₂S₂Cu₂Ca (%): C, 47.58; H, 4.56; S, 6.05; N, 7.93; Ca, 3.78; Cu, 11.99. Found (%): C, 46.71; H, 4.48; S, 5.91; N, 7.65 ; Ca, 3.9; Cu, 12.70. IR (KBr, ν_{\max} cm⁻¹): 3360s, 2939s, 2072vs, 1625vs, 1556s, 1474vs, 1398s, 1301s, 1223s, 1170s, 1109m, 1076s, 1050s, 966m, 853m, 781m, 739s, 632m, 563m, 487w. ESI-MS (m/z): 470.99 [Ca{Cu(HL)₂}₂]²⁺, 1003.98 [Ca{Cu(HL)₂}₂]²⁺(SCN⁻).

[Sr{Cu(HL¹)₂}₂](CH₃OH)₂ (5)

Ethanolamine (0.24 ml, 4 mmol) and *o*-vanillin (0.6 g, 4 mmol) were dissolved in 30 ml of methanol, forming a yellow solution, which was magnetically stirred for 10 minutes. Then, copper powder (0.06 g, 1 mmol), SrO (0.2 g, 2 mmol) and NH₄I (0.29 g, 2 mmol) were added to the yellow solution. The reaction mixture was magnetically stirred at 50-60 °C until the dissolution of copper powder was observed (*ca* 4 h). The solution was filtered and left for 1 day, then dark green crystals were formed. Yield: 0.21 g (33.72 %). Anal. Calc. for C₄₂H₅₆Cu₂I₂N₄O₁₄Sr (%): C, 38.52; H, 4.31; Cu, 9.71; N, 4.28; Sr, 6.69. Found (%): C, 36.17; H, 4.10; Cu, 9.63; N, 3.59; Sr, 6.72. IR (KBr, ν_{\max} cm⁻¹): 3417-3357s, 2931m, 2858m, 1625vs, 1612s, 1556m, 1475s, 1450s, 1400m, 1303s, 1248s, 1224vs, 1164m, 1078m, 1056m, 1045m, 970m, 854m, 768w, 746m, 630w, 561w. ESI-MS (m/z): 495.0 [Sr{Cu(HL)₂}₂]²⁺, 794.0 [SrCu₂(HL)₂]⁺, 921.9 [SrCu₂(HL)₂L]²⁺I⁻.

[Sr{Cu(HL¹)₂}₂](H₂O)₂](SCN)₂·0.65CH₃OH (6)

Ethanolamine (0.24 ml, 4 mmol) and *o*-vanillin (0.6 g, 4 mmol) were dissolved in 30 ml of methanol, forming a yellow solution, which was magnetically stirred for 10 minutes. Then, copper powder (0.06 g, 1 mmol), SrO (0.2 g, 2 mmol) and NH₄SCN (0.15 g, 2 mmol) were added to the yellow solution. The reaction mixture was magnetically stirred at 50-60 °C until the dissolution of copper powder was observed (*ca* 4 h). The solution was filtered and left for 1 day, then dark green crystals were formed. Yield: 0.23 g (41.48 %). Anal. Calc. for C_{42.65}H_{54.95}Cu₂N₆O_{14.65}S₂Sr (%): C, 43.97; H, 4.75; Cu, 10.91; N, 7.21; S, 5.50; Sr, 7.52. Found (%): C, 42.74; H, 4.51; Cu, 10.11; N, 6.87; S, 5.27; Sr, 7.11. IR (KBr, ν_{\max} cm⁻¹): 3366s, 2936s, 2835s, 2056s, 1626vs, 1551s, 1472vs, 1452vs, 1401s, 1305vs, 1243vs, 1222vs, 1170s, 1080s, 1051s, 968m, 855m, 782w, 738s, 628w,

564w. ESI-MS (m/z): 495.0 [Sr{Cu(HL)₂}₂]²⁺, 794.0 [SrCu₂(HL)L₂]⁺, 853.9 [SrCu₂(HL)₂L]²⁺(SCN)⁻, 1048.3 [Sr{Cu(HL)₂}₂]²⁺(SCN)⁻.

[Sr{Cu(HL¹)₂}₂NO₃]₂NO₃·CH₃OH (7)

Ethanolamine (0.24 ml, 4 mmol) and *o*-vanillin (0.6 g, 4 mmol) were dissolved in 30 ml of methanol, forming a yellow solution, which was magnetically stirred for 10 minutes. Then, copper powder (0.06 g, 1 mmol) and Sr(NO₃)₂ (0.21 g, 1 mmol) were added to the yellow solution. The reaction mixture was magnetically stirred at 50-60 °C until the dissolution of copper powder was observed (*ca* 4 h). The solution was filtered and left for 1 day, then dark green crystals were formed. Yield: 0.36 g (62.82%). Anal. Calc. for C₄₁H₅₂N₆O₁₉Cu₂Sr (%): C, 42.91; H, 4.57; N, 7.32; Sr, 7.64; Cu, 11.07. Found (%): C, 39.85; H, 4.34; N, 7.17; Sr, 8.59; Cu, 10.86. IR (KBr, ν_{\max} cm⁻¹): 3338s, 2943m, 1627vs, 1468s, 1449s, 1383s, 1298s, 1218vs, 1166m, 1067m, 1034m, 968m, 857m, 738m, 619w, 567w. ESI-MS (m/z): 495.93 [Sr{Cu(HL)₂}₂]²⁺, 1051.99 [Sr{Cu(HL)₂}₂(NO₃)]⁺.

[Ba{Cu(HL¹)₂}₂(CH₃OH)₂]₂I₂ (8)

Ethanolamine (0.24 ml, 4 mmol) and *o*-vanillin (0.6 g, 4 mmol) were dissolved in 30 ml of methanol, forming a yellow solution, which was magnetically stirred for 10 minutes. Then, copper powder (0.06 g, 1 mmol), BaO (0.3 g, 2 mmol) and NH₄I (0.29 g, 2 mmol) were added to the yellow solution. The reaction mixture was magnetically stirred at 50-60 °C until the dissolution of copper powder was observed (*ca* 4 h). The solution was filtered and left for 1 day, then dark green crystals were formed. Yield: 0.27 g (39.7%). Anal. Calc. for C₄₂H₅₆N₄O₁₄Cu₂BaI₂ (%): C, 37.12; H, 4.15; N, 4.12; Ba, 10.10; Cu, 9.35. Found (%): C, 38.64; H, 3.92; N, 4.03; Ba, 8.37; Cu, 9.8. IR (KBr, ν_{\max} cm⁻¹): 3382vs, 2932m, 1628vs, 1549s, 1473vs, 1447vs, 1395s, 1300s, 1242s, 1216vs, 1171m, 1082s, 1043s, 966m, 851m, 794w, 742s, 633m, 569w, 530w, 473w. ESI-MS (m/z): 472.66 [Ba{Cu(HL)₂}₂]²⁺, 1166.90 [Ba{Cu(HL)₂}₂]²⁺(I⁻).

[Ba{Cu(HL¹)₂}₂(CH₃OH)₂](SCN)₂ (9)

Ethanolamine (0.24 ml, 4 mmol) and *o*-vanillin (0.6 g, 4 mmol) were dissolved in 30 ml of methanol, forming a yellow solution, which was magnetically stirred for 10 minutes. Then, CuSCN (0.12 g, 1 mmol) and Ba(SCN)₂·2H₂O (0.29 g, 1 mmol) were added to the yellow solution. The reaction mixture was magnetically stirred at 50-60 °C until the dissolution of copper powder was observed (*ca* 4 h). The solution was filtered and left for 1 day, then dark green crystals were formed. Yield: 0.37 g (61.05 %). Anal. Calc. for C₄₄H₅₆N₆O₁₄S₂Cu₂Ba (%): C, 43.26; H, 4.62; N, 6.88; Ba, 11.24; Cu, 10.40. Found (%): C, 43.26; H, 4.13; S, 5.15; N, 6.77; Ba, 10.1; Cu, 10.2. IR

(KBr, ν_{\max} cm^{-1}): 3375s, 2926m, 2055s, 1626vs, 1556m, 1466s, 1447s, 1395m, 1306s, 1248s, 1226vs, 1171m, 1075m, 1056m, 975m, 845m, 742m, 627w, 556w, 473w. ESI-MS (m/z): 520.06 [Ba{Cu(HL)₂}₂]²⁺.

[Cu₄(HL¹)₂(L¹)₂(NCS)₂(CH₃OH)₂·2CH₃OH (10)

Mononuclear complex Cu(HL¹)₂ (0.2 g, 0.446 mmol), BaO (0.14 g, 0.893 mmol) and NH₄SCN (0.07 g, 0.893 mmol) were dissolved in 30 ml of methanol. The reaction mixture was magnetically stirred at 50-60 °C for 4 h. The solution was filtered and left for 1 day, then blue crystals were formed. Yield: 0.26 g (44.25 %). IR (KBr, ν_{\max} cm^{-1}): 3357br, 2940m, 2054s, 1627vs, 1553m, 1470vs, 1450vs, 1396m, 1305s, 1238s, 1222vs, 1172m, 1077m, 1048m, 967m, 845m, 757m. MALDI-TOF MS (m/z): 830.9 [Cu₄(HL¹)(L¹)₂]³⁺, 1025.0 [Cu₄(HL¹)(L¹)₃]⁺.

[Ca{Cu(HL²)₂}₂]₂ (11)

2-Aminobenzyl-alcohol (0.25 ml, 2 mmol) and *o*-vanillin (0.3 g, 2 mmol) were dissolved in 30 ml of methanol, forming a yellow solution, which was magnetically stirred for 10 minutes. Then, copper powder (0.06 g, 1 mmol), CaO (0.11 g, 2 mmol) and NH₄I (0.29 g, 2 mmol) were added to the yellow solution. The reaction mixture was magnetically stirred at 50-60 °C until the dissolution of copper powder was observed (*ca* 4 h). The solution was filtered and left for 1 day, then brown crystals were formed. Yield: 0.27 g (40 %). Anal. Calc. for C₆₀H₅₆N₄O₁₂Cu₂CaI₂ (%): C, 49.83; H, 3.90; N, 3.87; Ca, 2.77; Cu, 8.79. Found (%): C, 45.3; H, 3.4; N, 3.7; Ca, 2.3; Cu, 8.2. IR (KBr, ν_{\max} cm^{-1}): 3380br, 2932m, 1610vs, 1554s, 1486vs, 1388m, 1308s, 1238vs, 1180vs, 1102m, 1078m, 1012m, 974m, 852w, 764m, 740m, 642m, 560m, 542m, 466w.

[Cu(L³)₂Ca(NCS)₂(H₂O)] (12)

Copper powder (0.06 g, 1 mmol), CaO (0.11 g, 2 mmol), *o*-vanillin (0.3 g, 2 mmol) and NH₄SCN (0.15 g, 2 mmol) were added in 30 ml of methanol. The reaction mixture was stirred magnetically at 50-60 °C for *ca* 5 h until the complete dissolution of copper powder was observed. The solution was filtered and left for 1 day, then light-orange crystals were formed. Yield: 0.26 g (48 % per copper). Anal. Calc. for CaCuC₁₈N₄H₁₈O₅S₂(%): Ca 7.45, Cu 11.81, C 40.18, N 10.41, H 3.37, S 11.92. Found (%): Ca 8.1, Cu 11.2, C 36.5, N 10.1, H 3.2, S 11.4. FT-IR (KBr, ν_{\max} cm^{-1}): 3349vs, 3187vs 2942s, 2076vs, 1617vs, 1555m, 1464vs, 1386s, 1318s, 1245s, 1225vs, 1162m, 1074s, 1036m, 948m, 853m, 823m, 738s, 652m, 617m, 571m, 515m, 469m.

{[Mn(HL¹)₂]Cl}_n (13)

Ethanolamine (0.18 ml, 3 mmol) and *o*-vanillin (0.47 g, 3 mmol) were added to 30 ml of methanol and stirred magnetically for 15 min until the colour of the solution turned yellow. Then, manganese chloride tetrahydrate (0.59 g, 3 mmol) was added to the solution, and the reaction mixture was stirred at 50 °C for *ca* 1 h. A dark brown precipitate was collected after 1 day by filtration, washed with isopropanol and dried in air. Yield: 330 mg (21%, per Mn). Anal. Calc. for C₂₀H₂₄N₂O₆ClMn(%): C, 50.17; H, 5.05; N, 5.85; Mn, 11.47%. Found (%): C, 50.05; H, 4.97; N, 5.74; Mn, 11.35%. IR (ATR, ν_{\max} cm⁻¹): 3434br, 3396 w, 3186 br, 2936 w, 1607 vs, 1551 m, 1469 s, 1300 m, 1249 s, 1029 m, 864 s, 744 s, 640 m, 453 m.

{[Mn(HL¹)₂]Br}_n (14)

Ethanolamine (0.36 ml, 6 mmol) and *o*-vanillin (0.94 g, 6 mmol) were added to 30 ml of methanol and stirred magnetically for 15 min until the colour of the solution turned yellow. Then, manganese powder (0.11 g, 2 mmol) and NH₄Br (0.39 g, 4 mmol) were added to the solution, and the reaction mixture was stirred at 50 °C for *ca* 2 h. A dark brown precipitate was collected after 1 day by filtration, washed with isopropanol and dried in air. Yield: 320 mg (31 %). Anal. Calc. for C₂₀H₂₄N₂O₆BrMn (%): C, 45.91; H, 4.62; N, 5.35; Mn, 10.50. Found (%): C, 45.75; H, 4.52; N, 5.27; Mn, 10.35. IR (ATR, ν_{\max} cm⁻¹): 3437br, 3393w, 3184br, 2931w, 1610vs, 1548m, 1473s, 1315m, 1239s, 1019m, 867s, 746s, 645m, 455m.

[Mn(HL¹)₂(NCS)](15)

Ethanolamine (0.36 ml, 6 mmol) and *o*-vanillin (0.94 g, 6 mmol) were added to 30 ml of methanol and stirred magnetically for 15 min until the colour of the solution turned yellow. Then, manganese powder (0.11 g, 2 mmol) and NH₄NCS (0.31 g, 4 mmol) were added to the solution, and the reaction mixture was stirred at 50 °C for *ca* 2 h. A dark brown precipitate was collected after 1 day by filtration, washed with isopropanol and dried in air. Yield: 300 mg (30 %). Anal. Calc. for C₂₁H₂₄N₃O₆SMn (%): C, 50.30; H, 4.82; N, 8.38; S, 6.39; Mn, 10.96. Found (%): C, 50.16; H, 4.64; N, 7.98; S, 6.12; Mn, 11.30. IR (KBr, ν_{\max} cm⁻¹): 3420br, 2919w, 2071vs, 1616vs, 1553m, 1475s, 1452s, 1399m, 1353w, 1303vs, 1227s, 1193m, 1112w, 1086m, 1055m, 1024m, 979m, 902w, 864s, 784w, 742s, 639s, 590w, 528w, 471w.

{[Mn(HL⁴)₂]Br}_n (16)

Ethanolamine (0.36 ml, 6 mmol) and salicylaldehyde (0.56 g, 6 mmol) were added to 30 ml of methanol and stirred magnetically for 15 min until the colour of the solution turned yellow. Then, manganese powder (0.11 g, 2 mmol) and NH₄Br (0.39 g, 4 mmol) were added to the solution, the

reaction mixture was stirred at 50 °C for *ca* 2 h. A dark brown precipitate was collected after 1 day by filtration, washed with isopropanol and dried in air. Yield: 320 mg (35 %). Anal. Calc. for C₁₈H₂₀N₂O₄BrMn (%): C, 46.67; H, 4.35; N, 6.05; Mn, 11.86. Found (%): C, 46.54; H, 4.14; N, 5.85; Mn, 11.50. IR (ATR, ν_{max} cm⁻¹): 3151br, 2929w, 1607vs, 1546s, 1445s, 1300s, 1215s, 1025m, 884m, 767s, 638m, 456s.

{[Mn(HL⁴)₂]I}_n (17)

Ethanolamine (0.36 ml, 6 mmol) and salicylaldehyde (0.56 g, 6 mmol) were added to 30 ml of methanol and stirred magnetically for 15 min until the colour of the solution turned yellow. Then, manganese powder (0.11 g, 2 mmol) and NH₄I (0.58 g, 4 mmol) were added to the solution, and the reaction mixture was stirred at 50 °C for *ca* 2 h. A dark brown precipitate was collected after 1 day by filtration, washed with isopropanol and dried in air. Yield: 410 mg (40 %). Anal. Calc. for C₁₈H₂₀N₂O₄IMn (%): C, 42.37; H, 3.95; N, 5.49; Mn, 10.77. Found (%): C, 42.15; H, 3.83; N, 5.24; Mn, 10.46. IR (ATR, ν_{max} cm⁻¹): 3149br, 2915w, 1607vs, 1544s, 1439s, 1305s, 1218s, 1030m, 890m, 760m, 640m, 449s.

{[Mn(HL⁴)₂]NCS}_n (18)

Ethanolamine (0.36 ml, 6 mmol) and salicylaldehyde (0.56 g, 6 mmol) were added to 30 ml of methanol and stirred magnetically for 15 min until the colour of the solution turned yellow. Then, manganese powder (0.11 g, 2 mmol) and NH₄NCS (0.31 g, 4 mmol) were added to the solution, and the reaction mixture was stirred at 50 °C for *ca* 2 h. A dark brown precipitate was collected after 1 day by filtration, washed with isopropanol and dried in air. Yield: 220 mg (25 %). Anal. Calc. for C₁₉H₂₀N₃O₄SMn (%): C, 51.70; H, 4.57; N, 9.52; S, 7.26; Mn, 12.44. Found (%): C, 51.65; H, 4.28; N, 9.36; S, 7.15; Mn, 12.25. IR (ATR, ν_{max} cm⁻¹): 3145br, 3056w, 2924w, 2071s, 1599vs, 1543s, 1444s, 1293m, 1219m, 1025m, 885m, 757s, 683m, 456s.

[Mn₂(HL²)₂(NCS)₂]·2C₂H₅OH (19)

2-Aminobenzyl-alcohol (0.25 ml, 2 mmol) and *o*-vanillin (0.3 g, 2 mmol) were dissolved in 30 ml of methanol, forming a yellow solution, which was magnetically stirred for 10 minutes. Then, manganese powder (0.06 g, 1 mmol), CaO (0.11 g, 2 mmol) and NH₄SCN (0.15 g, 2 mmol) were added to the yellow solution. The reaction mixture was magnetically stirred at 50-60 °C until the dissolution of manganese powder was observed (*ca* 5 h). The solution was filtered and left for 1 day, then dark brown crystals were formed. Yield: 0.21 g (54.62%). Anal. Calc. for C₃₆H₄₀Mn₂N₄O₈S₂ (%): C, 52.05; H, 4.85; Mn, 13.23; N, 6.74; S, 7.72. Found (%): C, 56.08; H,

4.62; Mn, 14.2; N, 7.98; S, 8.21. IR (KBr, ν_{\max} cm^{-1}): 3464br, 2938m, 2044vs, 1636vs, 1614vs, 1600s, 1546m, 1504s, 1490s, 1456m, 1366m, 1236vs, 1176s, 1110w, 1020m, 966w, 746m.

Cu(L⁵)₂ (21)

To a yellow solution of HL⁵ (20 mg, 0.078 mmol) in DCM (3 mL), was added a solution of copper (II) acetate monohydrate (8 mg, 0.039 mmol) in methanol (3 mL). The reaction mixture was magnetically stirred at 65 °C for 2 hours. After 1-3 days of slow evaporation, dark red crystals were collected by filtration. Yield: 11 mg (48%). IR (KBr, ν_{\max} cm^{-1}): 3441br, 2938w, 1609vs, 1525vs, 1465m, 1433s, 1396m, 1314m, 1197m, 1149m, 1068w, 908w, 855w, 764m, 674w, 584w. ESI-MS (m/z): 317.0 [CuL⁵]⁺.

Co(L⁵)₂ (22)

To a yellow solution of HL⁵ (20 mg, 0.078 mmol) in DCM (3 mL), was added a solution of cobalt (II) hexafluoroacetylacetonate hydrate (18 mg, 0.039 mmol) in methanol (3 mL). The reaction mixture was magnetically stirred at 65 °C for 2 hours. After 1-3 days of slow evaporation, dark red crystals were collected by filtration. Yield: 10 mg (45.00 %). IR (ATR, ν_{\max} cm^{-1}): 3002w, 1736m, 1589vs, 1512vs, 1455s, 1428vs, 1383 vs, 1334s, 1282m, 1234m, 1213m, 1188s, 1142vs, 1125s, 1060s, 1049s, 1023s, 975m, 917m, 901s, 846s, 820s, 801s, 756s, 737vs, 601m, 580m, 525m, 495s, 474m, 453s, 419m, 408s. ESI-MS (m/z): 313.0 [CoL⁵]⁺, 568.1 [Co(L⁵)(HL⁵)]⁺.

Ni(L⁵)₂ (23)

To a yellow solution of HL⁵ (20 mg, 0.078 mmol) in DCM (3 mL), was added a solution of nickel (II) hexafluoroacetylacetonate hydrate (18 mg, 0.039 mmol) in methanol (3 mL). The reaction mixture was magnetically stirred at 65 °C for 2 hours. After 1-3 days of slow evaporation, dark red crystals were collected by filtration. Yield: 9 mg (40.5 %). IR (ATR, ν_{\max} cm^{-1}): 1739m, 1644s, 1593s, 1509m, 1456s, 1432s, 1384m, 1255s, 1191s, 1143vs, 1062m, 1021m, 976m, 904m, 848m, 823m, 799m, 754s, 738s, 672s, 583m, 528m, 510m, 495m, 451m, 415m. ESI-MS (m/z): 312.0 [NiL⁵]⁺, 567.1 [Ni(L⁵)(HL⁵)]⁺.

Zn(L⁵)₂ (24)

To a yellow solution of HL⁵ (20 mg, 0.078 mmol) in DCM (3 mL), was added a solution of zinc (II) hexafluoroacetylacetonate dihydrate (20 mg, 0.039 mmol) in methanol (3 mL). The reaction mixture was magnetically stirred at 65 °C for 2 hours. After 1-3 days of slow evaporation, yellow crystals were collected by filtration. Yield: 7 mg (31.3 %). IR (KBr, ν_{\max} cm^{-1}): 3332br, 1610vs, 1528s, 1500s, 1456s, 1440s, 1410w, 1390w, 1340w, 1280s, 1200s, 1148s, 1092w, 1070w, 1028w,

978w, 904m, 888m, 848m, 808m, 758vs, 654w, 522w, 452w. ESI-MS (m/z): 317.9 [ZnL⁵]⁺, 572.97 [Zn(L⁵)₂].

[Cu(L⁵)(Hfac)] (25)

To a yellow solution of HL⁵ (20 mg, 0.078 mmol) in DCM (3 mL), was added a solution of copper (II) hexafluoroacetylacetonate hydrate (37 mg, 0.078 mmol) in methanol (3 mL). The reaction mixture was magnetically stirred at 65 °C for 2 hours. After 1-3 days of slow evaporation, red needle-shaped crystals were collected by filtration. Yield: 26 mg (53.2 %). IR (KBr, ν_{\max} cm⁻¹): 3442br, 2938m, 1650s, 1610vs, 1584s, 1524vs, 1483s, 1431s, 1389m, 1321w, 1261vs, 1204vs, 1150vs, 909w, 808w, 751m, 740w, 655w, 448w, 425w. MALDI-TOF MS (m/z): 317.0 [CuL⁵]⁺.

Cu(L⁶)₂ (26)

To a red-orange solution of HL⁶ (20 mg, 0.070 mmol) in DCM (3 mL), was added a solution of copper (II) hexafluoroacetylacetonate hydrate (17 mg, 0.035 mmol) in methanol (3 mL). The reaction mixture was magnetically stirred at 65 °C for 2 hours. After 1-3 days of slow evaporation, red crystals were collected by filtration. Yield: 15 mg (67.72 %). IR (KBr, ν_{\max} cm⁻¹): 3449br, 2938m, 1605vs, 1544m, 1530s, 1466s, 1446s, 1390m, 1340w, 1244vs, 1210vs, 1082m, 1066w, 986w, 904w, 824w, 742m, 502w. MALDI-TOF MS (m/z): 347.0 [CuL⁶]⁺, 654.0 {Na[Cu(L⁶)₂]}⁺.

Zn(L⁶)₂ (27)

To a red-orange solution of HL⁶ (20 mg, 0.070 mmol) and triethylamine (0.01 mL, 0.070 mmol) in DCM (3 mL), was added a solution of zinc (II) acetate (6 mg, 0.035 mmol) in methanol (3 mL). The reaction mixture was magnetically stirred at 65 °C for 2 hours. After 1-3 days of slow evaporation, yellow-orange crystals were collected by filtration. Yield: 9 mg (43.54 %). IR (ATR, ν_{\max} cm⁻¹): 1739m, 1696m, 1643m, 1606s, 1532m, 1486m, 1435s, 1368s, 1255s, 1203vs, 1142vs, 1094m, 967m, 903m, 849m, 800s, 735s, 665s, 585m, 527m, 492s, 445m, 421m. MALDI-TOF MS: 655.0 {Na[Zn(L⁶)₂]}⁺.

[Co(L⁶)₂]·CH₂Cl₂ (28)

To a red-orange solution of HL⁶ (20 mg, 0.070 mmol) and triethylamine (0.01 mL, 0.070 mmol) in DCM (3 mL), was added a solution of cobalt (II) acetate tetrahydrate (9 mg, 0.035 mmol) in methanol (3 mL). The reaction mixture was magnetically stirred at 65 °C for 2 hours. After 1-3 days of slow evaporation, brown needle-shaped crystals were collected by filtration. Yield: 15 mg (61.07 %). Anal. Calc. for C₂₉H₂₂Cl₂CoN₆O₄S₂ (%): C, 48.89; H, 3.11; S, 9.00; N, 11.80. Found (%): C, 49.12; H, 2.98; S, 9.12; N, 12.65. IR (ATR, ν_{\max} cm⁻¹): 1740m, 1585s, 1526s, 1419vs,

1395vs, 1236s, 1201vs, 1166s, 1079s, 1059s, 977m, 900m, 846s, 800m, 732vs, 666m, 597m, 547m, 522m, 512m, 486m, 413m. MALDI-TOF MS: $m/z = 343.0$ $[\text{CoL}^6]^+$.

$[\text{Co}_2(\text{L}^7)_2\text{Cl}_4(\text{CH}_3\text{OH})_2]$ (29a)

To a light-yellow solution of L^7 (20 mg, 0.088 mmol) in DCM (3 mL), was added a solution of cobalt (II) chloride hexahydrate (21 mg, 0.088 mmol) in methanol (3 mL). The reaction mixture was magnetically stirred at 65 °C for 2 hours. After 1 days of slow evaporation, red crystals were collected by filtration. Yield: 13 mg (38.1%). ESI-MS (m/z): 321.0 $[\text{CoL}^7\text{Cl}]^+$.

$[\text{CuL}^7\text{Cl}_2]$ (30)

To a light-yellow solution of L^7 (20 mg, 0.088 mmol) in DCM (3 mL), was added a solution of copper (II) chloride dihydrate (15 mg, 0.088 mmol) in methanol (3 mL). The reaction mixture was magnetically stirred at 65 °C for 2 hours. After 1-3 days of slow evaporation, green crystals were collected by filtration. Yield: 16 mg (50.3 %). ESI-MS (m/z): 325.0 $[\text{CuL}^7\text{Cl}]^+$.

$[\text{ZnL}^7\text{Cl}_2]$ (31)

To a light-yellow solution of L^7 (20 mg, 0.088 mmol) in DCM (3 mL), was added a solution of zinc (II) chloride (12 mg, 0.088 mmol) in methanol (3 mL). The reaction mixture was magnetically stirred at 65 °C for 2 hours. After 1-3 days of slow evaporation, yellow crystals were collected by filtration. Yield: 24 mg (74.8 %). MALDI-TOF MS (m/z): 326 $[\text{ZnL}^7\text{Cl}]^+$.

$[\text{PtL}^7\text{Cl}_2]$ (32)

To a light-yellow solution of L^7 (20 mg, 0.088 mmol) in DCM (3 mL), was added a solution of platinum (II) chloride (23 mg, 0.088 mmol) in acetonitrile (3 mL). The reaction mixture was magnetically stirred at 65 °C for 2 hours. After 1-3 days of slow evaporation, brown crystals were collected by filtration. Yield: 19 mg (44.5 %). MALDI-TOF MS (m/z): 490.8 $[\text{PtL}^7\text{Cl}]^+$.

$[\text{MnL}^7(\text{Hfac})_2]$ (33)

To a light-yellow solution of L^7 (10 mg, 0.044 mmol) in DCM (3 mL), was added a solution of manganese (II) hexafluoroacetylacetonate hydrate (21 mg, 0.044 mmol) in methanol (3 mL). The reaction mixture was magnetically stirred at 65 °C for 2 hours. After 1-3 days of slow evaporation, pink needle-shaped crystals were collected by filtration. Yield: 27 mg (86.6%). ESI-MS (m/z): 488.9 $[\text{MnL}^7(\text{Hfac})]^+$.

[CoL⁷(Hfac)₂] (34)

To a light-yellow solution of L⁷ (10 mg, 0.044 mmol) in DCM (3 mL), was added a solution of cobalt (II) hexafluoroacetylacetonate hydrate (21 mg, 0.044 mmol) in methanol (3 mL). The reaction mixture was magnetically stirred at 65 °C for 2 hours. After 1-3 days of slow evaporation, red needle-shaped crystals were collected by filtration. Yield: 29 mg (93.3%). MALDI-TOF MS (m/z): 491.8 [CoL⁷(Hfac)]⁺.

[NiL⁷(Hfac)₂] (35)

To a light-yellow solution of L⁷ (10 mg, 0.044 mmol) in DCM (3 mL), was added a solution of nickel (II) hexafluoroacetylacetonate hydrate (21 mg, 0.044 mmol) in methanol (3 mL). The reaction mixture was magnetically stirred at 65 °C for 2 hours. After 1-3 days of slow evaporation, green needle-shaped crystals were collected by filtration. Yield: 23 mg (74.0%). MALDI-TOF MS (m/z): 492.7 [NiL⁷(Hfac)]⁺.

[CuL⁷(Hfac)₂] (36)

To a light-yellow solution of L⁷ (10 mg, 0.044 mmol) in DCM (3 mL), was added a solution of copper (II) hexafluoroacetylacetonate hydrate (21 mg, 0.044 mmol) in methanol (3 mL). The reaction mixture was magnetically stirred at 65 °C for 2 hours. After 1-3 days of slow evaporation, green needle-shaped crystals were collected by filtration. Yield: 26 mg (83.9 %). MALDI-TOF MS (m/z): 496.9 [CuL⁷(Hfac)]⁺.

[ZnL⁷(Hfac)₂] (37)

To a light-yellow solution of L⁷ (10 mg, 0.044 mmol) in DCM (3 mL), was added a solution of zinc (II) hexafluoroacetylacetonate dihydrate (23 mg, 0.044 mmol) in methanol (3 mL). The reaction mixture was magnetically stirred at 65 °C for 2 hours. After 1-3 days of slow evaporation, light-yellow needle-shaped crystals were collected by filtration. Yield: 24 mg (76.1 %). MALDI-TOF MS (m/z): 491.8 [ZnL⁷(Hfac)]⁺.

[CuL⁸(Hfac)₂] (38)

To a light-yellow solution of L⁸ (10 mg, 0.034 mmol) in chloroform (3 mL), was added a solution of copper (II) hexafluoroacetylacetonate hydrate (16 mg, 0.034 mmol) in methanol (3 mL). The reaction mixture was magnetically stirred at 65 °C for 1 hours. After a few days of slow evaporation, green crystals were collected by filtration. Yield: 15 mg (58.3%). ESI-MS (m/z): 561.0 [CuL⁸(Hfac)]⁺.

[Cu₂L⁸(Hfac)₄] (39)

To a light-yellow solution of L⁸ (10 mg, 0.034 mmol) in DCM (3 mL), was added a solution of copper (II) hexafluoroacetylacetonate hydrate (33 mg, 0.069 mmol) in n-heptane (3 mL). The reaction mixture was heated to n-heptane boiling point for five minutes. Upon cooling to room temperature, 2 mL of DCM were added, and the solution was left to slowly evaporate. Green crystals were formed in few days. Yield: 18 mg (41.8%). ESI-MS (m/z): 1038.7 [Cu₂L⁸(Hfac)₃]⁺.

[MnL⁹(Cl)₂]·**0.5CH₂Cl₂ (40)**

To a light-yellow solution of L⁹ (20 mg, 0.066 mmol) in DCM (3 mL), was added a solution of manganese (II) chloride tetrahydrate (13 mg, 0.066 mmol) in methanol (3 mL). The reaction mixture was magnetically stirred at 65 °C for 2 hours. After 1-3 days of slow evaporation, pink crystals were collected by filtration. Yield: 20 mg (64.5 %). ESI-MS (m/z): 393.9 [MnL⁹Cl]⁺.

[CoL⁹(H₂O)₂Cl]Cl·**3H₂O (41)**

To a light-yellow solution of L⁹ (20 mg, 0.066 mmol) in DCM (3 mL), was added a solution of cobalt (II) chloride hexahydrate (16 mg, 0.066 mmol) in methanol (3 mL). The reaction mixture was magnetically stirred at 65 °C for 2 hours. After 1-3 days of slow evaporation, dark brown crystals were collected by filtration. Yield: 16 mg (45.4 %). ESI-MS (m/z): 362.0 [CoL⁹]²⁺, 398.0 [CoL⁹Cl]⁺.

[CoL⁹Cl₂]·**0.25CH₂Cl₂ (42)**

To a light-yellow solution of L⁹ (20 mg, 0.066 mmol) in DCM (3 mL), was added a solution of cobalt (II) chloride (9 mg, 0.066 mmol) in methanol (3 mL). The reaction mixture was magnetically stirred at 65 °C for 2 hours. After 1-3 days of slow evaporation, green crystals were collected by filtration. Yield: 13 mg (41.3 %). ESI-MS (m/z): 398.0 [CoL⁹Cl]⁺.

[NiL⁹(H₂O)₃]Cl₂·**2H₂O (43)**

To a light-yellow solution of L⁹ (20 mg, 0.066 mmol) in DCM (3 mL), was added a solution of nickel (II) chloride hexahydrate (16 mg, 0.066 mmol) in methanol (3 mL). The reaction mixture was magnetically stirred at 65 °C for 2 hours. After 1-3 days of slow evaporation, green crystals were collected by filtration. Yield: 18 mg (51.1 %). ESI-MS (m/z): 362.0 [NiL⁹]²⁺, 398.0 [NiL⁹Cl]⁺.

[Ni₂(L⁹)₂Cl₄]·2H₂O (44)

To a light-yellow solution of L⁹ (20 mg, 0.066 mmol) in DCM (3 mL), was added a solution of nickel (II) chloride (9 mg, 0.066 mmol) in methanol (3 mL). The reaction mixture was magnetically stirred at 65 °C for 2 hours. After 1-3 days of slow evaporation, green brown crystals were collected by filtration. Yield: 22 mg (70.1 %). ESI-MS (m/z): 362.0 [NiL⁹]²⁺, 397.0 [NiL⁹Cl]⁺.

[CuL⁹Cl₂]·H₂O (45)

To a light-yellow solution of L⁹ (20 mg, 0.066 mmol) in DCM (3 mL), was added a solution of copper (II) chloride dihydrate (11 mg, 0.066 mmol) in methanol (3 mL). The reaction mixture was magnetically stirred at 65 °C for 2 hours. After 1-3 days of slow evaporation, green crystals were collected by filtration. Yield: 19 mg (64.4 %). ESI-MS (m/z): 367.0[CuL⁹]²⁺, 402.0 [CuL⁹Cl]⁺.

[ZnL⁹Cl₂] (46)

To a light-yellow solution of L⁹ (20 mg, 0.066 mmol) in DCM (3 mL), was added a solution of zinc (II) chloride (9 mg, 0.066 mmol) in methanol (3 mL). The reaction mixture was magnetically stirred at 65 °C for 2 hours. After 1-3 days of slow evaporation, yellow crystals were collected by filtration. Yield: 14 mg (47.8 %). ESI-MS (m/z): 402.8 [ZnL⁹Cl]⁺.

[NiL⁹(Hfac)(H₂O)](Hfac)·H₂O (47)

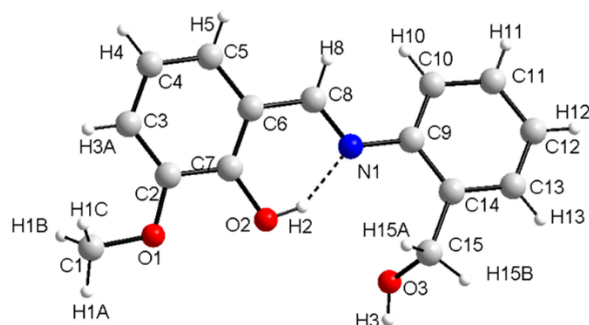
To a light-yellow solution of L⁹ (10 mg, 0.033 mmol) in chloroform (3 mL), was added a solution of nickel (II) hexafluoroacetylacetonate hydrate (16 mg, 0.033 mmol) in ethanol (3 mL). The reaction mixture was magnetically stirred at 65 °C for 2 hours. After 1-3 days of slow evaporation, green crystals were collected by filtration. Yield: 15 mg (55.7 %). IR (KBr, ν_{max} cm⁻¹): 3222br, 1671s, 1645vs, 1602m, 1554m, 1532vs, 1479vs, 1450s, 1258vs, 1208vs, 1149vs, 909w, 789m, 776m, 672m, 584m. ESI-MS (m/z): 569.0 [NiL⁹(Hfac)]⁺.

[CuL⁹(Hfac)(H₂O)](Hfac)·H₂O (48)

To a light-yellow solution of L⁹ (10 mg, 0.033 mmol) in chloroform (3 mL), was added a solution of copper (II) hexafluoroacetylacetonate hydrate (16 mg, 0.033 mmol) in methanol (3 mL). The reaction mixture was magnetically stirred at 65 °C for 2 hours. After 1-3 days of slow evaporation, green needle-shaped crystals were collected by filtration. Yield: 18 mg (65.7 %). IR (KBr, ν_{max} cm⁻¹): 32354br, 3093w, 2928m, 1672vs, 1602s, 1557s, 1531s, 1486m, 1457s, 1302m, 1252s, 1203vs, 1143vs, 1127vs, 906m, 885w, 837w, 826w, 789s, 727m, 661m, 591m, 572m, 521w. ESI-MS (m/z): 574.0 [CuL⁹(Hfac)]⁺.

[CuL⁹(Hfac)(C₂H₅OH)](Hfac) (49)

To a light-yellow solution of L⁹ (10 mg, 0.033 mmol) in chloroform (3 mL), was added a solution of copper (II) hexafluoroacetylacetonate hydrate (16 mg, 0.033 mmol) in ethanol (3 mL). The reaction mixture was magnetically stirred at 65 °C for 2 hours. After 1-3 days of slow evaporation, green needle-shaped crystals were collected by filtration. Yield: 20 mg (72.1 %). IR (KBr, ν_{\max} cm⁻¹): 3313br, 3079w, 1668vs, 1602m, 1554s, 1531vs, 1482s, 1455s, 1260vs, 1206vs, 1147vs, 1131vs, 913w, 783s, 659m, 577m, 568w. ESI-MS (m/z): 573.93 [CuL⁹(Hfac)]⁺. MALDI-TOF MS (m/z): 366.9 [CuL⁹]²⁺, 573.8 [CuL⁹(Hfac)]⁺, 622.0 [CuL⁹(Hfac)(CH₃CH₂OH)]⁺.

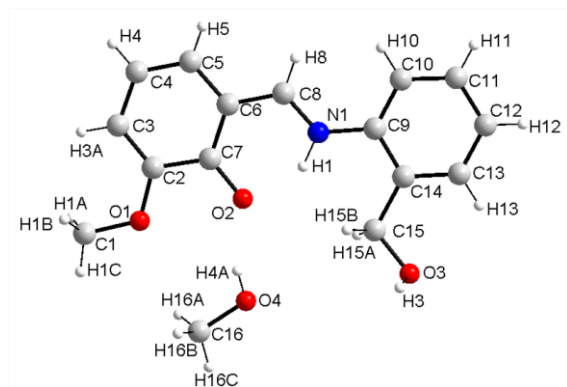
3-2-[[2-hydroxymethylbenzyl)imino]methyl]-6-methoxy-phenol, **H₂L²** (**20**)

Formula	C ₁₅ H ₁₅ NO ₃
M (g·mol ⁻¹)	257.28
T (K)	150
Wavelength (Å)	1.54184
Crystal system	Monoclinic
Space group	<i>P</i> 2 ₁ / <i>n</i>
a, (Å)	15.1282(5)
b, (Å)	5.07285(13)
c, (Å)	17.7873(6)
α, (°)	90
β, (°)	114.988(4)
γ, (°)	90
V, Å ³	1237.28(8)
Z, ρ _{calcd.} (g/cm ³)	4, 1.381
μ (mm ⁻¹)	0.790
<i>F</i> (000)	544
θ _{min} /θ _{max} (°)	5.040/73.258
Reflections collected/unique	8513/ 2451
R _{int}	0.0210
R ₁ [<i>I</i> > 2σ(<i>I</i>)]	0.0388, 0.1066
wR ₂ (all data)	0.0425, 0.1111
G.O.F.	1.039
Largest difference peak/hole (e ⁻ ·Å ⁻³)	0.250/ -0.197
N _o CCDC	1902225

Selected bond distances (Å) and angles (°) for **H₂L² (20)**.

O1—C1	1.4251(15)	C12—H12	0.93	C5—C6	1.4077(17)
O1—C2	1.3586(15)	C13—H13	0.93	C6—C7	1.4047(17)
O2—H2	0.90(2)	C8—H8	0.93	C6—C8	1.4492(17)
O2—C7	1.3446(14)	C10—H10	0.93	C9—C10	1.4015(17)
C12—C13	1.388(2)	C15—H15a	0.97	C9—C14	1.4029(18)
O3—C15	1.4215(16)	C15—H15b	0.97	C10—C11	1.3849(19)
N1—C8	1.2806(16)	C11—H11	0.93	C13—C14	1.3931(18)
N1—C9	1.4142(16)	C3—H3A	0.93	C14—C15	1.5092(17)
C3—C4	1.3992(19)	C4—H4	0.93	C2—C7	1.4113(17)
C1—H1b	0.96	C1—H1a	0.96	C11—C12	1.383(2)
C1—H1c	0.96	O3—H3	0.82	C4—C5	1.3729(19)
C2—C3	1.3833(17)				
C9—C10—H10	119.8	C11—C10—H10	119.8	C6—C8—H8	119.3
C13—C14—C15	120.33(11)	C10—C11—H11	119.9	C10—C9—N1	123.22(11)
O3—C15—C14	107.64(10)	O3—C15—H15a	110.2	C10—C9—C14	119.79(11)
C12—C11—C10	120.15(12)	C12—C11—H11	119.9	C14—C9—N1	116.98(10)
C11—C12—C13	119.71(12)	C11—C12—H12	120.1	N1—C8—C6	121.47(10)
H1a—C1—H1b	109.5	O3—C15—H15b	110.2	C11—C10—C9	120.34(12)
H1a—C1—H1c	109.5	N1—C8—H8	119.3	C2—O1—C1	117.83(10)
H1b—C1—H1c	109.5	O1—C1—H1a	109.5	C7—O2—H2	105.8(14)
O1—C2—C3	125.75(11)	O1—C1—H1b	109.5	C15—O3—H3	109.5
O1—C2—C7	113.93(10)	O1—C1—H1c	109.5	C8—N1—C9	122.68(10)
C3—C2—C7	120.31(11)	C13—C12—H12	120.1	C4—C5—C6	120.68(11)
C5—C6—C8	120.40(11)	C2—C3—H3a	120	C13—C14—C9	118.59(12)
C7—C6—C5	119.23(11)	C5—C4—H4	119.8	C4—C5—H5	119.7
C7—C6—C8	120.37(11)	C6—C5—H5	119.7	C2—C3—C4	119.97(12)
C14—C13—H13	119.3	C14—C15—H15b	110.2	O2—C7—C6	122.74(11)
C12—C13—H13	119.3	H15a—C15—H15b	108.5	C5—C4—C3	120.40(11)
C12—C13—C14	121.35(12)	C4—C3—H3a	120	C9—C14—C15	121.05(11)
C14—C15—H15a	110.2	C3—C4—H4	119.8	O2—C7—C2	117.86(10)

H₂L²·CH₃OH (20a)

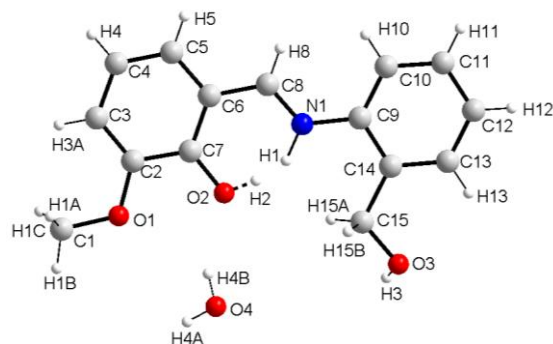


Formula	C ₁₆ H ₁₉ NO ₄
M (g·mol ⁻¹)	289.32
T (K)	150
Wavelength (Å)	1.54184
Crystal system	Orthorhombic
Space group	<i>Pna</i> 2 ₁
a, (Å)	20.7153(4)
b, (Å)	14.6858(3)
c, (Å)	4.76014(9)
α, (°)	90
β, (°)	90
γ, (°)	90
V, Å ³	1448.14(4)
Z, ρ _{calcd.} (g/cm ³)	4, 1.327
μ (mm ⁻¹)	0.784
<i>F</i> (000)	616
θ _{min} /θ _{max} (°)	3.689/73.217
Reflections collected/unique	8853/2840
R _{int}	0.0237
R ₁ [<i>I</i> > 2σ(<i>I</i>)]	0.0308, 0.0797
wR ₂ (all data)	0.0322, 0.0787
G.O.F.	1.039
Largest difference peak/hole (e ⁻ ·Å ⁻³)	0.157/ -0.171
N _o CCDC	1579661

Selected bond distances (Å) and angles (°) for **H₂L²·CH₃OH (20a)**.

N1—H1	0.93(3)	C6—C8	1.417(2)	C11—H11	0.93
N1—C8	1.308(2)	C13—C14	1.396(3)	C12—H12	0.93
N1—C9	1.416(2)	C9—C10	1.391(3)	C13—H13	0.93
C1—H1a	0.96	C9—C14	1.397(3)	C3—H3a	0.93
C1—H1b	0.96	O4—H4A	0.85(3)	C5—H5	0.93
C1—H1c	0.96	O4—C16	1.420(3)	C4—H4	0.93
C2—C3	1.373(3)	O1—C1	1.427(2)	C8—H8	0.93
C2—C7	1.443(3)	O1—C2	1.362(2)	C15—H15a	0.97
C11—C12	1.386(3)	O2—C7	1.292(2)	C15—H15b	0.97
C3—C4	1.413(3)	O3—H3	0.81(3)	C10—H10	0.93
C4—C5	1.366(3)	C5—C6	1.418(3)	C16—H16a	0.96
O3—C15	1.415(2)	C6—C7	1.429(3)	C16—H16b	0.96
C12—C13	1.380(3)	C10—C11	1.383(3)	C16—H16c	0.96
C14—C15	1.514(3)				
C2—O1—C1	116.88(16)	C10—C11—C12	119.9(2)	C11—C10—H10	120.1
C15—O3—H3	106.(2)	C13—C12—C11	120.07(19)	C10—C11—H11	120
C8—N1—H1	113.7(18)	C4—C5—C6	120.41(17)	O4—C16—H16a	109.5
C8—N1—C9	127.83(16)	C6—C5—H5	119.8	O4—C16—H16b	109.5
C9—N1—H1	118.5(18)	C5—C6—C7	120.52(16)	C12—C11—H11	120
C9—C14—C15	120.83(17)	C8—C6—C5	120.15(17)	C13—C12—H12	120
C13—C14—C9	117.75(18)	C8—C6—C7	119.32(16)	C12—C13—H13	119.4
O1—C1—H1c	109.5	O2—C7—C2	120.53(16)	C11—C12—H12	120
H1a—C1—H1b	109.5	O2—C7—C6	122.35(16)	C14—C13—H13	119.4
H1a—C1—H1c	109.5	C6—C7—C2	117.12(16)	C5—C4—H4	119.9
H1b—C1—H1c	109.5	N1—C8—C6	120.70(16)	C4—C5—H5	119.8
C2—C3—H3a	119.5	N1—C8—H8	119.6	O1—C1—H1a	109.5
C2—C3—C4	120.95(17)	C6—C8—H8	119.6	O1—C1—H1b	109.5
C4—C3—H3a	119.5	O1—C2—C3	126.41(18)	O3—C15—H15a	109.1
C3—C4—H4	119.8	O1—C2—C7	112.90(16)	O3—C15—H15b	109.1
C5—C4—C3	120.30(17)	C3—C2—C7	120.69(17)	C14—C15—H15a	109.1
C16—O4—H4a	110.(2)	C11—C10—C9	119.75(19)	C14—C15—H15b	109.1
C13—C14—C15	121.42(17)	C10—C9—N1	122.04(16)	H15a—C15—H15b	107.9
O3—C15—C14	112.28(17)	C10—C9—C14	121.19(18)	H16a—C16—H16c	109.5
O4—C16—H16c	109.5	C14—C9—N1	116.76(16)	H16b—C16—H16c	109.5
C12—C13—C14	121.30(19)	C9—C10—H10	120.1	H16a—C16—H16b	109.5

H₂L²·H₂O (20b)

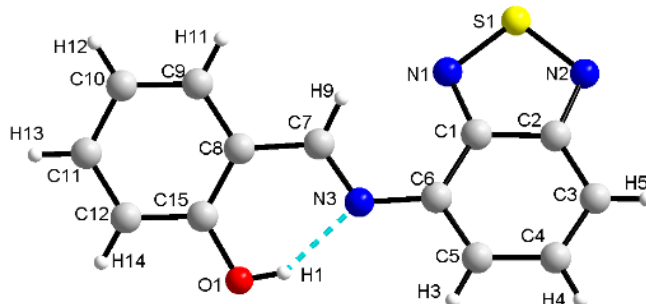


Formula	C ₁₅ H ₁₇ NO ₄
M (g·mol ⁻¹)	275.27
T (K)	150
Wavelength (Å)	0.71073
Crystal system	Orthorhombic
Space group	<i>Pna</i> 2 ₁
a, (Å)	20.6861(8)
b, (Å)	13.4035(5)
c, (Å)	4.78869(17)
α, (°)	90
β, (°)	90
γ, (°)	90
V, Å ³	1327.74(9)
Z, ρ _{calcd.} (g/cm ³)	4, 1.377
μ (mm ⁻¹)	0.100
<i>F</i> (000)	584
θ _{min} /θ _{max} (°)	3.623/28.927
Reflections collected/unique	20228/3120
R _{int}	0.0462
R ₁ [<i>I</i> > 2σ(<i>I</i>)]	0.0317, 0.0742
wR ₂ (all data)	0.0357, 0.0764
G.O.F.	1.054
Largest difference peak/hole (e ⁻ ·Å ⁻³)	0.202/ -0.202
N _o CCDC	1579663

Selected bond distances (Å) and angles (°) for H₂L²·H₂O (20b).

C10—C9	1.398(2)	C8—H8	0.93	C10—H10	0.93
O3—C15	1.417(2)	C8—C6	1.434(2)	C15—H15a	0.97
O2—C7	1.320(2)	C6—C5	1.410(2)	C15—H15b	0.97
O2—H2	0.83(8)	C6—C7	1.418(2)	C3—H3a	0.93
O1—C2	1.370(2)	O4—H4b	0.8504	C1—H1a	0.96
O1—C1	1.431(2)	O4—H4a	0.8507	C1—H1b	0.96
N1—C9	1.412(2)	C5—C4	1.372(3)	C1—H1c	0.96
N1—C8	1.296(2)	C4—C3	1.406(2)	C5—H5	0.93
N1—H1	0.98(7)	C3—C2	1.375(2)	C12—H12	0.93
C14—C13	1.394(2)	C2—C7	1.420(2)	C4—H4	0.93
C14—C9	1.400(2)	C11—C10	1.385(3)	C11—H11	0.93
C14—C15	1.515(2)	C12—C11	1.387(3)	O3—H3	0.82
C13—H13	0.93	C13—C12	1.384(3)		
C11—C10—C9	120.13(16)	O1—C2—C3	125.74(16)	C4—C5—H5	119.8
C8—N1—H1	114.(4)	O1—C2—C7	113.61(14)	C5—C4—H4	119.8
O3—C15—H15a	109.2	C3—C2—C7	120.66(15)	O1—C1—H1a	109.5
C12—C13—C14	121.21(16)	O2—C7—C6	121.88(15)	C14—C13—H13	119.4
C14—C15—H15b	109.2	O2—C7—C2	119.77(14)	N1—C8—H8	119.6
C14—C15—H15a	109.2	C6—C7—C2	118.35(14)	C3—C4—H4	119.8
C13—C14—C9	118.32(15)	C6—C8—H8	119.6	C4—C3—H3A	119.8
C5—C6—C7	119.87(15)	C5—C6—C8	120.55(15)	C9—C10—H10	119.9
C9—C14—C15	120.39(16)	C2—C3—H3a	119.8	C10—C11—H11	120.1
H15a—C15—H15b	107.9	C9—N1—H1	120.(4)	C11—C10—H10	119.9
C13—C12—C11	120.10(17)	C12—C13—H13	119.4	C7—O2—H2	109.4
C4—C5—C6	120.36(15)	C13—C12—H12	119.9	C15—O3—H3	109.5
C13—C14—C15	121.29(15)	C6—C5—H5	119.8	H4a—O4—H4b	109.4
N1—C8—C6	120.83(15)	C12—C11—H11	120.1	O3—C15—H15b	109.2
C7—C6—C8	119.57(15)	C11—C12—H12	119.9	O1—C1—H1b	109.5
C14—C9—N1	116.92(15)	C2—C3—C4	120.38(16)	O1—C1—H1c	109.5
C10—C9—N1	122.63(15)	C8—N1—C9	125.66(14)	H1a—C1—H1b	109.5
C10—C9—C14	120.44(16)	C2—O1—C1	116.55(14)	H1a—C1—H1c	109.5
O3—C15—C14	111.90(15)	C10—C11—C12	119.79(16)	H1b—C1—H1c	109.5
C5—C4—C3	120.38(16)				

2-[4-(2,1,3-benzothiadiazole)imino]methyl-phenol (**HL⁵**)

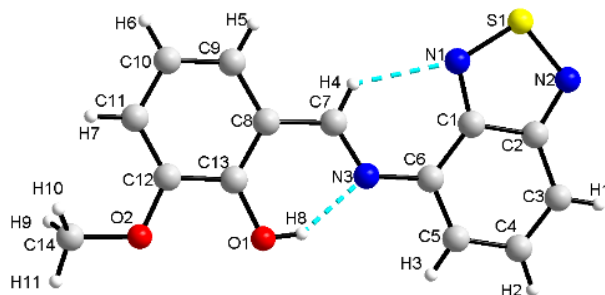


Formula	C ₁₃ H ₉ N ₃ OS
M (g·mol ⁻¹)	255.29
T (K)	150.00(10)
Wavelength (Å)	1.54184
Crystal system	Orthorhombic
Space group	<i>Pbca</i>
a, (Å)	12.9117(3)
b, (Å)	9.3341(2)
c, (Å)	18.8634(5)
α, (°)	90
β, (°)	90
γ, (°)	90
V, Å ³	2273.40(9)
Z, ρ _{calcd.} (g/cm ³)	8, 1.492
μ (mm ⁻¹)	2.452
<i>F</i> (000)	1056
θ _{min} /θ _{max} (°)	4.688 / 72.103
Reflections collected/unique	5479 / 2191
R _{int}	0.0215
R ₁ [I > 2σ(I)]	0.0338, 0.0916
wR ₂ (all data)	0.0378, 0.0950
G.O.F.	1.056
Largest difference peak/hole (e·Å ⁻³)	0.280 / -0.397
N _o CCDC	-

Selected bond distances (Å) and angles (°) for **HL**⁵.

C1-N1	1.3380(19)	C8-C15	1.4088(19)	C11-C12	1.383(2)
C1-C2	1.4369(18)	C9-C10	1.3797(19)	C11-H13	0.93
C1-C6	1.4371(19)	C9-H11	0.93	C12-C15	1.3962(19)
C2-N2	1.349(2)	C10-C11	1.397(2)	C12-H14	0.93
C2-C3	1.417(2)	C10-H12	0.93	C15-O1	1.3483(16)
C3-C4	1.361(2)	C6-N3	1.4067(17)	N1-S1	1.6126(12)
C3-H5	0.93	C7-N3	1.2903(18)	N2-S1	1.6175(14)
C4-C5	1.4230(19)	C7-C8	1.4512(18)	O1-H1	0.82
C4-H4	0.93	C7-H9	0.93	C8-C9	1.4063(19)
C5-C6	1.3738(19)	C5-H3	0.93		
N1-C1-C2	113.56(12)	C3-C4-C5	122.23(13)	N3-C7-H9	119.5
N1-C1-C6	126.57(12)	C3-C4-H4	118.9	C8-C7-H9	119.5
C2-C1-C6	119.83(12)	C5-C4-H4	118.9	C9-C8-C15	119.01(12)
N2-C2-C3	126.13(12)	C6-C5-C4	122.35(13)	C9-C8-C7	119.15(12)
N2-C2-C1	112.75(12)	C6-C5-H3	118.8	C15-C8-C7	121.83(12)
C3-C2-C1	121.11(13)	C4-C5-H3	118.8	C10-C9-C8	121.04(13)
C4-C3-C2	117.46(12)	C5-C6-N3	118.90(12)	C10-C9-H11	119.5
C4-C3-H5	121.3	C5-C6-C1	116.94(12)	C8-C9-H11	119.5
C2-C3-H5	121.3	N3-C6-C1	124.06(12)	C9-C10-C11	119.14(13)
C15-C12-H14	120.1	N3-C7-C8	121.09(12)	C9-C10-H12	120.4
O1-C15-C12	118.17(12)	C12-C15-C8	119.77(12)	C11-C10-H12	120.4
O1-C15-C8	122.06(11)	C1-N1-S1	106.39(9)	C12-C11-C10	121.14(12)
C7-N3-C6	121.19(12)	C2-N2-S1	106.24(10)	C12-C11-H13	119.4
C15-O1-H1	109.5	C11-C12-C15	119.89(13)	C10-C11-H13	119.4
N1-S1-N2	101.06(7)	C11-C12-H14	120.1		

2-[4-(2,1,3-benzothiadiazole)imino]methyl-6-methoxy-phenol (**HL**⁶)

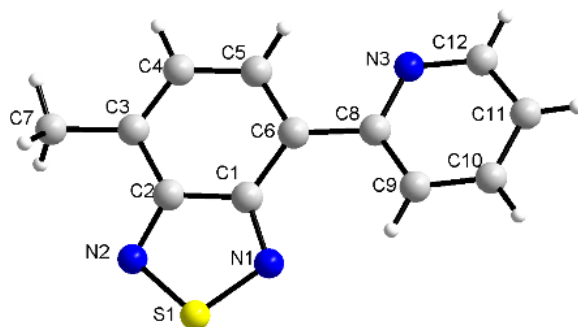


Formula	C ₁₄ H ₁₁ N ₃ O ₂ S
M (g·mol ⁻¹)	285.32
T (K)	150.00(10)
Wavelength (Å)	1.54184
Crystal system	Monoclinic
Space group	<i>P</i> 2 ₁ / <i>c</i>
a, (Å)	12.5784(4)
b, (Å)	5.23110(10)
c, (Å)	19.7962(7)
α, (°)	90
β, (°)	105.161(3)
γ, (°)	90
V, Å ³	1257.23(7)
Z, ρ _{calcd.} (g/cm ³)	4, 1.507
μ (mm ⁻¹)	2.343
<i>F</i> (000)	592
θ _{min} /θ _{max} (°)	3.641/ 72.176
Reflections collected/unique	4305 / 2405
R _{int}	0.0240
R ₁ [I > 2σ(I)]	0.0293, 0.0736
wR ₂ (all data)	0.0342, 0.0767
G.O.F.	1.051
Largest difference peak/hole (e ⁻ ·Å ⁻³)	0.263 / -0.271
N _o CCDC	-

Selected bond distances (Å) and angles (°) for **HL**⁶.

C1-N1	1.3449(17)	C9-H5	0.93	C14-H10	0.96
C1-C2	1.4383(18)	C10-C11	1.3996(19)	C14-H11	0.96
C1-C6	1.4411(18)	C10-H6	0.93	N1-S1	1.6182(11)
C2-N2	1.3466(18)	C11-C12	1.3805(19)	N2-S1	1.6178(12)
C2-C3	1.4206(19)	C11-H7	0.93	O1-H8	0.82
C3-C4	1.363(2)	C12-O2	1.3665(16)	C9-C10	1.3737(19)
C3-H1	0.93	C12-C13	1.4139(18)	C7-N3	1.2897(18)
C4-C5	1.4223(19)	C13-O1	1.3439(16)	C7-C8	1.4516(18)
C4-H2	0.93	C14-O2	1.4298(17)	C7-H4	0.93
C5-C6	1.3712(19)	C14-H9	0.96	C8-C13	1.4040(18)
C5-H3	0.93	C6-N3	1.4022(17)	C8-C9	1.4089(18)
N1-C1-C2	112.89(11)	C5-C6-C1	116.48(12)	O2-C12-C11	125.12(12)
N1-C1-C6	127.22(12)	N3-C6-C1	126.12(12)	O2-C12-C13	115.04(12)
C2-C1-C6	119.89(12)	N3-C7-C8	121.21(12)	C11-C12-C13	119.83(12)
N2-C2-C3	125.79(12)	N3-C7-H4	119.4	O1-C13-C8	122.30(11)
N2-C2-C1	113.24(12)	C8-C7-H4	119.4	O1-C13-C12	118.36(11)
C3-C2-C1	120.96(12)	C13-C8-C9	119.64(12)	C8-C13-C12	119.32(12)
C4-C3-C2	117.83(12)	C13-C8-C7	121.18(12)	O2-C14-H9	109.5
C4-C3-H1	121.1	C9-C8-C7	119.13(11)	O2-C14-H10	109.5
C2-C3-H1	121.1	C10-C9-C8	120.40(12)	H9-C14-H10	109.5
C3-C4-C5	121.47(13)	C10-C9-H5	119.8	H9-C14-H11	109.5
C3-C4-H2	119.3	C8-C9-H5	119.8	H10-C14-H11	109.5
C5-C4-H2	119.3	C9-C10-C11	120.09(13)	C1-N1-S1	106.68(9)
C6-C5-C4	123.33(12)	C9-C10-H6	120	C2-N2-S1	106.42(9)
C6-C5-H3	118.3	C11-C10-H6	120	O2-C14-H11	109.5
C4-C5-H3	118.3	C12-C11-C10	120.71(12)	C13-O1-H8	109.5
C5-C6-N3	117.39(11)	C12-C11-H7	119.6	C12-O2-C14	116.50(11)
C10-C11-H7	119.6	C7-N3-C6	122.94(11)	N2-S1-N1	100.77(6)

4-(2-pyridine)-7-methyl-2,1,3-benzothiadiazole (**L**⁷)

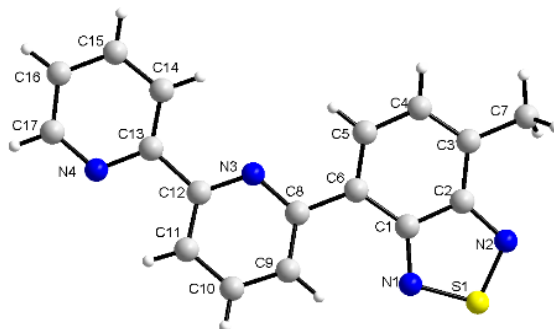


Formula	C ₁₂ H ₉ N ₃ S
M (g·mol ⁻¹)	227.28
T (K)	200.0(3)
Wavelength (Å)	1.54184
Crystal system	Monoclinic
Space group	<i>P</i> 2 ₁ / <i>n</i>
a, (Å)	14.2014(6)
b, (Å)	3.8339(3)
c, (Å)	19.1928(9)
α, (°)	90
β, (°)	96.994(4)
γ, (°)	90
V, Å ³	1037.21(10)
Z, ρ _{calcd.} (g/cm ³)	4, 1.455
μ (mm ⁻¹)	2.535
<i>F</i> (000)	472
θ _{min} /θ _{max} (°)	3.667 / 71.860
Reflections collected/unique	3803 / 1974
R _{int}	0.0373
R ₁ [I > 2σ(I)]	0.0503, 0.1320
wR ₂ (all data)	0.0599, 0.1445
G.O.F.	1.059
Largest difference peak/hole (e ⁻ ·Å ⁻³)	0.259 / -0.333

Selected bond distances (Å) and angles (°) for **L**⁷.

C1-N1	1.340(3)	C7-H16A	0.96	C10-H12	0.93
C1-C2	1.437(3)	C7-H16B	0.96	C11-C12	1.382(4)
C1-C6	1.448(3)	C7-H16C	0.96	C11-H13	0.93
C2-N2	1.351(3)	C8-N3	1.349(3)	C12-N3	1.328(3)
C2-C3	1.423(3)	C8-C9	1.391(3)	C12-H14	0.93
C3-C4	1.362(4)	C9-C10	1.382(3)	C10-C11-H13	121.4
C3-C7	1.498(3)	C9-H11	0.93	C6-C8	1.481(3)
C4-C5	1.416(3)	C10-C11	1.372(4)	N1-S1	1.6161(19)
C4-H8	0.93	C5-H9	0.93	N2-S1	1.615(2)
C5-C6	1.374(3)				
N1-C1-C2	112.95(19)	C3-C4-H8	118.7	H16B-C7-H16C	109.5
N1-C1-C6	126.86(19)	C5-C4-H8	118.7	N3-C8-C9	121.1(2)
C2-C1-C6	120.19(19)	C6-C5-C4	124.3(2)	N3-C8-C6	114.84(19)
N2-C2-C3	124.5(2)	C6-C5-H9	117.9	N3-C12-C11	124.6(2)
N2-C2-C1	113.32(19)	C4-C5-H9	117.9	N3-C12-H14	117.7
C3-C2-C1	122.2(2)	C5-C6-C1	114.8(2)	C11-C12-H14	117.7
C4-C3-C2	115.9(2)	C5-C6-C8	120.7(2)	C1-N1-S1	106.68(15)
C4-C3-C7	123.7(2)	C1-C6-C8	124.47(19)	C2-N2-S1	106.01(15)
C2-C3-C7	120.4(2)	C3-C7-H16A	109.5	C12-N3-C8	118.0(2)
C3-C4-C5	122.6(2)	C3-C7-H16B	109.5	N2-S1-N1	101.04(10)
H16A-C7-H16B	109.5	C11-C10-C9	119.7(2)	C12-C11-H13	121.4
C3-C7-H16C	109.5	C11-C10-H12	120.2	C10-C9-H11	120.3
H16A-C7-H16C	109.5	C9-C10-H12	120.2	C8-C9-H11	120.3
C9-C8-C6	124.1(2)	C10-C11-C12	117.3(2)	C10-C9-C8	119.4(2)

4-(2,2'-bipyridine)-7-methyl-2,1,3-benzothiadiazole (**L**⁹)

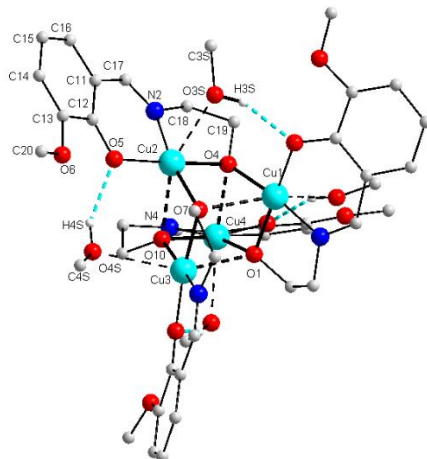


Formula	C ₁₇ H ₁₂ N ₄ S
M (g·mol ⁻¹)	304.37
T (K)	150.00(10)
Wavelength (Å)	1.54184
Crystal system	Monoclinic
Space group	<i>P</i> 2 ₁ / <i>n</i>
a, (Å)	3.8290(2)
b, (Å)	12.4811(7)
c, (Å)	28.6099(15)
α, (°)	90
β, (°)	91.088(4)
γ, (°)	90
V, Å ³	1367.02(13)
Z, ρ _{calcd.} (g/cm ³)	4, 1.479
μ (mm ⁻¹)	2.106
<i>F</i> (000)	632
θ _{min} /θ _{max} (°)	3.090 / 71.917
Reflections collected/unique	5154 / 2604
R _{int}	0.0269
R ₁ [I > 2σ(I)]	0.0680, 0.1754
wR ₂ (all data)	0.0724, 0.1772
G.O.F.	1.166
Largest difference peak/hole (e·Å ⁻³)	0.395 / -0.419
N _o CCDC	-

Selected bond distances (Å) and angles (°) for **L⁹**.

S1-N2	1.610(4)	C14-H14	0.93	C13-C14	1.386(6)
S1-N1	1.615(3)	C10-H10	0.93	C9-C10	1.383(6)
N3-C12	1.344(5)	N4-C13	1.350(5)	C9-H9	0.93
N3-C8	1.355(5)	N2-C2	1.354(5)	C14-C15	1.383(6)
N1-C1	1.347(5)	C12-C11	1.392(6)	C2-C3	1.420(6)
N4-C17	1.337(6)	C12-C13	1.497(5)	C4-C3	1.369(6)
C1-C2	1.439(6)	C1-C6	1.443(6)	C4-H4	0.93
C5-H5	0.93	C6-C5	1.363(6)	C3-C7	1.500(6)
C8-C9	1.391(6)	C6-C8	1.490(5)	C16-C17	1.380(7)
C11-C10	1.376(6)	C15-H15	0.93	C16-C15	1.382(6)
C11-H11	0.93	C17-H17	0.93	C16-H16	0.93
C5-C4	1.427(6)	C7-H7A	0.96	C7-H7C	0.96
C7-H7B	0.96				
N2-S1-N1	101.43(18)	N1-C1-C2	112.9(4)	N4-C13-C12	115.2(4)
C12-N3-C8	117.8(4)	N1-C1-C6	126.8(4)	C14-C13-C12	122.1(4)
C1-N1-S1	106.4(3)	C2-C1-C6	120.3(4)	C10-C9-C8	119.3(4)
C17-N4-C13	116.8(4)	C5-C6-C1	115.2(4)	C10-C9-H9	120.3
C2-N2-S1	106.1(3)	C5-C6-C8	121.3(4)	C8-C9-H9	120.3
N3-C12-C11	123.2(4)	C1-C6-C8	123.4(4)	C15-C14-C13	119.0(4)
N3-C12-C13	116.7(4)	N3-C8-C9	121.9(4)	C15-C14-H14	120.5
C11-C12-C13	120.0(4)	N2-C2-C3	124.6(4)	C13-C14-H14	120.5
N3-C8-C6	115.3(4)	N2-C2-C1	113.2(4)	C11-C10-C9	119.3(4)
C9-C8-C6	122.8(4)	C3-C2-C1	122.2(4)	C11-C10-H10	120.3
C10-C11-C12	118.4(4)	C3-C4-C5	122.2(4)	C9-C10-H10	120.3
C10-C11-H11	120.8	C3-C4-H4	118.9	C17-C16-C15	117.9(4)
C12-C11-H11	120.8	C5-C4-H4	118.9	C17-C16-H16	121
C6-C5-C4	124.2(4)	C4-C3-C2	115.9(4)	C15-C16-H16	121
C6-C5-H5	117.9	C4-C3-C7	123.4(4)	C16-C15-C14	119.2(4)
C4-C5-H5	117.9	C2-C3-C7	120.7(4)	C16-C15-H15	120.4
N4-C13-C14	122.7(4)	H7A-C7-H7C	109.5	C14-C15-H15	120.4
H7B-C7-H7C	109.5	C3-C7-H7A	109.5	N4-C17-C16	124.4(4)
H7A-C7-H7B	109.5	C3-C7-H7B	109.5	N4-C17-H17	117.8
C3-C7-H7C	109.5	C16-C17-H17	117.8		

[Cu₄(L¹)₄(CH₃OH)₄]·2,2CH₃OH (1)

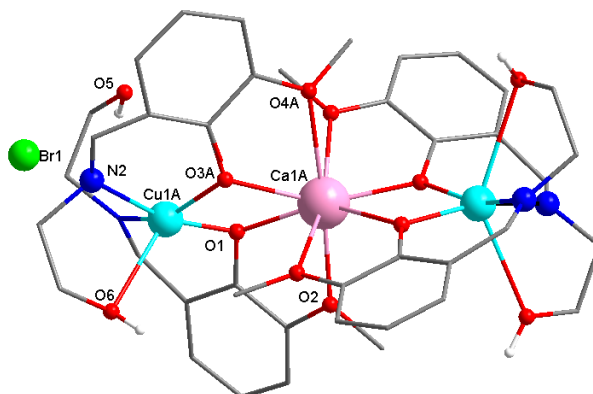


Formula	C _{46.2} H _{68.8} Cu ₄ N ₄ O _{18.2}
M (g·mol ⁻¹)	1225.61
T (K)	100
Wavelength (Å)	0.71073
Crystal system	Monoclinic
Space group	<i>P</i> 2 ₁ / <i>c</i>
a, (Å)	13.4225(5)
b, (Å)	23.1050(8)
c, (Å)	17.1866(5)
α, (°)	90
β, (°)	97.757(3)
γ, (°)	90
V, Å ³	5281.3(3)
Z, ρ _{calcd.} (g/cm ³)	4, 1.541
μ (mm ⁻¹)	1.664
<i>F</i> (000)	2542
θ _{min} /θ _{max} (°)	2.903/32.376
Reflections collected/unique	32912/16709
R _{int}	0.0716
R ₁ [I > 2σ(I)]	7.55, 13.11
wR ₂ (all data)	16.77, 16.46
G.O.F.	1.014
Largest difference peak/hole (e ⁻ ·Å ⁻³)	1.353/-0.926
N ₂ CCDC	1816649

Selected bond distances (Å) and angles (°) for [Cu₄(L¹)₄(CH₃OH)₄]·2,2CH₃OH (1).

Cu1—O4	1.949(3)	Cu3—O7	1.959(3)	Cu4—O10	1.978(3)
Cu1—O1	1.971(3)	Cu3—O10	1.937(3)	Cu4—O1	1.941(3)
Cu1—O2	1.926(3)	Cu3—O8	1.917(3)	Cu4—O11	1.933(3)
Cu1—N1	1.940(4)	Cu3—N3	1.933(4)	Cu4—N4	1.940(4)
Cu2—O7	1.937(3)	Cu2—O5	1.918(3)	Cu2—N2	1.942(4)
Cu2—O4	1.954(3)				
O2—Cu1—N1	93.52(15)	O2—Cu1—O1	174.80(14)	N3—Cu3—O10	169.95(14)
N1—Cu1—O4	170.66(14)	O4—Cu1—O1	87.36(13)	O8—Cu3—O7	173.67(14)
N1—Cu1—O1	83.57(14)	O2—Cu1—O4	95.69(14)	O11—Cu4—O10	170.69(14)
O7—Cu2—O4	88.41(13)	O5—Cu2—O7	95.64(13)	O11—Cu4—O1	96.13(14)
O7—Cu2—N2	170.28(16)	O5—Cu2—O4	175.65(14)	O11—Cu4—N4	93.52(17)
N4—Cu4—O10	83.42(16)	O5—Cu2—N2	91.92(16)	O8—Cu3—O10	93.84(13)
N4—Cu4—O1	168.85(18)	N2—Cu2—O4	84.22(15)	O8—Cu3—N3	93.23(15)
O10—Cu3—O7	88.82(12)	O1—Cu4—O10	87.88(13)	N3—Cu3—O7	84.88(14)

[Ca{Cu(HL¹)₂}₂]Br₂ (**2**)

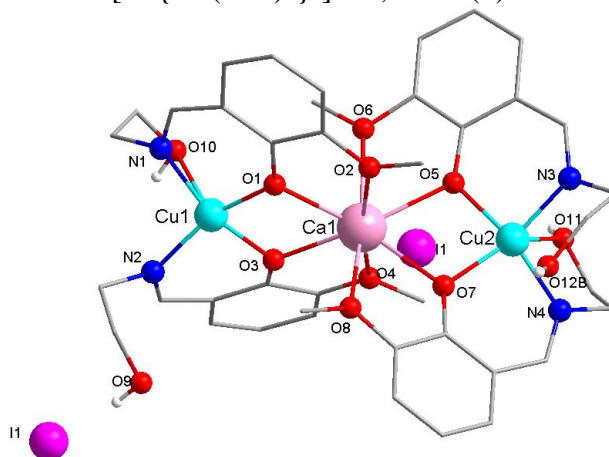
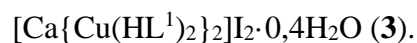


Formula	C ₄₀ H ₄₈ Br ₂ CaCu ₂ N ₄ O ₁₂
M (g·mol ⁻¹)	1103.80
T (K)	100
Wavelength (Å)	0.71073
Crystal system	Orthorhombic
Space group	<i>P</i> 2 ₁ 2 ₁ 2
a, (Å)	25.228(2)
b, (Å)	9.4014(8)
c, (Å)	9.4902(9)
α, (°)	90
β, (°)	90
γ, (°)	90
V, Å ³	2250.9(3)
Z, ρ _{calcd.} (g/cm ³)	2, 1.629
μ (mm ⁻¹)	2.897
<i>F</i> (000)	1120
θ _{min} /θ _{max} (°)	3.1420/22.3710
Reflections collected/unique	7105/3777
R _{int}	0.0625
R ₁ [I > 2σ(I)]	6.24, 10.35
wR ₂ (all data)	10.55, 11.94
G.O.F.	1.048
Largest difference peak/hole (e ⁻ ·Å ⁻³)	0.522/-0.637
N _o CCDC	1816647

Selected bond distances (Å) and angles (°) for [Ca{Cu(HL¹)₂}₂]Br₂ (**2**).

Cu1—O1	1.89(2)	Ca1a—O1a	2.35(2)	Ca1—O1	2.36(2)
Cu1—O3	1.936(11)	Ca1a—O2a	2.534(16)	Ca1—O2	2.515(15)
Cu1—N1	2.038(12)	Ca1a—O3a	2.323(12)	Ca1—O3	2.325(12)
Cu1—N2	1.958(13)	Ca1a—O4a	2.543(12)	Ca1—O4	2.554(12)
Cu1a—O1a	1.89(2)	Cu1a—N2a	1.955(13)	Cu1a—N1	1.874(12)
Cu1a—O3a	1.936(11)	Ca1a—C3a	3.22(2)		
O1—Cu1—O3	80.6(7)	O3a ⁱ —Ca1a—O4a	86.4(6)	O3a ⁱ —Ca1a—O1a	149.0(7)
O1—Cu1—N1	89.1(8)	O1a—Cu1a—O3a	81.1(7)	N1—Cu1a—O3a	149.5(7)
O1—Cu1—N2	159.4(10)	O1a—Cu1a—N2a	160.7(10)	N1—Cu1a—N2a	100.4(7)
O3—Cu1—N1	160.2(7)	O3a—Cu1a—N2a	89.9(8)	O2—Ca1—O2 ⁱ	111.0(8)
O3—Cu1—N2	91.7(7)	O1a ⁱ —Ca1a—O2a	79.2(7)	O1 ⁱ —Ca1—O2	83.9(7)
N2—Cu1—N1	103.3(7)	O1a ⁱ —Ca1a—O4a	84.5(6)	O1—Ca1—O2	63.2(6)
O2—Ca1—O4 ⁱ	77.8(5)	N1—Cu1a—O1a	95.8(7)	O1—Ca1—O2 ⁱ	83.9(7)
O2—Ca1—O4	170.4(5)	O1a ⁱ —Ca1a—O1a	133.3(10)	O1 ⁱ —Ca1—O2 ⁱ	63.2(6)
O2 ⁱ —Ca1—O4	77.8(5)	O1a—Ca1a—O4a	117.1(6)	O3 ⁱ —Ca1—O2	88.7(6)
O3 ⁱ —Ca1—O1	149.1(7)	O3a—Ca1a—O1a	64.4(5)	O3—Ca1—O3 ⁱ	129.7(9)
O3 ⁱ —Ca1—O1 ⁱ	63.9(5)	O3a—Ca1a—O2a	127.4(5)	O3 ⁱ —Ca1—O4 ⁱ	62.2(5)
O3—Ca1—O1 ⁱ	149.1(7)	O4a ⁱ —Ca1a—O4a	125.9(7)	O3 ⁱ —Ca1—O4	83.4(6)
O3—Ca1—O4 ⁱ	83.4(6)	O3a—Ca1a—C3a	84.8(5)	O1—Ca1—O4 ⁱ	97.3(7)
O3—Ca1—O4	62.2(5)	O3a—Ca1a—O4a	64.8(5)	O1—Ca1—O4	123.0(5)
O3—Ca1—O2	120.3(5)	O1a—Ca1a—O2a	64.0(6)	O3—Ca1—O1	63.9(5)
O4—Ca1—O4 ⁱ	93.6(8)	O2a ⁱ —Ca1a—O2a	75.4(8)	O1—Ca1—O1 ⁱ	121.2(11)
O1 ⁱ —Ca1—O4	97.3(7)	O2a—Ca1a—O4a	154.2(6)	O1 ⁱ —Ca1—O4 ⁱ	123.0(5)
O2 ⁱ —Ca1—O4 ⁱ	170.4(5)	O2a ⁱ —Ca1a—O4a	79.6(5)	O3 ⁱ —Ca1—O2 ⁱ	120.3(5)
O3—Ca1—O2 ⁱ	88.7(6)	O3a ⁱ —Ca1a—O3a	115.1(8)	O3a ⁱ —Ca1a—O2a	104.0(6)

Symmetry code: (i) -x, -2-y, z.

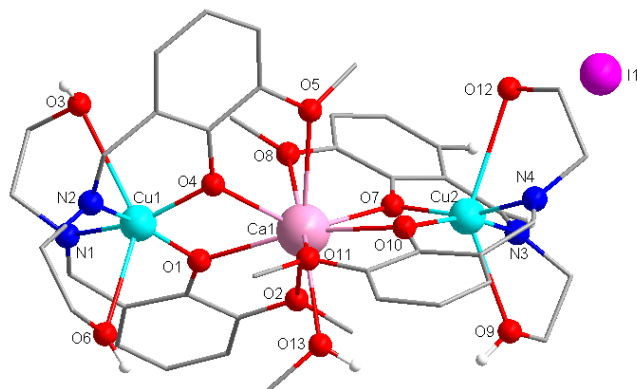


Formula	C ₄₀ H _{48.8} CaCu ₂ I ₂ N ₄ O _{12.4}
M (g·mol ⁻¹)	1204.99
T (K)	298
Wavelength (Å)	0.71073
Crystal system	Triclinic
Space group	<i>P</i> -1
a, (Å)	9.4367(4)
b, (Å)	10.7620(4)
c, (Å)	23.9900(8)
α, (°)	85.167(3)
β, (°)	79.469(3)
γ, (°)	85.260(3)
V, Å ³	2381.18(15)
Z, ρ _{calcd.} (g/cm ³)	2, 1.681
μ (mm ⁻¹)	2.359
F (000)	1200
θ _{min} /θ _{max} (°)	3.013/29.074
Reflections collected/unique	20018/10532
R _{int}	0.0338
R ₁ [I > 2σ(I)]	5.23, 9.09
wR ₂ (all data)	10.39, 10.88
G.O.F.	1.020
Largest difference peak/hole (e·Å ⁻³)	1.012/-0.536
N _o CCDC	1816648

Selected bond distances (Å) and angles (°) for [Ca{Cu(HL¹)₂}₂]₂·0,4H₂O (**3**).

Cu1—O1	1.908(3)	Cu2—O7	1.922(3)	Ca1—O1	2.357(3)
Cu1—O3	1.918(3)	Cu2—N3	1.961(4)	Ca1—O2	2.544(4)
Cu1—N1	1.945(4)	Cu2—N4	1.950(4)	Ca1—O3	2.368(3)
Cu1—N2	1.958(4)	Ca1—O6	2.582(3)	Ca1—O4	2.577(4)
Cu2—Ca1	3.4474(9)	Ca1—O7	2.321(3)	Ca1—O5	2.352(3)
Cu2—O5	1.913(3)	Ca1—O8	2.550(3)		
O1—Cu1—O3	81.66(13)	O8—Ca1—O4	107.66(11)	O7—Cu2—N3	153.17(17)
O1—Cu1—N1	93.03(14)	O8—Ca1—O6	164.45(12)	O7—Cu2—N4	90.75(15)
O1—Cu1—N2	157.91(15)	O7—Ca1—O5	63.92(10)	O1—Ca1—O2	63.0(1)
O3—Cu1—N1	159.25(15)	O7—Ca1—O6	124.71(10)	O1—Ca1—O3	63.95(11)
O3—Cu1—N2	91.19(14)	O7—Ca1—O8	63.69(10)	O1—Ca1—O4	123.26(11)
N1—Cu1—N2	100.49(15)	O5—Ca1—O8	120.36(11)	O1—Ca1—O6	79.46(11)
O5—Cu2—O7	80.35(12)	O7—Ca1—O1	148.99(13)	O1—Ca1—O8	88.55(11)
O5—Cu2—N3	92.26(15)	O7—Ca1—O2	96.53(11)	N4—Cu2—N3	104.23(16)
O5—Cu2—N4	157.79(17)	O7—Ca1—O3	125.07(12)	O3—Ca1—O2	125.79(10)
O2—Ca1—O4	170.12(11)	O7—Ca1—O4	80.70(12)	O3—Ca1—O4	62.4(1)
O2—Ca1—O6	86.52(12)	O5—Ca1—O3	145.47(13)	O3—Ca1—O6	94.27(11)
O2—Ca1—O8	79.18(12)	O5—Ca1—O4	89.92(12)	O3—Ca1—O8	89.24(11)
O4—Ca1—O6	87.32(12)	O5—Ca1—O6	62.29(10)	O5—Ca1—O2	80.38(12)
O5—Ca1—O1	128.34(11)				

[Ca{Cu(HL¹)₂}₂(CH₃OH)]I₂ (**3a**).

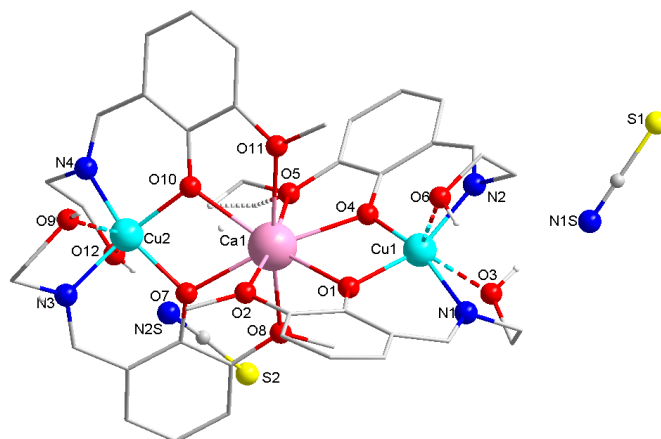


Formula	C ₄₁ H ₅₂ CaCu ₂ I ₂ N ₄ O ₁₃
M (g·mol ⁻¹)	1229.82
T (K)	100
Wavelength (Å)	0.71073
Crystal system	Orthorhombic
Space group	<i>P</i> 2 ₁ 2 ₁ 2 ₁
a, (Å)	9.5747(3)
b, (Å)	19.5355(6)
c, (Å)	25.2757(8)
α, (°)	90
β, (°)	90
γ, (°)	90
V, Å ³	4727.7(2)
Z, ρ _{calcd.} (g/cm ³)	4, 1.728
μ (mm ⁻¹)	2.379
<i>F</i> (000)	2456
θ _{min} /θ _{max} (°)	2.979/27.834
Reflections collected/unique	16421/9199
R _{int}	0.0315
R ₁ [I > 2σ(I)]	3.97, 6.73
wR ₂ (all data)	5.35, 7.25
G.O.F.	1.035
Largest difference peak/hole (e·Å ⁻³)	0.648/-0.499
No CCDC	1816650

Selected bond distances (Å) and angles (°) for [Ca{Cu(HL¹)₂}₂(CH₃OH)]₂ (**3a**).

Cu1—O4	1.925(5)	Ca1—O2	2.704(5)	Ca1—O10	2.424(5)
Cu1—N2	1.966(5)	Ca1—O7	2.349(5)	Ca1—O4	2.367(5)
Cu1—O1	1.916(5)	Ca1—O1	2.454(5)	Ca1—O5	2.661(5)
Cu1—N1	1.951(6)	Ca1—O11	2.688(5)	Ca1—O8	2.572(5)
Cu2—O7	1.917(5)	Cu2—N4	1.958(6)	Cu2—O10	1.928(5)
Cu2—N3	1.969(6)	Ca1—O13	2.463(5)		
O4—Cu1—N2	90.1(2)	N4—Cu2—N3	101.0(2)	O7—Cu2—N3	89.7(2)
O4—Cu1—N1	158.1(2)	O10—Cu2—N4	92.5(2)	O7—Cu2—O10	81.7(2)
O1—Cu1—O4	82.04(19)	O10—Cu2—N3	160.2(2)	O7—Cu2—N4	160.8(2)
O1—Cu1—N2	160.8(2)	O1—Ca1—O11	109.73(16)	O10—Ca1—O5	77.26(16)
O1—Cu1—N1	94.1(2)	O1—Ca1—O13	86.26(18)	O10—Ca1—O8	117.24(16)
N1—Cu1—N2	99.4(2)	O13—Ca1—O2	67.38(19)	O10—Ca1—O2	117.66(18)
O4—Ca1—O10	119.21(17)	O1—Ca1—O2	60.36(17)	O10—Ca1—O1	165.64(16)
O4—Ca1—O5	61.47(15)	O10—Ca1—O11	60.59(15)	O1—Ca1—O5	113.79(16)
O4—Ca1—O8	88.20(16)	O10—Ca1—O13	80.25(19)	O1—Ca1—O8	76.38(15)
O7—Ca1—O4	142.13(17)	O13—Ca1—O11	68.33(18)	O5—Ca1—O2	139.96(16)
O7—Ca1—O5	84.80(16)	O4—Ca1—O13	116.80(18)	O5—Ca1—O11	84.95(15)
O7—Ca1—O8	62.24(16)	O7—Ca1—O10	63.56(16)	O8—Ca1—O5	68.80(15)
O4—Ca1—O2	122.76(17)	O7—Ca1—O2	72.14(16)	O8—Ca1—O2	71.52(16)
O4—Ca1—O1	63.02(15)	O11—Ca1—O2	135.09(16)	O8—Ca1—O11	152.82(16)
O4—Ca1—O11	72.55(16)	O13—Ca1—O5	151.21(19)	O7—Ca1—O1	124.59(17)
O7—Ca1—O13	101.03(19)	O13—Ca1—O8	138.76(19)	O7—Ca1—O11	124.12(17)

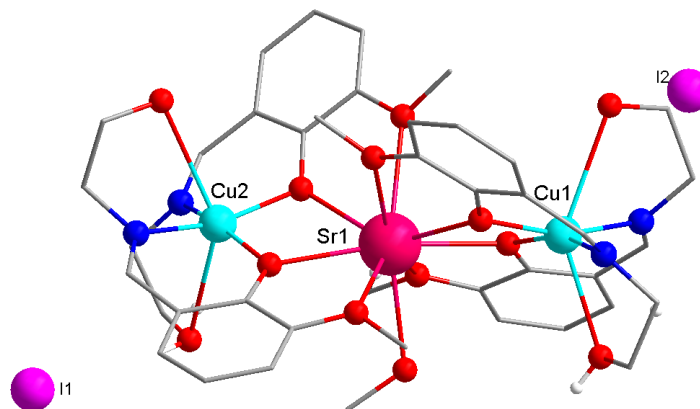
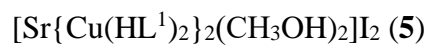
[Ca{Cu(HL¹)₂}₂](NCS)₂ (**4**).



Formula	C ₄₂ H ₄₈ CaCu ₂ N ₆ O ₁₂ S ₂
M (g·mol ⁻¹)	1060.14
T (K)	298
Wavelength (Å)	0.71073
Crystal system	Monoclinic
Space group	<i>P</i> 2 ₁ / <i>c</i>
a, (Å)	25.589(4)
b, (Å)	9.8501(6)
c, (Å)	20.6253(17)
α, (°)	90
β, (°)	111.634(14)
γ, (°)	90
V, Å ³	4832.5(10)
Z, ρ _{calcd.} (g/cm ³)	4, 1.457
μ (mm ⁻¹)	1.137
<i>F</i> (000)	2192
θ _{min} /θ _{max} (°)	2.965/30.000
Reflections collected/unique	27463/14065
R _{int}	0.0447
R ₁ [I > 2σ(I)]	5.16, 9.99
wR ₂ (all data)	11.92, 11.81
G.O.F.	0.935
Largest difference peak/hole (e·Å ⁻³)	0.579/-0.514
N _o CCDC	1816652

Selected bond distances (Å) and angles (°) for [Ca{Cu(HL¹)₂}₂](NCS)₂ (4).

Cu1—O1	1.9384(18)	Cu2—N4	1.972(2)	O1—Ca1	2.3771(19)
Cu1—N1	1.968(2)	Cu2—O7	1.9308(18)	Ca1—O4	2.3667(18)
Cu1—N2	1.967(2)	Cu2—O10	1.9219(18)	Ca1—O5	2.593(2)
Cu1—O4	1.9062(18)	Ca1—O11	2.615(2)	Cu2—N3	1.977(2)
O2—Ca1	2.606(2)	Ca1—O8	2.515(2)	Ca1—O10	2.3413(19)
Ca1—O7	2.3202(18)				
O1—Cu1—N2	153.47(9)	N4—Cu2—N3	103.94(9)	O8—Ca1—O5	80.46(7)
N2—Cu1—N1	103.48(9)	O7—Cu2—N3	90.59(9)	O7—Cu2—N4	155.50(9)
O4—Cu1—O1	81.11(7)	O1—Cu1—N1	90.67(9)	O10—Cu2—N3	157.43(9)
O4—Cu1—N1	157.46(9)	O7—Ca1—O11	123.36(7)	O10—Cu2—N4	91.92(9)
O4—Cu1—N2	92.69(8)	O10—Ca1—O2	94.67(7)	O10—Cu2—O7	80.65(7)
O1—Ca1—O2	62.30(6)	O10—Ca1—O4	123.77(7)	O2—Ca1—O11	87.99(7)
O1—Ca1—O5	123.51(7)	O10—Ca1—O5	78.89(7)	O4—Ca1—O1	63.60(6)
O1—Ca1—O8	87.85(7)	O10—Ca1—O8	119.98(7)	O7—Ca1—O2	78.85(7)
O7—Ca1—O5	98.39(7)	O7—Ca1—O8	63.66(6)	O7—Ca1—O4	152.82(7)
O4—Ca1—O2	122.39(7)	O8—Ca1—O11	168.15(7)	O10—Ca1—O11	61.88(6)
O4—Ca1—O5	62.14(6)	O7—Ca1—O10	64.66(6)	O5—Ca1—O11	88.74(7)
O4—Ca1—O8	93.00(7)	O7—Ca1—O1	124.90(7)	O10—Ca1—O1	148.44(8)
O8—Ca1—O2	103.23(7)	O4—Ca1—O11	77.53(7)	O1—Ca1—O11	94.15(7)
O5—Ca1—O2	173.56(7)				

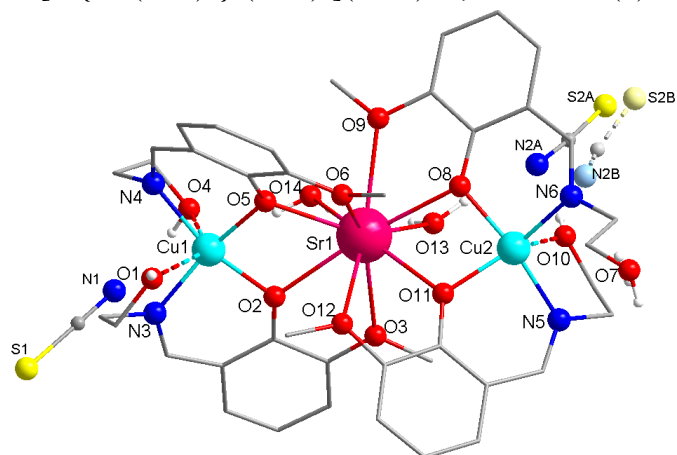


Formula	C ₄₁ H ₅₂ Cu ₂ I ₂ N ₄ O ₁₃ Sr
M (g·mol ⁻¹)	1277.36
T (K)	150.00(10)
Wavelength (Å)	0.71073
Crystal system	Orthorhombic
Space group	<i>P</i> 2 ₁ 2 ₁ 2 ₁
a, (Å)	9.65790(16)
b, (Å)	19.3437(4)
c, (Å)	25.6881(5)
α, (°)	90
β, (°)	90
γ, (°)	90
V, Å ³	4799.05(15)
Z, ρ _{calcd.} (g/cm ³)	4, 1.768
μ (mm ⁻¹)	3.336
<i>F</i> (000)	2528
θ _{min} /θ _{max} (°)	2.9570/28.6650
Reflections collected/unique	82557/11708
R _{int}	0.0632
R ₁ [I > 2σ(I)]	3.08, 5.56
wR ₂ (all data)	4.23, 5.95
G.O.F.	1.056
Largest difference peak/hole (e·Å ⁻³)	1.718/-1.127
No. CCDC	1898945

Selected bond distances (Å) and angles (°) for [Sr{Cu(HL¹)₂}₂(CH₃OH)₂]₂I₂ (**5**).

Sr1—O1	2.716(4)	Cu2—O8	1.920(3)	Cu1—O2	1.921(3)
Sr1—O2	2.557(3)	Cu2—O11	1.920(3)	Cu1—O5	1.924(3)
Sr1—O4	2.680(3)	Cu2—N3	1.949(4)	Cu1—N1	1.959(4)
Sr1—O5	2.475(3)	Cu2—N4	1.972(4)	Cu1—N2	1.973(4)
Sr1—O7	2.752(4)	Sr1—O10	2.749(3)	Sr1—O13	2.599(4)
Sr1—O8	2.570(3)	Sr1—O11	2.495(3)		
O2—Sr1—O10	78.7(1)	O4—Sr1—O1	152.17(11)	O5—Sr1—O8	126.11(11)
O2—Sr1—O13	81.68(13)	O4—Sr1—O7	71.99(11)	O5—Sr1—O10	86.04(10)
O8—Sr1—O1	113.11(11)	O4—Sr1—O10	67.28(10)	O5—Sr1—O11	141.27(11)
O8—Sr1—O4	78.70(11)	O5—Sr1—O1	119.8(1)	O11—Sr1—O1	76.10(11)
O1—Sr1—O10	84.91(11)	O5—Sr1—O2	60.88(10)	O11—Sr1—O2	120.29(10)
O8—Sr1—O10	108.67(10)	O5—Sr1—O4	59.35(10)	O11—Sr1—O4	89.84(10)
O8—Sr1—O13	88.78(12)	O1—Sr1—O7	135.84(12)	O11—Sr1—O7	118.36(10)
O10—Sr1—O7	139.08(11)	O8—Sr1—O7	58.3(1)	O11—Sr1—O8	60.54(10)
O13—Sr1—O1	68.98(14)	O2—Sr1—O1	58.97(10)	O11—Sr1—O10	58.89(10)
O13—Sr1—O4	138.31(13)	O2—Sr1—O4	111.63(11)	O11—Sr1—O13	118.21(13)
O13—Sr1—O7	67.67(14)	O2—Sr1—O7	121.19(11)	N1—Cu1—N2	100.51(16)
O5—Sr1—O7	76.50(11)	O2—Sr1—O8	169.36(11)	O8—Cu2—O11	83.41(13)
O2—Cu1—O5	83.09(13)	O8—Cu2—N4	161.01(15)	O11—Cu2—N3	160.17(15)
O2—Cu1—N1	91.85(15)	O8—Cu2—N3	93.33(15)	O11—Cu2—N4	89.87(14)
O2—Cu1—N2	160.33(15)	O5—Cu1—N2	89.58(14)	O13—Sr1—O10	152.93(13)
O5—Cu1—N1	161.28(16)	N3—Cu2—N4	98.77(15)		

[Sr{Cu(HL¹)₂}(H₂O)₂](SCN)₂·0,65CH₃OH (6)

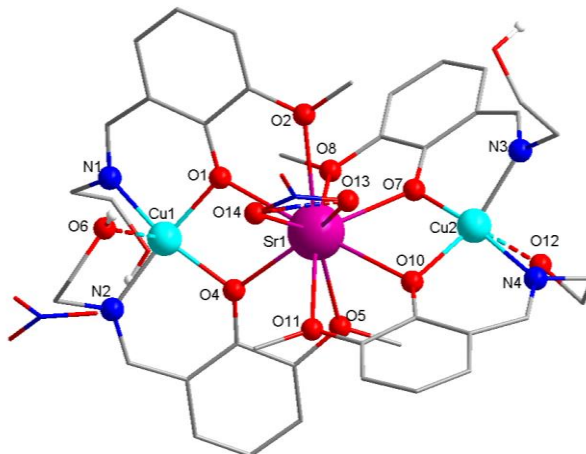


Formula	C _{42.65} H _{54.96} Cu ₂ N ₆ O _{14.65} S ₂ Sr
M (g·mol ⁻¹)	1164.90
T (K)	150.00(10)
Wavelength (Å)	0.71073
Crystal system	Triclinic
Space group	<i>P</i> -1
a, (Å)	11.3239(4)
b, (Å)	16.0333(3)
c, (Å)	16.0475(6)
α, (°)	104.815(3)
β, (°)	109.866(3)
γ, (°)	99.799(2)
V, Å ³	2540.97(15)
Z, ρ _{calcd.} (g/cm ³)	2, 1.523
μ (mm ⁻¹)	2.026
F (000)	1196
θ _{min} /θ _{max} (°)	2.7070/28.7010
Reflections collected/unique	23519/10776
R _{int}	0.0275
R ₁ [I > 2σ(I)]	5.60, 9.69
wR ₂ (all data)	4.25, 10.47
G.O.F.	1.047
Largest difference peak/hole (e ⁻ ·Å ⁻³)	1.474/-0.908
N _o CCDC	1966968

Selected bond distances (Å) and angles (°) for [Sr{Cu(HL¹)₂}₂(H₂O)₂](SCN)₂·0.65CH₃OH (6).

Sr1—O2	2.582(2)	Cu2—O8	1.908(2)	Cu1—O2	1.919(2)
Sr1—O3	2.721(2)	Cu2—O10	2.433(3)	Cu1—O5	1.929(2)
Sr1—O5	2.509(2)	Cu2—O11	1.932(2)	Cu1—N3	1.957(3)
Sr1—O6	2.816(2)	Cu2—N5	1.963(3)	Cu1—N4	1.984(3)
Sr1—O8	2.596(2)	Cu2—N6	1.980(2)	Sr1—O12	2.909(2)
Sr1—O9	2.712(2)	Sr1—O14	2.745(3)	Sr1—O13	2.640(3)
Sr1—O11	2.537(2)				
O2—Sr1—O3	58.73(7)	O8—Cu2—O10	95.97(10)	O3—Sr1—O6	141.25(7)
O2—Sr1—O6	105.63(7)	O8—Cu2—O11	82.27(9)	O3—Sr1—O12	77.54(7)
O2—Sr1—O8	172.32(7)	O8—Cu2—N5	162.42(10)	O3—Sr1—O14	83.54(9)
O2—Sr1—O9	128.88(7)	O8—Cu2—N6	92.62(10)	O5—Sr1—O2	61.18(7)
O2—Sr1—O12	69.62(7)	O11—Cu2—O10	120.57(10)	O5—Sr1—O3	119.91(7)
O2—Sr1—O13	109.79(9)	O11—Cu2—N5	89.94(10)	O5—Sr1—O6	57.98(7)
O2—Sr1—O14	67.17(9)	O11—Cu2—N6	150.18(10)	O5—Sr1—O8	123.05(7)
O5—Sr1—O12	82.05(7)	N5—Cu2—O10	74.43(10)	O5—Sr1—O9	79.04(7)
O5—Sr1—O13	137.65(10)	N5—Cu2—N6	101.76(11)	O5—Sr1—O11	132.99(7)
O5—Sr1—O14	74.22(9)	N6—Cu2—O10	89.12(10)	O9—Sr1—O3	144.10(7)
O8—Sr1—O3	116.60(7)	O13—Sr1—O14	65.03(11)	O9—Sr1—O6	74.34(7)
O8—Sr1—O6	74.08(7)	O14—Sr1—O6	125.53(9)	O9—Sr1—O12	137.89(7)
O8—Sr1—O9	58.68(7)	O14—Sr1—O12	136.62(8)	O9—Sr1—O14	72.28(9)
O8—Sr1—O12	103.90(7)	O2—Cu1—O5	84.67(9)	O11—Sr1—O2	113.37(7)
O8—Sr1—O13	71.78(9)	O2—Cu1—N3	91.39(10)	O11—Sr1—O3	73.88(7)
O8—Sr1—O14	119.47(9)	O2—Cu1—N4	161.21(10)	O11—Sr1—O6	83.04(7)
O6—Sr1—O12	63.73(7)	O11—Sr1—O14	151.02(9)	O11—Sr1—O8	58.96(7)
O13—Sr1—O9	78.15(10)	O11—Sr1—O12	55.79(6)	O11—Sr1—O9	117.23(7)
O13—Sr1—O6	143.89(9)	O11—Sr1—O13	89.27(10)	O5—Cu1—N3	162.31(10)
O13—Sr1—O3	67.56(10)	O13—Sr1—O12	136.59(10)	N3—Cu1—N4	100.27(11)
O5—Cu1—N4	88.34(11)				

[Sr{Cu(HL¹)₂}₂NO₃]NO₃·CH₃OH (7)

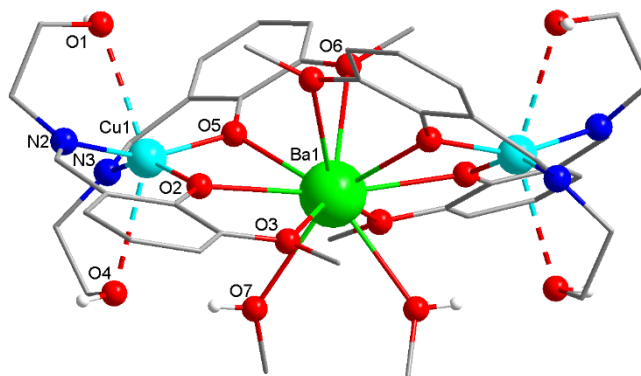


Formula	C ₄₁ H ₅₂ Cu ₂ N ₆ O ₁₉ Sr
M (g·mol ⁻¹)	1147.58
T (K)	298
Wavelength (Å)	0.71073
Crystal system	Orthorhombic
Space group	Pbca
a, (Å)	14.3048(5)
b, (Å)	21.5029(7)
c, (Å)	31.3751(10)
α, (°)	90
β, (°)	90
γ, (°)	90
V, Å ³	9650.8(6)
Z, ρ _{calcd.} (g/cm ³)	8, 1.580
μ (mm ⁻¹)	2.056
F (000)	4704
θ _{min} /θ _{max} (°)	2.962/31.105
Reflections collected/unique	57702/14740
R _{int}	0.0494
R ₁ [I > 2σ(I)]	4.78, 9.53
wR ₂ (all data)	9.50, 11.17
G.O.F.	1.008
Largest difference peak/hole (e·Å ⁻³)	0.500/-0.310
N _o CCDC	1816651

Selected bond distances (Å) and angles (°) for [Sr{Cu(HL¹)₂}₂NO₃]₂NO₃·CH₃OH (7).

Sr1—O1	2.5506(17)	Sr1—O11	2.732(2)	Cu1—O1	1.9210(17)
Sr1—O2	2.6796(19)	Sr1—O13	2.908(3)	Cu1—O4	1.9392(18)
Sr1—O4	2.5111(18)	Sr1—O14	2.686(2)	Cu1—O6	2.429(2)
Sr1—O5	2.763(2)	Cu2—N4	1.946(2)	Cu1—N2	1.971(2)
Sr1—O7	2.5114(17)	Cu2—N3	1.973(2)	Cu2—O7	1.9153(17)
Sr1—O8	2.903(2)	Cu1—N1	1.977(2)	Cu2—O10	1.9357(18)
Sr1—O10	2.5674(18)				
O1—Sr1—O2	59.77(6)	O1—Cu1—O6	93.39(8)	O2—Sr1—O13	67.96(8)
O1—Sr1—O5	111.85(6)	O1—Cu1—N1	91.19(9)	O2—Sr1—O14	69.48(8)
O1—Sr1—O8	69.22(6)	O4—Cu1—O6	117.74(9)	O4—Sr1—O1	61.14(5)
O1—Sr1—O10	175.36(6)	O4—Cu1—N1	157.42(9)	O4—Sr1—O2	120.90(6)
O1—Sr1—O11	120.38(6)	O4—Cu1—N2	89.96(9)	O4—Sr1—O5	58.22(6)
O1—Sr1—O13	109.42(7)	O7—Cu2—N4	163.43(9)	O4—Sr1—O7	134.25(7)
O1—Sr1—O14	73.61(7)	O2—Sr1—O11	132.41(7)	O4—Sr1—O8	86.50(6)
O2—Sr1—O5	151.56(7)	O14—Sr1—O8	136.52(7)	O4—Sr1—O10	122.20(6)
O2—Sr1—O8	72.72(7)	O14—Sr1—O11	66.29(7)	O7—Sr1—O5	86.01(6)
O4—Sr1—O11	80.00(6)	O14—Sr1—O13	44.68(8)	O7—Sr1—O8	57.10(6)
O4—Sr1—O13	135.89(8)	N2—Cu1—O6	74.54(9)	O7—Sr1—O10	61.91(6)
O4—Sr1—O14	94.88(7)	N2—Cu1—N1	100.88(10)	O7—Sr1—O11	120.86(6)
O5—Sr1—O8	78.93(6)	O11—Sr1—O5	75.95(6)	O7—Sr1—O13	89.26(8)
O5—Sr1—O13	135.18(7)	O11—Sr1—O8	154.87(7)	O7—Sr1—O14	130.27(7)
N4—Cu2—N3	97.82(10)	O10—Sr1—O8	113.42(6)	O10—Sr1—O11	58.96(6)
O7—Sr1—O1	118.66(6)	O10—Cu2—N3	156.51(9)	O10—Cu2—N4	91.14(9)
O7—Sr1—O2	76.94(6)	O10—Sr1—O13	65.96(7)	O10—Sr1—O2	116.83(6)
O8—Sr1—O13	133.04(8)	O10—Sr1—O14	102.42(7)	O10—Sr1—O5	72.67(6)
O7—Cu2—O10	85.45(8)	O1—Cu1—O4	83.66(7)	N1—Cu1—O6	84.43(9)
O7—Cu2—N3	91.56(9)	O11—Sr1—O13	68.62(8)	O14—Sr1—O5	137.21(7)

[Ba{Cu(HL¹)₂}(CH₃OH)₂]₂I₂ (**8**).



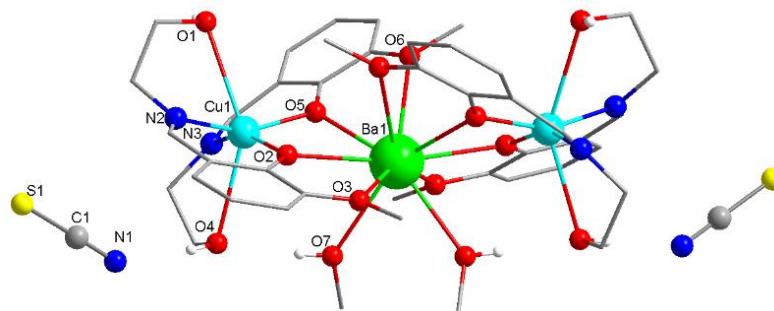
Formula	C ₄₂ H ₅₆ BaCu ₂ I ₂ N ₄ O ₁₄
M (g·mol ⁻¹)	1359.14
T (K)	150
Wavelength (Å)	1.54184
Crystal system	Monoclinic
Space group	C2/c
a, (Å)	30.8540(14)
b, (Å)	8.5135(2)
c, (Å)	24.6280(11)
α, (°)	90
β, (°)	129.439(7)
γ, (°)	90
V, Å ³	4996.1(5)
Z, ρ _{calcd.} (g/cm ³)	4, 1.807
μ (mm ⁻¹)	17.301
F (000)	2672
θ _{min} /θ _{max} (°)	3.668-73.679
Reflections collected/unique	17371/4961
R _{int}	0.0282
R ₁ [I > 2σ(I)]	3.19, 7.88
wR ₂ (all data)	3.36, 8.01
G.O.F.	1.081
Largest difference peak/hole (e·Å ⁻³)	1.160/-0.808
N _o CCDC	1898944

Selected bond distances (Å) and angles (°) for [Ba{Cu(HL¹)₂}₂(CH₃OH)₂]₂I₂ (**8**).

Ba1—O3 ⁱ	3.057(3)	Cu1—N1	1.974(3)	Ba1—O7 ⁱ	2.859(3)
Ba1—O3	3.057(3)	Ba1—O6 ⁱ	2.819(3)	Cu1—O2	1.915(3)
Ba1—O2	2.673(3)	Ba1—O7	2.859(4)	Cu1—O5	1.936(3)
Ba1—O2 ⁱ	2.673(3)	Ba1—O5 ⁱ	2.714(3)	Cu1—N2	1.964(3)
Ba1—O5	2.714(3)	Ba1—O6	2.819(3)		
O3—Ba1—O3 ⁱ	81.65(13)	O5 ⁱ —Ba1—O3 ⁱ	104.04(9)	O2 ⁱ —Ba1—O3 ⁱ	53.18(8)
O2—Ba1—O5	57.85(8)	O6 ⁱ —Ba1—O3 ⁱ	67.7(1)	O2 ⁱ —Ba1—O3	87.30(9)
O2 ⁱ —Ba1—O5	116.63(9)	O6—Ba1—O3 ⁱ	148.2(1)	O2—Ba1—O3	53.18(8)
O2—Ba1—O6	81.22(9)	O2 ⁱ —Ba1—O6 ⁱ	81.22(9)	O2—Ba1—O3 ⁱ	87.30(9)
O2—Ba1—O6 ⁱ	114.73(9)	O7 ⁱ —Ba1—O3	130.72(10)	O2—Ba1—O2 ⁱ	129.42(14)
O2 ⁱ —Ba1—O6	114.73(9)	O7 ⁱ —Ba1—O3 ⁱ	121.30(11)	O2 ⁱ —Ba1—O5 ⁱ	57.85(8)
O6—Ba1—O3	67.7(1)	O7—Ba1—O3 ⁱ	130.73(10)	O2—Ba1—O5 ⁱ	116.62(9)
O7—Ba1—O3	121.3(1)	O2 ⁱ —Ba1—O7 ⁱ	77.79(10)	O5—Ba1—O6	127.41(9)
O2 ⁱ —Ba1—O7	150.81(11)	O7 ⁱ —Ba1—O7	78.50(15)	O5 ⁱ —Ba1—O6	56.88(9)
O2—Ba1—O7 ⁱ	150.81(11)	O5—Cu1—N2	92.04(13)	O5 ⁱ —Ba1—O6 ⁱ	127.41(9)
O2—Ba1—O7	77.8(1)	O5—Cu1—N1	149.25(15)	O5 ⁱ —Ba1—O7 ⁱ	65.33(10)
O5 ⁱ —Ba1—O7	124.72(10)	N2—Cu1—N1	103.42(14)	O5—Ba1—O7	65.33(10)
O5 ⁱ —Ba1—O3	66.96(9)	O6 ⁱ —Ba1—O7	76.57(11)	O5—Ba1—O7 ⁱ	124.72(10)
O5—Ba1—O3	104.04(9)	O2—Cu1—O5	85.17(12)	O6 ⁱ —Ba1—O3	148.2(1)
O5—Ba1—O3 ⁱ	66.97(9)	O2—Cu1—N2	154.85(15)	O6—Ba1—O6 ⁱ	143.78(16)
O5 ⁱ —Ba1—O5	168.72(14)	O2—Cu1—N1	91.15(13)	O6—Ba1—O7	75.57(11)
O5—Ba1—O6 ⁱ	56.88(9)	O6 ⁱ —Ba1—O7 ⁱ	75.57(11)	O6—Ba1—O7 ⁱ	76.57(11)

Symmetry code: (i) 1-x, y, 1.5-z.

[Ba{Cu(HL¹)₂}₂(CH₃OH)₂](SCN)₂ (9)



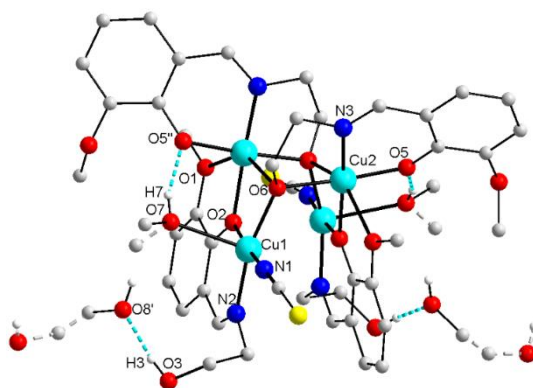
Formula	C ₄₄ H ₅₆ BaCu ₂ N ₆ O ₁₄ S ₂
M (g·mol ⁻¹)	1221.48
T (K)	149.99(10)
Wavelength (Å)	0.71073
Crystal system	Monoclinic
Space group	C2/c
a, (Å)	30.424(3)
b, (Å)	8.6589(5)
c, (Å)	25.061(3)
α, (°)	90
β, (°)	128.709(19)
γ, (°)	90
V, Å ³	5151.8(16)
Z, ρ _{calcd.} (g/cm ³)	4, 1.575
μ (mm ⁻¹)	1.723
F (000)	2480
θ _{min} /θ _{max} (°)	3.9930-28.7350
Reflections collected/unique	12033/5461
R _{int}	0.0462
R ₁ [I > 2σ(I)]	3.33, 6.70
wR ₂ (all data)	4.78, 7.27
G.O.F.	1.006
Largest difference peak/hole (e·Å ⁻³)	0.569/-0.885
No. CCDC	1864803

Selected bond distances (Å) and angles (°) for [Ba{Cu(HL¹)₂}₂(CH₃OH)₂](SCN)₂ (**9**).

Ba1—O2	2.7343(18)	Ba1—O6	3.057(2)	Ba1—O6 ⁱ	3.057(2)
Ba1—O2 ⁱ	2.7344(18)	Cu1—N2	1.951(2)	Ba1—O7	2.796(2)
Ba1—O3	2.835(2)	Cu1—N3	1.972(2)	Ba1—O7 ⁱ	2.796(2)
Ba1—O5 ⁱ	2.6687(18)	Cu1—O2	1.9173(19)	Ba1—O3 ⁱ	2.835(2)
Ba1—O5	2.6687(18)	Cu1—O5	1.9221(18)		
O2—Ba1—O2 ⁱ	168.76(9)	O5 ⁱ —Ba1—O6	87.16(6)	O2—Cu1—N3	153.6(1)
O2 ⁱ —Ba1—O6 ⁱ	103.45(5)	O5—Cu1—N2	154.63(10)	N2—Cu1—N3	101.43(9)
O2—Ba1—O3 ⁱ	127.62(5)	O2—Ba1—O3	55.94(6)	O5—Cu1—N3	90.08(9)
O2 ⁱ —Ba1—O3 ⁱ	55.94(5)	O2 ⁱ —Ba1—O7	122.57(6)	O2—Cu1—O5	85.97(8)
O2 ⁱ —Ba1—O3	127.63(5)	O2—Ba1—O7 ⁱ	122.57(6)	O2—Cu1—N2	92.95(9)
O2—Ba1—O6	103.45(5)	O3 ⁱ —Ba1—O3	150.17(10)	O5—Ba1—O7	79.20(7)
O2 ⁱ —Ba1—O6	67.45(6)	O3—Ba1—O6 ⁱ	65.79(6)	O2—Ba1—O7	67.55(6)
O2—Ba1—O6 ⁱ	67.44(5)	O3 ⁱ —Ba1—O6	65.79(6)	O6—Ba1—O6 ⁱ	79.08(8)
O3—Ba1—O6	143.81(6)	O5—Ba1—O6	53.52(5)	O5 ⁱ —Ba1—O6 ⁱ	53.52(5)
O3 ⁱ —Ba1—O6 ⁱ	143.81(6)	O5—Ba1—O7 ⁱ	148.74(7)	O5 ⁱ —Ba1—O2	116.68(6)
O5 ⁱ —Ba1—O7 ⁱ	79.20(7)	O5—Ba1—O2 ⁱ	116.68(6)	O5 ⁱ —Ba1—O3	79.13(6)
O5—Ba1—O5 ⁱ	130.63(9)	O7 ⁱ —Ba1—O7	73.91(10)	O5—Ba1—O3 ⁱ	79.13(6)
O7 ⁱ —Ba1—O3 ⁱ	79.46(7)	O7—Ba1—O3 ⁱ	76.79(7)	O5—Ba1—O3	113.80(6)
O5—Ba1—O6 ⁱ	87.16(6)	O7 ⁱ —Ba1—O3	76.79(7)	O5 ⁱ —Ba1—O3 ⁱ	113.81(6)
O7 ⁱ —Ba1—O6 ⁱ	123.06(7)	O5 ⁱ —Ba1—O7	148.74(7)	O5—Ba1—O2	57.94(6)
O7—Ba1—O6	123.06(7)	O7—Ba1—O6 ⁱ	133.39(6)	O5 ⁱ —Ba1—O2 ⁱ	57.95(6)
O2 ⁱ —Ba1—O7 ⁱ	67.55(6)	O7 ⁱ —Ba1—O6	133.39(6)		

Symmetry code: (i) 1-x, y, 1.5-z.

[Cu₄(HL¹)₂(L¹)₂(NCS)₂(CH₃OH)₂·2CH₃OH (**10**)



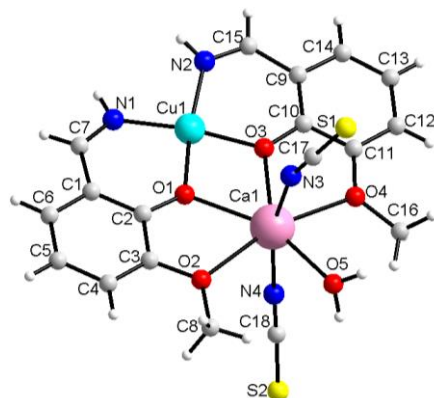
Formula	C ₂₃ H _{30.97} Cu ₂ N ₃ O ₈ S
M (g·mol ⁻¹)	636.61
T (K)	150.00(10)
Wavelength (Å)	0.71073
Crystal system	Monoclinic
Space group	C2/c
a, (Å)	24.1441(7)
b, (Å)	18.5534(5)
c, (Å)	11.7949(4)
α, (°)	90
β, (°)	91.192(2)
γ, (°)	90
V, Å ³	5282.4(3)
Z, ρ _{calcd.} (g/cm ³)	8, 1.601
μ (mm ⁻¹)	1.741
F (000)	2624
θ _{min} /θ _{max} (°)	2.195- 28.864
Reflections collected/unique	10909/10909
R _{int}	-
R ₁ [I > 2σ(I)]	4.64, 11.64
wR ₂ (all data)	5.39, 11.94
G.O.F.	1.090
Largest difference peak/hole (e·Å ⁻³)	0.771/-0.845
N _o CCDC	1966967

Selected bond distances (Å) and angles (°) for [Cu₄(HL¹)₂(L¹)₂(NCS)₂(CH₃OH)₂·2CH₃OH (**10**).

Cu1—O2	1.945(3)	Cu2—O6	1.989(3)	Cu2—O1 ⁱ	2.372(3)
Cu1—O6	1.957(3)	Cu2—O6 ⁱ	2.352(3)	Cu2—O2 ⁱ	2.014(3)
Cu1—O7	2.427(4)	Cu2—N3	1.940(3)	Cu2—O5	1.930(3)
Cu1—N1	1.940(4)	Cu1—N2	1.983(4)		
O6—Cu1—N2	162.60(12)	N1—Cu1—O2	174.11(14)	N2—Cu1—O7	102.15(16)
O2 ⁱ —Cu2—O1 ⁱ	72.79(10)	N1—Cu1—O6	91.89(14)	O6 ⁱ —Cu2—O1 ⁱ	144.66(10)
O2 ⁱ —Cu2—O6 ⁱ	71.94(10)	N1—Cu1—O7	95.11(15)	O6—Cu2—O1 ⁱ	95.21(11)
O5—Cu2—O1 ⁱ	87.13(12)	N1—Cu1—N2	94.20(15)	O6—Cu2—O2 ⁱ	90.85(11)
O5—Cu2—O2 ⁱ	92.90(11)	O2—Cu1—O6	82.75(11)	O6—Cu2—O6 ⁱ	83.19(9)
O5—Cu2—O6 ⁱ	96.76(11)	O2—Cu1—O7	82.84(12)	N3—Cu2—O1 ⁱ	102.23(12)
O5—Cu2—O6	176.04(12)	O2—Cu1—N2	91.63(13)	N3—Cu2—O2 ⁱ	172.72(11)
O6—Cu1—O7	93.50(14)	O5—Cu2—N3	92.14(13)	N3—Cu2—O6	84.25(13)
N3—Cu2—O6 ⁱ	112.66(12)				

Symmetry code: (i) 1-x, y, 0.5-z.

[Cu(L³)₂Ca(NCS)₂(H₂O)] (12)

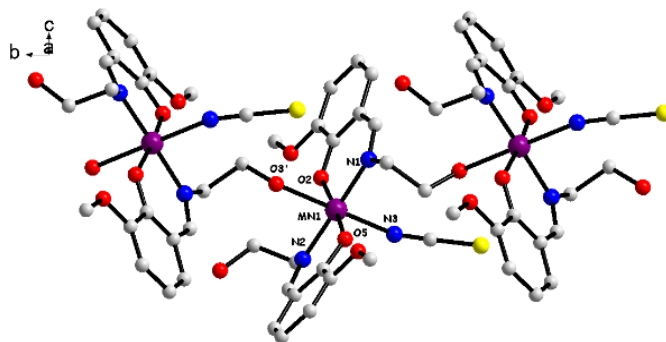


Formula	C ₁₈ H ₁₈ CaCuN ₄ O ₅ S ₂
M (g·mol ⁻¹)	538.10
T (K)	298
Wavelength (Å)	0.71073
Crystal system	Monoclinic
Space group	<i>P</i> 2 ₁ / <i>n</i>
a, (Å)	8.5623(3)
b, (Å)	10.5377(3)
c, (Å)	24.4439(7)
α, (°)	90
β, (°)	90.768(3)
γ, (°)	90
V, Å ³	2205.30(13)
Z, ρ _{calcd.} (g/cm ³)	4, 1.621
μ (mm ⁻¹)	1.450
<i>F</i> (000)	1100
θ _{min} /θ _{max} (°)	3.066–30.395
Reflections collected/unique	15524/5827
R _{int}	0.0366
R ₁ [I > 2σ(I)]	4.39, 8.62
wR ₂ (all data)	8.33, 10.00
G.O.F.	1.018
Largest difference peak/hole (e ⁻ ·Å ⁻³)	0.532/-0.449
N _o CCDC	1984001

Selected bond distances (Å) and angles (°) for [Cu(L³)₂Ca(NCS)₂(H₂O)] (12).

Cu1—O1	1.9183(17)	Ca1—O2	2.509(2)	Ca1—O5	2.350(2)
Cu1—O3	1.9248(17)	Ca1—O4	2.521(2)	Ca1—O1	2.3552(17)
Cu1—N2	1.929(2)	Cu1—Ca1	3.4269(6)	Ca1—N4	2.422(3)
Cu1—N1	1.941(2)	Ca1—O3	2.3393(17)	Ca1—N3	2.441(3)
O1—Cu1—O3	82.10(7)	O3—Ca1—O4	64.16(6)	O3—Ca1—O5	144.15(8)
O1—Cu1—N2	171.82(8)	O5—Ca1—O4	82.24(7)	O3—Ca1—O1	65.04(6)
O3—Cu1—N2	91.50(9)	O1—Ca1—O4	128.40(6)	O5—Ca1—O1	149.31(8)
O1—Cu1—N1	91.46(9)	O2—Ca1—O4	165.47(6)	O3—Ca1—N4	101.41(8)
O3—Cu1—N1	172.35(9)	O3—Ca1—O2	128.92(6)	O5—Ca1—N4	84.40(8)
N2—Cu1—N1	95.27(10)	O5—Ca1—O2	86.08(7)	O1—Ca1—N4	100.55(8)
O3—Ca1—N3	91.05(8)	N4—Ca1—O4	81.11(8)	O1—Ca1—O2	63.91(6)
O5—Ca1—N3	79.27(8)	N3—Ca1—O4	95.05(8)	N4—Ca1—O2	89.18(8)
O1—Ca1—N3	94.33(8)	N4—Ca1—N3	163.60(9)	N3—Ca1—O2	91.23(8)

[Mn(HL¹)₂(NCS)] (15)



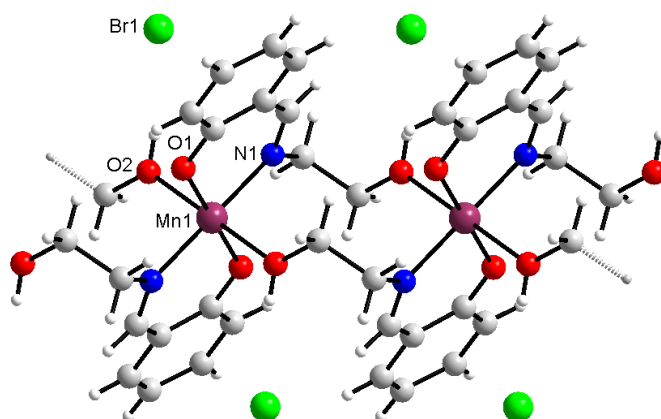
Formula	C ₂₁ H ₂₄ N ₃ O ₆ SMn
M (g·mol ⁻¹)	501.43
T (K)	295.65(10)
Wavelength (Å)	1.54184
Crystal system	Monoclinic
Space group	<i>P</i> 2 ₁ / <i>n</i>
a, (Å)	10.8561(6)
b, (Å)	11.6732(5)
c, (Å)	17.5981(9)
α, (°)	90
β, (°)	96.457(5)
γ, (°)	90
V, Å ³	2215.98(19)
Z, ρ _{calcd.} (g/cm ³)	4, 1.503
μ (mm ⁻¹)	6.104
<i>F</i> (000)	1040
θ _{min} /θ _{max} (°)	4.4640/73.1450
Reflections collected/unique	7292/4237
R _{int}	0.0239
R ₁ [<i>I</i> > 2σ(<i>I</i>)]	0.0333/0.0824
wR ₂ (all data)	0.0401/0.0871
G.O.F.	1.035
Largest difference peak/hole (e ⁻ ·Å ⁻³)	0.259/-0.330
No CCDC	1891125

Selected bond distances (Å) and angles (°) for [Mn(HL¹)₂(NCS)] (15).

Mn1—O5	1.8437(15)	Mn1—N1	2.0528(17)	Mn1—N3	2.2305(19)
Mn1—O2	1.8643(15)	O3—Mn1 ⁱⁱ	2.3396(15)	Mn1—O3 ⁱ	2.3396(15)
Mn1—N2	2.0309(17)				
N1—Mn1—O3 ⁱ	88.14(6)	O5—Mn1—O2	173.02(7)	N2—Mn1—N1	178.38(7)
N3—Mn1—O3 ⁱ	178.42(7)	O5—Mn1—N2	90.01(7)	O5—Mn1—N3	93.88(8)
O5—Mn1—O3 ⁱ	84.77(7)	O2—Mn1—N2	89.54(7)	O2—Mn1—N3	93.09(8)
O2—Mn1—O3 ⁱ	88.26(7)	O5—Mn1—N1	89.22(7)	N2—Mn1—N3	90.46(7)
O2—Mn1—N1	91.05(7)	N1—Mn1—N3	91.01(7)	N2—Mn1—O3 ⁱ	90.37(6)

Symmetry code: (i) 1.5-x, 0.5+y, 1.5-z; (ii) 1.5-x, -0.5+y, 1.5-z.

{[Mn(HL⁴)₂]Br}_n (16)



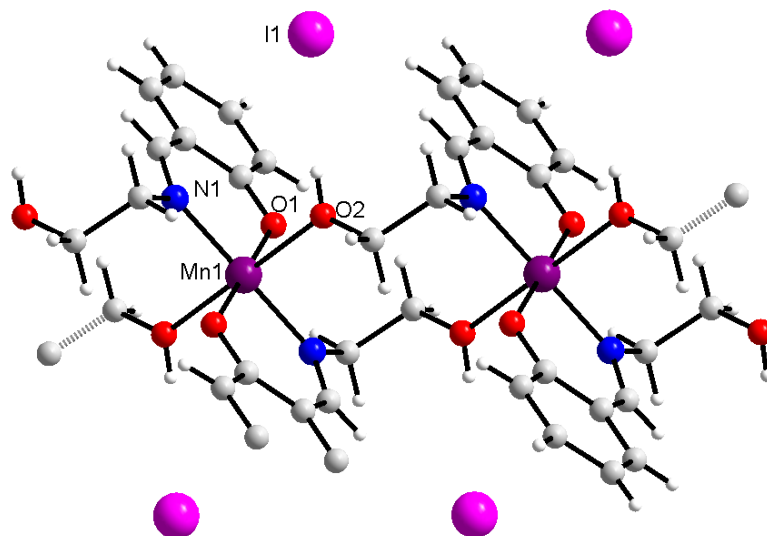
Formula	C ₁₈ H ₂₀ N ₂ O ₄ BrMn
M (g·mol ⁻¹)	463.20
T (K)	150.00(10)
Wavelength (Å)	1.54184
Crystal system	Monoclinic
Space group	C2/c
a, (Å)	18.5786(9)
b, (Å)	5.7196(3)
c, (Å)	18.1494(10)
α, (°)	90
β, (°)	105.278(5)
γ, (°)	90
V, Å ³	1860.44(17)
Z, ρ _{calcd.} (g/cm ³)	4, 1.654
μ (mm ⁻¹)	8.513
F (000)	936
θ _{min} /θ _{max} (°)	4.935/72.279
Reflections collected/unique	3207/1766
R _{int}	0.0242
R ₁ [I > 2σ(I)]	0.0256/0.0641
wR ₂ (all data)	0.0303/ 0.0672
G.O.F.	1.043
Largest difference peak/hole (e ⁻ ·Å ⁻³)	0.346/-0.244
N _o CCDC	1842146

Selected bond distances (Å) and angles (°) for {[Mn(HL⁴)₂]Br}_n (16).

Mn1—O1 ⁱ	1.8727(14)	Mn1—N1	2.0285(16)	Mn1—O2 ⁱⁱ	2.2867(15)
Mn1—O1	1.8727(14)	O2—Mn1 ^{iv}	2.2867(15)	Mn1—O2 ⁱⁱⁱ	2.2867(15)
Mn1—N1 ⁱ	2.0284(16)				
O1 ⁱ —Mn1—O1	180	O1 ⁱ —Mn1—O2 ⁱⁱⁱ	91.02(6)	O1 ⁱ —Mn1—O2 ⁱⁱ	88.98(6)
O1 ⁱ —Mn1—N1 ⁱ	89.91(6)	O1—Mn1—O2 ⁱⁱⁱ	88.98(6)	O1—Mn1—O2 ⁱⁱ	91.02(6)
O1—Mn1—N1 ⁱ	90.09(6)	O2 ⁱⁱ —Mn1—O2 ⁱⁱⁱ	180.0(1)	N1 ⁱ —Mn1—O2 ⁱⁱ	86.97(6)
O1 ⁱ —Mn1—N1	90.09(6)	N1 ⁱ —Mn1—O2 ⁱⁱⁱ	93.03(6)	N1—Mn1—O2 ⁱⁱ	93.03(6)
O1—Mn1—N1	89.91(6)	N1—Mn1—O2 ⁱⁱⁱ	86.97(6)	N1 ⁱ —Mn1—N1	180

Symmetry code: (i) -x, -y, -z; (ii) -x, -1-y, -z; (iii) x, 1+y, z; (iv) x, -1+y, z.

{[Mn(HL⁴)₂]I}_n (**17**)



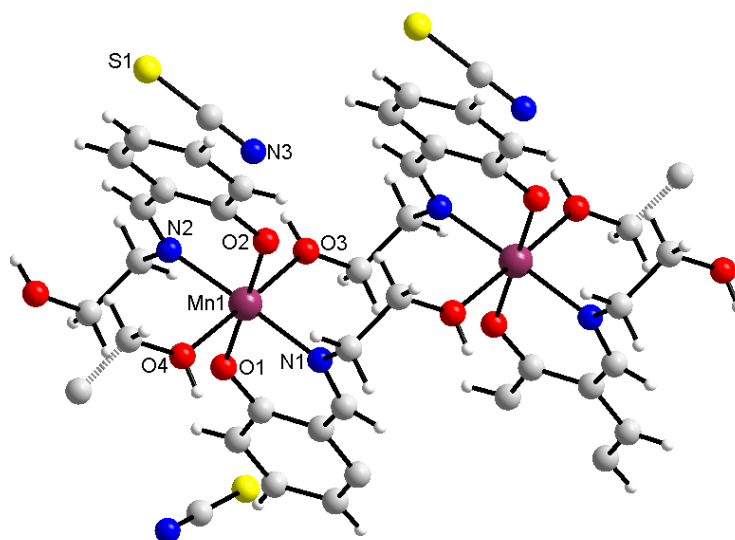
Formula	C ₁₈ H ₂₀ N ₂ O ₄ IMn
M (g·mol ⁻¹)	510.20
T (K)	150.01(10)
Wavelength (Å)	1.54184
Crystal system	Monoclinic
Space group	C2/c
a, (Å)	19.3631(5)
b, (Å)	5.7552(2)
c, (Å)	17.9767(5)
α, (°)	90
β, (°)	102.470(3)
γ, (°)	90
V, Å ³	1956.04(10)
Z, ρ _{calcd.} (g/cm ³)	4, 1.732
μ (mm ⁻¹)	18.096
F (000)	1008
θ _{min} /θ _{max} (°)	4.678/72.593
Reflections collected/unique	6408/1909
R _{int}	0.0265
R ₁ [I > 2σ(I)]	0.0192/0.0469
wR ₂ (all data)	0.0207/0.0477
G.O.F.	1.036
Largest difference peak/hole (e ⁻ ·Å ⁻³)	0.379/-0.422
N _o CCDC	1842148

Selected bond distances (Å) and angles (°) for {[Mn(HL⁴)₂]I}_n (**17**).

Mn1—O1 ⁱ	1.8706(12)	Mn1—O2	2.2877(14)	Mn1—N1	2.0256(15)
Mn1—O1	1.8706(12)	Mn1—N1 ⁱ	2.0256(15)	Mn1—O2 ⁱ	2.2877(14)
O1 ⁱ —Mn1—O1	180	N1—Mn1—O2 ⁱ	87.33(5)	O1 ⁱ —Mn1—N1 ⁱ	90.30(6)
N1 ⁱ —Mn1—N1	180	O2 ⁱ —Mn1—O2	180.00(4)	O1—Mn1—N1 ⁱ	89.70(6)
O1 ⁱ —Mn1—O2 ⁱ	90.87(6)	N1—Mn1—O2	92.67(5)	O1 ⁱ —Mn1—N1	89.70(6)
O1—Mn1—O2 ⁱ	89.13(6)	O1—Mn1—O2	90.87(6)	O1—Mn1—N1	90.30(6)
N1 ⁱ —Mn1—O2 ⁱ	92.67(5)	N1 ⁱ —Mn1—O2	87.33(5)	O1 ⁱ —Mn1—O2	89.13(6)

Symmetry code: (i) 1-x, 2-y, 1-z.

{[Mn(HL⁴)₂]NCS}_n (**18**)

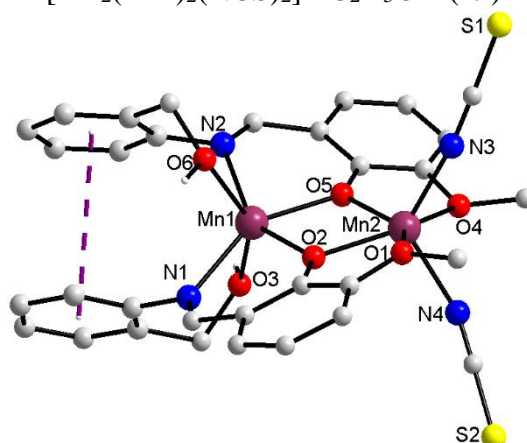


Formula	C ₁₉ H ₂₀ N ₃ O ₄ SMn
M (g·mol ⁻¹)	441.38
T (K)	150.00(10)
Wavelength (Å)	1.54184
Crystal system	Orthorhombic
Space group	<i>P</i> 2 ₁ 2 ₁ 2 ₁
a, (Å)	5.7247(3)
b, (Å)	16.7646(7)
c, (Å)	20.4425(8)
α, (°)	90
β, (°)	90
γ, (°)	90
V, Å ³	1961.91(15)
Z, ρ _{calcd.} (g/cm ³)	4, 1.494
μ (mm ⁻¹)	6.733
<i>F</i> (000)	912
θ _{min} /θ _{max} (°)	3.409/72.241
Reflections collected/unique	4995/3291
R _{int}	0.0364
R ₁ [<i>I</i> > 2σ(<i>I</i>)]	0.0373/0.0918
wR ₂ (all data)	0.0408/0.1003
G.O.F.	1.087
Largest difference peak/hole (e ⁻ ·Å ⁻³)	0.304/-0.394
N _o CCDC	1842149

Selected bond distances (Å) and angles (°) for {[Mn(HL⁴)₂]NCS}_n (**18**).

Mn1—O2	1.861(3)	Mn1—O4	2.282(3)	Mn1—N1	2.049(4)
Mn1—O1	1.876(3)	Mn1—N2	2.037(4)	Mn1—O3	2.242(3)
O1—Mn1—N2	89.90(15)	O1—Mn1—O3	92.09(15)	O2—Mn1—O1	179.06(16)
O2—Mn1—N1	90.84(14)	N2—Mn1—O3	88.44(13)	O2—Mn1—N2	89.77(14)
O1—Mn1—N1	89.46(14)	N1—Mn1—O3	93.57(13)	O1—Mn1—O4	88.11(14)
N2—Mn1—N1	177.91(15)	O2—Mn1—O4	91.01(14)	N2—Mn1—O4	90.47(13)
O2—Mn1—O3	88.79(14)	O3—Mn1—O4	178.89(12)	N1—Mn1—O4	87.52(14)

[Mn₂(HL²)₂(NCS)₂]₂·2C₂H₅OH (**19**)

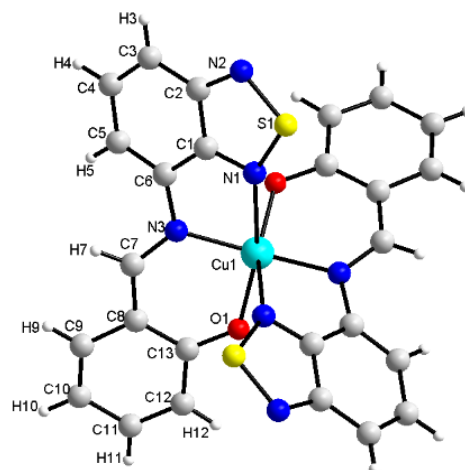


Formula	C ₃₆ H ₄₀ Mn ₂ N ₄ O ₈ S ₂
M (g·mol ⁻¹)	830.72
T (K)	140.0(4)
Wavelength (Å)	1.54184
Crystal system	Triclinic
Space group	<i>P</i> -1
a, (Å)	11.7392(4)
b, (Å)	12.5238(4)
c, (Å)	14.2096(5)
α, (°)	84.196(3)
β, (°)	87.881(3)
γ, (°)	67.315(3)
V, Å ³	1917.59(12)
Z, ρ _{calcd.} (g/cm ³)	2, 1.439
μ (mm ⁻¹)	6.834
<i>F</i> (000)	860
θ _{min} /θ _{max} (°)	3.126/ 72.687
Reflections collected/unique	11866/ 7275
R _{int}	0.0322
R ₁ [I > 2σ(I)]	3.83, 10.04
wR ₂ (all data)	4.06, 10.48
G.O.F.	1.048
Largest difference peak/hole (e·Å ⁻³)	1.267/ -0.500
N _o CCDC	-

Selected bond distances (Å) and angles (°) for [Mn₂(HL²)₂(NCS)₂]₂·2C₂H₅OH (**19**).

Mn1—O2	2.1098(14)	Mn2—O1	2.4227(15)	Mn2—N3	2.092(2)
Mn1—O5	2.1255(14)	Mn2—O4	2.4309(15)	Mn2—N4	2.0998(19)
Mn1—N2	2.2157(17)	Mn1—O6	2.2407(15)	Mn2—O5	2.1260(14)
Mn1—N1	2.2241(17)	Mn1—O3	2.2272(15)	Mn2—O2	2.1334(14)
O5—Mn1—N1	149.42(6)	O2—Mn1—O5	74.70(5)	N2—Mn1—O6	81.35(6)
N2—Mn1—N1	125.35(6)	O2—Mn1—N2	149.12(6)	N1—Mn1—O6	83.51(6)
O2—Mn1—O3	116.17(6)	O5—Mn1—N2	82.19(6)	O3—Mn1—O6	146.06(6)
O5—Mn1—O3	90.96(5)	O2—Mn1—N1	82.89(6)	N3—Mn2—N4	115.43(8)
N3—Mn2—O5	104.96(7)	N2—Mn1—O3	83.93(6)	N4—Mn2—O1	80.75(7)
N4—Mn2—O5	127.43(7)	N1—Mn1—O3	80.41(6)	O5—Mn2—O1	138.30(5)
N3—Mn2—O2	125.63(7)	O2—Mn1—O6	91.01(6)	O2—Mn2—O1	68.45(5)
N4—Mn2—O2	104.76(7)	O5—Mn1—O6	116.89(6)	N3—Mn2—O4	83.29(7)
O5—Mn2—O2	74.21(5)	O2—Mn2—O4	137.90(5)	N4—Mn2—O4	83.88(6)
N3—Mn2—O1	83.08(7)	O1—Mn2—O4	152.65(5)	O5—Mn2—O4	68.44(5)

Cu(L⁵)₂ (**21**)



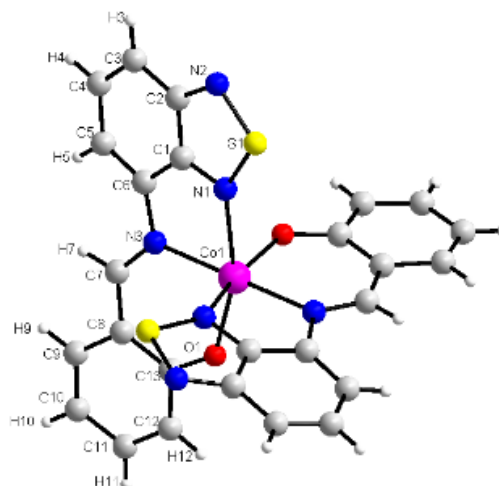
Formula	C ₂₆ H ₁₆ CuN ₆ O ₂ S ₂
M (g·mol ⁻¹)	572.11
T (K)	149.3(5)
Wavelength (Å)	1.54184
Crystal system	Orthorhombic
Space group	<i>Pbcn</i>
a, (Å)	20.8093(14)
b, (Å)	8.0705(5)
c, (Å)	13.9314(8)
α, (°)	90
β, (°)	90
γ, (°)	90
V, Å ³	2339.7(3)
Z, ρ _{calcd.} (g/cm ³)	4, 1.624
μ (mm ⁻¹)	3.317
F (000)	1164
θ _{min} /θ _{max} (°)	4.249 / 72.368
Reflections collected/unique	5562 / 2271
R _{int}	0.0935
R ₁ [I > 2σ(I)]	0.0800, 0.2076
wR ₂ (all data)	0.0930, 0.2220
G.O.F.	1.088
Largest difference peak/hole (e ⁻ ·Å ⁻³)	0.802 / -1.203
N ₂ CCDC	-

Selected bond distances (Å) and angles (°) for Cu(L⁵)₂ (**21**).

N3-Cu1	1.970(4)	Cu1-O1 ⁱ	1.930(3)
O1-Cu1	1.930(3)	Cu1-N3 ⁱ	1.970(4)
N3 ⁱ -Cu1-N3	162.7(2)	O1 ⁱ -Cu1-N3 ⁱ	94.03(15)
O1 ⁱ -Cu1-O1	134.4(2)	O1-Cu1-N3 ⁱ	92.66(15)
O1-Cu1-N3	94.03(15)	O1 ⁱ -Cu1-N3	92.66(15)

Symmetry code: (i) -x+1,y,-z+1/2.

Co(L⁵)₂ (**22**)



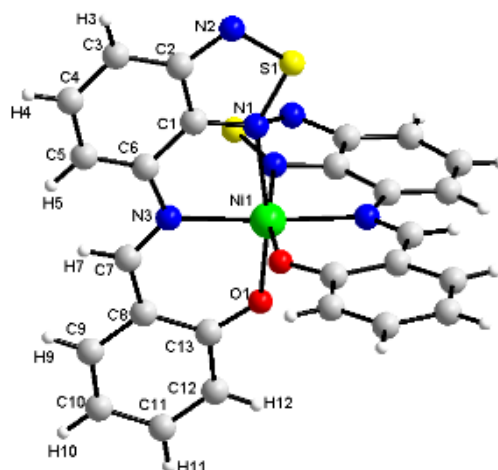
Formula	C ₂₆ H ₁₆ CoN ₆ O ₂ S ₂
M (g·mol ⁻¹)	567.50
T (K)	150.01(10)
Wavelength (Å)	1.54184
Crystal system	Orthorhombic
Space group	Pbcn
a, (Å)	18.6048(7)
b, (Å)	8.8596(3)
c, (Å)	13.8679(6)
α, (°)	90
β, (°)	90
γ, (°)	90
V, Å ³	2285.86(15)
Z, ρ _{calcd.} (g/cm ³)	4, 1.649
μ (mm ⁻¹)	7.933
F (000)	1156
θ _{min} /θ _{max} (°)	4.754 - 72.418
Reflections collected/unique	5617 / 2225
R _{int}	0.0286
R ₁ [I > 2σ(I)]	0.0335, 0.0788
wR ₂ (all data)	0.0428, 0.0838
G.O.F.	1.062
Largest difference peak/hole (e·Å ⁻³)	0.312 / -0.281
N _o CCDC	-

Selected bond distances (Å) and angles (°) for Co(L⁵)₂ (**22**).

Co1-O1 ⁱ	1.9979(16)	Co1-N1	2.2856(18)	Co1-N3	2.1138(18)
Co1-O1	1.9979(16)	Co1-N3 ⁱ	2.1138(18)	Co1-N1 ⁱ	2.2856(18)
O1-Co1-N1	161.68(7)	O1 ⁱ -Co1-O1	104.60(10)	O1-Co1-N3 ⁱ	88.85(7)
N3 ⁱ -Co1-N1	77.16(7)	N3 ⁱ -Co1-N1 ⁱ	102.21(7)	O1 ⁱ -Co1-N3	88.85(7)
N3-Co1-N1	102.21(7)	N3-Co1-N1 ⁱ	77.16(7)	O1-Co1-N3	91.66(7)
N1 ⁱ -Co1-N1	83.77(9)	O1 ⁱ -Co1-N1	87.78(7)	N3 ⁱ -Co1-N3	179.17(10)
O1-Co1-N1 ⁱ	87.78(7)	O1 ⁱ -Co1-N3 ⁱ	91.66(7)	O1 ⁱ -Co1-N1 ⁱ	161.68(7)

Symmetry code: (i) -x+1,y,-z+1/2.

Ni(L⁵)₂ (**23**)



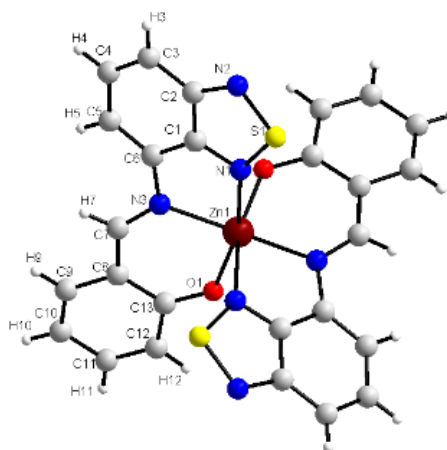
Formula	C ₂₆ H ₁₆ N ₆ NiO ₂ S ₂
M (g·mol ⁻¹)	567.28
T (K)	120.01(10)
Wavelength (Å)	1.54184
Crystal system	Orthorhombic
Space group	<i>Pbcn</i>
a, (Å)	18.7879(7)
b, (Å)	8.8858(3)
c, (Å)	13.6750(5)
α, (°)	90
β, (°)	90
γ, (°)	90
V, Å ³	2282.98(14)
Z, ρ _{calcd.} (g/cm ³)	4, 1.650
μ (mm ⁻¹)	3.275
<i>F</i> (000)	1160
θ _{min} /θ _{max} (°)	4.707 / 72.463
Reflections collected/unique	5551 / 2214
R _{int}	0.0203
R ₁ [<i>I</i> > 2σ(<i>I</i>)]	0.0327, 0.0876
wR ₂ (all data)	0.0356, 0.0913
G.O.F.	1.069
Largest difference peak/hole (e ⁻ ·Å ⁻³)	0.330 / -0.291
N _o CCDC	-

Selected bond distances (Å) and angles (°) for Ni(L⁵)₂ (**23**).

N1-Ni1	2.2207(16)	Ni1-N3 ⁱ	2.0587(15)	Ni1-O1 ⁱ	1.9977(13)
N3-Ni1	2.0587(15)	Ni1-N1 ⁱ	2.2208(16)	Ni1-O1	1.9977(13)
O1 ⁱ -Ni1-N3 ⁱ	92.28(6)	O1-Ni1-O1 ⁱ	97.63(8)	N3 ⁱ -Ni1-N1 ⁱ	79.42(6)
O1-Ni1-N3	92.28(6)	O1-Ni1-N3 ⁱ	90.14(6)	N3 ⁱ -Ni1-N1	97.87(6)
O1 ⁱ -Ni1-N3	90.14(6)	N3 ⁱ -Ni1-N3	176.32(8)	N3-Ni1-N1	79.42(6)
O1-Ni1-N1 ⁱ	168.05(5)	O1-Ni1-N1	88.66(6)	N3-Ni1-N1 ⁱ	97.88(6)
O1 ⁱ -Ni1-N1 ⁱ	88.66(6)	O1 ⁱ -Ni1-N1	168.05(5)	N1-Ni1-N1 ⁱ	87.04(8)

Symmetry code: (i) -x+1,y,-z+1/2.

Zn(L⁵)₂ (**24**)



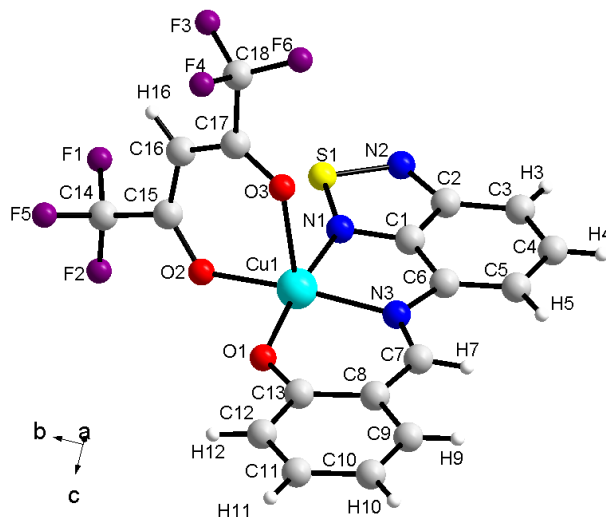
Formula	C ₂₆ H ₁₆ N ₆ O ₂ S ₂ Zn
M (g·mol ⁻¹)	573.94
T (K)	150.00(10)
Wavelength (Å)	1.54184
Crystal system	Orthorhombic
Space group	<i>Pbcn</i>
a, (Å)	19.8956(10)
b, (Å)	8.3892(4)
c, (Å)	13.8731(7)
α, (°)	90
β, (°)	90
γ, (°)	90
V, Å ³	2315.5(2)
Z, ρ _{calcd.} (g/cm ³)	4, 1.646
μ (mm ⁻¹)	3.494
<i>F</i> (000)	1168
θ _{min} /θ _{max} (°)	4.445/ 73.535
Reflections collected/unique	5220 / 2281
R _{int}	0.0340
R ₁ [I > 2σ(I)]	0.0354, 0.0925
wR ₂ (all data)	0.0451, 0.1011
G.O.F.	1.040
Largest difference peak/hole (e ⁻ ·Å ⁻³)	0.383 / -0.371
№ CCDC	-

Selected bond distances (Å) and angles (°) for Zn(L⁵)₂ (**24**).

Zn1-O1	1.9878(17)	Zn1-N1	2.510(2)	Zn1-N1 ⁱ	2.5104(19)
Zn1-O1 ⁱ	1.9878(17)	Zn1-N3 ⁱ	2.0783(18)	Zn1-N3	2.0783(18)
O ⁱ -Zn1-N3	90.98(7)	N1 ⁱ -Zn1-N1	81.14(9)	N3 ⁱ -Zn1-N1 ⁱ	97.11(6)
O1-Zn1-N3 ⁱ	90.98(7)	O1 ⁱ -Zn1-N1 ⁱ	158.93(7)	O1-Zn1-N1	158.93(7)
O1 ⁱ -Zn1-N3 ⁱ	95.17(7)	N3-Zn1-N1 ⁱ	74.46(7)	O1 ⁱ -Zn1-N1	85.75(7)
N3-Zn1-N3 ⁱ	169.12(10)	O1-Zn1-O1 ⁱ	111.13(10)	N3-Zn1-N1	97.11(7)
O1-Zn1-N1 ⁱ	85.75(7)	O1-Zn1-N3	95.17(7)	N3 ⁱ -Zn1-N1	74.46(7)

Symmetry code: (i) -x+1,y,-z+3/2.

[CuL⁵(Hfac)] (25)

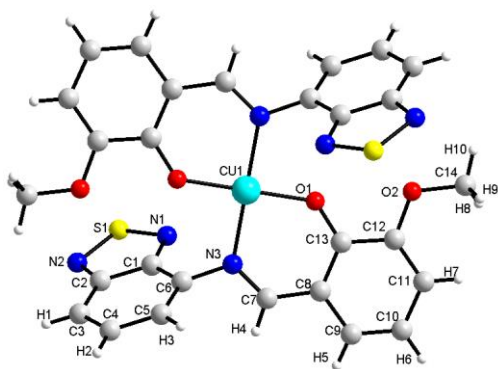


Formula	C ₁₈ H ₉ CuF ₆ N ₃ O ₃ S
M (g·mol ⁻¹)	524.88
T (K)	294.21(10)
Wavelength (Å)	1.54184
Crystal system	Monoclinic
Space group	<i>P</i> ₂ ₁ / <i>c</i>
a, (Å)	8.3214(2)
b, (Å)	21.7762(4)
c, (Å)	10.5087(2)
α, (°)	90
β, (°)	93.263(2)
γ, (°)	90
V, Å ³	1901.18(7)
Z, ρ _{calcd.} (g/cm ³)	4, 1.834
μ (mm ⁻¹)	3.468
<i>F</i> (000)	1044
θ _{min} /θ _{max} (°)	4.060 / 72.350
Reflections collected/unique	7569 / 3640
R _{int}	0.0176
R ₁ [I > 2σ(I)]	0.0446, 0.1212
wR ₂ (all data)	0.0515, 0.1272
G.O.F.	1.056
Largest difference peak/hole (e ⁻ ·Å ⁻³)	1.134 / -0.587
N _o CCDC	-

Selected bond distances (Å) and angles (°) for [CuL⁵(Hfac)] (25).

N1-Cu1	2.071(3)	O3-Cu1	2.244(2)	O1-Cu1	1.884(2)
N3-Cu1	1.971(2)	O2-Cu1	1.979(2)		
N3-Cu1-N1	82.78(10)	O1-Cu1-N1	168.96(11)	O1-Cu1-N3	93.10(9)
O2-Cu1-N1	89.71(10)	N1-Cu1-O3	88.20(9)	O1-Cu1-O2	92.12(9)
O1-Cu1-O3	102.77(10)	O2-Cu1-O3	86.69(8)	N3-Cu1-O2	166.08(10)
N3-Cu1-O3	104.69(9)				

Cu(L⁶)₂ (**26**)



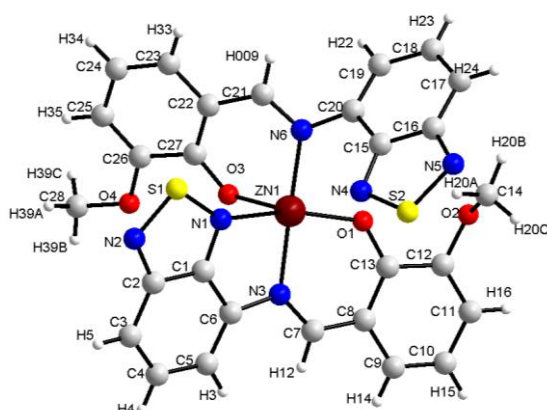
Formula	C ₂₈ H ₂₀ CuN ₆ O ₄ S ₂
M (g·mol ⁻¹)	632.16
T (K)	150.00(10)
Wavelength (Å)	1.54184
Crystal system	Monoclinic
Space group	<i>P</i> 2 ₁ / <i>c</i>
a, (Å)	7.2857(2)
b, (Å)	22.5527(5)
c, (Å)	7.8865(2)
α, (°)	90
β, (°)	98.126(2)
γ, (°)	90
V, Å ³	1282.84(6)
Z, ρ _{calcd.} (g/cm ³)	2, 1.637
μ (mm ⁻¹)	3.148
<i>F</i> (000)	646
θ _{min} /θ _{max} (°)	3.920 / 72.550
Reflections collected/unique	4865 / 2455
R _{int}	0.0203
R ₁ [I > 2σ(I)]	0.0383, 0.1115
wR ₂ (all data)	0.0423, 0.1147
G.O.F.	1.058
Largest difference peak/hole (e ⁻ ·Å ⁻³)	0.441 / -0.923
N ₂ CCDC	-

Selected bond distances (Å) and angles (°) for Cu(L⁶)₂ (**26**).

N3-Cu1	2.010(2)	Cu1-O1 ⁱ	1.8879(17)
O1-Cu1	1.8880(17)	Cu1-N3 ⁱ	2.010(2)
O1 ⁱ -Cu1-N3 ⁱ	90.43(8)	O1 ⁱ -Cu1-O1	180
O1-Cu1-N3 ⁱ	89.57(8)	O1 ⁱ -Cu1-N3	89.57(8)
N3-Cu1-N3 ⁱ	180	O1-Cu1-N3	90.43(8)

Symmetry code: (i) -x,-y+2,-z+1.

Zn(L⁶)₂ (**27**)

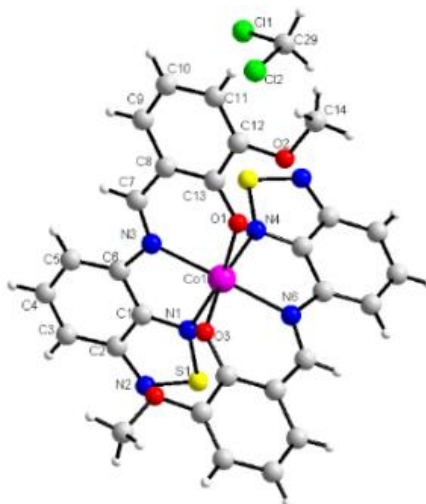


Formula	C ₂₈ H ₂₀ N ₆ O ₄ S ₂ Zn
M (g·mol ⁻¹)	633.99
T (K)	149.3(4)
Wavelength (Å)	1.54184
Crystal system	Monoclinic
Space group	<i>P</i> ₂ ₁ / <i>c</i>
a, (Å)	14.2736(3)
b, (Å)	8.39650(10)
c, (Å)	21.6214(4)
α, (°)	90
β, (°)	99.887(2)
γ, (°)	90
V, Å ³	2552.80(8)
Z, ρ _{calcd.} (g/cm ³)	4, 1.650
μ (mm ⁻¹)	3.293
<i>F</i> (000)	1296
θ _{min} /θ _{max} (°)	3.143 / 72.577
Reflections collected/unique	8238 / 4909
R _{int}	0.0712
R ₁ [I > 2σ(I)]	0.0719, 0.1950
wR ₂ (all data)	0.0739, 0.1995
G.O.F.	1.059
Largest difference peak/hole (e ⁻ ·Å ⁻³)	0.634 / -0.956
N ₂ CCDC	-

Selected bond distances (Å) and angles (°) for Zn(L⁶)₂ (**27**).

N1-Zn1	2.425(2)	N3-Zn1	2.058(2)	N6-Zn1	2.034(2)
O3-Zn1	1.971(2)	O1-Zn1	1.968(2)		
O1-Zn1-O3	117.20(9)	N3-Zn1-N1	75.95(9)	O1-Zn1-N1	155.44(9)
O1-Zn1-N6	94.25(9)	N6-Zn1-N3	162.14(9)	O3-Zn1-N1	86.25(9)
O3-Zn1-N6	91.83(9)	O3-Zn1-N3	100.35(9)	N6-Zn1-N1	92.02(9)
O1-Zn1-N3	91.74(9)				

[Co(L⁶)₂]·CH₂Cl₂ (**28**)

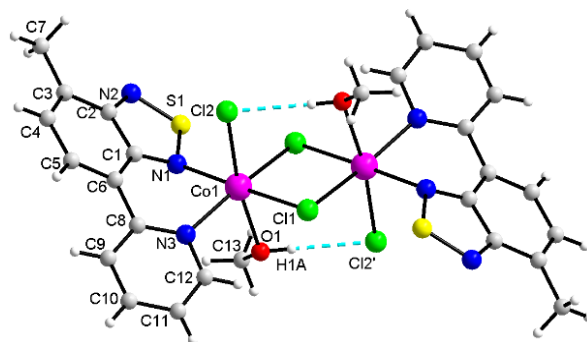


Formula	C ₂₉ H ₂₂ Cl ₂ CoN ₆ O ₄ S ₂
M (g·mol ⁻¹)	712.47
T (K)	149.3(4)
Wavelength (Å)	1.54184
Crystal system	Triclinic
Space group	<i>P</i> -1
a, (Å)	11.0894(7)
b, (Å)	12.3519(8)
c, (Å)	13.0378(8)
α, (°)	90.231(5)
β, (°)	111.019(6)
γ, (°)	114.765(6)
V, Å ³	1488.43(18)
Z, ρ _{calcd.} (g/cm ³)	2, 1.590
μ (mm ⁻¹)	7.887
<i>F</i> (000)	726
θ _{min} /θ _{max} (°)	3.694/ 73.777
Reflections collected/unique	10877 / 5673
R _{int}	0.0800
R ₁ [I > 2σ(I)]	0.0734, 0.1852
wR ₂ (all data)	0.0964, 0.2075
G.O.F.	1.028
Largest difference peak/hole (e·Å ⁻³)	1.669 / -1.822
No CCDC	-

Selected bond distances (Å) and angles (°) for [Co(L⁶)₂]·CH₂Cl₂ (**28**).

N1-Co1	2.221(4)	O3-Co1	2.004(3)	O1-Co1	1.997(3)
N4-Co1	2.248(4)	N6-Co1	2.088(4)	N3-Co1	2.103(4)
O1-Co1-O3	96.04(14)	N6-Co1-N1	86.75(16)	N6-Co1-N3	159.13(15)
O1-Co1-N6	105.46(14)	N3-Co1-N1	78.02(16)	O1-Co1-N1	167.22(15)
O3-Co1-N6	89.91(14)	O1-Co1-N4	88.04(14)	O3-Co1-N1	87.59(15)
N6-Co1-N4	77.64(15)	O3-Co1-N4	167.54(14)	O1-Co1-N3	89.21(14)
N3-Co1-N4	88.33(15)	N1-Co1-N4	90.98(16)	O3-Co1-N3	103.46(14)

[Co₂(L⁷)₂Cl₄(CH₃OH)₂] (**29a**)



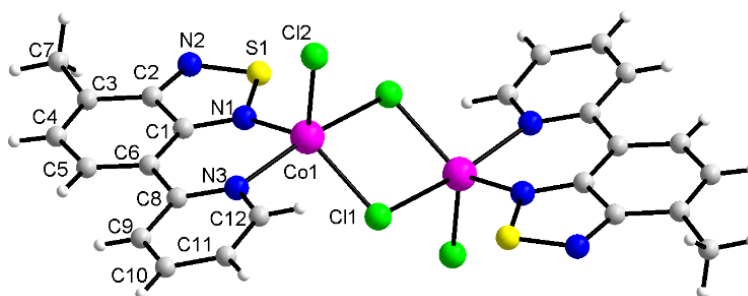
Formula	C ₂₆ H ₂₆ Cl ₄ Co ₂ N ₆ O ₂ S ₂
M (g·mol ⁻¹)	778.31
T (K)	149.97(10)
Wavelength (Å)	1.54184
Crystal system	Triclinic
Space group	<i>P</i> -1
a, (Å)	7.9130(6)
b, (Å)	8.8737(7)
c, (Å)	11.4632(8)
α, (°)	72.308(6)
β, (°)	79.447(6)
γ, (°)	78.700(6)
V, Å ³	745.37(10)
Z, ρ _{calcd.} (g/cm ³)	1, 1.734
μ (mm ⁻¹)	13.644
<i>F</i> (000)	394
θ _{min} /θ _{max} (°)	4.084 / 72.096
Reflections collected/unique	5199 / 2815
R _{int}	0.0257
R ₁ [<i>I</i> > 2σ(<i>I</i>)]	0.0346, 0.0923
wR ₂ (all data)	0.0355, 0.0936
G.O.F.	1.038
Largest difference peak/hole (e ⁻ ·Å ⁻³)	0.829 / -0.391
N ₂ CCDC	-

Selected bond distances (Å) and angles (°) for [Co₂(L⁷)₂Cl₄(CH₃OH)₂] (**29a**).

Co1-N3	2.1371(19)	Cl11-Co1 ⁱ	2.4713(6)	Co1-Cl11	2.4538(6)
Co1-N1	2.1580(19)	Co1-Cl12	2.4090(6)	Co1-Cl11 ⁱ	2.4713(6)
Co1-O1	2.1604(16)				
N3-Co1-N1	84.15(7)	N3-Co1-Cl11 ⁱ	167.44(5)	N1-Co1-Cl11	177.45(5)
N3-Co1-O1	86.56(7)	N1-Co1-Cl11 ⁱ	90.14(5)	O1-Co1-Cl11	84.14(5)
N1-Co1-O1	98.38(7)	O1-Co1-Cl11 ⁱ	83.22(5)	Cl12-Co1-Cl11	89.76(2)
N3-Co1-Cl12	100.12(5)	Cl12-Co1-Cl11 ⁱ	90.80(2)	N3-Co1-Cl11	95.62(6)
N1-Co1-Cl12	87.78(5)	O1-Co1-Cl12	171.39(5)	Cl11-Co1-Cl11 ⁱ	90.58(2)

Symmetry code: (i) -x+1,-y+1,-z+2.

[Co₂(L⁷)₂Cl₄] (**29b**)



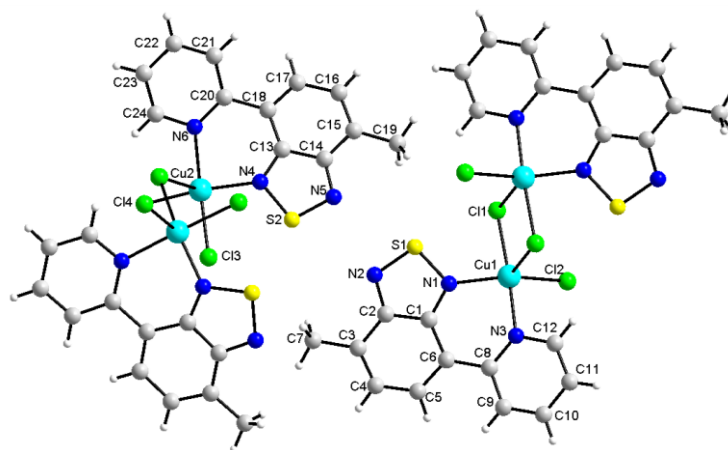
Formula	C ₂₄ H ₁₈ Cl ₄ Co ₂ N ₆ S ₂
M (g·mol ⁻¹)	714.22
T (K)	150.00(10)
Wavelength (Å)	1.54184
Crystal system	Triclinic
Space group	<i>P</i> -1
a, (Å)	8.3351(6)
b, (Å)	8.4938(5)
c, (Å)	10.1982(7)
α, (°)	106.063(5)
β, (°)	103.924(6)
γ, (°)	101.738(5)
V, Å ³	644.59(8)
Z, ρ _{calcd.} (g/cm ³)	1, 1.840
μ (mm ⁻¹)	15.655
<i>F</i> (000)	358
θ _{min} /θ _{max} (°)	4.755 / 72.041
Reflections collected/unique	4387 / 2443
R _{int}	0.0198
R ₁ [I > 2σ(I)]	0.0267, 0.0738
wR ₂ (all data)	0.0268, 0.0739
G.O.F.	1.038
Largest difference peak/hole (e ⁻ ·Å ⁻³)	0.489 / -0.348
N _o CCDC	-

Selected bond distances (Å) and angles (°) for [Co₂(L⁷)₂Cl₄] (**29b**).

Cl1-Co1	2.3205(5)	Cl1-Co1 ⁱ	2.5748(5)	Cl2-Co1	2.2724(6)
N1-Co1-N3	87.67(6)	N3-Co1-Cl1 ⁱ	167.21(5)	N1-Co1-Cl2	109.74(5)
N3-Co1-Cl1	93.59(4)	Cl2-Co1-Cl1 ⁱ	94.294(19)	N3-Co1-Cl2	98.41(5)
Cl2-Co1-Cl1	119.35(2)	Cl1-Co1-Cl1 ⁱ	81.393(18)	N1-Co1-Cl1	130.06(5)
N1-Co1-Cl1 ⁱ	86.65(4)				

Symmetry code: (i) -x+1,-y+1,-z.

[CuL⁷Cl₂] (30)



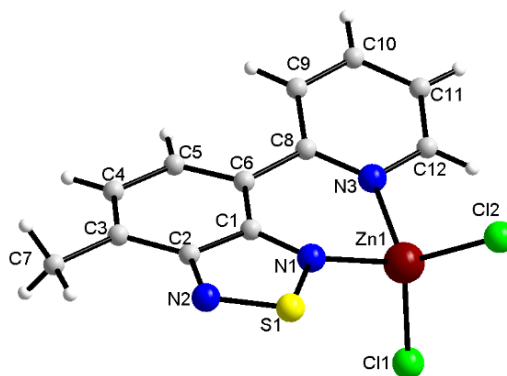
Formula	C ₂₄ H ₁₈ Cl ₄ Cu ₂ N ₆ S ₂
M (g·mol ⁻¹)	723.44
T (K)	150 K
Wavelength (Å)	0.71073 Å
Crystal system	Monoclinic
Space group	<i>P</i> 2 ₁ / <i>c</i>
a, (Å)	19.102
b, (Å)	18.812
c, (Å)	7.188
α, (°)	90
β, (°)	91.36
γ, (°)	90
V, Å ³	2582.2
Z, ρ _{calcd.} (g/cm ³)	4, 1.861
μ (mm ⁻¹)	2.252
<i>F</i> (000)	1448
θ _{min} /θ _{max} (°)	2.392 / 27.512
Reflections collected/unique	58998 / 5830
R _{int}	0.0911
R ₁ [I > 2σ(I)]	0.0589, 0.0868
wR ₂ (all data)	0.1199, 0.1034
G.O.F.	1.135
Largest difference peak/hole (e ⁻ ·Å ⁻³)	0.633 / -0.620
N _o CCDC	-

Selected bond distances (Å) and angles (°) for [CuL⁷Cl₂] (30).

Cl1-Cu1	2.3351(13)	Cl4-Cu2	2.2824(14)	Cl3-Cu2	2.3191(14)
Cl1-Cu1 ⁱ	2.5997(13)	Cl4-Cu2 ⁱⁱ	2.7277(14)	Cl2-Cu1	2.2736(14)
N4-Cu2-Cl3	88.19(12)	N1-Cu1-N3	87.53(16)	N1-Cu1-Cl1	88.93(12)
N6-Cu2-Cl3	170.36(12)	N1-Cu1-Cl2	152.45(12)	N3-Cu1-Cl1	176.46(12)
Cl4-Cu2-Cl3	92.85(5)	N3-Cu1-Cl2	91.17(12)	Cl2-Cu1-Cl1	91.95(5)
N4-Cu2-Cl4 ⁱⁱⁱ	109.02(12)	N4-Cu2-N6	88.60(16)	N1-Cu1-Cl1 ⁱ	106.14(12)
N6-Cu2-Cl4 ⁱⁱⁱ	83.88(12)	N4-Cu2-Cl4	154.97(13)	N3-Cu1-Cl1 ⁱ	93.97(12)
Cl4-Cu2-Cl4 ⁱⁱⁱ	96.01(5)	N6-Cu2-Cl4	93.90(12)	Cl2-Cu1-Cl1 ⁱ	101.41(5)
Cl3-Cu2-Cl4 ⁱⁱⁱ	88.58(5)	Cl1-Cu1-Cl1 ⁱ	87.06(4)		

Symmetry code: (i) -x+1,-y+1,-z+1; (ii) x,-y+3/2,z+1/2; (iii) x,-y+3/2,z-1/2.

[ZnL⁷Cl₂] (31)

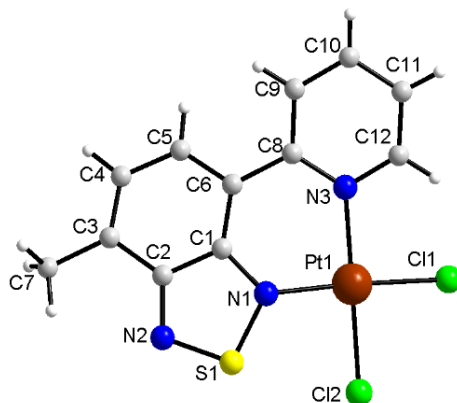


Formula	C ₁₂ H ₉ Cl ₂ N ₃ SZn
M (g·mol ⁻¹)	363.55
T (K)	293(2)
Wavelength (Å)	0.71073
Crystal system	Monoclinic
Space group	C2/c
a, (Å)	12.995
b, (Å)	10.601
c, (Å)	21.575
α, (°)	90
β, (°)	103.92
γ, (°)	90
V, Å ³	2885.0
Z, ρ _{calcd.} (g/cm ³)	8, 1.674
μ (mm ⁻¹)	2.205
F (000)	1456
θ _{min} /θ _{max} (°)	3.543 / 27.500
Reflections collected/unique	14816 / 3152
R _{int}	0.0785
R ₁ [I > 2σ(I)]	0.0459, 0.1036
wR ₂ (all data)	0.1026, 0.1227
G.O.F.	1.035
Largest difference peak/hole (e·Å ⁻³)	0.487 / -0.657
N _o CCDC	-

Selected bond distances (Å) and angles (°) for [ZnL⁷Cl₂] (31).

C11-Zn1	2.2115(11)	N3-Zn1	2.039(3)	N1-Zn1	2.047(3)
C12-Zn1	2.2076(12)				
N3-Zn1-N1	91.26(12)	Cl2-Zn1-Cl1	116.67(5)	N1-Zn1-Cl1	110.77(9)
N3-Zn1-Cl2	111.95(10)	N3-Zn1-Cl1	111.10(10)	N1-Zn1-Cl2	112.32(9)

[PtL⁷Cl₂] (**32**)

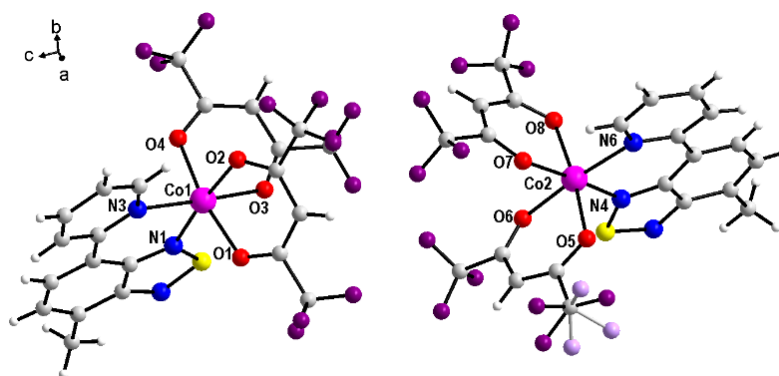


Formula	C ₁₂ H ₉ Cl ₂ N ₃ PtS
M (g·mol ⁻¹)	493.27
T (K)	293(2)
Wavelength (Å)	0.71073
Crystal system	Orthorhombic
Space group	<i>Pna</i> 2 ₁
a, (Å)	14.971
b, (Å)	12.530
c, (Å)	7.194
α, (°)	90
β, (°)	90
γ, (°)	90
V, Å ³	1349.5
Z, ρ _{calcd.} (g/cm ³)	4, 2.428
μ (mm ⁻¹)	10.935
<i>F</i> (000)	920
θ _{min} /θ _{max} (°)	3.929 / 27.515
Reflections collected/unique	10439 / 2774
R _{int}	0.0390
R ₁ [I > 2σ(I)]	0.0283, 0.0390
wR ₂ (all data)	0.0478, 0.0422
G.O.F.	1.017
Largest difference peak/hole (e ⁻ ·Å ⁻³)	0.776/ -0.836
N ₂ CCDC	-

Selected bond distances (Å) and angles (°) for [PtL⁷Cl₂] (**32**).

C11-Pt1	2.308(2)	N3-Pt1	2.068(5)	N1-Pt1	1.990(6)
Cl2-Pt1	2.3066(18)				
N1-Pt1-N3	90.3(2)	Cl2-Pt1-Cl1	88.67(9)	N3-Pt1-Cl1	93.39(18)
N1-Pt1-Cl2	88.01(17)	N1-Pt1-Cl1	173.24(17)	N3-Pt1-Cl2	175.6(6)

[CoL⁷(Hfac)₂] (34)

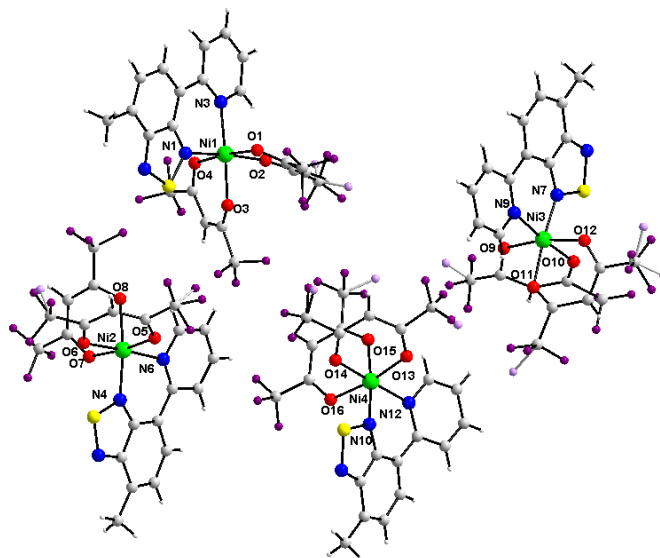


Formula	C ₂₂ H ₁₁ CoF ₁₂ N ₃ O ₄ S
M (g·mol ⁻¹)	700.33
T (K)	150.01(10)
Wavelength (Å)	1.54184 Å
Crystal system	Triclinic
Space group	<i>P</i> -1
a, (Å)	8.6909(4)
b, (Å)	17.1214(9)
c, (Å)	17.7647(8)
α, (°)	87.050(4)
β, (°)	80.729(4)
γ, (°)	82.968(4)
V, Å ³	2587.9(2)
Z, ρ _{calcd.} (g/cm ³)	4, 1.797
μ (mm ⁻¹)	7.120
<i>F</i> (000)	1388
θ _{min} /θ _{max} (°)	2.521/ 72.149
Reflections collected/unique	20278 / 9919
R _{int}	0.0554
R ₁ [I > 2σ(I)]	0.0747, 0.1829
wR ₂ (all data)	0.0976, 0.2001
G.O.F.	1.039
Largest difference peak/hole (e·Å ⁻³)	1.252 / -0.567
No. CCDC	-

Selected bond distances (Å) and angles (°) for [CoL⁷(Hfac)₂] (34).

Co1-O4	2.060(4)	Co2-N4	2.073(5)	Co1-O2	2.062(4)
Co1-N1	2.068(5)	Co2-O5	2.083(4)	Co1-O1	2.068(4)
Co1-O3	2.121(4)	Co2-O6	2.078(4)	Co1-N3	2.169(4)
Co2-O7	2.052(4)	Co2-O8	2.065(4)	Co2-N6	2.141(5)
O4-Co1-N1	96.53(17)	N4-Co2-O6	87.61(18)	O4-Co1-O2	88.21(15)
N1-Co1-N3	85.99(18)	O7-Co2-O5	86.65(17)	O1-Co1-N3	99.47(15)
O3-Co1-N3	175.96(17)	O8-Co2-O5	172.95(16)	O2-Co1-N3	96.57(17)
O4-Co1-N3	90.89(15)	O6-Co2-O5	86.89(16)	O1-Co1-O3	83.88(15)
N1-Co1-O3	91.91(17)	O8-Co2-N6	93.65(18)	O2-Co1-O3	85.81(16)
O4-Co1-O3	85.92(14)	N4-Co2-N6	86.77(18)	N1-Co1-O1	87.92(17)
O2-Co1-O1	86.95(16)	N4-Co2-O5	94.91(18)	O4-Co1-O1	169.00(15)
O2-Co1-N1	174.59(17)	O7-Co2-N6	98.71(18)	O5-Co2-N6	91.20(17)
O7-Co2-O8	87.56(17)	O6-Co2-N6	173.88(18)	O7-Co2-N4	174.28(17)
O8-Co2-N4	90.47(18)	O7-Co2-O6	86.99(17)	O8-Co2-O6	88.80(17)

[NiL⁷(Hfac)₂] (35)

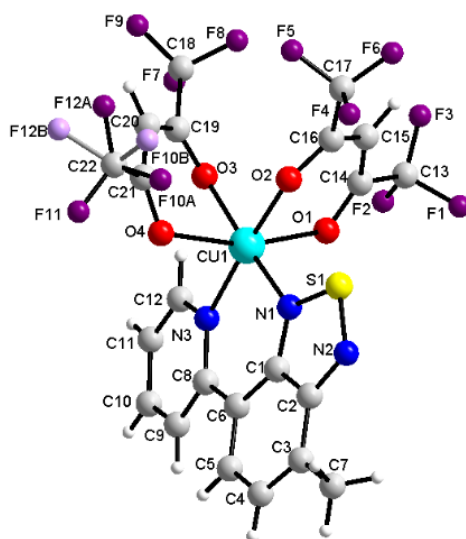


Formula	C ₂₂ H ₁₁ F ₁₂ N ₃ NiO ₄ S
M (g·mol ⁻¹)	700.08
T (K)	150.0(1)
Wavelength (Å)	1.54184 Å
Crystal system	Triclinic
Space group	<i>P</i> -1
a, (Å)	8.5783(6)
b, (Å)	25.9296(16)
c, (Å)	26.5961(17)
α, (°)	62.767(6)
β, (°)	85.651(6)
γ, (°)	81.229(6)
V, Å ³	5198.4(6)
Z, ρ _{calcd.} (g/cm ³)	8, 1.789
μ (mm ⁻¹)	2.990
<i>F</i> (000)	2784
θ _{min} /θ _{max} (°)	3.241 / 72.862
Reflections collected/unique	41505 / 19892
R _{int}	0.1159
R ₁ [<i>I</i> > 2σ(<i>I</i>)]	0.0936, 0.2292
wR ₂ (all data)	0.1785, 0.3018
G.O.F.	0.975
Largest difference peak/hole (e ⁻ ·Å ⁻³)	1.702 / -0.864
N _o CCDC	-

Selected bond distances (Å) and angles (°) for [NiL⁷(Hfac)₂] (35).

Ni1-O1	2.044(5)	Ni1-O2	2.036(5)	N9-Ni3	2.124(7)
Ni1-O4	2.044(5)	Ni1-O3	2.047(6)	Ni4-O13	2.022(8)
N1-Ni1	2.035(6)	N3-Ni1	2.091(6)	Ni4-O14	2.047(7)
Ni2-O5	2.028(6)	Ni2-O7	2.023(5)	N12-Ni4	2.062(9)
Ni2-O8	2.060(6)	Ni2-O6	2.050(5)	N7-Ni3	2.002(8)
N6-Ni2	2.081(6)	N4-Ni2	2.015(7)	Ni4-O15	2.032(7)
Ni3-O11	2.033(7)	Ni3-O12	2.028(6)	Ni4-O16	2.051(8)
Ni3-O10	2.057(6)	Ni3-O9	2.051(6)	N10-Ni4	2.033(8)
N1-Ni1-O2	174.2(2)	O4-Ni1-N3	91.9(2)	O11-Ni3-N9	98.0(3)
O4-Ni1-O3	88.6(2)	O1-Ni1-O3	86.2(2)	O13-Ni4-O15	86.5(3)
O2-Ni1-N3	96.9(2)	N1-Ni1-N3	88.8(2)	O15-Ni4-O16	86.5(3)
N1-Ni1-O3	88.1(2)	O1-Ni1-N3	93.4(2)	N10-Ni4-O14	89.6(3)
N1-Ni1-O1	89.3(2)	O2-Ni1-O1	89.5(2)	O13-Ni4-O14	88.5(3)
O1-Ni1-O4	174.4(2)	O2-Ni1-O4	88.1(2)	O13-Ni4-N10	98.5(3)
O3-Ni1-N3	176.9(2)	O2-Ni1-O3	86.1(2)	O14-Ni4-O16	85.5(3)
N1-Ni1-O4	92.5(2)	N4-Ni2-O5	97.6(3)	O15-Ni4-N12	93.7(4)
N4-Ni2-O7	88.0(3)	O5-Ni2-N6	91.7(2)	O14-Ni4-N12	175.9(4)
O7-Ni2-O6	88.7(2)	N4-Ni2-O6	88.5(2)	O9-Ni3-N9	95.2(3)
N4-Ni2-O8	173.4(3)	O5-Ni2-O6	88.2(2)	O10-Ni3-N9	174.9(3)
O5-Ni2-O8	85.8(2)	O7-Ni2-O8	88.3(2)	N10-Ni4-O16	88.3(4)
N4-Ni2-N6	88.8(3)	O6-Ni2-O8	86.0(2)	O13-Ni4-O16	170.9(3)
O7-Ni2-N6	91.7(2)	O7-Ni2-O5	173.5(2)	O15-Ni4-O14	88.5(3)
O6-Ni2-N6	177.3(2)	O8-Ni2-N6	96.7(3)	O15-Ni4-N10	174.6(4)
O12-Ni3-O11	86.9(3)	N7-Ni3-O9	96.2(3)	O13-Ni4-N12	88.2(4)
N7-Ni3-O12	91.6(3)	N7-Ni3-O11	173.9(3)	N10-Ni4-N12	88.5(4)
O11-Ni3-O9	84.5(3)	O12-Ni3-O9	169.2(2)	O16-Ni4-N12	98.1(4)
O12-Ni3-O10	86.6(3)	N7-Ni3-O10	87.0(3)	N7-Ni3-N9	88.0(3)
O9-Ni3-O10	86.4(3)	O11-Ni3-O10	87.0(3)	O12-Ni3-N9	92.4(2)

[CuL⁷(Hfac)₂] (36)

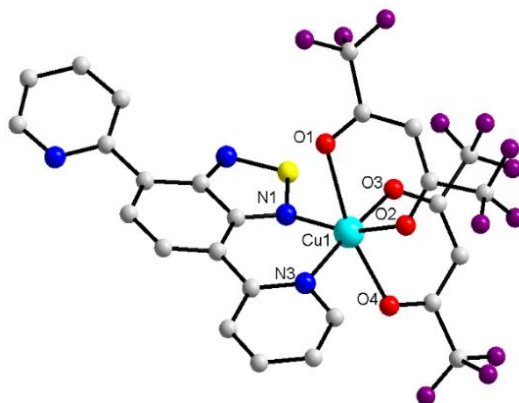


Formula	C ₂₂ H ₁₁ CuF ₁₂ N ₃ O ₄ S
M (g·mol ⁻¹)	704.94
T (K)	149.99(10)
Wavelength (Å)	1.54184 Å
Crystal system	Triclinic
Space group	<i>P</i> -1
a, (Å)	8.5296(7)
b, (Å)	11.1616(10)
c, (Å)	13.5876(12)
α, (°)	89.345(7)
β, (°)	81.332(7)
γ, (°)	82.820(7)
V, Å ³	1268.75(19)
Z, ρ _{calcd.} (g/cm ³)	2, 1.845
μ (mm ⁻¹)	3.174
<i>F</i> (000)	698
θ _{min} /θ _{max} (°)	3.290 / 71.999
Reflections collected/unique	9312 / 4832
R _{int}	0.0639
R ₁ [I > 2σ(I)]	0.0670, 0.1504
wR ₂ (all data)	0.0998, 0.1706
G.O.F.	1.076
Largest difference peak/hole (e ⁻ ·Å ⁻³)	0.520 / -0.473
N ₂ CCDC	-

Selected bond distances (Å) and angles (°) for [CuL⁷(Hfac)₂] (36).

Cu1-N1	1.972(4)	Cu1-O1	2.246(4)	Cu1-N3	2.041(4)
Cu1-O4	2.318(4)	Cu1-O2	1.991(4)	Cu1-O3	1.987(4)
N1-Cu1-O3	173.24(17)	N3-Cu1-O1	94.67(16)	N1-Cu1-O2	85.49(16)
N1-Cu1-N3	90.11(17)	O3-Cu1-O4	82.97(16)	O3-Cu1-O2	88.38(15)
O2-Cu1-N3	175.59(17)	N3-Cu1-O4	94.24(16)	O3-Cu1-N3	96.02(17)
O3-Cu1-O1	84.48(16)	O1-Cu1-O4	165.29(13)	N1-Cu1-O1	97.90(17)
N1-Cu1-O4	93.75(17)	O2-Cu1-O4	86.05(15)	O2-Cu1-O1	85.96(15)

[CuL⁸(Hfac)₂] (38)

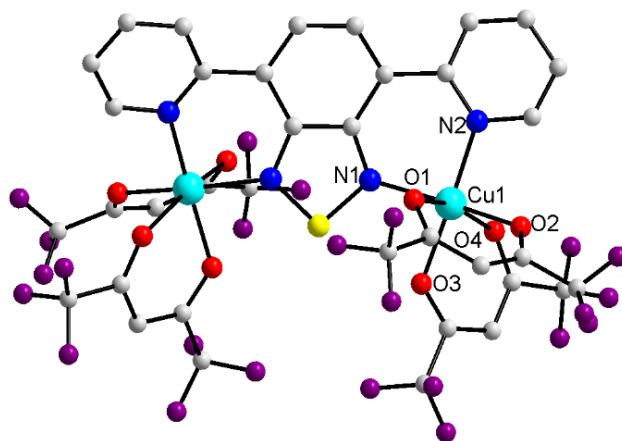


Formula	C ₂₆ H ₁₂ CuF ₁₂ N ₄ O ₄ S
M (g·mol ⁻¹)	768.00
T (K)	149.8(2)
Wavelength (Å)	1.54184
Crystal system	Monoclinic
Space group	<i>P</i> 2 ₁ / <i>c</i>
a, (Å)	8.3373(4)
b, (Å)	18.4314(6)
c, (Å)	19.1423(8)
α, (°)	90
β, (°)	97.620(4)
γ, (°)	90
V, Å ³	2915.6(2)
Z, ρ _{calcd.} (g/cm ³)	4, 1.750
μ (mm ⁻¹)	2.836
<i>F</i> (000)	1524
θ _{min} /θ _{max} (°)	3.343 / 71.890
Reflections collected/unique	11669 / 5540
R _{int}	0.0666
R ₁ [I > 2σ(I)]	0.0616, 0.1513
wR ₂ (all data)	0.0835, 0.1686
G.O.F.	1.028
Largest difference peak/hole (e ⁻ ·Å ⁻³)	1.356 / -0.489
No CCDC	-

Selected bond distances (Å) and angles (°) for [CuL⁸(Hfac)₂] (38).

Cu1-O3	1.968(3)	Cu1-O2	2.016(3)	Cu1-O4	2.215(3)
Cu1-O1	2.402(3)	Cu1-N1	2.007(3)	Cu1-N3	2.007(3)
O3-Cu1-N3	173.62(12)	N3-Cu1-O4	87.81(12)	O3-Cu1-N1	88.52(12)
O3-Cu1-O4	86.19(11)	O2-Cu1-O4	90.41(12)	N3-Cu1-O2	92.76(13)
N1-Cu1-O2	160.88(13)	N1-Cu1-O1	80.13(12)	O3-Cu1-O2	89.45(12)
N1-Cu1-O4	108.41(12)	O3-Cu1-O1	84.03(10)	O4-Cu1-O1	166.86(10)
N3-Cu1-O1	102.23(11)	O2-Cu1-O1	80.76(12)	N1-Cu1-N3	91.32(13)

[Cu₂L⁸(Hfac)₄] (**39**)

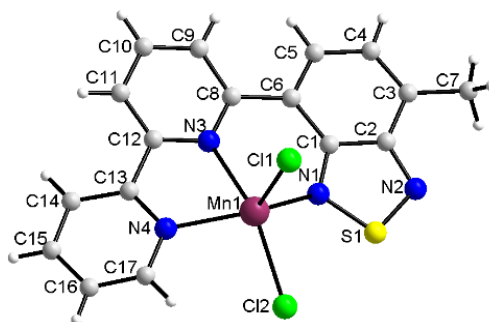


Formula	C ₃₆ H ₁₄ Cu ₂ F ₂₄ N ₄ O ₈ S
M (g·mol ⁻¹)	1245.65
T (K)	293(2)
Wavelength (Å)	0.71073
Crystal system	Monoclinic
Space group	C2/c
a, (Å)	21.567
b, (Å)	11.752
c, (Å)	17.878
α, (°)	90
β, (°)	103.25
γ, (°)	90
V, Å ³	4410.5
Z, ρ _{calcd.} (g/cm ³)	4, 1.876
μ (mm ⁻¹)	1.169
F (000)	2448
θ _{min} /θ _{max} (°)	3.467 / 27.528
Reflections collected/unique	23970 / 5061
R _{int}	0.1836
R ₁ [I > 2σ(I)]	0.0828, 0.2059
wR ₂ (all data)	0.2300, 0.2795
G.O.F.	0.926
Largest difference peak/hole (e ⁻ ·Å ⁻³)	0.904 / -0.623
N _o CCDC	-

Selected bond distances (Å) and angles (°) for [Cu₂L⁸(Hfac)₄] (**39**).

Cu1-O3	1.981(5)	Cu1-N1	2.064(6)	Cu1-O1	2.267(6)
Cu1-O2	1.998(6)	Cu1-N2	2.032(6)	Cu1-O4	2.287(6)
O3-Cu1-N2	169.9(2)	N2-Cu1-N1	90.3(2)	N2-Cu1-O4	89.3(2)
O2-Cu1-N2	93.8(2)	O3-Cu1-O1	84.9(2)	N1-Cu1-O4	107.2(2)
O3-Cu1-N1	85.0(2)	O2-Cu1-O1	84.6(2)	O1-Cu1-O4	164.9(2)
O2-Cu1-N1	166.0(2)	N2-Cu1-O1	103.3(2)	O3-Cu1-O4	83.6(2)
O3-Cu1-O2	92.8(2)	N1-Cu1-O1	81.4(2)	O2-Cu1-O4	86.2(2)

[MnL⁹Cl₂] \cdot 0,5CH₂Cl₂ (**40**)

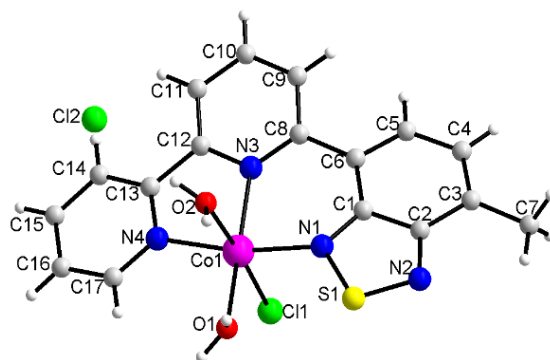


Formula	C ₃₅ H ₂₆ Cl ₆ Mn ₂ N ₈ S ₂
M (g·mol ⁻¹)	945.34
T (K)	293(2)
Wavelength (Å)	0.71073
Crystal system	Monoclinic
Space group	C2/c
a, (Å)	13.254
b, (Å)	10.633
c, (Å)	27.322
α, (°)	90
β, (°)	99.70
γ, (°)	90
V, Å ³	3795.4
Z, ρ _{calcd.} (g/cm ³)	4, 1.654
μ (mm ⁻¹)	1.238
F (000)	1904
θ _{min} /θ _{max} (°)	3.528/ 27.516
Reflections collected/unique	18786 / 4275
R _{int}	0.0389
R ₁ [I > 2σ(I)]	0.0466, 0.1241
wR ₂ (all data)	0.0863, 0.1369
G.O.F.	1.078
Largest difference peak/hole (e ⁻ ·Å ⁻³)	1.174 / -0.429
N _o CCDC	-

Selected bond distances (Å) and angles (°) for [MnL⁹Cl₂] \cdot 0,5CH₂Cl₂ (**40**).

Cl1-Mn1	2.3654(10)	Mn1-N1	2.183(3)	Mn1-N4	2.170(3)
Cl2-Mn1	2.3966(10)	Mn1-N3	2.318(3)		
N1-Mn1-Cl1	101.50(8)	N4-Mn1-Cl1	109.51(9)	N4-Mn1-N1	143.59(11)
N3-Mn1-Cl1	100.31(7)	Cl1-Mn1-Cl2	110.79(4)	N4-Mn1-N3	75.38(10)
N4-Mn1-Cl2	96.12(8)	N3-Mn1-Cl2	148.77(8)	N1-Mn1-N3	80.81(9)
N1-Mn1-Cl2	90.14(8)				

[CoL⁹(H₂O)₂Cl]Cl·3H₂O (**41**)

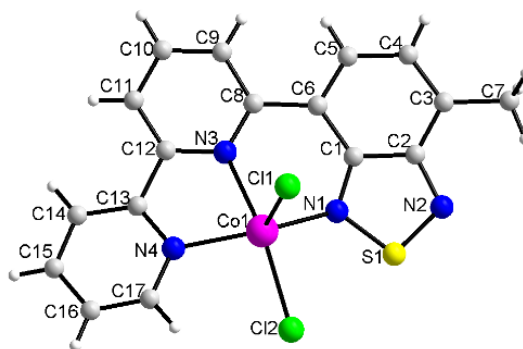


Formula	C ₁₇ H ₂₂ Cl ₂ CoN ₄ O ₅ S
M (g·mol ⁻¹)	524.27
T (K)	293(2)
Wavelength (Å)	0.71073
Crystal system	Triclinic
Space group	<i>P</i> -1
a, (Å)	7.7532(18)
b, (Å)	9.1039(8)
c, (Å)	16.3180(12)
α, (°)	76.219(10)
β, (°)	79.793(7)
γ, (°)	83.815(12)
V, Å ³	1098.3(3)
Z, ρ _{calcd.} (g/cm ³)	2, 1.585
μ (mm ⁻¹)	1.156
<i>F</i> (000)	538
θ _{min} /θ _{max} (°)	2.383/ 27.499
Reflections collected/unique	39560 / 5024
R _{int}	0.0445
R ₁ [I > 2σ(I)]	0.0324, 0.0753
wR ₂ (all data)	0.0561, 0.0823
G.O.F.	1.041
Largest difference peak/hole (e ⁻ ·Å ⁻³)	0.488 / -0.431
N _o CCDC	-

Selected bond distances (Å) and angles (°) for [CoL⁹(H₂O)₂Cl]Cl·3H₂O (**41**).

Co1-N1	2.0895(17)	Cl1-Co1	2.4280(7)	Co1-O2	2.2204
Co1-N3	2.1299(16)	Co1-N4	2.0742(17)	Co1-O1	2.1304(16)
N4-Co1-O1	102.67(7)	N4-Co1-N1	169.04(7)	N1-Co1-O2	90.26(6)
N3-Co1-O2	89.74(5)	N4-Co1-N3	79.94(7)	N3-Co1-Cl1	94.69(5)
O1-Co1-O2	83.31(6)	N1-Co1-N3	89.63(6)	O1-Co1-Cl1	92.35(6)
N4-Co1-Cl1	92.93(5)	N1-Co1-O1	87.26(7)	O2-Co1-Cl1	175.33(3)
N1-Co1-Cl1	91.26(5)	N3-Co1-O1	172.36(7)	N4-Co1-O2	86.36(6)

[CoL⁹Cl₂] \cdot 0,25CH₂Cl₂ (**42**)

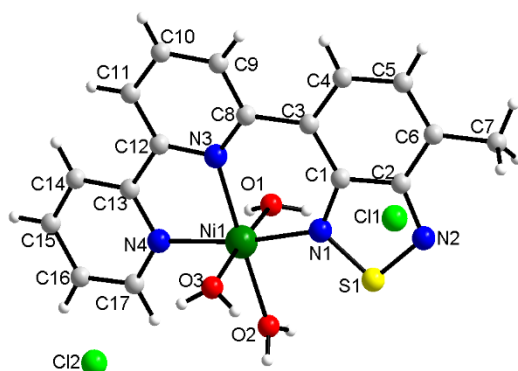


Formula	C _{17,25} H _{12,5} Cl _{2,5} CoN ₄ S
M (g·mol ⁻¹)	455.43
T (K)	293(2)
Wavelength (Å)	0.71073
Crystal system	Monoclinic
Space group	C2/c
a, (Å)	13.187(2)
b, (Å)	10.5419(5)
c, (Å)	27.153(5)
α, (°)	90
β, (°)	100.570(10)
γ, (°)	90
V, Å ³	3710.7(9)
Z, ρ _{calcd.} (g/cm ³)	8, 1.630
μ (mm ⁻¹)	1.406
F (000)	1836
θ _{min} /θ _{max} (°)	3.573 / 27.798
Reflections collected/unique	32517 / 4324
R _{int}	0.0647
R ₁ [I > 2σ(I)]	0.0443, 0.1070
wR ₂ (all data)	0.1075, 0.1250
G.O.F.	1.041
Largest difference peak/hole (e ⁻ ·Å ⁻³)	0.582/-0.558
No CCDC	-

Selected bond distances (Å) and angles (°) for [CoL⁹Cl₂] \cdot 0,25CH₂Cl₂ (**42**).

Cl1-Co1	2.3144(10)	Co1-N4	2.068(3)	Co1-N1	2.076(3)
Cl2-Co1	2.3460(11)	Co1-N3	2.196(3)		
N3-Co1-Cl1	96.13(7)	N3-Co1-Cl2	155.50(7)	N4-Co1-N3	78.35(10)
N4-Co1-Cl2	95.26(9)	Cl1-Co1-Cl2	108.34(4)	N1-Co1-N3	84.89(10)
N1-Co1-Cl2	89.88(8)	N4-Co1-N1	150.25(11)	N4-Co1-Cl1	107.15(9)
N1-Co1-Cl1	98.88(8)				

[NiL⁹(H₂O)₃]Cl₂·2H₂O (**43**)

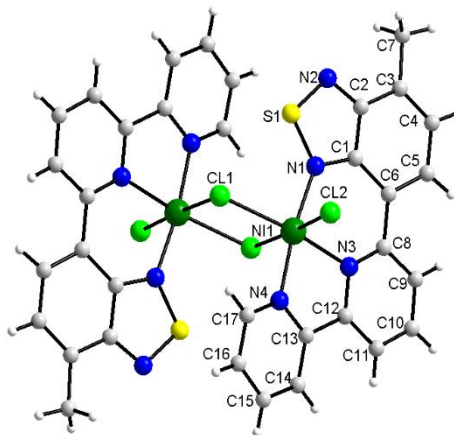


Formula	C ₁₇ H ₂₂ Cl ₂ N ₄ NiO ₅ S
M (g·mol ⁻¹)	524.05
T (K)	293(2)
Wavelength (Å)	1.54184
Crystal system	Triclinic
Space group	<i>P</i> -1
a, (Å)	7.3508(2)
b, (Å)	10.8385(4)
c, (Å)	14.5746(5)
α, (°)	105.928(3)
β, (°)	90.807(3)
γ, (°)	102.858(3)
V, Å ³	1085.10(7)
Z, ρ _{calcd.} (g/cm ³)	2, 1.604
μ (mm ⁻¹)	4.786
<i>F</i> (000)	540
θ _{min} /θ _{max} (°)	3.163 / 72.654
Reflections collected/unique	6887 / 4156
R _{int}	0.0220
R ₁ [I > 2σ(I)]	0.0323, 0.0855
wR ₂ (all data)	0.0330, 0.0858
G.O.F.	1.066
Largest difference peak/hole (e ⁻ ·Å ⁻³)	0.530/-0.627
N _o CCDC	-

Selected bond distances (Å) and angles (°) for [NiL⁹(H₂O)₃]Cl₂·2H₂O (**43**).

N1-Ni1	2.0253(14)	Ni1-O3	2.0622	N3-Ni1	2.0963(14)
Ni1-O1	2.0604	Ni1-O2	2.0897	N4-Ni1	2.0362(14)
N1-Ni1-N4	171.16(6)	N1-Ni1-O2	89.25(4)	O1-Ni1-O2	88.1
N1-Ni1-O1	91.05(5)	N4-Ni1-O2	99.58(4)	O3-Ni1-O2	86.2
N4-Ni1-O1	89.67(5)	O1-Ni1-N3	90.49(4)	N1-Ni1-N3	90.16(6)
N1-Ni1-O3	90.42(5)	O3-Ni1-N3	95.18(4)	N4-Ni1-N3	81.02(6)
N4-Ni1-O3	89.74(5)	O2-Ni1-N3	178.49(4)		
O1-Ni1-O3	174.1				

[Ni₂(L⁹)₂Cl₄]·2H₂O (**44**)



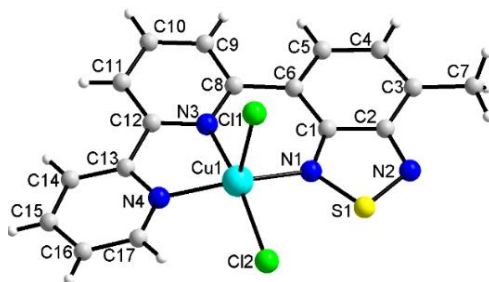
Formula	C ₃₄ H ₂₈ Cl ₄ N ₃ Ni ₂ O ₂ S ₂
M (g·mol ⁻¹)	903.98
T (K)	293(2)
Wavelength (Å)	1.54184
Crystal system	Triclinic
Space group	<i>P</i> -1
a, (Å)	9.2795(6)
b, (Å)	9.9546(6)
c, (Å)	10.5049(8)
α, (°)	77.380(6)
β, (°)	84.953(6)
γ, (°)	68.550(6)
V, Å ³	881.31(11)
Z, ρ _{calcd.} (g/cm ³)	1, 1.703
μ (mm ⁻¹)	5.615
F (000)	460
θ _{min} /θ _{max} (°)	4.313 / 72.033
Reflections collected/unique	6093 / 3341
R _{int}	0.0328
R ₁ [I > 2σ(I)]	0.0542, 0.1425
wR ₂ (all data)	0.0662, 0.1534
G.O.F.	1.070
Largest difference peak/hole (e ⁻ ·Å ⁻³)	0.933/-0.496
N _o CCDC	-

Selected bond distances (Å) and angles (°) for [Ni₂(L⁹)₂Cl₄]·2H₂O (**44**).

Ni1-N1	2.013(3)	Ni1-N3	2.087(3)	Ni1-Cl1	2.4192(10)
Ni1-N4	2.028(3)	Ni1-Cl2	2.3965(12)	Ni1-Cl1 ⁱ	2.5560(11)
Cl1-Ni1 ⁱ	2.5559(11)				
N3-Ni1-Cl1	168.11(10)	N1-Ni1-N4	171.83(13)	N1-Ni1-N3	90.49(14)
Cl2-Ni1-Cl1	93.93(4)	Cl2-Ni1-Cl1 ⁱ	177.22(4)	N4-Ni1-N3	81.35(13)
N1-Ni1-Cl1 ⁱ	89.86(10)	Cl1-Ni1-Cl1 ⁱ	83.37(4)	N1-Ni1-Cl2	89.57(10)
N4-Ni1-Cl1 ⁱ	89.89(10)	N1-Ni1-Cl1	91.43(10)	N4-Ni1-Cl2	91.06(10)
N3-Ni1-Cl1 ⁱ	84.90(9)	N4-Ni1-Cl1	96.65(9)	N3-Ni1-Cl2	97.82(9)

Symmetry code: (i) -x+1,-y,-z+1

[CuL⁹Cl₂]-H₂O (**45**)

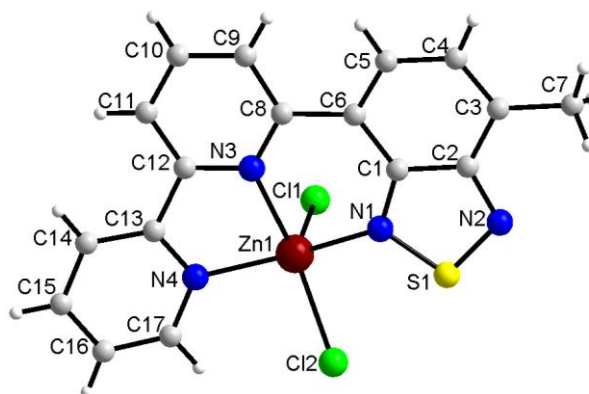


Formula	C ₁₇ H ₁₄ Cl ₂ CuN ₄ OS
M (g·mol ⁻¹)	456.82
T (K)	149.9(4)
Wavelength (Å)	1.54184
Crystal system	Monoclinic
Space group	C2/c
a, (Å)	12.9460(4)
b, (Å)	10.2914(3)
c, (Å)	26.7719(8)
α, (°)	90
β, (°)	100.575(3)
γ, (°)	90
V, Å ³	3506.30(19)
Z, ρ _{calcd.} (g/cm ³)	8, 1.731
μ (mm ⁻¹)	5.807
F (000)	1848
θ _{min} /θ _{max} (°)	3.359 / 72.497
Reflections collected/unique	6406 / 3355
R _{int}	0.0533
R ₁ [I > 2σ(I)]	0.0679, 0.1787
wR ₂ (all data)	0.0706, 0.1841
G.O.F.	1.125
Largest difference peak/hole (e·Å ⁻³)	2.414 / -1.123
N _o CCDC	-

Selected bond distances (Å) and angles (°) for [CuL⁹Cl₂]-H₂O (**45**).

Cu1-N1	1.979(3)	Cu1-Cl2	2.2968(10)	Cu1-N3	2.070(3)
Cu1-N4	1.992(4)	Cu1-Cl1	2.4699(11)		
N1-Cu1-N4	162.72(14)	N3-Cu1-Cl2	162.91(10)	N3-Cu1-Cl1	94.65(9)
N1-Cu1-N3	89.51(13)	N1-Cu1-Cl1	93.38(10)	N4-Cu1-Cl2	94.30(11)
N4-Cu1-N3	82.04(14)	N4-Cu1-Cl1	102.27(11)	Cl2-Cu1-Cl1	102.44(4)
N1-Cu1-Cl2	89.38(10)				

[ZnL⁹Cl₂] (**46**)

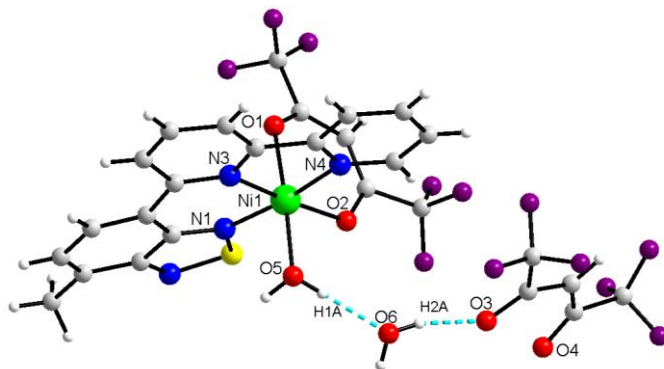


Formula	C ₁₇ H ₁₂ C ₁₂ N ₄ SZn
M (g·mol ⁻¹)	440.64
T (K)	149.99(18)
Wavelength (Å)	1.54184
Crystal system	Monoclinic
Space group	C2/c
a, (Å)	13.1070(3)
b, (Å)	10.3418(2)
c, (Å)	26.7348(8)
α, (°)	90
β, (°)	99.801(2)
γ, (°)	90
V, Å ³	3571.01(15)
Z, ρ _{calcd.} (g/cm ³)	8, 1.639
μ (mm ⁻¹)	5.818
F (000)	1776
θ _{min} /θ _{max} (°)	3.355 / 72.634
Reflections collected/unique	11535 / 3492
R _{int}	0.0267
R ₁ [I > 2σ(I)]	0.0337, 0.0929
wR ₂ (all data)	0.0355, 0.0942
G.O.F.	1.089
Largest difference peak/hole (e·Å ⁻³)	0.893/-0.639
No CCDC	-

Selected bond distances (Å) and angles (°) for [ZnL⁹Cl₂] (**46**).

N4-Zn1	2.0614(18)	Cl2-Zn1	2.3261(5)	N3-Zn1	2.2592(16)
Cl1-Zn1	2.2773(5)	N1-Zn1	2.0919(17)		
N4-Zn1-N1	146.20(7)	Cl1-Zn1-Cl2	108.27(2)	N1-Zn1-Cl1	100.57(5)
N4-Zn1-N3	77.07(6)	N4-Zn1-Cl1	108.70(6)	N3-Zn1-Cl1	98.92(4)
N1-Zn1-N3	82.12(6)	N3-Zn1-Cl2	152.64(5)	N4-Zn1-Cl2	96.50(5)
N1-Zn1-Cl2	89.88(5)				

[NiL⁹(Hfac)(H₂O)](Hfac)·H₂O (**47**)

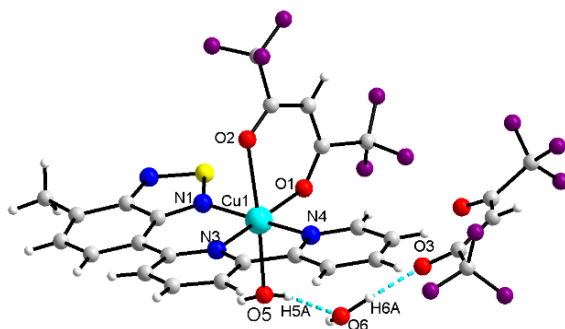


Formula	C ₂₇ H ₁₈ F ₁₂ N ₄ NiO ₆ S
M (g·mol ⁻¹)	813.22
T (K)	293(2)
Wavelength (Å)	1.54184
Crystal system	Triclinic
Space group	<i>P</i> -1
a, (Å)	10.9339(4)
b, (Å)	11.8302(4)
c, (Å)	12.1233(4)
α, (°)	76.150(3)
β, (°)	82.818(3)
γ, (°)	82.140(3)
V, Å ³	1501.30(9)
Z, ρ _{calcd.} (g/cm ³)	2, 1.799
μ (mm ⁻¹)	2.752
<i>F</i> (000)	816
θ _{min} /θ _{max} (°)	3.773 / 72.145
Reflections collected/unique	11467 / 5773
R _{int}	0.0246
R ₁ [I > 2σ(I)]	0.0405, 0.1078
wR ₂ (all data)	0.0441, 0.1121
G.O.F.	1.059
Largest difference peak/hole (e·Å ⁻³)	0.782/-0.469
N ₂ CCDC	-

Selected bond distances (Å) and angles (°) for [NiL⁹(Hfac)(H₂O)](Hfac)·H₂O (**47**).

N1- Ni1	2.0144(18)	O5- Ni1	2.0737(14)	O1- Ni1	2.0927(14)
N3- Ni1	2.0657(17)	N4- Ni1	2.0333(18)	O2- Ni1	2.0677(14)
N1- Ni1-N4	172.79(7)	N3- Ni1-O2	175.20(7)	N3- Ni1-O5	89.71(6)
N1- Ni1-N3	91.55(7)	N1- Ni1-O5	91.09(7)	O2- Ni1-O5	90.88(6)
N4- Ni1-N3	81.93(7)	N4- Ni1-O5	91.96(7)	N1- Ni1-O1	84.73(7)
N1- Ni1-O2	93.19(7)	O2- Ni1-O1	88.92(6)	N4- Ni1-O1	92.24(7)
N4- Ni1-O2	93.29(7)	O5- Ni1-O1	175.80(6)	N3- Ni1-O1	90.83(6)

[CuL⁹(Hfac)(H₂O)](Hfac)·H₂O (**48**)

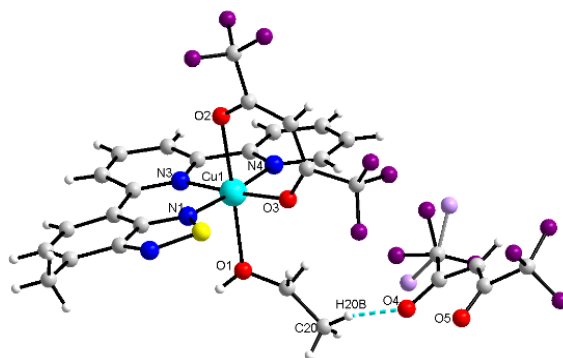


Formula	C ₂₇ H ₁₈ CuF ₁₂ N ₄ O ₆ S
M (g·mol ⁻¹)	818.05
T (K)	293(2)
Wavelength (Å)	1.54184
Crystal system	Triclinic
Space group	<i>P</i> -1
a, (Å)	10.6738(10)
b, (Å)	11.9907(14)
c, (Å)	12.2608(11)
α, (°)	76.439(9)
β, (°)	83.021(8)
γ, (°)	84.120(9)
V, Å ³	1509.7(3)
Z, ρ _{calcd.} (g/cm ³)	2, 1.800
μ (mm ⁻¹)	2.831
<i>F</i> (000)	818
θ _{min} /θ _{max} (°)	3.727 / 72.083
Reflections collected/unique	11159 / 5751
R _{int}	0.0360
R ₁ [I > 2σ(I)]	0.0437, 0.1045
wR ₂ (all data)	0.0578, 0.1155
G.O.F.	1.018
Largest difference peak/hole (e·Å ⁻³)	0.709/-0.543
N _o CCDC	-

Selected bond distances (Å) and angles (°) for [CuL⁹(Hfac)(H₂O)](Hfac)·H₂O (**48**).

Cu1-N1	1.967(3)	Cu1-N3	2.034(2)	Cu1-O2	2.397(2)
Cu1-N4	1.970(3)	Cu1-O5	2.2945(18)	Cu1-O1	2.0157(18)
N1- Cu1-N4	173.65(10)	N1- Cu1-O2	82.03(9)	N4- Cu1-N3	83.08(10)
N1- Cu1-O1	91.34(9)	N4- Cu1-O2	94.25(9)	O1- Cu1-N3	175.37(10)
N4- Cu1-O1	93.41(9)	O1- Cu1-O2	84.22(7)	N1- Cu1-O5	91.21(8)
N1- Cu1-N3	91.95(10)	N3- Cu1-O2	93.01(8)	N4- Cu1-O5	92.67(8)
N3- Cu1-O5	89.34(8)	O5- Cu1-O2	172.91(7)	O1- Cu1-O5	93.84(7)

[CuL⁹(Hfac)(C₂H₅OH)](Hfac) (**49**)



Formula	C ₂₉ H ₂₀ CuF ₁₂ N ₄ O ₅ S
M (g·mol ⁻¹)	828.09
T (K)	293(2)
Wavelength (Å)	1.54184
Crystal system	Triclinic
Space group	<i>P</i> -1
a, (Å)	10.5929(5)
b, (Å)	11.9389(6)
c, (Å)	12.5134(7)
α, (°)	75.772(5)
β, (°)	82.796(4)
γ, (°)	85.505(4)
V, Å ³	1520.02(14)
Z, ρ _{calcd.} (g/cm ³)	2, 1.809
μ (mm ⁻¹)	2.796
<i>F</i> (000)	830
θ _{min} /θ _{max} (°)	3.666/ 71.920
Reflections collected/unique	10591 / 5757
R _{int}	0.0304
R ₁ [I > 2σ(I)]	0.0559, 0.1467
wR ₂ (all data)	0.0656, 0.1553
G.O.F.	1.021
Largest difference peak/hole (e ⁻ ·Å ⁻³)	0.729/-1.320
N ₂ CCDC	-

Selected bond distances (Å) and angles (°) for [CuL⁹(Hfac)(C₂H₅OH)](Hfac) (**49**).

Cu1-N1	1.966(3)	Cu1-N3	2.028(3)	Cu1-O2	2.3982(12)
Cu1-N4	1.977(3)	Cu1-O1	2.3388(12)	Cu1-O3	2.0022
N1- Cu1-N4	174.74(12)	N4- Cu1-O1	91.20(8)	O3- Cu1-O2	84
N1- Cu1-O3	91.08(8)	O3- Cu1-O1	93.4	N3- Cu1-O2	93.96(8)
N4- Cu1-O3	93.34(9)	N3- Cu1-O1	88.96(8)	N1- Cu1-O2	83.25(8)
N1- Cu1-N3	92.43(11)	N1- Cu1-O1	91.37(8)	N4- Cu1-O2	94.38(8)
N4- Cu1-N3	83.03(11)	O1- Cu1-O2	174	O3- Cu1-N3	175.73(8)

Computational details

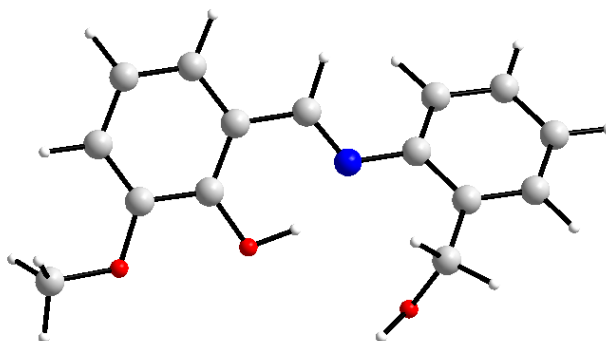
Density functional theory (DFT) and *ab initio* methods have been performed for complexes **13-18** to get the zero-field splitting contribution. The spin-orbit coupling contribution to D and E was calculated using the state-averaged complete active space self-consistent field (CASSCF) approach, with four electrons in 5 orbitals (5 quintet and lowest 35 triplet states were taken into account)¹⁻³. Functional B3LYP in the ORCA software package^{4,5} was employed with TZVPP basis set for Mn and all coordinated atoms and SVP^{6,7} bases set for all remaining atoms. The “coupled-perturbed” scheme implementing in ORCA was used to calculate the spin-spin contribution. To verify the presence of exchange interactions between Mn (III) centres DFT calculation was performed in the ORCA program using similarly as in the calculations of D above, functional and basis sets.

All calculations for compounds **20-20b** have used the Density Functional Theory (DFT) method implemented in the Gaussian 09 package⁸. The PBE0 functional⁹ and 6-311++G(2df,2pd)^{10,11} basis set with an ultra-fine grid were used. Starting geometries for compounds **20-20b** were derived from the experimentally observed X-ray structures; only moving the H positions was applied to generate the keto and enol isomers. Optimized geometries were then tested as global minima by frequencies calculations providing the Gibbs free energies. Finally, to reproduce the absorption and emission properties, Time Dependent DFT (TD-DFT) calculations were performed with the same functional and basis set. For emission the first singlets were optimized. The spectra have been generated with a Gaussian approximation (Full width at half maximum of 3000 cm⁻¹) with the GaussSum program¹².

DFT and TD-DFT calculations have been done using Gaussian 09 package⁸, with the PBE0 functional⁹ and TZVP^{6,13} (**HL**⁵ and **HL**⁶) or 6-311++G(2df, 2pd)^{10,11} (**L**⁷, **L**⁹ and **L**¹⁰) basis set. Optimized geometries were then confirmed as global minima by frequency calculations. Starting geometries were derived from the X-ray structures.

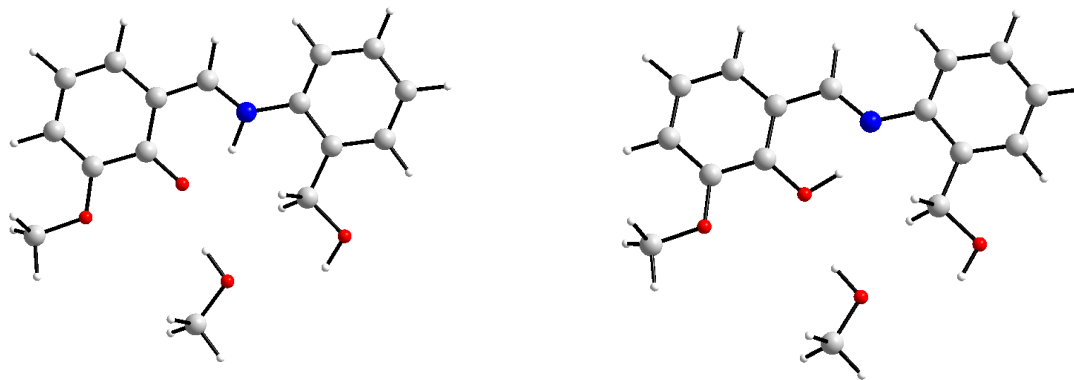
DFT calculation details

Converged Cartesian coordinates of calculated compound **H₂L² (20)**



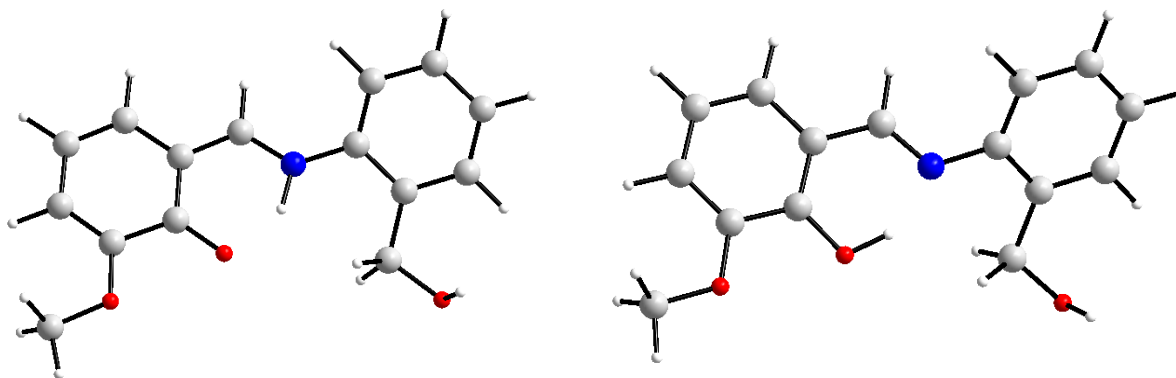
O	9.346530	-0.632871	6.929578
C	10.041858	-1.637619	7.622415
C	8.181813	-0.199737	7.453601
O	8.083132	1.228645	5.586352
H	7.468413	1.917942	5.201407
C	7.523305	0.802622	6.709430
O	8.145126	3.602412	3.240319
H	9.017511	3.362451	3.556286
C	7.670878	4.704321	3.995209
N	6.081172	2.822123	5.358535
C	5.614986	2.347899	6.453799
C	5.404930	3.794746	4.621150
H	10.937602	-1.843374	7.040537
H	9.448303	-2.554171	7.704472
H	10.332470	-1.307845	8.625441
C	7.617877	-0.661469	8.628393
H	8.119871	-1.431231	9.198490
C	6.403837	-0.148690	9.096473
H	5.985792	-0.528369	10.019485
C	5.755955	0.828612	8.384950
H	4.815383	1.238387	8.734947
C	6.302609	1.314639	7.186574
H	4.681982	2.724534	6.888457
C	4.014880	3.825619	4.520722
C	6.173226	4.742231	3.926542
H	3.427577	3.057380	5.009309
C	3.385706	4.803631	3.767817
H	2.305177	4.809245	3.690713
C	4.137846	5.758743	3.102921
H	3.651302	6.522241	2.509046
C	5.522851	5.716193	3.184815
H	6.117584	6.451730	2.654626
H	8.071004	5.644746	3.597818
H	7.990304	4.619444	5.039621

Converged Cartesian coordinates of calculated compound $\text{H}_2\text{L}^2 \cdot \text{CH}_3\text{OH}$ (20a).



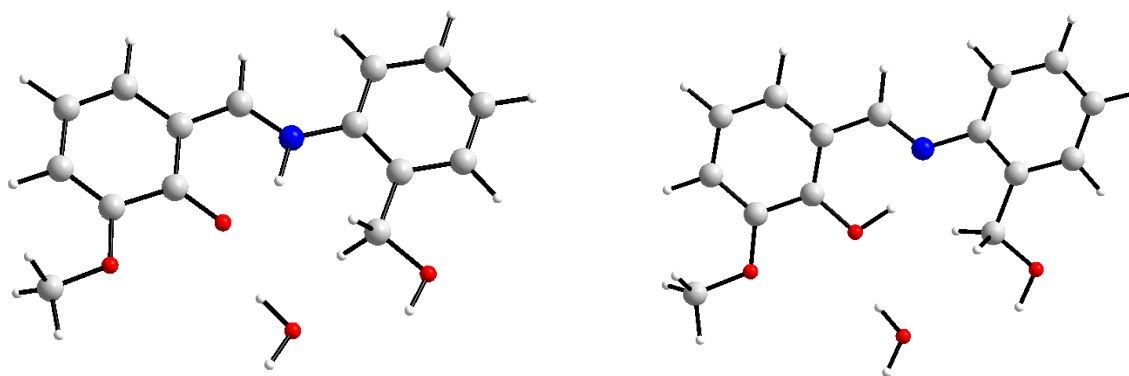
keto				enol			
O	10.99600	11.53579	-1.27422	C	16.82574	10.83091	4.58595
C	10.00554	11.57739	-2.26918	C	15.87152	10.90624	3.58204
C	11.68064	12.67019	-1.02861	C	15.43511	12.17059	3.15974
O	12.85952	11.43784	0.60490	C	15.92987	13.31738	3.77981
C	12.67668	12.53666	0.00653	C	16.87282	13.22131	4.78957
O	14.76686	8.70735	3.51987	C	17.32847	11.97537	5.18933
H	14.11729	8.14221	3.09215	N	14.47034	12.24238	2.14827
C	14.63260	9.96250	2.91263	C	14.54278	13.14457	1.23936
N	14.66621	12.54354	1.96960	C	13.53477	13.31497	0.22242
H	14.02151	11.79295	1.61800	C	12.39826	12.48931	0.20058
C	14.42833	13.65489	1.31227	C	11.42568	12.68395	-0.80202
C	15.58843	12.26956	2.98406	C	11.60826	13.67920	-1.74468
H	10.42926	11.83266	-3.24632	C	12.74209	14.49696	-1.71981
H	9.21863	12.29782	-2.02172	C	13.69370	14.31676	-0.74829
H	9.57566	10.57909	-2.31495	O	10.36812	11.85013	-0.74748
C	11.49475	13.86646	-1.66681	C	9.36684	11.99791	-1.72203
H	10.74421	13.95341	-2.44154	O	12.20645	11.52671	1.09366
C	12.26497	15.00982	-1.34009	C	15.33166	9.66069	2.92717
H	12.08397	15.93524	-1.87057	O	15.64910	8.47175	3.61027
C	13.21616	14.93824	-0.37294	H	15.16856	8.45811	4.43986
H	13.81238	15.80609	-0.11354	H	12.99146	11.54912	1.70299
C	13.44496	13.71848	0.31665	H	9.75965	11.83211	-2.73060
H	15.00872	14.54159	1.54846	H	8.90365	12.98904	-1.67568
C	16.46502	13.22328	3.48904	H	8.61615	11.24206	-1.50235
C	15.59292	10.95924	3.48419	H	10.86544	13.83059	-2.51592
H	16.46270	14.23513	3.10407	H	12.85934	15.26764	-2.47024
C	17.35064	12.87684	4.49475	H	14.57808	14.94259	-0.71517
H	18.03210	13.62177	4.88601	H	15.39897	13.82683	1.19672
C	17.36342	11.58348	4.99664	H	15.54006	14.28560	3.48861
H	18.05673	11.31383	5.78345	H	17.24051	14.11979	5.26990
C	16.48765	10.63383	4.49095	H	18.06734	11.89107	5.97660
H	16.48418	9.62086	4.87071	H	17.17933	9.85322	4.88882
H	13.60745	10.33803	3.03696	H	14.24972	9.76123	2.78591
H	14.80000	9.88155	1.82964	H	15.75939	9.55366	1.92670
O	12.45158	8.71824	1.22871	C	16.82574	10.83091	4.58595
H	12.46021	9.62819	0.89285	C	15.87152	10.90624	3.58204
C	11.46765	7.99173	0.53722	C	15.43511	12.17059	3.15974
H	11.66794	7.94755	-0.53969	C	15.92987	13.31738	3.77981
H	10.46532	8.41032	0.68530	C	16.87282	13.22131	4.78957
H	11.46948	6.97176	0.92432	C	17.32847	11.97537	5.18933

Converged Cartesian coordinates of calculated compound **20a** (no CH₃OH).



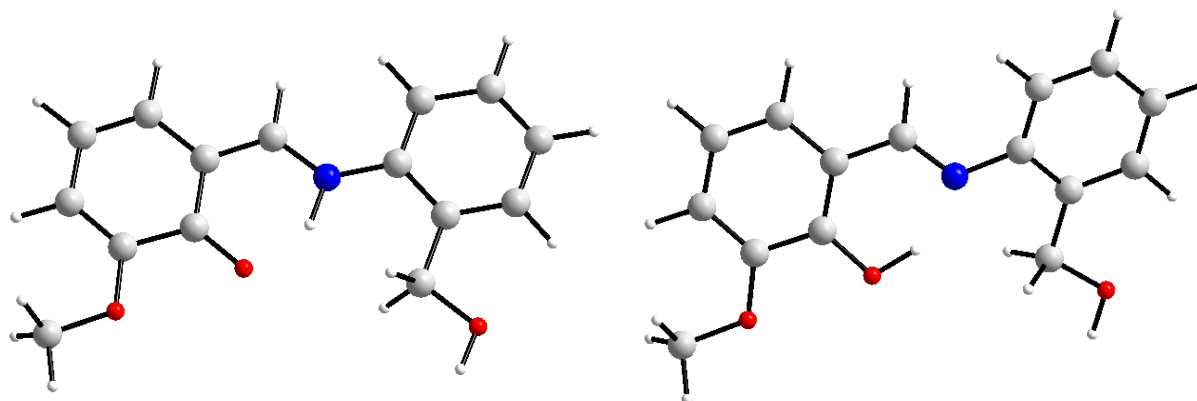
keto				enol			
C	9.67172	11.60019	-1.86766	C	16.49009	10.64621	4.48766
C	11.54371	12.58682	-0.84411	C	15.59298	10.96655	3.48052
O	12.64479	11.41430	0.88604	C	15.57229	12.27331	2.96757
C	12.57446	12.43998	0.16704	C	16.45001	13.23053	3.47475
O	15.03817	8.60121	3.80100	C	17.33952	12.89600	4.47984
H	14.57371	8.66969	4.63651	C	17.36036	11.60363	4.98702
C	14.86792	9.80049	3.08814	N	14.63700	12.50636	1.95540
N	14.64382	12.42011	2.04379	C	14.44646	13.61734	1.34335
H	13.89957	11.71235	1.81078	C	13.44399	13.73023	0.31054
C	14.51789	13.46194	1.24295	C	12.66107	12.61378	-0.03792
C	15.57881	12.23009	3.06466	C	11.68753	12.73759	-1.04692
H	10.07367	11.66654	-2.88457	C	11.51497	13.95490	-1.68068
H	9.00596	12.45222	-1.69172	C	12.29381	15.06247	-1.33281
H	9.10658	10.67634	-1.76506	C	13.24594	14.95214	-0.35027
C	11.49117	13.70492	-1.62728	O	10.98732	11.61403	-1.31115
H	10.71882	13.80027	-2.37937	C	10.00081	11.67953	-2.31078
C	12.43102	14.76140	-1.48700	O	12.82223	11.44099	0.56753
H	12.34776	15.62632	-2.13192	C	14.63834	9.95942	2.91706
C	13.41457	14.68192	-0.55724	O	14.78499	8.70747	3.53417
H	14.13716	15.48213	-0.43965	O	12.43905	8.57811	1.26991
C	13.51062	13.53977	0.28575	C	11.47554	7.77999	0.62477
H	15.23260	14.27408	1.33253	H	14.13980	8.13207	3.11484
C	16.35710	13.27621	3.55360	H	13.56649	11.59955	1.24291
C	15.71291	10.94174	3.60276	H	10.43143	11.93863	-3.28337
H	16.22766	14.27982	3.16972	H	9.22080	12.40494	-2.05806
C	17.28603	13.04731	4.55316	H	9.56003	10.68674	-2.36845
H	17.88310	13.87027	4.92576	H	10.76879	14.05705	-2.45672
C	17.43950	11.77428	5.07866	H	12.13811	16.00303	-1.84462
H	18.16657	11.58861	5.85906	H	13.85586	15.80388	-0.07201
C	16.65159	10.73693	4.60275	H	15.02239	14.51983	1.56734
H	16.76826	9.73569	4.99718	H	16.44293	14.24185	3.08751
H	13.80973	10.08992	3.06495	H	18.01802	13.64549	4.86843
H	15.14083	9.58021	2.05181	H	18.05690	11.34174	5.77407

Converged Cartesian coordinates of calculated compound $\text{H}_2\text{L}^2 \cdot \text{H}_2\text{O}$ (20b).



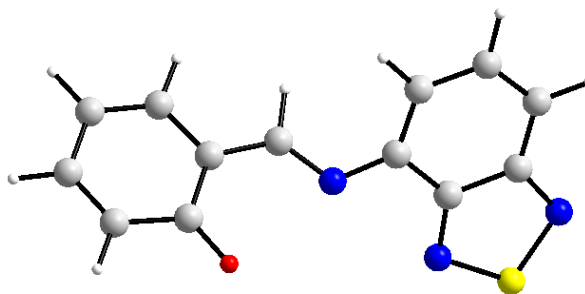
keto				enol			
C	13.76190	6.63024	5.10795	C	12.96274	4.94188	3.53091
C	12.50922	6.68169	5.65644	C	11.82946	4.77309	4.33982
C	11.51696	5.69012	5.31761	C	11.65072	5.58869	5.47078
C	11.92436	4.66631	4.38485	C	12.61037	6.57208	5.77419
C	13.23612	4.65421	3.84178	C	13.72182	6.71196	4.96207
C	14.13199	5.61221	4.19468	C	13.89949	5.89644	3.84146
O	10.35580	5.72403	5.81569	C	10.83030	3.78950	3.99230
O	12.07460	7.61170	6.53009	N	9.80254	3.59387	4.73245
C	12.97990	8.61515	6.91223	C	8.79289	2.67334	4.43486
C	11.00909	3.67336	4.01379	C	9.00536	1.50864	3.70093
N	9.78754	3.65165	4.49474	C	7.95380	0.64326	3.45049
C	8.73666	2.76073	4.25556	C	6.68749	0.93549	3.93529
C	7.53666	3.01503	4.93539	C	6.47596	2.08493	4.68442
C	6.46338	2.16208	4.73382	C	7.51968	2.95642	4.95129
C	6.57041	1.07656	3.87670	C	7.33548	4.19602	5.77193
C	7.76213	0.83408	3.20903	O	6.00437	4.32128	6.20514
C	8.84664	1.67354	3.39592	O	10.58612	5.45976	6.26053
C	7.46020	4.19658	5.85194	O	12.34683	7.31594	6.86928
O	6.19811	4.30710	6.44946	C	13.27573	8.31099	7.22156
O	8.21403	6.66500	7.39489	O	8.22945	6.78146	7.41626
H	6.24508	5.08443	7.01318	H	5.96751	5.10848	6.75224
H	9.66260	4.46066	5.15151	H	10.05231	4.69698	5.86422
H	5.54178	2.36598	5.26240	H	5.49584	2.31702	5.07918
H	5.72274	0.41906	3.72961	H	5.86381	0.25907	3.74257
H	7.85103	-0.01175	2.53888	H	8.12733	-0.26577	2.88776
H	9.77211	1.47568	2.87019	H	10.00189	1.26388	3.35306
H	8.23942	4.10624	6.62131	H	8.01453	4.15264	6.63266
H	7.69421	5.10791	5.28448	H	7.63485	5.07153	5.18270
H	11.31256	2.90194	3.31263	H	10.97598	3.24460	3.05420
H	13.50645	3.86947	3.14390	H	13.08493	4.30836	2.66001
H	15.13370	5.61082	3.78585	H	14.77697	6.02797	3.22214
H	14.49670	7.38003	5.37050	H	14.46513	7.46304	5.19176
H	13.85950	8.19335	7.41007	H	14.25898	7.88233	7.44031
H	12.44817	9.25850	7.60998	H	12.88630	8.78662	8.11893
H	13.30671	9.20918	6.05212	H	13.37815	9.06227	6.43191
H	8.36376	7.44935	7.92151	H	8.37971	7.36126	8.16283
H	9.05270	6.50371	6.93186	H	9.11195	6.53914	7.10681

Converged Cartesian coordinates of calculated compound **20b** (no H₂O).



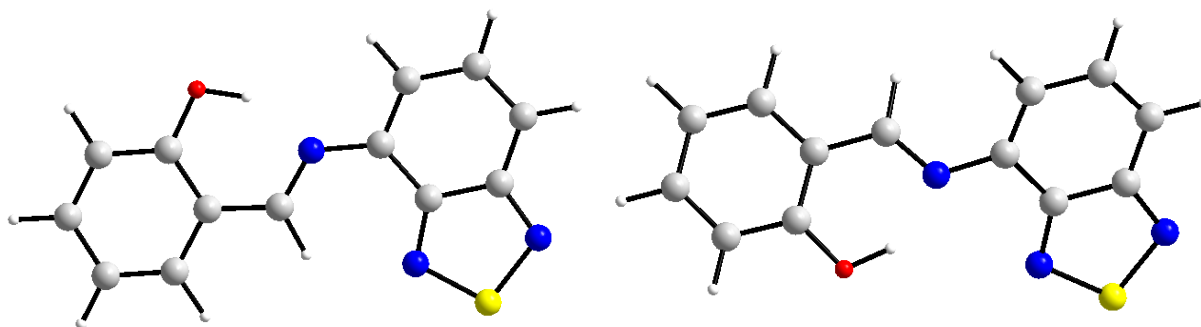
keto				enol			
C	13.68123	6.62912	5.13040	C	9.08122	1.44891	3.99930
C	12.41422	6.70729	5.63591	C	8.69018	2.70271	4.46523
C	11.42092	5.70466	5.30073	C	7.33256	2.97042	4.68988
C	11.85991	4.64504	4.41574	C	6.39710	1.98814	4.40479
C	13.19111	4.60878	3.91617	C	6.79064	0.74694	3.92292
C	14.07677	5.57486	4.26456	C	8.13492	0.47492	3.72660
O	10.25245	5.76238	5.75701	N	9.61796	3.70626	4.76896
O	11.95865	7.66903	6.45953	C	10.66227	3.88004	4.04459
C	12.85623	8.68029	6.83523	C	11.67486	4.85768	4.35803
C	10.95311	3.65085	4.05554	C	11.54940	5.67168	5.49662
N	9.71033	3.64895	4.49738	C	12.55594	6.61807	5.77969
C	8.69041	2.73235	4.23084	C	13.64482	6.72905	4.93441
C	7.44296	2.95838	4.83010	C	13.76402	5.91793	3.80181
C	6.41174	2.06452	4.58317	C	12.79042	4.99438	3.51678
C	6.59930	0.96426	3.76067	O	12.35635	7.35605	6.89027
C	7.83568	0.74807	3.17216	C	13.33105	8.31082	7.22531
C	8.87794	1.62722	3.40508	O	10.51034	5.58274	6.31708
C	7.24282	4.15044	5.72009	C	6.92448	4.31457	5.21548
O	5.92127	4.17011	6.20407	O	5.52663	4.35727	5.39147
H	5.81962	4.93753	6.76736	H	5.29324	5.21306	5.75070
H	9.56832	4.48488	5.12269	H	9.92570	4.86494	5.95019
H	5.45351	2.24709	5.04964	H	5.35116	2.20699	4.57129
H	5.78138	0.27818	3.58053	H	6.04543	-0.01103	3.71544
H	7.99398	-0.10784	2.52797	H	8.45152	-0.49955	3.37530
H	9.83711	1.44498	2.93865	H	10.13633	1.22894	3.88819
H	7.96162	4.11203	6.55064	H	7.44614	4.49856	6.16391
H	7.46593	5.06834	5.15822	H	7.25549	5.09389	4.51685
H	11.27403	2.85354	3.39292	H	10.81924	3.28832	3.13616
H	13.48077	3.79857	3.25588	H	12.86822	4.35827	2.64259
H	15.09177	5.55641	3.88997	H	14.62652	6.02655	3.15748
H	14.41225	7.38416	5.38882	H	14.41854	7.45378	5.14804
H	13.71757	8.27250	7.37551	H	14.30523	7.84466	7.40611
H	12.30531	9.34984	7.49229	H	12.98731	8.78663	8.14108
H	13.21500	9.24225	5.96598	H	13.43632	9.07005	6.44325

Converged Cartesian coordinates of calculated compound (**L⁵**).



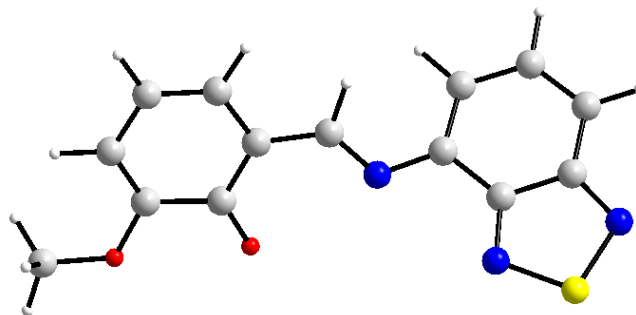
C	2.6559	0.2384	0.1925
C	3.5486	1.0192	0.9624
C	1.2855	0.5926	0.276
C	3.1734	-0.8531	-0.6425
C	4.8991	0.7925	1.0038
H	3.1241	1.8315	1.5511
C	5.4199	-0.2767	0.2371
H	5.5524	1.4101	1.61
C	4.611	-1.0575	-0.5333
H	6.4895	-0.4766	0.2636
H	5.0152	-1.8731	-1.1253
O	2.4814	-1.5514	-1.3942
N	0.2555	-0.0289	-0.2055
N	-2.1803	-1.4772	0.3255
H	1.0997	1.5055	0.8706
C	-0.9503	0.5843	-0.2169
C	-2.1487	-0.1899	0.021
C	-1.1586	1.9277	-0.5097
C	-3.461	0.4287	-0.0296
C	-2.4441	2.5084	-0.5612
H	-0.2959	2.5369	-0.7538
C	-3.5956	1.8047	-0.3308
N	-4.457	-0.4168	0.2282
S	-3.7552	-1.8751	0.5168
H	-2.5134	3.5653	-0.8033
H	-4.5774	2.2579	-0.3759

Converged Cartesian coordinates of calculated compound **HL⁵**.



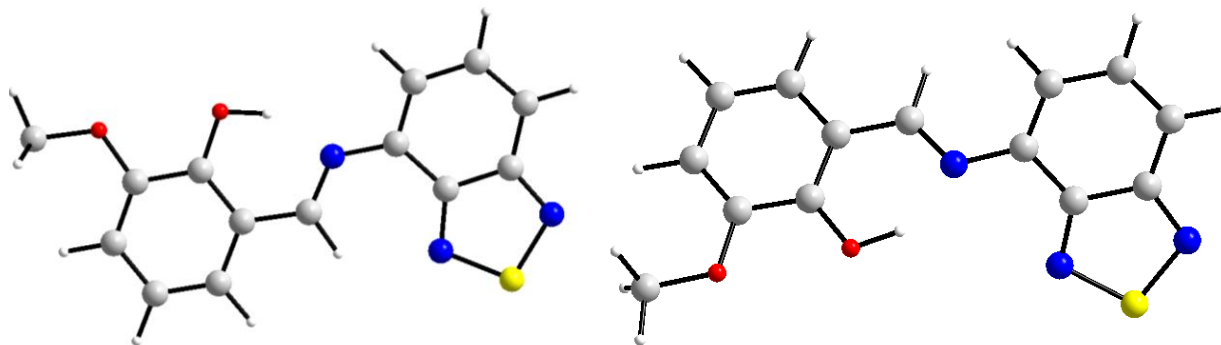
<i>A-HL⁵</i>				<i>B- HL⁵</i>			
C	1.9731	-0.1416	0.0024	C	2.9554	-0.8249	-0.4208
N	1.7155	-1.4459	0.022	C	2.6578	0.4129	0.1995
C	3.3895	0.156	-0.0041	C	3.7021	1.1723	0.7466
C	1.0168	0.9329	-0.0091	C	5.0084	0.742	0.6828
N	4.159	-0.9288	0.0101	C	5.2889	-0.4787	0.0642
C	3.858	1.4914	-0.023	C	4.2836	-1.2529	-0.4783
C	2.925	2.4846	-0.0325	C	1.3046	0.8942	0.282
H	4.9222	1.6879	-0.0287	N	0.3169	0.2411	-0.2143
C	1.5367	2.2069	-0.0243	C	-0.9689	0.7596	-0.1925
H	3.2415	3.5213	-0.0462	C	-2.0593	-0.1416	0.0174
H	0.8329	3.0312	-0.0316	C	-3.4155	0.3474	0.017
N	-0.3641	0.814	-0.0029	C	-3.6849	1.7193	-0.2102
C	-0.996	-0.3124	-0.0288	C	-2.6225	2.5457	-0.4265
C	-2.4346	-0.3563	-0.0167	C	-1.2824	2.0766	-0.4232
H	-0.4666	-1.265	-0.0597	N	-4.3189	-0.6059	0.2343
C	-3.0867	-1.5981	-0.0482	S	-3.484	-1.9972	0.4198
C	-3.2129	0.8266	0.0255	N	-1.9579	-1.4465	0.2372
C	-4.4611	-1.6856	-0.0387	O	2.0109	-1.5963	-0.9467
H	-2.4803	-2.4982	-0.0803	H	-4.7073	2.0745	-0.2168
C	-5.2146	-0.5102	0.003	H	-2.7944	3.5989	-0.6188
H	-4.9518	-2.6509	-0.0632	H	-0.4848	2.7763	-0.6471
C	-4.6054	0.7282	0.0348	H	1.1455	1.8441	0.8074
H	-6.2979	-0.567	0.0109	H	3.4599	2.1172	1.2241
H	-5.1848	1.6432	0.0672	H	5.8066	1.3386	1.107
O	-2.6493	2.0302	0.0568	H	6.3141	-0.8287	0.0082
S	3.1588	-2.2147	0.0305	H	4.4957	-2.2021	-0.9557
H	-1.6609	1.881	0.0426	H	1.1358	-1.1464	-0.8001

Converged Cartesian coordinates of calculated compound (**L**⁶):



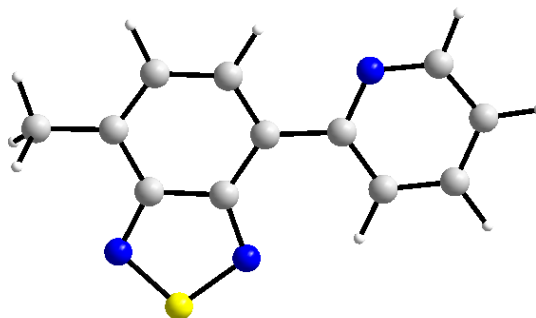
C	1.6669	0.6119	-0.2546
C	2.0112	1.8705	-0.7377
C	2.7814	-0.2653	0.0328
N	0.4029	0.1574	-0.1026
C	3.3492	2.2776	-0.9252
H	1.2118	2.5433	-1.0259
C	4.4244	1.4749	-0.6522
H	3.5249	3.2774	-1.3128
C	4.151	0.1767	-0.1603
H	5.4472	1.7953	-0.8026
N	5.057	-0.7431	0.1659
N	2.6833	-1.4957	0.5089
C	-0.5195	0.9625	0.3261
C	-1.9233	0.7767	0.3522
H	-0.1935	1.9171	0.7769
C	-2.5933	-0.3436	-0.3014
C	-2.6745	1.7616	1.0452
O	-2.0353	-1.2153	-0.97
C	-4.0571	-0.3622	-0.111
O	-4.6546	-1.433	-0.706
C	-4.7265	0.6076	0.5777
C	-4.0305	1.6966	1.1663
H	-5.8054	0.5614	0.6852
H	-4.5835	2.4585	1.7046
H	-2.1294	2.5873	1.4983
C	-6.0396	-1.5382	-0.5838
H	-6.3294	-2.4472	-1.113
H	-6.5607	-0.6812	-1.0345
H	-6.3572	-1.6193	0.4656
S	4.2109	-2.055	0.6823

Converged Cartesian coordinates of calculated compound **HL⁶**.



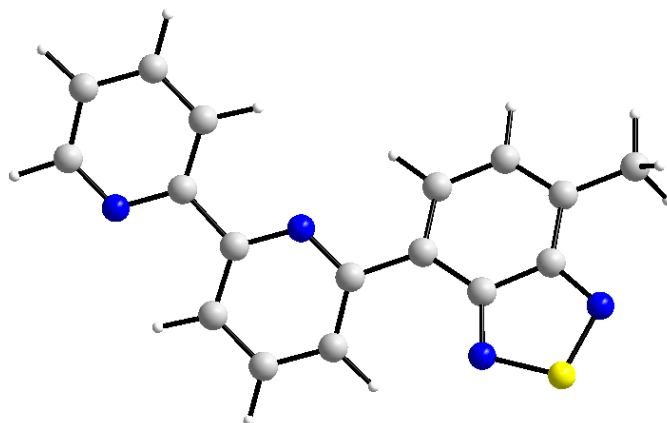
<i>A-HL⁶</i>				<i>B-HL⁶</i>			
S	4.0618	-1.9887	0	C	-2.8237	2.0102	-0.8391
N	2.5431	-1.3821	0.0001	C	-1.9431	1.0409	-0.3256
C	2.6565	-0.0574	0	C	-2.4424	-0.1864	0.1516
C	4.0321	0.3932	-0.0001	C	-3.8368	-0.4179	0.1128
N	4.9156	-0.601	0	C	-4.6781	0.5561	-0.3931
C	4.3517	1.772	-0.0001	C	-4.1737	1.7722	-0.8697
C	3.3156	2.6571	-0.0001	C	-0.53	1.3113	-0.2993
C	1.9659	2.2295	-0.0001	N	0.3228	0.47	0.1635
C	1.5883	0.9062	0	C	1.6687	0.7917	0.2503
N	0.2288	0.6369	0	C	2.6308	-0.2291	-0.0279
C	-0.2773	-0.5519	0.0001	C	4.0406	0.0527	0.0807
C	-1.7024	-0.7564	0.0001	C	4.4883	1.3353	0.4822
C	-2.5914	0.3367	0.0001	C	3.5429	2.2781	0.7579
C	-3.983	0.0908	0	C	2.1521	2.0137	0.6493
C	-4.4467	-1.2119	-0.0002	N	4.8107	-0.9909	-0.2184
C	-3.559	-2.295	-0.0001	S	3.7989	-2.2142	-0.6023
C	-2.2063	-2.0705	0	N	2.3583	-1.4709	-0.4089
O	-2.169	1.5935	0.0004	O	-1.6602	-1.1408	0.634
O	-4.7617	1.1944	0	O	-4.2327	-1.6162	0.5902
C	-6.1563	1.0097	-0.0002	C	-5.6097	-1.9058	0.5729
H	5.388	2.0837	-0.0002	H	5.5487	1.534	0.5688
H	3.5168	3.7223	-0.0002	H	3.8512	3.2659	1.0821
H	1.1763	2.972	-0.0001	H	1.4499	2.7921	0.9266
H	0.3528	-1.4414	0.0001	H	-0.2031	2.2733	-0.7126
H	-1.5052	-2.8982	0	H	-2.4165	2.9466	-1.2061
H	-3.9514	-3.3047	-0.0003	H	-4.8573	2.5152	-1.262
H	-5.5121	-1.4037	-0.0003	H	-5.7459	0.3807	-0.4241
H	-6.4929	0.4706	0.8931	H	-6.0102	-1.9035	-0.4474
H	-6.4927	0.4707	-0.8935	H	-6.1795	-1.1974	1.1853
H	-6.592	2.0072	0.0001	H	-5.7117	-2.9043	0.9941
H	-1.1691	1.5489	0.0006	H	-0.7214	-0.8159	0.5671

Converged Cartesian coordinates of calculated compound **L⁷**.



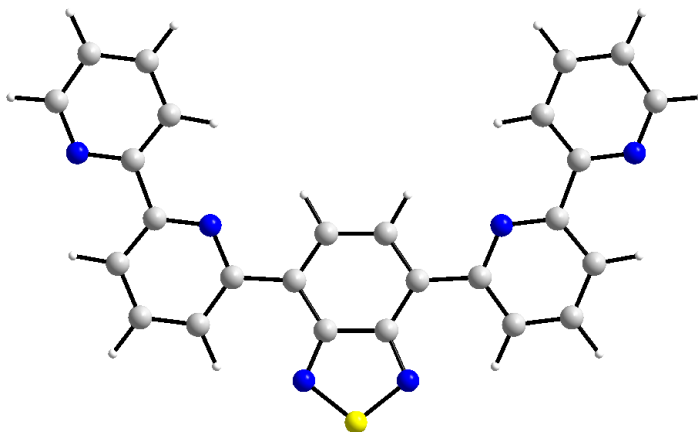
S	4.3327	0.35286	5.44996
N	4.97451	0.84278	4.06318
N	5.52733	0.69177	6.47026
C	6.52275	1.22364	5.75241
C	6.19315	1.30841	4.35037
N	9.46763	2.1229	7.86582
C	9.93469	2.12224	9.10214
C	8.23858	1.64413	7.63444
C	7.79256	1.68141	6.22378
C	8.63064	2.1864	5.25975
C	7.44778	1.1473	8.67281
C	8.29683	2.2645	3.88867
H	9.59939	2.54093	5.58602
C	7.09634	1.83979	3.39242
H	9.0304	2.68072	3.20719
C	6.71955	1.91078	1.95269
C	7.95049	1.15305	9.96293
H	6.46013	0.76612	8.4645
C	9.22053	1.64898	10.19452
H	7.34843	0.7708	10.77867
H	9.65198	1.6722	11.18679
H	10.93644	2.52148	9.23392
H	6.48897	0.91766	1.5602
H	7.5248	2.34297	1.35953
H	5.81928	2.51395	1.81416

Converged Cartesian coordinates of calculated compound **L⁹**.



S	3.28572	6.78949	15.85947
N	2.93495	6.67954	17.42375
N	2.52363	8.1484	15.47361
C	2.17605	7.73703	17.73164
C	1.94191	8.58943	16.59275
C	2.21316	5.93222	20.2091
C	2.32297	5.24725	21.4073
C	1.81906	7.27087	20.23709
H	2.42904	5.44878	19.26901
C	2.04793	5.89621	22.59446
C	1.665	7.23519	22.53511
H	2.12021	5.40764	23.55542
C	0.9432	10.63012	15.48565
C	1.16949	9.77708	16.6862
H	1.89184	10.97643	15.06903
H	0.33231	11.49785	15.73263
H	0.44605	10.0654	14.6936
C	0.9009	9.23395	19.05211
C	1.63551	8.07531	19.00976
C	0.67163	10.05975	17.92748
H	0.47699	9.51921	20.00581
N	1.55496	7.89444	21.38732
N	1.39725	7.30127	24.92242
C	1.13525	7.94537	26.05079
C	1.36843	7.98862	23.7794
H	2.62376	4.20633	21.40927
C	1.07963	9.35145	23.73798
C	0.80912	10.01159	24.92193
H	1.07844	9.86008	22.78451
C	0.83393	9.29782	26.10973
H	1.16731	7.35081	26.959
H	0.58315	11.07128	24.91908
H	0.62821	9.77248	27.06044
H	0.07184	10.953	18.06237

Converged Cartesian coordinates of calculated compound **L¹⁰**.



N	-3.4538	0.128	-0.1034	H	-3.3053	-3.201	-0.4742
C	-2.9351	-1.0967	-0.2167	H	-5.767	-2.9012	-0.5828
C	-3.7455	-2.2196	-0.3894	H	-6.7138	-0.5875	-0.3552
C	-5.1175	-2.0449	-0.445	H	-3.3679	2.5427	0.3594
C	-5.6506	-0.7772	-0.3229	H	-8.178	3.1575	-0.1111
C	-4.7713	0.2908	-0.1506	H	-4.3081	4.8512	0.5963
C	-1.4599	-1.1758	-0.186	H	-6.7816	5.1584	0.3512
C	-0.7234	-2.3558	0.127	H	-3.3053	-3.201	-0.4742
C	0.7234	-2.3558	0.127	H	1.2281	0.851	-0.7067
C	1.4599	-1.1758	-0.186	H	-1.2281	0.851	-0.7067
C	0.7037	-0.0646	-0.4673	H	3.3053	-3.201	-0.4741
C	-0.7037	-0.0646	-0.4673	H	5.767	-2.9012	-0.5826
N	1.2349	-3.5409	0.4756	H	6.7138	-0.5875	-0.3551
S	0	-4.5226	0.7629	H	3.3679	2.5427	0.3594
N	-1.2349	-3.5409	0.4755	H	8.178	3.1575	-0.1111
C	2.9351	-1.0967	-0.2167	H	4.3081	4.8512	0.5962
C	3.7455	-2.2196	-0.3893	H	6.7816	5.1584	0.3511
C	5.1175	-2.045	-0.4448	C	-5.2891	1.6741	-0.0029
C	5.6506	-0.7772	-0.3228	C	-4.4264	2.7365	0.2598
C	4.7713	0.2908	-0.1506	C	-4.9554	4.0069	0.3906
N	3.4538	0.128	-0.1033	C	-6.3236	4.1822	0.2568
C	5.2891	1.6741	-0.0029	C	-7.1016	3.0635	-0.0013
C	4.4264	2.7365	0.2597	N	-6.6068	1.8405	-0.1283
C	4.9554	4.007	0.3904	C	7.1017	3.0635	-0.0013
C	6.3236	4.1822	0.2567	N	6.6068	1.8405	-0.1283

References

1. Shova, S.; Vlad, A.; Cazacu, M.; Krzystek, J.; Bucinsky, L.; Breza, M.; Darvasiová, D.; Rapta, P.; Cano, J.; Telsler, J.; Arion, V. B. *Dalton Trans.* **2017**, 46 (35), 11817–11829.
2. Duboc, C.; Ganyushin, D.; Sivalingam, K.; Collomb, M.-N.; Neese, F. *J. Phys. Chem. A* **2010**, 114 (39), 10750–10758.
3. Pascual-Álvarez, A.; Vallejo, J.; Pardo, E.; Julve, M.; Lloret, F.; Krzystek, J.; Armentano, D.; Wernsdorfer, W.; Cano, J. *Chem. Eur. J.* **2015**, 21 (48), 17299–17307.
4. Neese, F. *Comput. Mol. Sci.* **2012**, 2 (1), 73–78.
5. Chen, H.; Adams, S. *IUCrJ* **2017**, 4 (5), 614–625.
6. Schäfer, A.; Horn, H.; Ahlrichs, R. *J. Chem. Phys.* **1992**, 97 (4), 2571–2577.
7. Eichkorn, K.; Weigend, F.; Treutler, O.; Ahlrichs, R. *Theor. Chem. Acc.* **1997**, 97 (1), 119–124.
8. Frisch, M. J.; Trucks, G. W.; Schlegel, H. B.; Scuseria, G. E.; Robb, M. A.; Cheeseman, J. R.; Scalmani, G.; Barone, V.; Mennucci, B.; Petersson, G. A.; Nakatsuji, H.; Caricato, M.; Li, X.; Hratchian, H. P.; Izmaylov, A. F.; Bloino, J.; Zheng, G.; Sonnenberg, J. L.; Hada, M.; Ehara, M.; Toyota, K.; Fukuda, R.; Hasegawa, J.; Ishida, M.; Nakajima, T.; Honda, Y.; Kitao, O.; Nakai, H.; Vreven, T.; Montgomery, J. A., Jr.; Peralta, J. E.; Ogliaro, F.; Bearpark, M.; Heyd, J. J.; Brothers, E.; Kudin, K. N.; Staroverov, V. N.; Kobayashi, R.; Normand, J.; Raghavachari, K.; Rendell, A.; Burant, J. C.; Iyengar, S. S.; Tomasi, J.; Cossi, M.; Rega, N.; Millam, J. M.; Klene, M.; Knox, J. E.; Cross, J. B.; Bakken, V.; Adamo, C.; Jaramillo, J.; Gomperts, R.; Stratmann, R. E.; Yazyev, O.; Austin, A. J.; Cammi, R.; Pomelli, C.; Ochterski, J. W.; Martin, R. L.; Morokuma, K.; Zakrzewski, V. G.; Voth, G. A.; Salvador, P.; Dannenberg, J. J.; Dapprich, S.; Daniels, A. D.; Farkas, Ö.; Foresman, J. B.; Ortiz, J. V.; Cioslowski, J.; Fox, D. J. Gaussian~09 Revision E.01.
9. Adamo, C.; Barone, V. *J. Chem. Phys.* **1999**, 110 (13), 6158–6170.
10. Adamo, C.; Barone, V. *J. Chem. Phys.* **1999**, 110 (13), 6158–6170.
11. Krishnan, R.; Binkley, J. S.; Seeger, R.; Pople, J. A. *J. Chem. Phys.* **1980**, 72 (1), 650–654.
12. Frisch, M. J.; Pople, J. A.; Binkley, J. S. *J. Chem. Phys.* **1984**, 80 (7), 3265–3269.
13. O’Boyle, N. M.; Tenderholt, A. L.; Langner, K. M. *J. Comput. Chem.* **2008**, 29 (5), 839–845.
14. Schäfer, A.; Huber, C.; Ahlrichs, R. *J. Chem. Phys.* **1994**, 100 (8), 5829–5835.

Composés de Coordination Basés sur des Métaux 3d avec des Ligands Multidentates N- ou N,O-donneurs : Synthèse, Structure et Propriétés

Mots clés : Complexes métalliques, 2,1,3-Benzothiadiazole, Pyridine, 2,2'-Bipyridine, DFT, Bases de Schiff, Magnétisme, Luminescence

Résumé : Cette thèse est dédiée à la synthèse de nouveaux complexes à base de métaux 3d avec des ligands multidentates, la caractérisation de leurs structures et propriétés. Le travail est divisé en trois parties.

Dans la première partie nous décrivons la synthèse de complexes polynucléaires avec des ligands bases de Schiff dérivés de la *o*-vaniline ou le salicylaldéhyde. L'approche "synthèse directe" pour obtenir des complexes hétéro-métalliques cuivre-métaux alcalins terreux a été développée. Le tautomerism d'un ligand base de Schiff a été étudié. Dans les polymères de coordination, de très faibles interactions antiferromagnétiques entre les ions manganèse (III) *via* les ponts {-NCCO-} ont été observées.

La deuxième partie décrit des ligands bases de Schiff à base de 2,1,3-benzothiadiazole. Les possibilités de coordination de ces ligands sont discutées. Une série de complexes de métaux de transition a été obtenue et caractérisée. Les propriétés magnétiques des complexes de cuivre et cobalt sont présentées.

Dans la troisième partie nous décrivons la synthèse de ligands comportant l'unité 2,1,3-benzothiadiazole et des fragments pyridine et 2,2'-bipyridine. Des complexes mono- et binucléaires ont été préparés. Les propriétés photophysiques des ligands ainsi obtenus et des complexes de zinc ont été étudiées. Les résultats expérimentaux sont étayés par des calculs DFT et TD-DFT.

Coordination Compounds Based on 3d-Metals with Multidentate N- or N,O-donor Ligands: Synthesis, Structure and Properties

Keywords: Metal complexes, Schiff bases, 2,1,3-Benzothiadiazole, Pyridine, 2,2'-Bipyridine, DFT, Magnetism, Luminescence

Abstract: This thesis is devoted to the synthesis of new complexes based on 3d-metals with multidentate ligands, characterization of their structures and properties. This work consists of three main parts.

In the first part, we present the synthesis of polynuclear complexes with Schiff base ligands, derivatives of *o*-vanillin or salicylic aldehyde. The "direct synthesis" approach for obtaining heterometallic copper-alkaline earth metal complexes was developed. The tautomerism of a Schiff base ligand was studied. In the coordination polymers very weak antiferromagnetic exchange interactions between manganese (III) ions through {-NCCO-} bridges have been found.

The second part is devoted to Schiff base ligands based on 2,1,3-benzothiadiazole. The coordination possibilities of these ligands were discussed. A series of transition metal complexes was obtained and characterized. The magnetic properties for copper and cobalt complexes are described.

In the third part, we focus on the design and the synthesis of ligands containing 2,1,3-benzothiadiazole and pyridine or 2,2'-bipyridine fragments. Mono- and binuclear complexes were synthesized. The photophysical properties of the obtained ligands and zinc complexes are described. The crystallographic results and physical properties were supported by DFT and TD-DFT calculations.